DISSERTATION
AT THE FACULTY OF BIOLOGY OF THE
LUDWIG-MAXIMILIANS-UNIVERSITÄT MÜNCHEN

FOR THE AWARD OF THE DEGREE
Doctor rerum naturalium

Mitochondrial Genome Segregation Dynamics and Quality Control in *S.cerevisiae*

RODARIA ROUSSOU

FROM ATHENS, GREECE

August 2024

Mitochondrial Genome Segregation Dynamics and Quality Control in *S. cerevisiae*

Dissertation von Rodaria Roussou

München 2024

Mitochondrial Genome Segregation Dynamics and Quality Control in *S. cerevisiae*

Dissertation der Fakultät für Biologie

der Ludwig-Maximilians-Universität München

Rodaria Roussou

München, 2024

Diese Dissertation wurde angefertigt
unter der Leitung von Prof. Dr. Christof Osman
im Bereich von Zell- und Entwicklungsbiologie
an der Ludwig-Maximilians-Universität München

Erstgutachter/in:	Prof. Dr. Christof Osman
Zweitgutachter/in:	Prof. Dr. Dejana Morkranjac
Tag der Abgabe:	07.08.2024
Tag der mündlichen Prüfung:	06.12.2024

Erklärung

Ich versichere hiermit an Eides statt, dass meine Dissertation selbstständig und ohne unerlaubte Hilfsmittel angefertigt worden ist.
Die vorliegende Dissertation wurde weder ganz noch teilweise bei einer anderen Prüfungskommission vorgelegt.
Ich habe noch zu keine früheren Zeitpunkt versucht, eine Dissertation einzureichen oder an einer Doktorprüfung teilzunehmen.

München, den 20. Januar 2025

Rodaria Roussou

The submitted dissertation was prepared under the supervision of Prof. Dr. Christof Osman at the Department of Cell Biology, in the Faculty of Biology of the Ludwig-Maximillians-University (LMU) in Munich.

First examiner: Prof. Dr. Christof Osman
Second examiner: Prof. Dr. Dejana Mokranjac
Day of submission: August 7, 2024
Day of oral examination: December 6, 2024

If you know the question, you know half.

- Herb Boyer

I dedicate this work to my beloved grandmother Rodaria,
who always reminded me what's important in life.

Affidavit

I hereby declare, that the submitted thesis entitled 'Mitochondrial Genome Segregation Dynamics and Quality Control in *S.cerevisiae*' is my own work.

I have only used the sources indicated and have not made unauthorized use of services of a third party. Where the work of others has been quoted or reproduced, the source is always given.

I further declare that the dissertation presented here has not been submitted in the same or similar form to another examination committee nor to any other institution for the purpose of obtaining an academic degree.

Munich, 07.08.2024 Rodaria Roussou

Eigenständigkeitserklärung

Hiermit versichere ich an Eides statt, dass die vorliegende schriftliche Dissertation / Masterarbeit / Bachelorarbeit / Zulassungsarbeit mit dem Titel

Mitochondrial Genome Segregation Dynamics and Quality Control in S. cerevisiae

von mir selbstständig verfasst wurde und dass keine anderen als die angegebenen Quellen und Hilfsmittel benutzt wurden. Die Stellen der Arbeit, die anderen Werken dem Wortlaut oder dem Sinne nach entnommen sind, wurden in jedem Fall unter Angabe der Quellen (einschließlich des World Wide Web und anderer elektronischer Text- und Datensammlungen) kenntlich gemacht. Weiterhin wurden alle Teile der Arbeit, die mit Hilfe von Werkzeugen der künstlichen Intelligenz de novo generiert wurden, durch Fußnote/Anmerkung an den entsprechenden Stellen kenntlich gemacht und die verwendeten Werkzeuge der künstlichen Intelligenz gelistet. Die genutzten Prompts befinden sich im Anhang. Diese Erklärung gilt für alle in der Arbeit enthaltenen Texte, Graphiken, Zeichnungen, Kartenskizzen und bildliche Darstellungen.

Planegg-Martinsried, 07.08.24

(Ort / Datum)

RODARIA ROUSSOU

(Vor und Nachname in Druckbuchstaben)

Rodaria Roussou

(Unterschrift)

Affidavit

Herewith I certify under oath that I wrote the accompanying Dissertation / MSc thesis / BSc thesis / Admission thesis myself.

Title: Mitochondrial Genome Segregation Dynamics and Quality Control in S. cerevisiae

In the thesis no other sources and aids have been used than those indicated. The passages of the thesis that are taken in wording or meaning from other sources have been marked with an indication of the sources (including the World Wide Web and other electronic text and data collections). Furthermore, all parts of the thesis that were de novo generated with the help of artificial intelligence tools were identified by footnotes/annotations at the appropriate places and the artificial intelligence tools used were listed. The prompts used were listed in the appendix. This statement applies to all text, graphics, drawings, sketch maps, and pictorial representations contained in the Work.

Planegg-Martinsried, 07.08.24

(Location/date)

RODARIA ROUSSOU

(First and last name in block letters)

Rodaria Roussou

(Signature)

Erklärung
Declaration

Hiermit erkläre ich, *
Hereby I declare

☒ dass die Dissertation nicht ganz oder in wesentlichen Teilen einer anderen Prüfungskommission vorgelegt worden ist.
that this work, complete or in parts, has not yet been submitted to another examination institution

☒ dass ich mich anderweitig einer Doktorprüfung ohne Erfolg **nicht** unterzogen habe.
*that I did **not** undergo another doctoral examination without success*

☒ dass ich mich mit Erfolg der Doktorprüfung im Hauptfach
that I successfully completed a doctoral examination in the main subject

und in den Nebenfächern
and in the minor subjects

bei der Fakultät für
at the faculty of Biology

der
at Ludwig Maximillians University
(Hochschule/*University*)

unterzogen habe.

☐ dass ich ohne Erfolg versucht habe, eine Dissertation einzureichen oder mich der Doktorprüfung zu unterziehen.
that I submitted a thesis or did undergo a doctoral examination without success

Planegg-Martinsried, 20.01.25
Ort, Datum/*place, date*

Rodaria Roussou
Unterschrift/*signature*

*) Nichtzutreffendes streichen/
delete where not applicable

Contents

List of Figures

List of Abbreviations

Amp	ampicillin
ADP	adenosine diphosphate
ATP	adenosine triphosphate
ATPase	adenosine triphosphate hydrolase
bp	base pairs
°C	degree Celsius
CJ	contact junction
C-terminal	carboxy-terminal
CS	contact sites
COB	Cytochrome b
COX	cytochrome c oxidase
DNM1	dynamin 1
EM	electron microscope
ETC	electron transport chain
ER	endoplasmic reticulum
textbfDNA	deoxy-ribonucleic acid
Δ**p**	proton-motive force
$\Delta\psi$	membrane potential
E.coli	escherichia coli
Fig.	figure
g	gram or gravitational constant (9.81 m/s2)
GTP	guanosine triphosphate
hr	hour
Hek	human embryonic kidney
HeLa	Henrietta Lacks (patient from whom cell line is derived)
HMG	high mobility group
IMM	inner mitochondrial membrane
IMS	intermembrane space
Kan	kanamycin
kDa	kilo dalton
kb	kilo bases
l	litre
µ	micro
m	milli
M	molar
min	minute

MAT	mating type
MGM1	Mitochondrial Genome Maintenance 1
MRX6	MIOREX complex component 6
MICOS	Mitochondrial contact site and cristae organising system
MIOREX	Mitochondrial organization of gene expression
mtDNA	mitochondrial DNA
mRNA	messenger RNA
MW	molecular weight
n	nano
NAD	nicotinamide adenine dinucleotide
NADH	nicotinamide adenine dinucleotide Hydride
nDNA	nuclear DNA
NG	NeonGreen
N-terminal	amino-terminal
OD	optical density
OMM	outer mitochondrial membrane
OPA1	optical atrophy 1
ORF	open reading frame
ori	origin-like
OXPHOS	oxidative phosphorylation
PBS	phosphate buffered saline
PCR	polymerase chain reaction
Pi	inorganic phosphate
Pol	polymerase
RNA	ribonucleic acid
rRNA	ribosomal RNA
RT	room temperature
ROS	reactive oxygen species
sec	seconds
SC	synthetic complete
S. cerevisiae	Saccharomyces cerevisiae
S. pombe	Schizosaccharomyces pombe
su	subunit
TIM	transporter of the inner mitochondrial membrane
TOM	transporter of the outer mitochondrial membrane
tRNA	transfer RNA
UTR	untranslated region
v/v	volume per volume
w/v	weight per volume
WT	wild type
YPD	yeast peptone dextrose
YPG	yeast peptone glycerol

List of Publications

Publication 1:
R. Roussou, D. Metzler, F. Padovani, F. Thoma, R. Schwarz, B. Shraiman, K. M. Schmoller, and C. Osman. (Aug. 2024). "Real-time assessment of mitochondrial DNA heteroplasmy dynamics at the single-cell level". The EMBO Journal 0.0, pp. 1–20, Aug 5; doi: 10.1038/s44318-024-00183-5.

Publication 2:
C. Jakubke, R. Roussou, A. Maiser, C. Schug, F. Thoma, D. Bunk, D. Hörl, H. Leonhardt, P. Walter, T. Klecker and C. Osman. (Sep. 2021). "Cristae-dependent quality control of the mitochondrial genome". Science Advances 7 (36), eabi8886, Sep 3; doi: 10.1126/sciadv.abi8886.

Confirmation of co-authors

As part of this cumulative dissertation, the second publication entitled: "Cristae-dependent quality control of the mitochondrial genome" was produced as a shared first co-authorship together with Christopher Jakubke.

In Figure 1 of the manuscript both me and Christopher worked closely. Specifically, figure 1B was prepared by me and in Figures 1C, 1F and 1G were prepared together with Christopher and the corresponding experiments were also carried out by both. Figures 2, 3 and 4 were predominantly prepared by Christopher. The electron microscopy in Figures 3E and 3F, as well as the images in Figure S8 of the appendix, were prepared and analysed by Christina Schug and Till Klecker from the University of Bayreuth. For the generation of Figure 5 both me and Christopher contributed equally. Most experiments for the re-submission of the manuscript during the revision period were executed by me, while Felix Thoma contributed majorly with the time-lapse microscopy and image analysis.

Munich, 07.08.2024 Christopher Jakubke

Munich, 07.08.2024 Rodaria Roussou

Abstract

Mitochondrial DNA (mtDNA), present as multiple copies within cells, encodes crucial subunits of the mitochondrial respiratory chain and is essential for ATP generation. Within individual cells, mtDNA copies can vary in sequence, leading to a state known as heteroplasmy. Dynamic changes in heteroplasmy are not well understood due to the challenge of real-time monitoring. We employ mtDNA-based fluorescent markers, microfluidics, and automated cell tracking to observe mtDNA variants in live heteroplasmic yeast populations at the single-cell level. This method, combined with direct mtDNA tracking and data-driven mathematical modeling, reveals that asymmetric partitioning of mtDNA copies during cell division and limited mitochondrial fusion and fission frequencies are critical for mtDNA variant segregation and homoplasmy establishment.

Mutations in mtDNA can lead to cellular energy shortages and numerous mitochondrial diseases, and the mechanisms by which cells maintain mtDNA integrity over generations remain unclear. By using *S. cerevisiae*, we investigated whether cells can intracellularly distinguish between functional and defective mtDNA. Our findings indicate that mother cells promote the generation of daughter cells with healthier mtDNA content. Purifying selection for functional mtDNA occurs within a continuous mitochondrial network and relies on stable mitochondrial subdomains and intact cristae morphology. We suggest that cristae-dependent proximity of mtDNA and its encoded proteins creates a spatial 'sphere of influence,' linking lack of functional fitness to the clearance of defective mtDNA.

These comprehensive approaches offer new insights into mtDNA heteroplasmy dynamics and the role of mitochondrial architecture and essential mechanisms in mtDNA quality control.

Zusammenfassung

Die mitochondriale DNA (mtDNA), die in Form von mehreren Kopien in Zellen vorhanden ist, kodiert wichtige Untereinheiten der mitochondrialen Atmungskette und ist für die ATP-Erzeugung unerlässlich. Innerhalb einzelner Zellen können die mtDNA-Kopien in ihrer Sequenz variieren, was zu einem Zustand führt, der als Heteroplasmie bekannt ist. Die dynamischen Veränderungen in der Heteroplasmie sind aufgrund der Schwierigkeit der Echtzeitbeobachtung nicht gut verstanden. Wir setzen mtDNA-basierte Fluoreszenzmarker, Mikrofluidik und automatisierte Zellverfolgung ein, um mtDNA Varianten in lebenden heteroplasmatischen Hefepopulationen auf Einzelzellniveau zu beobachten. Diese Methode, kombiniert mit direkter mtDNA-Analyse und datengetriebener mathematischer Modellierung, zeigt, dass die asymmetrische Aufteilung der mtDNA Kopien während der Zellteilung und die begrenzten mitochondrialen Fusions- und Fissions- frequenzen für die Segregation der mtDNA Varianten und die Etablierung der Homoplasmie entscheidend sind.

Mutationen in der mtDNA können zu zellulärem Energiemangel und zahlreichen mitochondrialen Krankheiten führen, und die Mechanismen, durch die die Zellen die Integrität der mtDNA über Generationen hinweg aufrechterhalten, sind noch unklar. Mit Hilfe von S. cerevisiae haben wir untersucht, ob Zellen intrazellulär zwischen funktioneller und defekter mtDNA unterscheiden können. Unsere Ergebnisse deuten darauf hin, dass Mutterzellen die Erzeugung von Tochterzellen mit gesünderem mtDNA Gehalt fördern. Die Selektion auf funktionelle mtDNA findet innerhalb eines kontinuierlichen mitochondrialen Netzwerks statt und hängt von stabilen mitochondrialen Subdomänen und einer intakten Cristae Morphologie ab. Wir vermuten, dass die cristae-abhängige Nähe von mtDNA und den kodierten Proteinen eine räumliche "Einflusssphäre" schafft, die einen Mangel an funktioneller Fitness mit der Beseitigung defekter mtDNA verbindet.

Diese umfassenden Ansätze bieten neue Einblicke in die Dynamik der mtDNA Heteroplasmie sowie in die Rolle der mitochondrialen Architektur und der wesentlichen Mechanismen bei der Qualitätskontrolle der mtDNA.

Introduction

1 The eukaryotic cell and Mitochondria

Mitochondria are widely recognized as the primary energy generators in eukaryotic cells, producing ATP through aerobic respiration. Their name as "powerhouses" was branded already in 1957 by Peter Siekevitz (Siekevitz, 1957). They were initially documented in 1857 by the Swiss anatomist Rudolf Albrecht von Kölliker, and in 1890, Richard Altman hypothesized that they functioned as intracellular parasites. However, these structures were coined the term "mitochondria" by the German scientist Carl Benda, from the Greek words "mitos" meaning thread and "khondros" meaning granule. It took nearly fifty more years to isolate mitochondria and demonstrate their role in catalyzing respiration.

Research conducted over the last decades has unveiled a plethora of additional functions carried out by mitochondria. Mitochondrial proteomes typically consist of more than 1,000 proteins that participate in a variety of biochemical processes crucial for cell function. These processes include - but are not limited to - protein synthesis, metabolism of amino acids and nucleotides, breakdown of fatty acids, lipid, quinone and steroid biosynthesis, biogenesis of iron-sulfur clusters, regulation of apoptosis, and maintenance of ion balance within the cell (Kauppila, Kauppila, and Larsson, 2017; Malina, Larsson, and Nielsen, 2018; Calvo and Mootha, 2010).

1.1 Origin of mitochondria

Mitochondria's origin can be traced back to the endosymbiotic theory proposed by Lynn Margulis in 1970 (Margulis, 1970; Embley and Martin, 2006). Subsequent genetic analyses provided support for the notion that mitochondria have evolved from endosymbiotic bacteria. Specifically, mitochondria have their origins in endosymbiotic purple non-sulphur bacteria ($alpha$-proteobacteria), although the precise mechanisms of their evolution have remained under debate (John and Whatley, 1975; Andersson et al., 2003). There are also controversies around the nature of the host and the initial advantages that led to the intracellular engulfment (Martin and Müller, 1998; Andersson et al., 2003). The most recent studies support the theory that mitochondria evolved from an endosymbiotic alpha-proteobacterium within an archaeal host cell related to Asgard archaea. Proto-mitochondria developed from the earliest known precursor, the pre-mitochondrial $alpha$-proteobacterium, with forms that slowly transitioned to the mitochondrial cenancestor, in the last eukaryotic common ancestor (LECA). During eukaryogenesis, the complexity of the proto-eukaryotic genome and proteome gradually expanded, in contrast to the genome and proteome of the mitochondrial endosymbiont, which underwent reduction as the organelle amalgamated proteins of both host(inner) and foreign(outer) sources (Wang and Wu, 2015; Roger, Muñoz-Gómez, and Kamikawa, 2017). Recent evidence suggests that the host organism, related to the Asgard archaea, already possessed some characteristics resembling those of eukaryotes, such as a dynamic cytoskeleton and membrane trafficking. Vosseberg et al. suggest that, upon mitochondrial acquisition,

there was a further increase in complexity, marked by the development of a signaling and transcription regulation network, as well as the shaping of the endomembrane system (Vosseberg et al., 2020).

1.2 Evolution of the mitochondrial genome

Due to their origin, mitochondria are cellular organelles possessing their own genetic material (Figure 1). In human cells on average 1-10 copies are estimated to exist in each organelle (Margulis, 1970; Wiesner, Rüegg, and Morano, 1992). Additional studies have confirmed that several thousand copies of mitochondrial DNA (mtDNA) can be found in just one animal cell (Spelbrink, 2010; Montoya et al., 1982). However, as different cell types have different tasks and thus exhibit different energetic needs, the amount of mtDNA they harbor greatly varies. For example, human lung cells contain 5,000 - 20,000 mtDNA copies per cell (D'Erchia et al., 2015), while the oocytes contain 100,000 mtDNA molecules (Chen et al., 1995). Importantly, mitochondrial genomes are much simpler than those of their bacterial ancestors, containing only a fraction of the genes. This reduction occurred over time through the combination of increased mutation rates and gene loss, probably due to the genomes' inability to replicate outside host cells. Furthermore, as a protein import system evolved, essential genes could recombine into the host genome, which led to a further reduction of the mitochondrial gene content (McCutcheon and Moran, 2011; Boussau et al., 2004).

The reason for the retention of mitochondrial genomes, despite the integration of numerous genes into the nuclear genome, remains a subject of inquiry. Two main hypotheses have emerged to shed light on this phenomenon (Daley and Whelan, 2005). The Co-location for Redox Regulation (CoRR) hypothesis posits that certain genes crucial to the electron transport chain (ETC) must remain within mitochondria to rapidly regulate gene expression in response to the organelle's redox state. Efficient ETC function requires swift adjustments in gene expression to prevent the formation of harmful reactive oxygen species. Therefore, retaining these genes within the mitochondrial genome provides a selective advantage by facilitating localized regulation (Allen, 1992; Allen, 2015). The second hypothesis, so-called Barrier to Evolutionary Transfer, proposes that specific proteins retained in the mitochondrial genome cannot be efficiently synthesized in the cytosol and further targeted to mitochondria due to their characteristics, such as being large hydrophobic proteins with multiple transmembrane domains. When these genes are expressed in the nucleus, they may mis-localize to the endoplasmic reticulum (ER), hindering their proper function, and thus acting as a barrier to their evolutionary transfer (Björkholm et al., 2016). Both of these theories are reinforced by the observation that components of the ETC encoded by the mitochondrial genome, particularly those in the center of those complexes, are the least likely to be transferred to the nucleus (Johnston and Jones, 2016). It is worth noting that the two hypotheses are not mutually exclusive, and also that neither of them fully addresses the consistent retention of mitochondrial ribosomal RNA (rRNA) genes on organellar chromosomes. One explanation for this retention could be attributed to the challenges associated with translocating large structured RNAs across membranes and the risk of mis-assembly (Roger, Muñoz-Gómez, and Kamikawa, 2017).

2 Budding yeast as model organism for mitochondrial research

The budding yeast *Saccharomyces cerevisiae* has become a potent system for investigating mitochondrial dynamics, due to its numerous experimental advantages. Unlike most organisms, which cannot survive when the mitochondrial genome is mutated or lost, leading to a halt in oxidative phosphorylation (OXPHOS) and ATP production, yeast cells lacking functional mtDNA can still thrive and be studied. However, this can only take place provided they maintain mitochondria and are supplied with a fermentable carbon source, like glucose. Moreover, since many nuclear mutations that impact mitochondrial morphology and physiology also result in mtDNA loss, *S. cerevisiae* stands out as one of the rare model organisms where the consequences of these mutations can be scrutinized, and the corresponding genes can be thoroughly characterized (Shaw and Nunnari, 2002).

Another advantage of baker's yeast is that not only its nuclear, but also its mitochondrial genome can be edited (Lasserre et al., 2015). This enables direct manipulation of mtDNA, further allowing specialized experimental setups, such as tagging of mtDNA-encoded genes, rendered almost impossible in other model organisms. The short replication cycle of yeast is another of its advantages as it allows experiments spanning across multiple generations. Since one generation in yeast takes on average 90 minutes, it enables tracking of cellular and mitochondrial dynamics at the single cell level in populations, within reasonable time periods. Last but not least, the vast majority of mitochondrial and nuclear genes in budding yeast have been preserved throughout evolution. This suggests that the same proteins utilized for energy production and mitochondrial biology in yeast most likely also hold significant roles in energy production in other more complex eukaryotes. Consequently, findings from mitochondrial research in yeast can be extrapolated to humans (Shaw and Nunnari, 2002; Shadel, 1999).

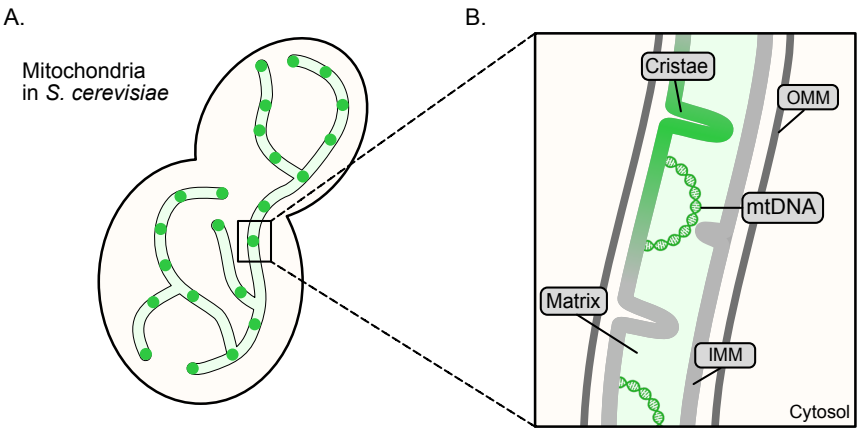

FIGURE 1: Simplified representation of mitochondrial morphology in *S. cerevisiae*. **(A)** Mitochondria in budding yeast appear as a continuous tubular network, with the mitochondrial DNA molecules dispersed evenly throughout. **(B)** Mitochondria are comprised of an outer membrane (OMM) that encloses the inner membrane (IMM), creating an intermembrane space. Copies of mtDNA are distributed across the mitochondrial network, within the matrix. Cristae structures emerge due to invaginations of the inner mitochondrial membrane.

3 Main functions of mitochondria (a very brief summary)

Cells utilize various fuels such as sugars, amino acids, and fatty acids to produce energy in the form of ATP and GTP. The mitochondria, acting as the metabolic center of the cell, undertake numerous crucial tasks apart from just producing ATP. Their primary function might be producing ATP via the tricarboxylic acid (TCA) cycle and oxidative phosphorylation (Spinelli and Haigis, 2018; Nolfi-Donegan, Braganza, and Shiva, 2020), nonetheless they also take part in metabolic activities, including amino acid, lipid and intermediary metabolism, synthesis of iron–sulfur clusters and heme, and maintenance of the cellular redox state. They essentially generate intermediate metabolites, facilitate inter-organelle communication, and contribute in the maintenance of the balance in calcium ions and reactive oxygen species (ROS). All the aforementioned functions are intricately linked, relying on the health of individual mitochondria as well as the overall mitochondrial network. Notably, these processes are affected by aging, which eventually leads to mitochondrial dysfunctions.

Specifically, the breakdown of mitochondrial substrates, such as pyruvate, produces acetyl-CoA, which is metabolized by the citric acid cycle. Importantly, it has been reported that different substrates lead to different effects on the kinetics and efficiency of OXPHOS in isolated mitochondria (Tomar et al., 2022). In the breakdown process, electron donors, nicotinamide adenine dinucleotide (NADH) and flavin adenine dinucleotide ($FADH_2$), are generated and transfer electrons to the ETC (Saraste, 1999). Electron flow in the ETC, which is located in the inner mitochondrial membrane (Figure 2), results in the pumping of protons into the intermembrane space (Sazanov, 2015). The fundamental mechanism of ATP generation by the ETC is largely conserved from yeast to mammalian cells. In mammals, the electron donors are NADH and $FADH_2$, and in budding yeast NADH and succinate (Lenaz and Genova, 2013). Either way, the translocation of protons (H^+) across the inner membrane into the intermembrane space (IMS) establishes an electrochemical proton gradient, known as mitochondrial membrane potential($\Delta\Psi$). This potential, in conjunction with proton concentration (pH), generates a proton-motive force, which plays a pivotal role in storing energy during OXPHOS. The proton-motive force (Δp) serves as a crucial element linking the electron transport (complexes I-IV) and oxygen consumption to the function of Complex V (ATP synthase). It is the movement of protons down their electrochemical gradient through the ATP synthase that generates ATP and this re-entry of protons into the matrix that dissipates the proton gradient (Watt et al., 2010; Nolfi-Donegan, Braganza, and Shiva, 2020). The proton-motive force is also responsible for facilitating the transport of ADP and phosphate into the mitochondria, while expelling ATP into the cytosol for cellular utilization. Apart from that, Δp plays also a vital role in regulating the movement of calcium ions, ensuring ion homeostasis within both the cytosol and mitochondrial matrix, and hence influencing pathways involved in calcium-related signaling (Brand et al., 2013).

In mammalian cells, the ETC consists of four multi-subunit complexes and two electron carriers, cytochrome c and ubiquinone (Vries and Marres, 1987). Notably, budding yeast lacks complex I, but compensates with two types of NADH dehydrogenases, one which oxidizes NADH in the matrix, termed internal or Ndi, and one facing the IMS, termed external or Nde (Vries and Marres, 1987; Iwata et al., 2012; Luttik et al., 1998). Certain subunits of ATP synthase and cytochrome c oxidase are encoded by the mitochondrial genome, while the remaining subunits are nuclear-encoded and imported into the mitochondria. Of note, disruptions in the ETC can lead to the development of numerous diseases, such as myopathies and

brain disorders (DiMauro and Schon, 2003).

The electron transport chain organizes into large, stable supra-molecular structures, known as respirasomes (Dudkina et al., 2011; Boekema and Braun, 2007; Wittig and Schägger, 2009). These structures improve substrate transport efficiency and minimize the generation of ROS, which is a consequence of electrons deviating from their typical pathway to oxygen (Lasserre et al., 2015). ROS generated by ETC, including hydrogen peroxide (H_2O_2) and superoxide anion radical (O^{2-}), serve as redox signaling agents in various cellular pathways. ROS are implicated in stimulating cell proliferation and potentially influencing transcription factors and mitochondrial DNA replication (Nolfi-Donegan, Braganza, and Shiva, 2020; Sauer, Wartenberg, and Hescheler, 2001). Mitochondrial ROS can trigger ferroptosis, a form of iron-dependent cell death, distinct from apoptosis (Dixon et al., 2012; Dai et al., 2024). Lastly, mitochondria are also involved in the activation of apoptosis (Lopez and Tait, 2015).

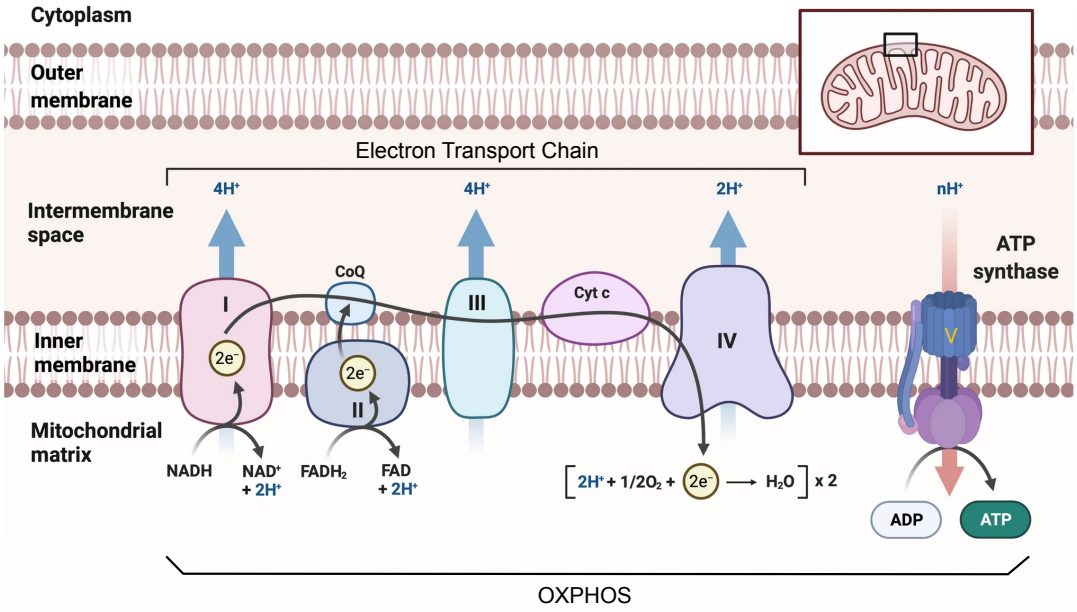

FIGURE 2: Brief overview of the oxidative phosphorylation, adapted from Wu, Ho, and Lu, 2021. The mitochondrial electron transport chain consists of four enzymatic protein complexes located in the inner mitochondrial membrane: complex I (NADH dehydrogenase - in yeast: Nde and Ndi), complex II (succinate dehydrogenase), complex III (cytochrome bc1 complex), and complex IV (cytochrome c oxidase). These complexes facilitate electron transport from NADH or $FADH_2$ to molecular oxygen. During this process, protons (H^+) are transported across the inner mitochondrial membrane to the intermembrane space, establishing a proton gradient. This gradient is utilized by complex V (ATP synthase) to generate ATP from ADP phosphorylation, the process known as oxidative phosphorylation.

4 Mitochondrial morphology

4.1 Mitochondrial structure in *S. cerevisiae*

Mitochondria are enclosed by two membranes that create four distinct compartments: the outer membrane, the IMS, the inner membrane, and the matrix (Figures 1). The outer mitochondrial membrane (OMM), encapsulating the entire organelle, has a protein to phospholipid ratio akin to that of the eukaryotic plasma membrane, approximately 1:1 by weight (Alberts and Watson, 1994). It harbors protein complexes facilitating the translocation of newly synthesized proteins, as well as voltage-dependent anion channels (VDACs or porins) which render the organelle permeable to other molecules, such as calcium cations (Khan, Kuriachan, and Mahalakshmi, 2021).

The inner mitochondrial membrane (IMM), characterized by extensive folding which creates the cristae, carries more than one fifth of the total mitochondrial proteins. Comprising roughly of 20% lipids and 80% proteins, the IMM has the highest protein to lipid ratio among cellular membranes. Importantly, the majority of mitochondrial proteins are translated in the cytoplasm and then targeted and transported into the mitochondrial subcompartments. This process is mediated by distinct preprotein translocases located in the outer (TOM complex) and inner membrane (TIM complex) of the mitochondria (Figure 3), with interactions between TOM and TIM being highly dynamic (Segui-Real et al., 1993; Neupert, 1997).

Approximately 5% of the total mitochondrial proteins inhabit the intermembrane space, with roles in maintaining mitochondrial morphology, electron transport, apoptosis, iron-sulfur cluster biogenesis, and protein translocation. The mitochondrial matrix serves as the hotspot for metabolic processes, such as the oxidation of pyruvate and fatty acids as well as the citric acid cycle, and contains a myriad of enzymes, mitochondrial ribosomes, tRNAs, and multiple mitochondrial DNA molecules.

4.2 Cristae morphology and function

The cristae are elaborately folded structures of the inner mitochondrial membrane, characterized by invaginations that project into the matrix of the organelle (Figure 3). These structures are integral to the function of mitochondria in cellular respiration. Specifically, the connections between the inner membrane and the cristae are known as crista junctions (CJs). These narrow crista junctions link the IMM to the cristae. Additionally, the IMM and the OMM are firmly connected by contact sites (CS), which are stabilized by the mitochondrial contact sites (MICOS) complex (Harner et al., 2011). Cristae significantly increase the surface area of the inner mitochondrial membrane, providing ample space for numerous protein complexes involved in oxidative phosphorylation. The main benefit of this increased surface area is that it facilitates efficient ATP production, as it maximizes the space for the subunits of the respiratory chain, thus directly optimizing the coupling of electron transport to ATP synthesis.

Furthermore, cristae play a crucial role in creating specific sub-compartments within the mitochondrial network, aiding in the isolation of metabolic processes. This compartmentalization helps to segregate enzymes and substrates, and could potentially serve as a physical barrier for mutated mtDNA copies, providing a mechanism for containing and even mitigating the impact of deleterious mutations on

mitochondrial function. Notably, it has been suggested that mtDNA and the proteins it encodes exert a localized influence, affecting mitochondrial functionality only in close proximity (Busch, Kowald, and Spelbrink, 2014). This indicates the possibility that cristae structures are involved in the process of mtDNA quality control, although it remains uncertain whether they play a role in maintainance and inheritance of mtDNA copies. Put together, beyond their role in energy production, cristae also serve as dynamic organizers of the mitochondrial contents, due to their compartmentalization ability (Zorkau et al., 2021; Iovine, Claypool, and Alder, 2021).

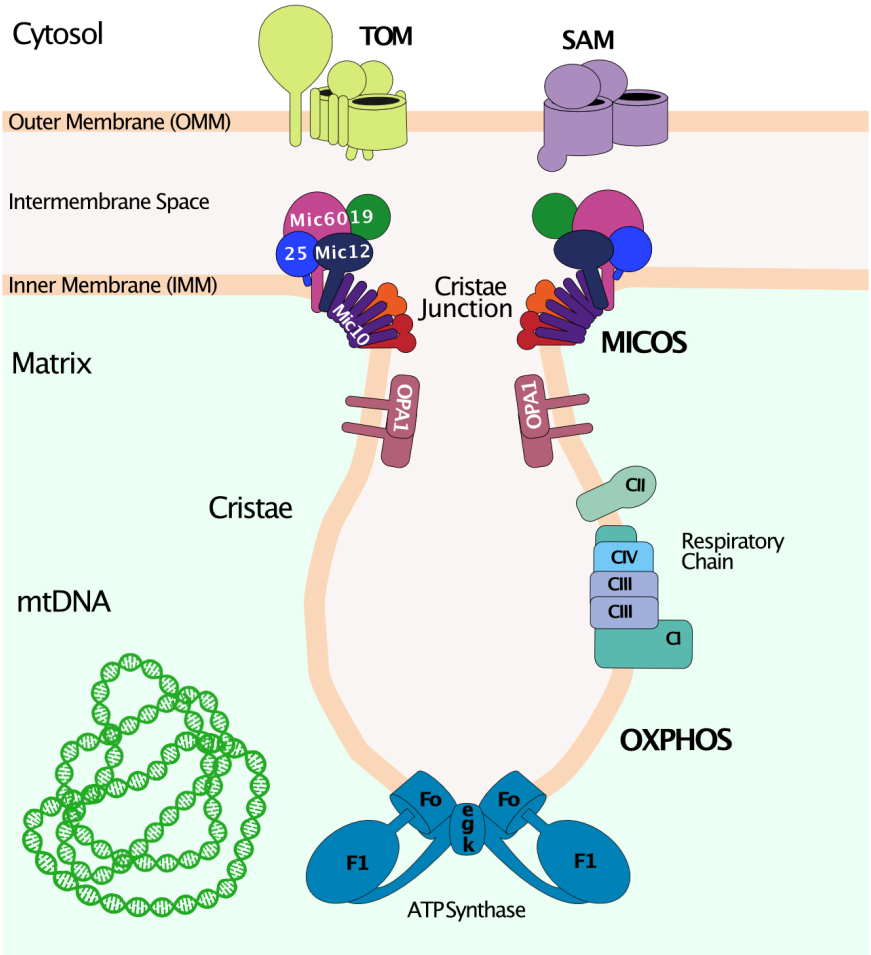

FIGURE 3: Schematic representation of cristae architecture and its determinants, adapted from Colina-Tenorio et al., 2020. The MICOS complex maintains the stability of cristae junctions by inducing membrane curvatures and establishing contact sites with outer membrane protein complexes. The mitochondrial F_1F_o-ATP synthase creates the pronounced curvature of cristae rims and tubules by forming membrane-bending dimers and oligomers dependent on the subunits e (*ATP21*), g (*ATP20*), and k (*ATP19*). The dynamin-related GTPase Opa1 (yeast Mgm1) facilitates fusion of the inner membrane, through homotypic interactions, participating in cristae biogenesis and maintenance. CI, CII, CIII, CIV refer to the respiratory chain complexes. OXPHOS represents the oxidative phosphorylation machinery. SAM denotes the sorting and assembly machinery. TOM represents the translocase of the outer mitochondrial membrane.

4.3 Atp20, Mic60 and their role in cristae formation

Two necessary components for the aforementioned cristae architecture and the overall function of mitochondria are the MICOS complex and the ATP synthase. These two complexes are required for oxidative phosphorylation and normal mitochondrial ultrastructure and morphology.

Specifically, the F_1F_o-ATP synthase acts as a molecular rotary motor and it comprises a catalytic sector (head piece), a membrane sector (base piece), and two connecting stalks (Figure 3). The F_1 sector, containing the head piece, is a water-soluble component capable of ATP hydrolysis, detached from the F_o sector. In contrast, the F_o sector is integrated into the membrane and primarily consists of hydrophobic subunits that establish a dedicated proton-conducting pathway. Upon coupling of the F_1 and F_o sectors, the enzyme operates as a reversible H^+-transporting ATPase, which facilitates the conversion of ADP and P_i into ATP within the mitochondrial membranes of both eukaryotes (Frasch, Bukhari, and Yanagisawa, 2022; Kühlbrandt, 2019; Berden and Hartog, 2000). The F_1F_o-ATP synthase is a highly conserved molecular apparatus. It forms dimers arranged in rows along the curvatures of cristae (Figure 3). In yeast, the molecular mass of the ATP synthase is around 600 kDa, and comprises thirteen core subunits (α3, β3, γ, δ, ϵ, OSCP, 4, 6, 8, 9, 10, d, f, and h), and this structure does remain consistent across eukaryotes and bacteria. In yeast, four substructures of the ATP synthase are formed as follows: the catalytic head group [α3, β3,], the central stalk (γ, δ, ϵ,), the peripheral stalk (4, d, h), and the membrane region (9, 10, 6, 8, f). The first two units create the F_1 subcomplex and the latter two the F_o subcomplex. The oligomycin sensitivity conferral protein (OSCP) subunit bridges the peripheral stalk and the catalytic domain, enabling the ATP synthase to adopt various rotational states by acting as a hinge (Davies et al., 2012; Murphy et al., 2019).

The yeast F_1F_o-ATP synthase includes four supplementary protein subunits (e, g, i, and k), with e, g, and k identified within the ATP synthase dimer (Arselin et al., 2004; Velours and Arselin, 2000; Arnold, 1998). Specifically, subunits e (*ATP21*) and g (*ATP20*), which are also present in mammals, are small, integral membrane proteins featuring a single predicted transmembrane helix containing a GXXXG motif. Subunit g possesses a minor N-terminal matrix domain capable of crosslinking with subunit 4, while subunit e carries a short C-terminal domain with a predicted coiled-coil motif exposed to the intermembrane space. Together they stabilize bent cristae rims, as they are directly involved in the formation of ATP synthase dimers. Specifically, within the dimers of the ATP synthase both of the monomers are arranged in a 86° angle, which leads to the bending of the membrane (Harner et al., 2016). Yeast mutants lacking either subunit e or g, or both, fail to form dimers. Lack of the dimeric ATP synthase has been described to lead to an onion-like morphology of mitochondria, where uncontrolled proliferation of cristae membranes leads to a multilayered appearance (Paumard et al., 2002). Interestingly, a reduction in subunit e quantities results in a decrease in the amount of subunit g, whereas a decrease in subunit g does not impact subunit e levels. The complete loss of either subunit e or g results in the loss of supramolecular ATP synthase structures, leading to a 50% reduction in mitochondrial ATPase activity (Arselin et al., 2004). Electron cryotomography of mitochondrial membranes has revealed extensive rows of dimers along the highly curved cristae ridges in mammals, plants, and fungi. Importantly, within each dimer the two F_1 subcomplexes have been observed to be consistently 28 nm apart, in contrast to the spacing between adjacent dimers that vary along the rows (Davies et al., 2012).

As introduced already, further stabilization of cristae junctions occurs via the MICOS complex (Figure 3). It is situated within the IMM, with domains facing the intermembrane space, facilitating the formation of extended heterogeneous scaffold-like structures, localized towards the inner boundary membrane (Hoppins et al., 2011; Friedman et al., 2015). This multiprotein complex is comprised of six nuclear-encoded core subunits (Mic60, Mic10, Mic19, Mic27, Mic26, and Mic12) in yeast, and most of them have a mammalian counterpart (Darshi et al., 2011; Friedman et al., 2015; Alkhaja et al., 2012; Weber et al., 2013). It plays a central role in regulating the shape and organization of the mitochondrial inner membrane (Harner et al., 2011; Hoppins et al., 2011; Malsburg et al., 2011; Pfanner et al., 2014), by interacting with cardiolipin, the import machinery, and respiratory complexes (Weber et al., 2013; Harner et al., 2016; Harner et al., 2011; Rabl et al., 2009; Hoppins et al., 2011; Zerbes et al., 2012; Bohnert et al., 2012; Harner et al., 2014). Since it has such a crucial role, deletion of any single subunit leads to characteristic morphological IMM defects, including extended lamellar structures and reduced cristae junctions, resulting in a lamellar mitochondrial shape defect.

From the aforementioned subunits, Mic60 and Mic10 are characterised as the "core components" coordinating the MICOS assembly in a stepwise manner. Deleting Mic60 was shown to destabilize Mic19, whereas deletion of Mic10 destabilizes Mic27 (Harner et al., 2014; Hoppins et al., 2011; Malsburg et al., 2011). Moreover, double deletions of different subunits exhibit diverse genetic interactions, indicating collaborative yet distinct functions within mitochondria (Hoppins et al., 2011). For example, Mic60's role in import operates independently of the MICOS complex (Malsburg et al., 2011). It has also been observed that the assembly of Mic27/Mic10/Mic12 at cristae junctions relies on respiratory complexes and cardiolipin (Friedman et al., 2015). Additionally, in contrast to the assembly of Mic27/Mic10/Mic12 at cristae junctions, Mic60's assembly occurs autonomously of the respiratory complexes, indicating its potential involvement in marking nascent cristae junctions. Furthermore, Mic60 has the capability to engage with both the TOM complex and the sorting and assembly machinery (SAM) complex (Figure 3). Notably, the Mic60-Mic19 subcomplex is believed to link CJs to the OMM. Previous studies have demonstrated that Mic19 facilitates the interaction between the mitochondrial outer and inner membranes through the Sam50-Mic19-Mic60 axis (Tang et al., 2019). Deletion of *MIC19* results in alterations in mitochondrial ultrastructure, characterized by aberrant mitochondrial cristae and the absence of cristae junctions, consequently hindering ATP production (Darshi et al., 2011). Importantly, since Mic19 can also act as a bridge between MICOS subcomplexes, it has been suggested to play a role in mtDNA copy number regulation and positioning of cristae junctions (Sastri et al., 2017).

4.4 Fission-Fusion and their role in mitochondrial dynamics

Taking into account that the impermeability of the IMM is such that even small hydrogen ions cannot pass through (Lemasters, 2007), the question arises on how the contents of mitochondria get exchanged and travel along the tubular network. It is known that the overall cell function is significantly controlled by the mitochondrial morphology and throughout the lifespan of a cell mitochondria undergo continuous growth, division, and fusion. Thereby, the balance between fission and fusion events inevitably influences the organelle's morphology at steady state (Shaw and Nunnari, 2002). In budding yeast, where mitochondria form a dynamic network, fission-fusion events occur every two minutes (Nunnari et al., 1997), and it

is these continuous dynamics that maintain the tubular reticulum, which supports mitochondrial function.

Fission events are governed by the Dnm1 GTPase (mammalian Drp1), and occur specifically within a tubule or at a branchpoint within the mitochondrial network (Otsuga et al., 1998; Mozdy, McCaffery, and Shaw, 2000; Bleazard et al., 1999) (Otsuga D, et al. 1998; Bleazard W, et al., 1999; Sesaki H, Jensen RE, 1999). Dnm1 localises to the OMM, and is recruited to the mitochondria from the cytosol only after post-translational activation (Archer, 2013). Importantly, Dnm1 assembles into multimeric contractile rings at the fission site (Figure 4). Cardiolipin, which is synthesized within the IMM, has been show to be transported to the OMM and directly interact with Drp1 in mammalian cell lines (Bustillo-Zabalbeitia et al., 2014; Ugarte-Uribe et al., 2014). This interaction promotes Drp1 oligomerization and GTPase activity, consequently amplifying the process of mitochondrial fission (Ugarte-Uribe et al., 2014). Fusion, on the other hand, is regulated by the mitofusin Fzo1 (mammalian Mfn1 and Mfn2) and exclusively occurs between two mitochondrial tips (Figure 4) or between a tip and the side of a tubule (Hermann et al., 1998; Rapaport et al., 1998). Fzo1 has been also shown to localize on the OMM, with Fzo1's GTPase domain exposed to the cytoplasm (Hermann et al., 1998).

Another GTPase involved in remodeling of mitochondrial compartments, the so-called Mgm1 (human Opa1), localizes within the intermembrane space (Shepard and Yaffe, 1999; Wong et al., 2000), with its long form embedded in the IMM, and mediates inner membrane fission (Figure 4). Few proteins have been identified to work together with Dnm1 on the outer membrane fission machinery. The two key players are the Fis1 and Mdv1 proteins (Tieu and Nunnari, 2000; Mozdy, McCaffery, and Shaw, 2000; Cerveny, McCaffery, and Jensen, 2001). In a yeast two-hybrid assay, Mdv1 was found to interact and co-localize with Dnm1 (Figure 4), in punctate structures on the OMM (Tieu and Nunnari, 2000; Uetz et al., 2000; Cerveny, McCaffery, and Jensen, 2001), which indicates that these two proteins are part of a complex marking future division sites. Interestingly, Mdv1 seems to be specific for yeast mitochondrial division, as no homologs have been identified in higher eukaryotes. In contrast, homologs of Mgm1 and Dnm1 have been identified in a range of other organisms. Mutations in the human homolog of Mgm1 have been associated with a form of dominant optic atrophy that causes childhood blindness (Alexander et al., 2000; Delettre et al., 2000).

In cells lacking Dnm1, mitochondria appear with 'net-like' structures, due to halted mitochondrial fission, while fusion of mitochondrial tips persists (Sesaki and Jensen, 1999). Conversely, in Fzo1 mutant cells, mitochondrial networks rapidly disintegrate due to the obstruction of mitochondrial fusion, while fission continues unimpeded (Rapaport et al., 1998). When Mgm1 function is impaired in yeast, mitochondrial tubules quickly fragment, leading to subsequent loss of mtDNA (Shepard and Yaffe, 1999; Wong et al., 2000). Interestingly, the observed mitochondrial fragmentation is blocked when fission is inhibited by deletion of *DNM1* (Wong et al., 2000; Fekkes, Shepard, and Yaffe, 2000). Fis1 and Mdv1 mutations have also been shown to prevent this fragmentation, and mtDNA loss in fzo1 mutants (Tieu and Nunnari, 2000; Mozdy, McCaffery, and Shaw, 2000; Cerveny, McCaffery, and Jensen, 2001).

Recently, there have been two distinct types of fission characterized in mice, one associated with mitochondrial proliferation and one with mitochondrial degradation (Kleele et al., 2021), both involving Drp1 (yeast Dnm1). Firstly, midzone mitochondrial fission, which occurs within the central half (middle) of a mitochondrion,

at specific sites guided by actin and mitochondrial–ER tethering, is believed to primarily support cell proliferation and mitochondrial biogenesis (Nagashima et al., 2020). Secondly, peripheral fission events occur at the outer 0–25% of the mitochondrion and rely on Fis1 and lysosome contact to facilitate the Dnm1 assembly. It is believed that division at the periphery allows damaged material to be discarded into smaller mitochondria parts destined for mitophagy, which could be a direct mechanism involved in mitochondrial quality control (Colpman, Dasgupta, and Archer, 2023).

All in all, mitochondrial fusion and fission processes are facilitated by numerous large GTPases, collectively shaping the dynamic mitochondrial networks across various cell types, and improper regulation of those two mechanisms is associated with several genetic neuro-degenerative diseases, like Parkinson's disease (Poole et al., 2010; Ziviani, Tao, and Whitworth, 2010).

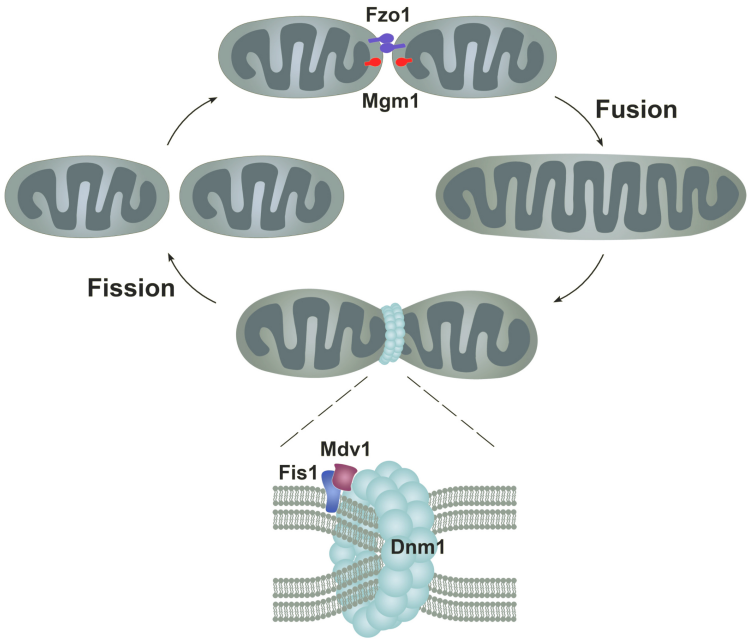

FIGURE 4: Schematic description of fission and fusion dynamics, adapted from Navarro-Espíndola, Suaste-Olmos, and Peraza-Reyes, 2020. Mitochondria dynamics are regulated by fusion and fission processes. Fusion is facilitated by Fzo1 (mitofusin) and Mgm1 (human Opa1) at the outer and inner mitochondrial membranes, respectively, while Dnm1 is responsible for mediating fission, upon interaction with Mdv1.

5 mtDNA structure and composition

5.1 mtDNA structure in *S.cerevisiae*

The mitochondrial genome is structured either as a circular or linear double-stranded DNA molecule. The two strands, termed heavy (H-strand) and light (L-strand) in mammals, are distinguished by their nucleotide composition, with the H-strand being guanine-rich and the L-strand being cytosine-rich (Berk and Clayton, 1974). The length of mtDNA varies among species. In humans it is approximately 16,5 kilobases (kb), while in yeast it has a length of 86 kb. There are few major differences between the mammalian and the yeast mtDNA, such as the intron content

and the amount of proteins encoded, however in both organisms mtDNA exists in multiple copies within individual cells, which can further vary depending on the cellular energy requirements.

Regarding the structural configurations of mtDNA, there are three different ones in yeast: linear filaments, open circles, and closed circles, based on their sediment behavior (Shapiro et al., 1968). Early investigations suggest that the predominant conformation is in the form of linear filaments, denoted as concatemers, with heterogeneous sizes (Maleszka, Skelly, and Clark-Walker, 1991). Importantly, the major species of mtDNA in the mother cells are in the form of concatemers, while in daughter cells are as circular monomers (Ling, Hori, and Shibata, 2007). While the precise functional significance of these diverse conformations remains not fully understood, it is postulated that they play a major role in the process of mtDNA replication.

The human mitochondrial genome contains 37 genes, with 28 located on the H-strand and 9 on the L-strand. Thirteen of these genes encode a single polypeptide component of the mitochondrial respiratory chain, which serves as the primary site for cellular energy production via OXPHOS. The remaining 24 genes produce mature RNA products, including 22 mitochondrial tRNA molecules, a 16S rRNA (large ribosomal subunit), and a 12S rRNA (small ribosomal subunit). In yeast, mtDNA encodes 7 proteins required for oxidative phosphorylation (Figure 5), including three subunits of the ATP synthase complex (Atp6, Atp8, and Atp9), apocytochrome b (Cob), three subunits of cytochrome c oxidase (Cox1, Cox2, and Cox3) and one mitochondrial ribosomal protein (Var1). Yeast mtDNA also encodes for 2 ribosomal RNAs (rRNAs), 24 transfer RNAs (tRNAs), the 9S RNA component of RNase P and several intron-related open reading frames (ORFs) (Foury et al., 1998; Miyakawa, 2017).

Unlike the nuclear genome (nDNA), mtDNA is highly dense with approximately 93% representing coding regions in mammals. In the higher eukaryotes, mtDNA genes lack introns, and some genes, such as ATP6 and ATP8, feature overlapping regions. Most genes are contiguous, separated by one or two non-coding base pairs. Mammalian mtDNA contains only one significant non-coding region, known as the displacement loop (D-loop) (Andrews et al., 1999), which houses the site for mtDNA replication initiation, as well as both H-strand transcription promoters (Hsp1 and Hsp2) (Chinnery and Hudson, 2013). Notably, in *S.cerevisiae*, coding regions consist of approximately 30% GC and the intergenic regions, which occupy two-thirds of the yeast mtDNA, are separated by long repetitive AT-rich spacers, separated by GC-rich clusters (Zamaroczy and Bernardi, 1986). Also, in contrast to mammalian mtDNA genes, yeast coding regions contain introns. The yeast mitochondrial genome is equipped with eight replication origin-like (ori) elements (Tzagoloff and Myers, 1986).

Importantly, the mitochondrial genetic code exhibits slight variations compared to the nuclear one. The mitochondrial DNA has only two stop codons: 'AGA' and 'AGG', as opposed to the three stop codons 'UAA', 'UGA', and 'UAG' in nDNA. Additionally, 'UGA' in mtDNA encodes for tryptophan instead (Temperley et al., 2010). Furthermore, 'AUA', typically representing isoleucine in nDNA, codes for methionine in mtDNA.

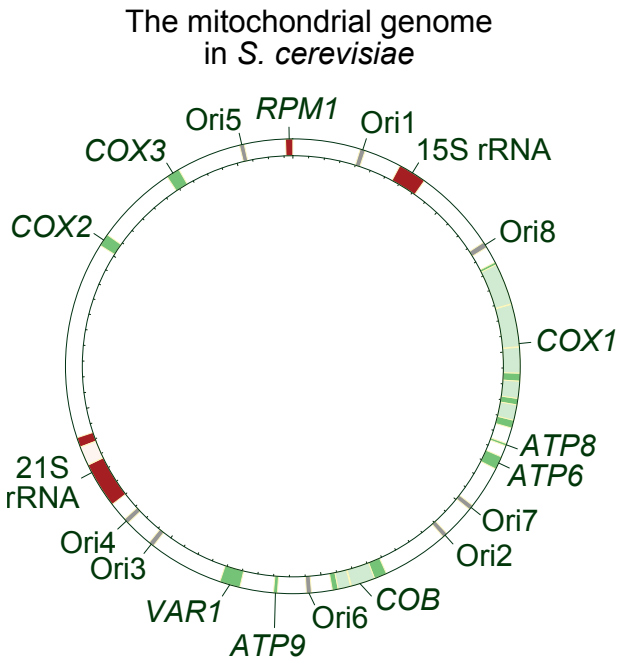

FIGURE 5: The mitochondrial genome in *S. cerevisiae*. mtDNA encodes 8 protein-encoding genes and several tRNAs and rRNAs. Among these, 7 of the proteins serve as subunits of the electron transport chain, while one encodes a ribosomal protein (Var1). In budding yeast, these subunits are cytochrome c oxidase subunits I, II, and III (COX1, COX2, and COX3), ATP synthase subunits 6, 8, and 9 (*ATP6, ATP8, ATP9*) and apocytochrome b (*COB*).

5.2 mtDNA organization in *S.cerevisiae*

Since mitochondria do not contain histones, mtDNA had been initially thought to be free from protective and packaging proteins. In 1982, Kuroiwa et al. demonstrated that mtDNA in *Physarum polycepharum* is localized into electron-dense bodies, termed "mitochondrial nuclei" at the center of a mitochondrion (Kuroiwa et al., 1982). Essentially, Kuroiwa described the nucleoids, nucleoprotein complexes that mtDNA molecules are organized into (Spelbrink, 2010; Chen and Butow, 2005a). Eukaryotic cells harbor numerous copies of mtDNA, dispersed throughout the mitochondrial matrix, with each nucleoid generally hosting an average of 1-3 mtDNA copies (Kukat et al., 2011; Seel et al., 2023). A typical yeast cell contains 30 to even 100 copies of mtDNA (Göke et al., 2020; Seel et al., 2023), depending also on the strain or sugar source. However, there is a contradiction, termed “the ploidy paradox” between the large physical number of mtDNA molecules per cell and the small number (1–3) of heritable units, estimated from mitochondrial genetics (Piškur, 1994). Research in yeast and stable human cell lines has shown that nucleoids are maintained in a semi-regular pattern, with each mtDNA copy positioned at approximately equal distances from adjacent ones (Osman et al., 2015; Jajoo et al., 2016; Iborra, Kimura, and Cook, 2004). Even distribution is thought to be supported by the additional anchorage of nucleoids to the IMM, which further facilitates the regulation of mitochondrial genome inheritance (Nunnari et al., 1997; Cho et al., 1998; Rickwood, Chambers, and Barat, 1981).

The key protein responsible for proper organization and packaging of mtDNA is TFAM in mammals (Ekstrand, 2004), and its counterpart Abf2 in *S. cerevisiae*

(Zelenaya-Troitskaya et al., 1998). Both proteins are functionally similar and contain two adjacent HMG-boxes each, capable of binding to mtDNA, inducing bends in the DNA strands, thereby aiding in packaging (Kukat et al., 2011; Cuppari et al., 2019; Chakraborty et al., 2016; Choi and Garcia-Diaz, 2021). Both TFAM and Abf2 play a regulatory role in determining the mtDNA copy number, with their expression levels directly influencing this parameter, establishing a dose-dependent correlation. It has been shown that moderate overexpression of both TFAM and Abf2 leads to an increase in mtDNA levels (Ikeda et al., 2015; Kanki et al., 2004; Zelenaya-Troitskaya et al., 1998). However, excessive Abf2 overexpression can lead to mtDNA loss (Zelenaya-Troitskaya et al., 1998). Importantly, Abf2, apart from stabilizing mtDNA, is presumed to also play a role in mtDNA recombination, potentially facilitating mtDNA replication (MacAlpine, Perlman, and Butow, 1998). TFAM, on the other hand, can act as a transcription factor, a function not shared by Abf2 (Miyakawa, 2017).

More precisely, in budding yeast, Abf2 induces negative supercoiling in the circular mtDNA, and subsequently folds the mtDNA, facilitated by a DNA topoisomerase (Diffley and Stillman, 1992). Alternatively, linear DNA is packaged in a relaxed manner and has limited binding affinity to Abf2, potentially allowing enzymes to access regulatory sites within mtDNA more easily (Brewer et al., 2003). Absence of *ABF2* leads to rapid loss of mtDNA, resulting in rho0 or rho- petite cells, when cultivated and kept on fermentable media (Diffley and Stillman, 1992). In such a case, nucleoids display a less compact structure and exhibit a diffused organization (Newman, 1996). Importantly, when yeast cells are kept on glycerol, they maintain their mtDNA, as it is needed for survival under a non-fermentable selective environment. Recently, alongside Abf2, a few other proteins have been identified as being associated with nucleoids (Miyakawa, 2017), such as the HMG-box protein Cim1, which acts antagonistically to Abf2, with Δ*cim1* cells exhibiting increased mtDNA levels (Schrott and Osman, 2023), and the helicase Hmi1, required for maintenance of functional mtDNA (Sedman et al., 2000). Another protein playing an important role in mtDNA copy number regulation is Mrx6, as its deletion, like that of Cim1, leads to a previosuly reported 1.5-fold increase in mtDNA levels (Göke et al., 2020).

6 mtDNA Heteroplasmy (Emergence and Dynamics)

In mitochondria, the maintenance of mtDNA is vital for the organelle's proper function and the respiratory chain. This necessitates meticulous regulation of processes governing its replication, transmission, and maintenance of integrity. Unlike nDNA, mtDNA lacks protection from histones, rendering it more vulnerable to both intrinsic and extrinsic assaults. However, the previously reported Cim1 and Abf2 are proteins involved in packaging and protection of mtDNA. Notably, because mtDNA is located proximal to the IMM where the mitochondrial respiratory chain generates free electrons and ROS, it is exposed to mutagenic factors (Habbane et al., 2021). This leads to mitochondrial DNA copies exposed to various stress conditions, which can lead to changes in their sequence, even if that is silent mutations. The coexistence of various mtDNA haplotypes within a single cell is known as heteroplasmy (Figure 6). Accordingly, mtDNA homoplasmy translates to the state where all the mitochondrial DNA molecules within a cell or organism are identical.

By referring to mtDNA heteroplasmy dynamics one inevitably encompasses the changes that occur in mtDNA over time, and these alterations can alter the degree of heteroplasmy within a single yeast cell, as well as within a population. These

dynamics can be both temporal and spatial. Mutations leading to morphological re-organization, due to increased fusion and fission frequencies for example, have been reported to increase heteroplasmy variance in theoretical studies (Glastad and Johnston, 2023; Tam et al., 2013; Kowald and Kirkwood, 2011). On the other hand, time, which often translates to cell divisions and aging, has also been shown to increase heteroplasmy variance and result in significant alterations on the degree of heteroplasmy within cells (Johnston, 2019; Johnston et al., 2015). All in all, both intra-cellular and inter-cellular shifts are attributed to the spatio-temporal mtDNA dynamics.

More specifically, there are few different mechanisms believed to contribute to this phenomenon. Briefly, the most prominent explanations for the observed mtDNA segregation dynamics are 1) vegetative segregation, which describes the stochastic partitioning of mtDNA copies at cell divisions (Birky, Fuerst, and Maruyama, 1989); 2) intracellular random drift, due to gene conversion resulting in recombinant genomes, or random replication of a subset of mtDNA molecules (Birky, Fuerst, and Maruyama, 1989); 3) active intracellular selection for mtDNA with a specific genotype, which can include selective replication of few wildtype mtDNA copies in a competitive scenario (Hill, Chen, and Xu, 2014; Wai, Teoli, and Shoubridge, 2008); 4) reduction of mtDNA copies given to the daughter cells, via selective (or not) transmission (Cree et al., 2008; Klucnika and Ma, 2019) and at the population level 5) intercellular selection of a subset of cells (Dujon, Slonimski, and Weill, 1974; Backer and Birky, 1985). However, vegetative segregation and relaxed replication, mtDNA replication independently of the cell cycle, are the two most widely accepted explanations in the field for the emergence and persistence (or cessation) of heteroplasmy.

Since heteroplasmy emerges by *de novo* mutagenesis, the degree of heteroplasmy changes in accordance to the mutation accumulation. Specifically, deletion mutations tend to accumulate more in non-dividing tissues. This leads to the age-related buildup of biochemically deficient cells, where OXPHOS is impaired, which can contribute to diseases associated with aging, such as Alzheimer's and Parkinson's diseases. Additionally, it has been reported that single nucleotide variants in mtDNA progressively accumulate throughout a cell's and thus individual's lifespan, with a higher concentration detected in the D-loop region, which is essential for mtDNA transcription and replication in cells (Michikawa et al., 1999; Pinto and Moraes, 2015). Put together, either due to deletions or single-nucleotide substitutions, heteroplasmy levels change dramatically over time, and clonal expansion plays a pivotal role in determining the severity of the phenotype.

6.1 Relaxed replication

To be more specific, one parameter directly influencing the degree of heteroplasmy and severity of phenotype is relaxed replication. Replication of the mitochondrial genome, unlike the nuclear one, is not linked to the cell cycle. In other words, mtDNA molecules replicate randomly, resulting in one or multiple copies of the template molecule at a time (Birky, 1994). This way individual mtDNA molecules can be clonally expanded independent of segregation (Figure 6). It is worth noting that relaxed replication impacts the degree of heteroplasmy in both dividing and non-dividing cells (Stewart and Chinnery, 2021).

In cases where there are two or more distinct types of mtDNA molecules present

in a cell, it remains rather stochastic which type will undergo replication more frequently than another, which eventually leads to a variation in the level of heteroplasmy within the cell, also known as intracellular drift. Importantly, regardless of mitochondrial types (i.e. a neutral scenario, or not) and assuming the cell's bioenergetic demands remain constant, it has been suggested that cells most likely maintain a relatively stable number of mtDNA molecules (Chinnery and Samuels, 1999). It is worth mentioning though that the mtDNA copy number has its own implications on the mtDNA heteroplasmy levels, as previous studies in mice have shown that alterations of mtDNA copy number can improve the pathological manifestations of a heteroplasmic mutation in rapidly proliferating tissues (Filograna et al., 2019), likely due to enhanced clonal expansion and selective elimination of mutated mtDNA. Intriguingly, the reverse has also been observed with the levels of heteroplasmy remaining identical, while the total mtDNA levels increase (Filograna et al., 2019).

Given that mtDNA proliferation is most often a response to the absence of an optimal number of mtDNA molecules, cells harboring mtDNA haplotypes that have a negative impact on mtDNA function will experience elevated rates of mtDNA proliferation. This is proposed to occur in human cells as high numbers of mtDNA molecules may protect against accumulation of mutant alleles during a cell's lifetime. This makes sense as the dilution of the mutant alleles by the overall increase of mtDNA copies inside a cell can delay potential pathologies (Chinnery and Samuels, 1999). In such cases, within a heteroplasmic cell, mutated mtDNA may undergo favored replication, because they copy faster if the target molecule is smaller, which would also lead to all replication factors being available sooner to replicate another mtDNA molecule (Diaz, 2002). Under these non-neutral scenarios, instances of selfish replication combined with the relaxed nature of the mitochondrial genomes can become the major drivers for shifts in the degree of heteroplasmy.

6.2 Vegetative segregation

Changes in allele frequency can further occur when mtDNA molecules are partitioned during cell divisions (Figure 6). Specifically, the uneven distribution of different mtDNA variants across daughter cells has been shown to result in drastically diverse heteroplasmic states. Notably, unlike relaxed replication, vegetative segregation influences the mtDNA heteroplasmy levels only in mitotic (proliferating) cells (Pérez-Amado et al., 2021).

Importantly, within a yeast lineage, the number of division events is tightly linked to the level of heteroplasmy. This happens since the mother cell inevitably ages through various segregation rounds. Thus, the quality of the mitochondrial genome it contains and gets transferred to the newly formed daughter cells inevitably dictates their mitochondrial fitness (Figure 6). With this in mind, and given that in higher eukaryotes mtDNA content is exclusively passed from mothers to progeny, a process known as uniparental (maternal) inheritance, segregation events take on a particularly significant role in determining and establishing the degree of heteroplasmy in newly formed cells.

Vegetative segregation arises from a combination of processes such as organelle genome replication and partitioning. Importantly, the frequency and manner of vegetative segregation are influenced not only by the quantities of genomes and organelles, but also by their spatial distribution within the cell, the variability in replication instances per molecule, and the variance in both numerical and genotypic partitioning of organelles and genomes (Birky, 1994).

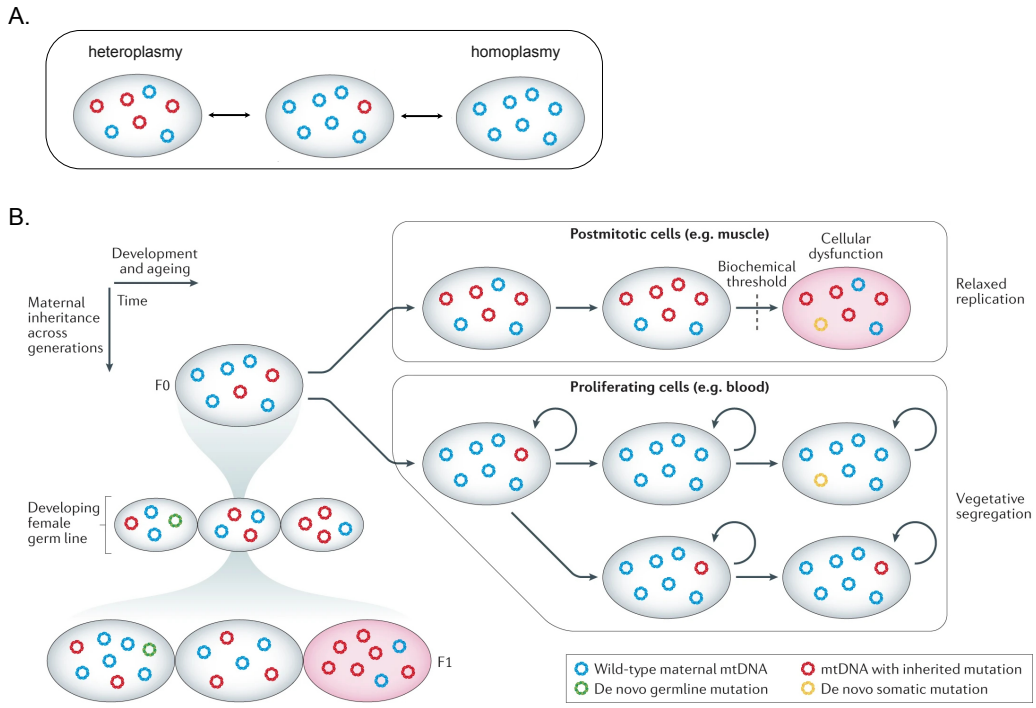

FIGURE 6: Factors influencing mtDNA heteroplasmy dynamics, adapted from Stewart and Chinnery, 2021. **(A)** Depiction of a heteroplasmic cell versus a homoplasmic cell. A cell is characterized heteroplasmic solely by the presence of distinct types of mtDNA within the single cell, and not by the quality of those mtDNA molecules. **(B)** Levels of heteroplasmy in mtDNA can undergo alterations over the course of an individual's life. These changes are influenced by vegetative segregation during cell division and relaxed replication in dividing and non-dividing cells. In non-dividing cells, relaxed replication occurring throughout life may result in an elevated proportion of mutant mtDNA. If this proportion surpasses a critical threshold, it can lead to a biochemical deficiency in oxidative phosphorylation. The genetic bottleneck in the germline accelerates the segregation of mtDNA variants between generations, leading to big fluctuations in heteroplasmy levels. Importantly, heteroplasmy can also arise from de novo mutations, somatic while aging or during germline development (in higher eukaryotes).

It has been previously shown that in yeast, zygotes initially containing more than one type of mtDNA reproduce vegetatively, and result in homoplasmic diploid progeny (Dujon, Slonimski, and Weill, 1974). The generation of homoplasmic daughter cells has been thought to occur stochastically during cell division. Taking into account the difficulty in pinpointing whether the degree of heteroplasmy is directly correlated with vegetative segregation, researchers have developed equations to calculate the number of segregating units and their distribution between mother and daughter cells. By analyzing mitochondrial allele frequencies in middle buds, budding off of the middle of a zygote, they found that most zygotes have few segregating units, with only a fraction entering the bud. This suggested that mitochondria or their fragments, containing multiple genomes, segregate randomly during reproduction, supporting the hypothesis of stochastic vegetative segregation (Birky et al., 1978).

7 mtDNA quality control

7.1 Units of selection

When thinking about the mechanisms of mtDNA segregation and quality control, it is necessary to first consider where the control is happening. Purifying selection for example, defined as the selection of WT against mutant mtDNA, is likely to occur on phenotypes. However, mtDNA phenotypes can be manifested on different levels, at the level of a whole organism, a cell or even an individual organelle, i.e. mitochondrion. In the simple setting of a yeast population for example, if the unit of selection is the cell, then an individual cell with too many mutant mtDNA copies most likely will not prosper and therefore will not be represented in subsequent generations. On the other hand, if quality control is active at the level of mitochondria, then those organelles with dysfunctional copies would be selectively eliminated, for example via mitophagy or by preventing their genome from replicating. However, since yeast mitochondria exist in a continuous tubular network with nucleoids distributed throughout, it becomes even more complex to decipher how cells eliminate or prevent replication within individual nucleoids. A recent study, utilizing super-resolution STED microscopy, revealed that approximately 1.4 mtDNA molecules exist per nucleoid, suggesting that the smallest heritable/segregation unit consists of a single molecule of mtDNA (Kukat et al., 2011; Raap et al., 2012).

7.2 Purifying Selection

The first direct real-time experimental observations of purifying selection were done in mice about a decade ago, by Fan et al., 2008 and Stewart et al., 2008. More recent studies conducted in *Drosophila melanogaster* and mice have unveiled that in the female germline, mutant copies of mtDNA are eliminated through purifying selection (Fan et al., 2008; Hill, Chen, and Xu, 2014; Stewart et al., 2008). Despite existing data that almost all metazoans transmit mitochondria and mtDNA to offspring only through their female lineage, we still know little about the stage and the mechanisms by which deleterious mtDNA molecules get eliminated in the germline. In part, this is due to limitations in tools for imaging purifying selection, as well as due to the dynamic spatio-temporal nature of the phenomenon itself. However, we have gained significant knowledge on the quality control pathways throughout the past decades. For example, mitochondrial quality has been shown to determine motility, with well-functioning mitochondria being more efficiently transported, and that cell division events significantly influence the heteroplasmic state of newly formed cells (Higuchi-Sanabria et al., 2016; Aretz, Jakubke, and Osman, 2019). Furthermore, recent findings in *Drosophila melanogaster* indicate that mitochondrial fragmentation, caused by fission events, is necessary and sufficient for germline mtDNA selection (Lieber et al., 2019). Specifically, mitochondrial fission generates small mitochondrial fragments containing only one or a few mitochondrial genomes, which effectively segregates mtDNA copies and prevents complementation of mutant mtDNA by gene products of intact mtDNA copies. Subsequently, the mitochondrial fragments harboring mutated mtDNA are believed to be identified based on a reduction in membrane potential or ATP content, leading to their removal via mitophagy (Lieber et al., 2019; Chen, Berquez, and Luciani, 2020).

It is worth mentioning that the mechanisms for mtDNA maintenance, replication, degradation as well as selection likely evolved to prevent the gradual accumulation of deleterious mtDNA mutations across generations, thus averting a mutational meltdown, known as Muller's ratchet (Muller, 1964; Palozzi, Jeedigunta, and Hurd, 2018). The susceptibility of mtDNA to Muller's ratchet is due to its asexual transmission and absence of recombination (Stewart and Larsson, 2014; Hagstrom et al., 2013). Nevertheless, not all deleterious mtDNA mutations are effectively eliminated in the germline by purifying selection (Stewart and Larsson, 2014; Stewart et al., 2008). Moreover, even for those mutations that are successfully eliminated by purifying selection, it often takes several generations to fully remove them (Fan et al., 2008; Hill, Chen, and Xu, 2014; Ma, Xu, and O'Farrell, 2014; Stewart et al., 2008).

7.3 mtDNA maintenance

The mechanism by which cells preserve the integrity of mtDNA intra- and intercellularly and across generations, despite the presence of high mitochondrial mutation rates, has long remained elusive. It is an immense challenge for the cell to maintain a functional level of mtDNA copy number which supports optimal cellular function, since deviations in mtDNA numbers frequently coincide with mitochondrial dysfunction, and diminished oxidative phosphorylation efficiency (Nicolson, 2014). In budding yeast, mtDNA replication factors have been demonstrated to influence mtDNA copy number, including the mtDNA-packaging factor Abf2 (Zelenaya-Troitskaya et al., 1998), as well as the mitochondrial DNA polymerase Mip1 (Stumpf et al., 2010), as mutations in both have been shown to alter mtDNA copy numbers (Westermann, 2014). Additionally, mutations in the recently characterised Cim1 were shown to display increased mtDNA levels and improve mitochondrial function (Schrott and Osman, 2023).

Interestingly, a direct correlation of mtDNA copy number and cell volume has been suggested in HeLa and budding yeast cells, as the volume of the cells was shown to linearly correlate with their mitochondrial content (Rafelski et al., 2012; Miettinen and Björklund, 2016; Kitami et al., 2012; Posakony, England, and Attardi, 1977). Studies in fission yeast have demonstrated a proportional increase in nucleoids relative to cell volume (Jajoo et al., 2016). Moreover, recently, Seel et al. showed that mtDNA copy number is dependent on the concentrations of mtDNA-maintenance factors, such as Abf2 and Mip1 (Seel et al., 2023). By linking mtDNA maintenance to nuclear protein synthesis, and its correlation with cell growth, they posit that constant mtDNA levels can be reliably maintained without a tight regulation from the cell cycle. Also recently, scientists showed that in damaged mitochondria the efficiency in protein import is compromised. This can result in diminished mtDNA replication, thereby hindering the propagation of mtDNA copies (Zhang et al., 2019). One additional study has suggested a role of the citric acid cycle enzyme aconitase (Aco1), coupling mtDNA maintenance with metabolic regulation (Chen and Butow, 2005b). Specifically, the reallocation of Aco1 from the Krebs cycle to nucleoids has been suggested to stabilize mtDNA under oxidative stress conditions (Shadel, 2005). Lastly, another factor influencing mtDNA maintenance is selective mtDNA degradation. In mammalian cells, degradation of the mitochondrial genome has been repeatedly suggested to serve as a protective mechanism against mutagenesis, reducing the energy cost of repair (Moretton et al., 2017; Bacman et al., 2013; Chapman, Ng, and Nicholls, 2020).

7.4 mtDNA Inheritance

Mitochondrial genome inheritance refers to the transmission of mtDNA from one generation to the next. Proper segregation and adequate transmission of mtDNA molecules across generations are essential for daughter cell viability and the continuity of lineages and populations. Taking into account that yeast divides asymmetrically and mitochondria are self-replicating and cannot be synthesized *de novo*, it becomes clear why the active transfer of mitochondria and mtDNA is of such high importance (Leite, Costa, and Pereira, 2023). However, in numerous animal species, the inheritance of mtDNA is influenced by a phenomenon known as mitochondrial genetic bottleneck, taking place during germline development (Burgstaller et al., 2018; Stewart and Chinnery, 2015; Zhang, Burr, and Chinnery, 2018a; Johnston, 2019). Briefly, this genetic bottleneck describes a threshold of transmittable mtDNA molecules from one generation to the next (Figure 6), which leads to substantial removal of deleterious mutations (Jenuth et al., 1996; Koehler et al., 1991; Tang et al., 2022). In humans, the genetic bottleneck appears to be more restricted compared to the bottleneck observed in mice, and other lower eukaryotes (Cree et al., 2008; Wai, Teoli, and Shoubridge, 2008; Floros et al., 2018). Interestingly, decreasing mtDNA levels during the crucial stage of germ cell development are thought to expose variants to selection mechanisms that operate at the cellular, organelle, or mtDNA level. This can even be a life-saving process as the mutation rate of mtDNA is orders of magnitude higher compared to nuclear DNA (Haag-Liautard et al., 2008). Therefore, the reduction of mtDNA copies facilitates the removal of the mutated ones, keeping the cell under the biochemical threshold for clinical manifestation of a disease.

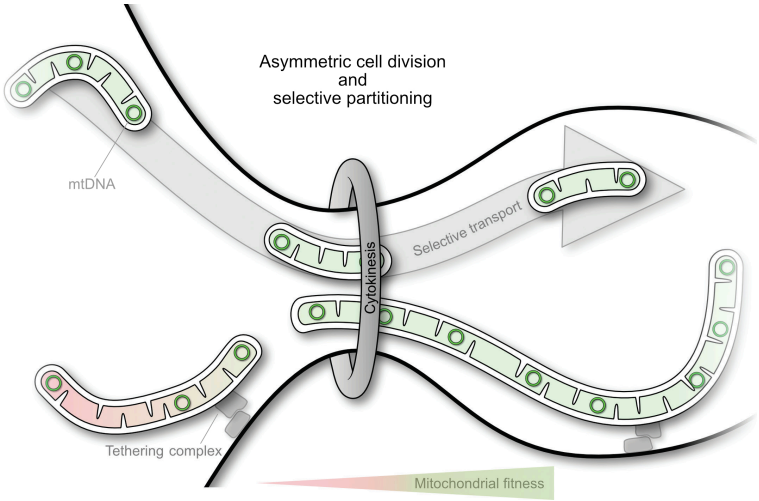

FIGURE 7: Asymmetric division as part of the mitochondrial quality control, adapted from Aretz, Jakubke, and Osman, 2019. Mitochondria are tethered to the plasma membrane via anchoring complexes, which can contribute to the selective transport of mitochondrial fragments from mother to daughter cells. During cytokinesis, the mitochondria crossing the bud neck undergo stringent control, in order to make sure that healthy mtDNA copies are preferentially inherited to the newly formed buds. Simultaneously, relaxed mtDNA replication within the transferable mitochondrial fragments can influence the mitochondrial fitness of the newly formed daughter cell. The colour gradient represents mitochondrial fitness, based on membrane and redox potential.

Currently, two main theories exist as explanations for the rapid mtDNA reduction occurring during cell division, although the exact mechanism of segregation remains a topic of debate. Either it is attributed to an unequal segregation of mtDNA

molecules or of mtDNA nucleoids from the mother's to the daughter's mitochondria during cell division, leading to rapid shifts on the heteroplasmy levels from one generation to the next (Carling, Cree, and Chinnery, 2011). However, it is worth keeping in mind that a combination of both, unequal partitioning and relaxed replication, can lead to rapid heteroplasmic alterations. Importantly, since mitochondria are such dynamic organelles, the process of mtDNA inheritance also highly relies on the mitochondrial fusion and fission machinery, which continuously fragments, shuffles and fuses mitochondrial tubules across a cell's lifespan, thereby directly shaping the distribution of mtDNA content (Figure 7). Apart from experimental data, mathematical modeling has also suggested that mitochondrial network structure and fission-fusion dynamics can generate useful variability in the cell's mtDNA content and thereby contribute to the mtDNA inheritance process (Glastad and Johnston, 2023; Tam et al., 2013; Kowald and Kirkwood, 2011). Other *in silico* studies have identified cell division as a parameter influencing mtDNA inheritance, since it was shown to increase mtDNA heteroplasmy variance (Johnston, 2019; Johnston et al., 2015). Moreover, a recent study in cybrids has established that the process of mtDNA segregation and inheritance is non-random (Figure 7), such that generation of novel heteroplasmic levels occurs due to transient rearrangement of mtDNA copies inside the segregation unit before replication and segregation (Raap et al., 2012).

8 mtDNA and Disease

Mitochondrial diseases can stem from either primary mtDNA defects or defects in nuclear-encoded mitochondrial proteins. Mitochondrial DNA variations occur through time due to oxidative damage and are attributed to factors such as heteroplasmy and inherited mutations. Rare mtDNA mutations and large-scale deletions exhibit heterogeneity and can manifest at any stage of life, affecting various tissues and causing a diverse range of diseases. Therefore, understanding mtDNA heteroplasmy is crucial, as the clinical expression of pathogenic mutations depends on the proportion of mutant genomes within a cell. In eukaryotes, there are developmental and genetic mechanisms in place to constrain the transmission of heteroplasmy (Edwards et al., 2021). Due to this heteroplasmic nature, clinical manifestations of mitochondrial diseases vary widely. Conditions like Leber's hereditary optic neuropathy (LHON), myoclonus epilepsy with ragged red fibers (MERRF) and mitochondrial encephalomyopathy with lactic acidosis and stroke-like episodes (MELAS) are associated with specific mtDNA point mutations. Other disorders, such as the Kearns–Sayre syndrome (KSS), are linked to mtDNA deletions.

Currently, over 150 pathogenic mutations in mtDNA have been documented in humans, spanning across more than 30 of the 37 mitochondrial genes (Habbane et al., 2021). Since mtDNA originates solely from the maternal lineage, it is subsequently inherited by all offspring from their mother, with only the daughters passing it on to the next generations. The genetic basis of diseases associated with mitochondrial genome abnormalities is often explained due to this maternal transmission (Zhang, Burr, and Chinnery, 2018a). Specifically, recent studies have suggested that offspring of men carrying a point mutation face no risk, whereas the risk is elevated for offspring and siblings of women with an mtDNA mutation. However, failure to eliminate paternal mitochondria can lead to the development of mitochondrial diseases (Habbane et al., 2021). Global estimates suggest that around 1 in 5000 individuals may have manifested mitochondrial disease (Chinnery and Hudson, 2013). All in all, molecular genetic testing, preferably from affected tissues, and factors

such as maternal inheritance patterns, help identify mtDNA mutations and aid in appropriate diagnosis.

Aim of this study

So far, it is known that mtDNA quantity and quality can change rapidly during a cell's lifespan and across generations. In higher eukaryotes, dramatic shifts in heteroplasmy, defined as the presence of different mtDNA haplotypes in a cell, are attributed to unequal partitioning of mtDNA (Wei et al., 2019; Burgstaller et al., 2018; Otten et al., 2016; Lee et al., 2012; Ashley, Laipis, and Hauswirth, 1989; Olivo et al., 1983; Hauswirth and Laipis, 1982) or preferential replication during germline development (Otten et al., 2016; Cree et al., 2008; Wai, Teoli, and Shoubridge, 2008; Stewart and Larsson, 2014; Cao et al., 2009). Mathematical simulations in yeast suggest that cell divisions, mitochondrial structure, and fission-fusion dynamics significantly influence mtDNA segregation, by directly affecting the heteroplasmy variance (Johnston, 2019; Johnston et al., 2015; Glastad and Johnston, 2023; Tam et al., 2013; Kowald and Kirkwood, 2011).

Studies in *Drosophila melanogaster* and mice reveal that defective mtDNA copies are selectively eliminated in the female germline through purifying selection (Fan et al., 2008; Hill, Chen, and Xu, 2014; Stewart et al., 2008). In *D. melanogaster*, fission has been also proposed as a key player in the clearance process (Lieber et al., 2019; Chen, Berquez, and Luciani, 2020). Furthermore, cristae morphology has been indirectly shown to be involved in mitochondrial health, as defective compartmentalization leads to mitochondrial dysfunction (Zorkau et al., 2021).

Despite recent advancements in the field, mtDNA segregation and the quality control across generations remains poorly understood. This work aims to better understand the temporal dynamics of mtDNA heteroplasmy and quality control in proliferating cell populations at the single-cell level, using *S. cerevisiae*. By using mtDNA variants encoding fluorescent proteins, mtDNA quantities in dividing cells will be estimated. The study will also investigate heteroplasmy levels across populations to assess the speed of reaching homoplasmy and the effects of asymmetric partitioning during cell division. These results will be evaluated with mathematical modeling, which will be further used to identify factors of mtDNA segregation dynamics not directly revealed by empirical data. For delineating the mtDNA quality control in *S. cerevisiae* cells, pedigree analyses will be conducted, starting from heteroplasmic zygotes with competing mtDNA qualities. Furthermore, live-cell microscopy will be used to investigate the mtDNA integrity and distribution in the mitochondrial network of heteroplasmic cells. Lastly, genes involved in fission (*DNM1*) and cristae architecture (*ATP20, MIC60*) will be deleted to evaluate their influence on purifying selection.

Put together, this study will provide insights into mtDNA dynamics, by exploring the speed at which cells attain mtDNA homoplasmy, while identifying key factors for successful phenotypic segregation. Additionally, it will investigate the presence of a selection mechanism under non-neutral mtDNA scenarios, and evaluate the influence of mitochondrial architecture in the mtDNA purifying selection process.

Publication 1:
Real-time assessment of mitochondrial DNA heteroplasmy dynamics at the single-cell level

THE EMBO JOURNAL

Real-time assessment of mitochondrial DNA heteroplasmy dynamics at the single-cell level

Rodaria Roussou, Dirk Metzler, Francesco Padovani, Felix Thoma, Rebecca Schwarz, Boris Shraiman, Kurt Schmoller, and Christof Osman

Corresponding author(s): Christof Osman (osman@bio.lmu.de)

Review Timeline:

Submission Date:	7th Mar 24
Editorial Decision:	8th Apr 24
Revision Received:	7th Jun 24
Accepted:	17th Jul 24

Editor: Hartmut Vodermaier

Transaction Report:

(Note: With the exception of the correction of typographical or spelling errors that could be a source of ambiguity, letters and reports are not edited. Depending on transfer agreements, referee reports obtained elsewhere may or may not be included in this compilation. Referee reports are anonymous unless the Referee chooses to sign their reports.)

Article

SOURCE DATA | TRANSPARENT PROCESS | OPEN ACCESS | CHECK FOR UPDATES

THE EMBO JOURNAL

Real-time assessment of mitochondrial DNA heteroplasmy dynamics at the single-cell level

Rodaria Roussou[1,2], Dirk Metzler[1], Francesco Padovani[3], Felix Thoma[1,2], Rebecca Schwarz[1], Boris Shraiman[4], Kurt M Schmoller[3] & Christof Osman[1]✉

Abstract

Mitochondrial DNA (mtDNA) is present in multiple copies within cells and is required for mitochondrial ATP generation. Even within individual cells, mtDNA copies can differ in their sequence, a state known as heteroplasmy. The principles underlying dynamic changes in the degree of heteroplasmy remain incompletely understood, due to the inability to monitor this phenomenon in real time. Here, we employ mtDNA-based fluorescent markers, microfluidics, and automated cell tracking, to follow mtDNA variants in live heteroplasmic yeast populations at the single-cell level. This approach, in combination with direct mtDNA tracking and data-driven mathematical modeling reveals asymmetric partitioning of mtDNA copies during cell division, as well as limited mitochondrial fusion and fission frequencies, as critical driving forces for mtDNA variant segregation. Given that our approach also facilitates assessment of segregation between intact and mutant mtDNA, we anticipate that it will be instrumental in elucidating the mechanisms underlying the purifying selection of mtDNA.

Keywords mtDNA; Heteroplasmy; Mitochondrial Fission; Mitochondria; Mathematical Modeling
Subject Categories Computational Biology; Organelles
https://doi.org/10.1038/s44318-024-00183-5
Received 7 March 2024; Revised 7 June 2024;
Accepted 17 July 2024
Published online: 05 August 2024

Introduction

The mitochondrial genome (mtDNA) encodes core subunits of the respiratory chain, making it essential for mitochondrial ATP production. Most eukaryotic cells contain multiple copies of mtDNA. From yeast to human cells, these copies are distributed throughout the mitochondrial network in a semiregular manner, with each mtDNA copy located roughly equidistantly from adjacent copies (Iborra et al, 2004; Jajoo et al, 2016; Osman et al, 2015). mtDNA is packaged into nucleoprotein complexes known as nucleoids (Chen and Butow, 2005; Spelbrink, 2010), containing on average 1–3 copies of mtDNA in mammalian and yeast cells (Kukat et al, 2011; Seel et al, 2023). Mutations in individual mtDNA copies can result in heteroplasmy, where different mtDNA variants coexist within a cell (Stewart and Chinnery, 2021). This scenario can occur with neutral mutations having no impact on mitochondrial function, but becomes relevant for cellular and organismal health when mutations affect mitochondrial function (Park and Larsson, 2011). In this latter case, the ratio of mutant over intact mtDNA amounts in combination with the nature of the mutation determines the severity of the mutant phenotype.

Throughout the lifespan of an organism, the degree of heteroplasmy, representing the proportion of distinct mtDNA variants within individual cells, can change (Kauppila et al, 2017). The proposed mechanisms underlying this change include relaxed replication and vegetative segregation. Relaxed replication, wherein the amplification of mtDNA is uncoupled from the cell cycle, may lead to some mtDNA copies undergoing multiple replications while others remain unreplicated. Uneven distribution of mtDNA copies between mother and daughter cells, known as vegetative segregation, can further alter the degree of heteroplasmy in proliferating cell populations (Birky, 1994; Stewart and Chinnery, 2021). Additionally, intracellular selection resulting from favoring or disfavoring specific mtDNA variants for replication or degradation (Floros et al, 2018; Hill et al, 2014; Jakubke et al, 2021; Lieber et al, 2019; Ma et al, 2014) or selection acting on the level of cellular fitness (Kotrys et al, 2024) have been proposed to contribute to alterations in heteroplasmic levels in cell populations. Striking examples of changes in heteroplasmy are observed during germline development, where ratios of different mtDNA variants can rapidly shift from one generation to the next (Ashley et al, 1989; Burgstaller et al, 2018; Lee et al, 2012; Olivo et al, 1983; Otten et al, 2016; Wei et al, 2019). This rapid change is proposed to occur due to a bottleneck effect in oocyte development, either through partitioning of a limited number of mtDNA into primordial germ cells or preferential replication of a subset of mtDNA copies in developing oocytes (Cao et al, 2009; Cree et al, 2008; Otten et al, 2016; Stewart and Larsson, 2014; Wai et al, 2008).

The concept of heteroplasmy is widespread among eukaryotic cells. In the single-celled budding yeast, the degree of heteroplasmy in individual cells changes during the growth of a population derived from a single heteroplasmic zygote (Dujon et al, 1974). Eventually, this results in the complete segregation of mtDNA

[1]Faculty of Biology, Ludwig-Maximilians-Universität München, 82152 Planegg-Martinsried, Germany. [2]Graduate School Life Science Munich, 82152 Planegg-Martinsried, Germany. [3]Institute of Functional Epigenetics, Molecular Targets and Therapeutics Center, Helmholtz Zentrum München, 85764 Neuherberg, Germany. [4]Kavli Institute for Theoretical Physics, University of California, 93106 Santa Barbara, CA, USA. ✉E-mail: osman@bio.lmu.de

variants (Birky, 1994, 2001; Jakubke et al, 2021), such that most cells retain only one variant present in the heteroplasmic founder cell. So far, studying heteroplasmic dynamics has remained challenging regardless of the organism, because it has not been possible to infer the quantity of mtDNA variants within living cells over time. However, theoretical modeling has supported the view that heteroplasmy variance increases with cell divisions (Johnston, 2019; Johnston et al, 2015). Furthermore, modeling has also suggested that mitochondrial network structure and fission-fusion dynamics contribute to the emergence of heteroplasmic variance (Glastad and Johnston, 2023; Kowald and Kirkwood, 2011; Tam et al, 2013).

Here, we present an important step forward in understanding the temporal dynamics of mtDNA heteroplasmy in proliferating cell populations at single-cell resolution in *S. cerevisiae*. By employing two mtDNA variants encoding Atp6 fused to either red or green fluorescent proteins as surrogate markers for neutral mtDNA haplotypes in *S. cerevisiae*, we infer quantities of mtDNA variants in living cells. Using this approach, we observe a rapid shift in heteroplasmy levels across populations and find that asymmetric partitioning of mtDNA copies during cell division, as well as mitochondrial fusion-fission frequencies, are important determinants for mtDNA variant segregation.

Results

Real-time single-cell tracking of mtDNA heteroplasmy dynamics in *S. cerevisiae*

To investigate the dynamics of heteroplasmy, we aimed to develop a system, which would allow real-time assessment of the segregation of two different mtDNA genotypes across multiple generations. For this purpose, we opted for two recently established yeast strains with opposing mating types, each homoplasmic for a different mtDNA variant. Specifically, these strains harbor mtDNA encoding Atp6 tagged C-terminally either with NeonGreen ($mtDNA^{Atp6\text{-}NG}$) or mKate2 ($mtDNA^{Atp6\text{-}mKate2}$) and hence exhibit green or red fluorescence within mitochondria, respectively, depending on the presence and expression of the respective mtDNA haplotype. According to our rationale, the mating of both strains and subsequent mitochondrial fusion would result in heteroplasmic zygotes, carrying ~50% $mtDNA^{Atp6\text{-}NG}$ and ~50% $mtDNA^{Atp6\text{-}mKate2}$ (Jakubke et al, 2021; Nunnari et al, 1997; Okamoto et al, 1998). Upon growth, each heteroplasmic zygote would give rise to progeny, whose heteroplasmic state would be reflected by ongoing expression and fluorescence of Atp6-NG and/or Atp6-mKate2 (Fig. 1A). In the following analyses, the heteroplasmy state of each cell will be characterized by an "h-value," calculated by dividing the amount of $mtDNA^{Atp6\text{-}mKate2}$ by the sum of $mtDNA^{Atp6\text{-}NG}$ and $mtDNA^{Atp6\text{-}mKate2}$, inferred by the respective fluorescent signals (Fig. 1B). Unless otherwise stated, for all experiments, cells were pre-grown in glucose-containing rich medium, because of higher mating efficiency, while imaging was performed in minimal medium containing glucose, due to lower background fluorescence.

In order to continuously monitor heteroplasmy changes on a single-cell level, we used a microfluidic system, that allowed tracking of progeny derived from single zygotes for up to six generations. Segmentation and tracking of individual cells as well as lineage tracing enabled the construction of genealogical trees for every single population (Fig. 1C,D).

Characterization of haploid $mtDNA^{Atp6\text{-}NG}$ and $mtDNA^{Atp6\text{-}mKate2}$ parental strains

Before generating heteroplasmic zygotes, it was important to compare growth and mtDNA maintenance between strains harboring $mtDNA^{Atp6\text{-}NG}$ or $mtDNA^{Atp6\text{-}mKate2}$ to determine potential influences of growth properties on segregational dynamics of both mtDNA variants in the following heteroplasmic segregation experiments. In line with previous analyses (Jakubke et al, 2021), both strains exhibited virtually wildtype-like growth under fermentable and non-fermentable carbon sources at 30 and 37 °C in plate growth assays (Appendix Fig. S1A,B). We furthermore quantified doubling times of $mtDNA^{Atp6\text{-}NG}$ or $mtDNA^{Atp6\text{-}mKate2}$ strains in our microfluidic setup by segmenting and counting cells over a time course of 8 h. In line with our growth assay on plates, both strains exhibited very similar doubling times (Appendix Fig. S1C). Similarly, petite levels, indicative of loss or dysfunctional mtDNA, were equivalent between $mtDNA^{Atp6\text{-}NG}$, $mtDNA^{Atp6\text{-}mKate2}$, and wildtype strains (Appendix Fig. S1D).

Next, we aimed to assess the validity of using Atp6-NG or Atp6-mKate2 fluorescence intensities as proxies for mtDNA presence within single cells. First, we examined $mtDNA^{Atp6\text{-}NG}$ or $mtDNA^{Atp6\text{-}mKate2}$ strains in our microfluidic setup and monitored fluorescent signals across multiple generations for 8 h. In every population derived from single haploid cells, we observed homogeneous fluorescent signal intensities in the mitochondrial networks across all cells after 8 h (Fig. 2A,B; Movies EV1, EV2). Next, we assessed Atp6-NG and Atp6-mKate2 fluorescence in cell populations lacking the mitochondrial HMG-box protein Abf2. Δ*abf2* cells are known to gradually lose mtDNA if grown in a fermentable carbon source (YPD) (Schrott and Osman, 2023; Sia et al, 2009; Zelenaya-Troitskaya et al, 1998). We cultured Δ*abf2* cells in a non-fermentable carbon source (YPG) to prevent mtDNA loss and monitored Atp6-NG and Atp6-mKate2 fluorescence upon transition to a minimal medium. Consistent with the occasional loss of mtDNA, Δ*abf2* populations exhibited indeed a higher signal variability across cells, which is quantitatively revealed by a higher coefficient of variation for either $mtDNA^{Atp6\text{-}NG}$ or $mtDNA^{Atp6\text{-}mKate2}$ in Δ*abf2*, compared to the respective WT cells (Fig. 2C,D; Appendix Fig. S2; Movies EV3, EV4). Some cells exhibited fluorescence, indicative of mtDNA presence, while others appeared to have fully lost mtDNA, as they were only visible in the DIC channel. We interpret these findings to reflect that all wildtype cells maintain mtDNA and continue to express the fluorescent Atp6 variants with relatively little cell-to-cell variability, while mtDNA maintenance deficits associated with Δ*abf2* cells result in heterogeneity of Atp6-NG or Atp6-mKate2 fluorescence signals.

To further support that Atp6-NG or Atp6-mKate2 fluorescence reflects the expression of the respective mtDNA, we measured the fluorescent decay rates by inhibiting mitochondrial translation with Chloramphenicol (CAP). Of note, this experiment was performed in strains lacking *PDR5*, a multidrug transporter localized in the plasma membrane, to prevent CAP export from the cell and allow efficient translational inhibition (Leonard et al, 1994). *PDR5*

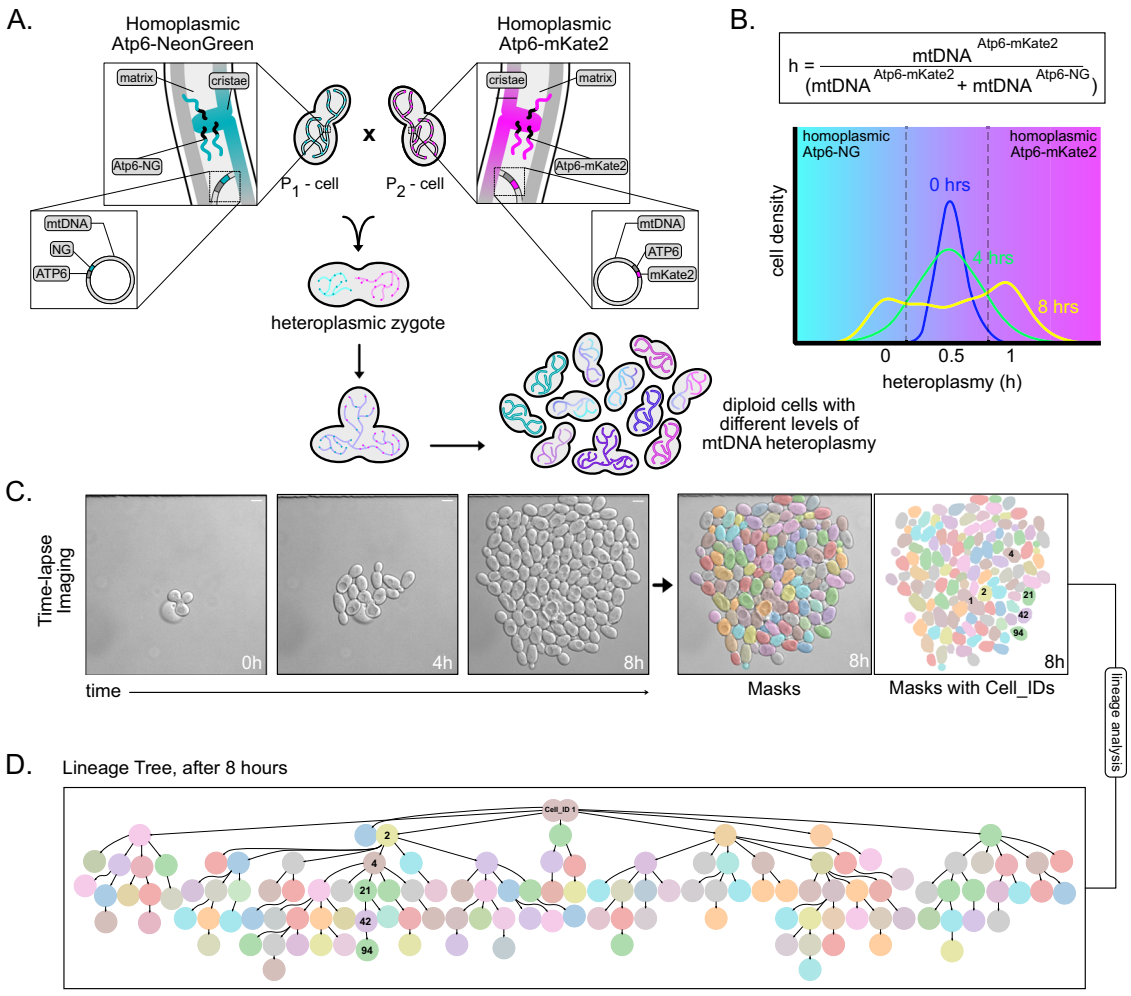

Figure 1. Schematic of the mtDNA heteroplasmy pipeline.

(A) Strains harboring either mtDNA$^{Atp6\text{-}NG}$ or mtDNA$^{Atp6\text{-}mKate2}$ are mated. The growth of a population derived from single zygotes is monitored in a microfluidic chamber, resulting in diploid cells with different levels of mtDNA heteroplasmy. **(B)** The heteroplasmy value (h) of each cell is calculated by dividing the fluorescent signal of Atp6-mKate2 by the sum of Atp6-NG and Atp6-mKate2. Example of heteroplasmy distributions at three indicated timepoints. Cells with h-values lower than 0.5 (cyan area) contain a higher proportion of mtDNA$^{Atp6\text{-}NG}$, while cells with h-values above 0.5 (magenta area) contain a higher proportion of mtDNA$^{Atp6\text{-}mKate2}$. **(C)** Representative bright-field images of a cell population derived from a single zygote, after an 8-h time-lapse video. Cell segmentation and masking was performed with the Cell-ACDC software. Scale bars: 5 µm. **(D)** Lineage tree derived from the zygote shown in **(C)**, at the end of the recording. One lineage is annotated as an example, with cell identities matching the mask IDs in **(C)**.

deletion did not lead to a growth phenotype (Appendix Fig. S1A,B). Upon addition of CAP, we observed a decrease in both Atp6-mKate2 and Atp6-NG intensities, where within 5 h, signal intensities appeared to reach a bottom plateau, likely representing background fluorescence of cells and absence of the respective fluorophore (Fig. 2E; Appendix Fig. S3A–D; Movies EV5–EV8). By fitting exponential decay curves (Alber et al, 2018), we assessed the fluorescence decay rates (k) for both fusion proteins, which were virtually identical ($k_{mKate2} = 0.31$, SEM:±0.01), $k_{NG} = 0.31$, SEM: ± 0.01) (Fig. 2F). Of note, in the absence of CAP, the wildtype mtDNA$^{Atp6\text{-}NG}$ strain exhibited an increase of fluorescence over time, while the mtDNA$^{Atp6\text{-}mKate2}$ strain exhibited a slight decrease over time. We also assessed the reappearance of fluorescent signals upon removal of CAP after a 6-h treatment. While both fluorescent signals reappeared rapidly, reflecting the maintenance of mtDNA, the Atp6-NG signal reemerged slightly faster compared to Atp6-mKate2 (Figs. 2F and EV1; Movie EV9). We speculate the difference in fluorescence levels over time between Atp6-NG and Atp6-mKate2 to be the result of a combination of various factors, including the switch from rich to minimal medium, which may affect mtDNA expression, the biophysical properties of the fluorescent proteins, as well as differences in the maturation time between NG and mKate2. To account for the difference, in all following experiments, NG and mKate2 fluorescence is always normalized to the median fluorescence per timeframe in the respective channel.

Based on the aforementioned experiments, we conclude that the presence of mtDNA$^{Atp6\text{-}NG}$ or mtDNA$^{Atp6\text{-}mKate2}$ is unlikely to substantially alter cellular fitness, mtDNA maintenance, or influence the outcome of segregation dynamics within our heteroplasmic model. Furthermore, our findings support that

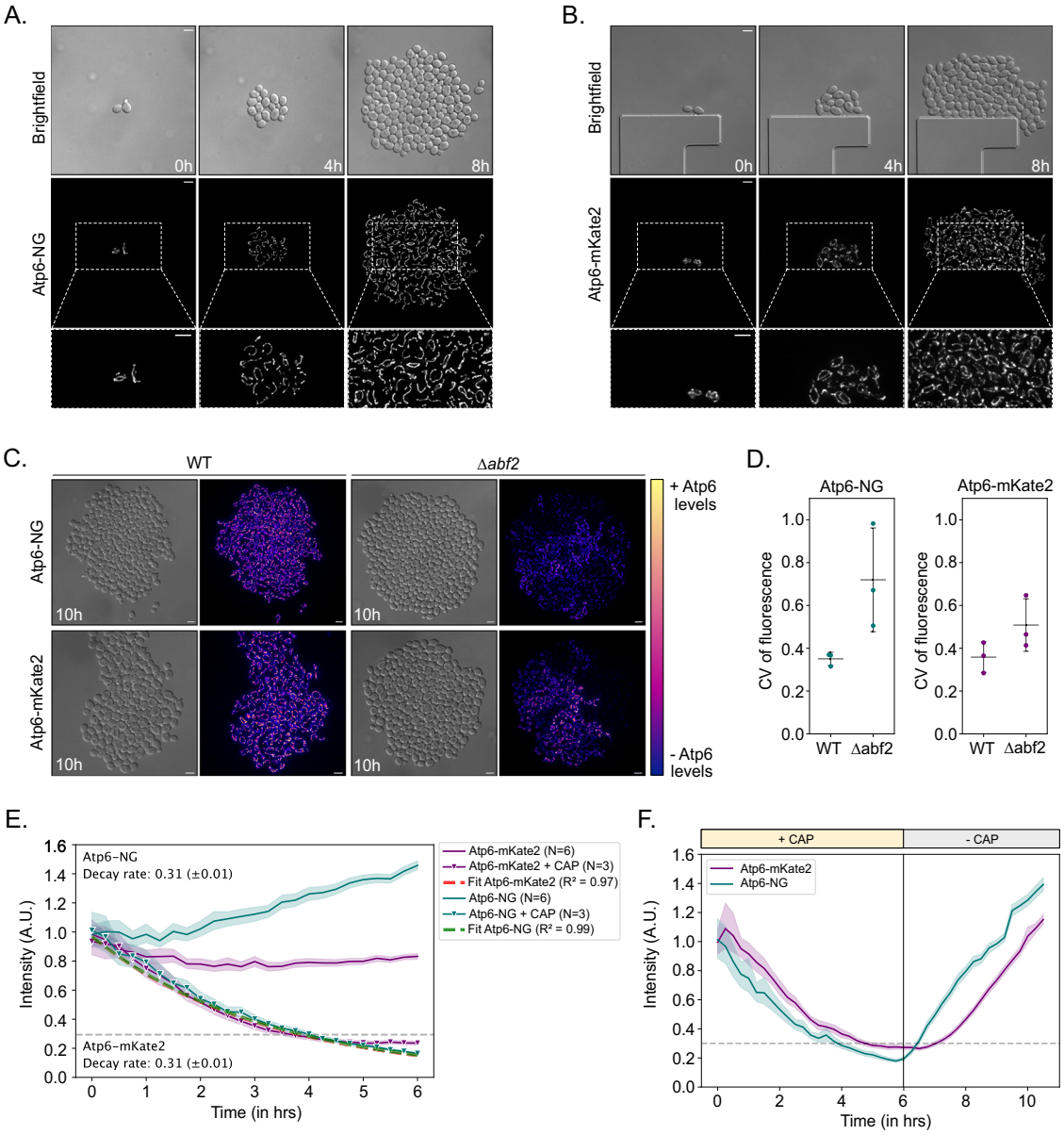

Figure 2. Atp6-NG and Atp6-mKate2 are valid proxies for mtDNA variants.

(**A**, **B**) Yeast cells harboring Atp6-NG (**A**) or Atp6-mKate2 (**B**) mtDNA were imaged for 8 h on a microfluidic chip. Fluorescence images are maximum-intensity projections of z-stacks, after deconvolution. Scale bars: 5 µm. (**C**) Wildtype and Δ*abf2* cells harboring Atp6-NG or Atp6-mKate2 mtDNA were imaged for 10 h. Cells were first grown in YPG and supplied with minimal media during the microfluidic imaging. The color representation on the heatmap bar corresponds to the pixel intensity of Atp6. Fluorescence images are maximum-intensity projections of z-stacks, after deconvolution. Scale bars: 5 µm. (**D**) The coefficient of variation (CV) of fluorescence among cells at the last timepoint was calculated for indicated strains. Strains were pre-cultured in YPG and put into minimal media for microfluidic imaging. Each dot represents the CV of a population derived from single cells ($n > 1000$ cells analyzed in total per strain). The mean and SD of the CV per strain is shown ($N = 3$). (**E**) Line graph showing the normalized fluorescent intensities of Atp6-NG or Atp6-mKate2 assessed during growth of $mtDNA^{Atp6\text{-}NG}$ or $mtDNA^{Atp6\text{-}mKate2}$ strains. Cells were constantly supplied with minimal medium containing ($N = 6$) or lacking ($N = 3$) 1 mg/ml Chloramphenicol (CAP) for mtDNA translation inhibition. Intensities were normalized to the median fluorescence intensity of the first timepoint per replicate. Data represent mean and shaded areas show the 95% confidence interval per strain. Decay rates for each fluorophore were calculated by fitting an exponential to the intensity levels of fluorescence upon CAP treatment. (**F**) Line graph represents the normalized fluorescent intensities of cells expressing Atp6-NG or Atp6-mKate2, during a 12-hr recording. Cells were first incubated for 6 h in minimal media with 1 mg/ml CAP and upon washing off the drug, cells were kept in minimal media until the end of each experiment. Data represent the mean and the shadow areas show the 95% confidence interval per strain ($N = 3$). Source data are available online for this figure.

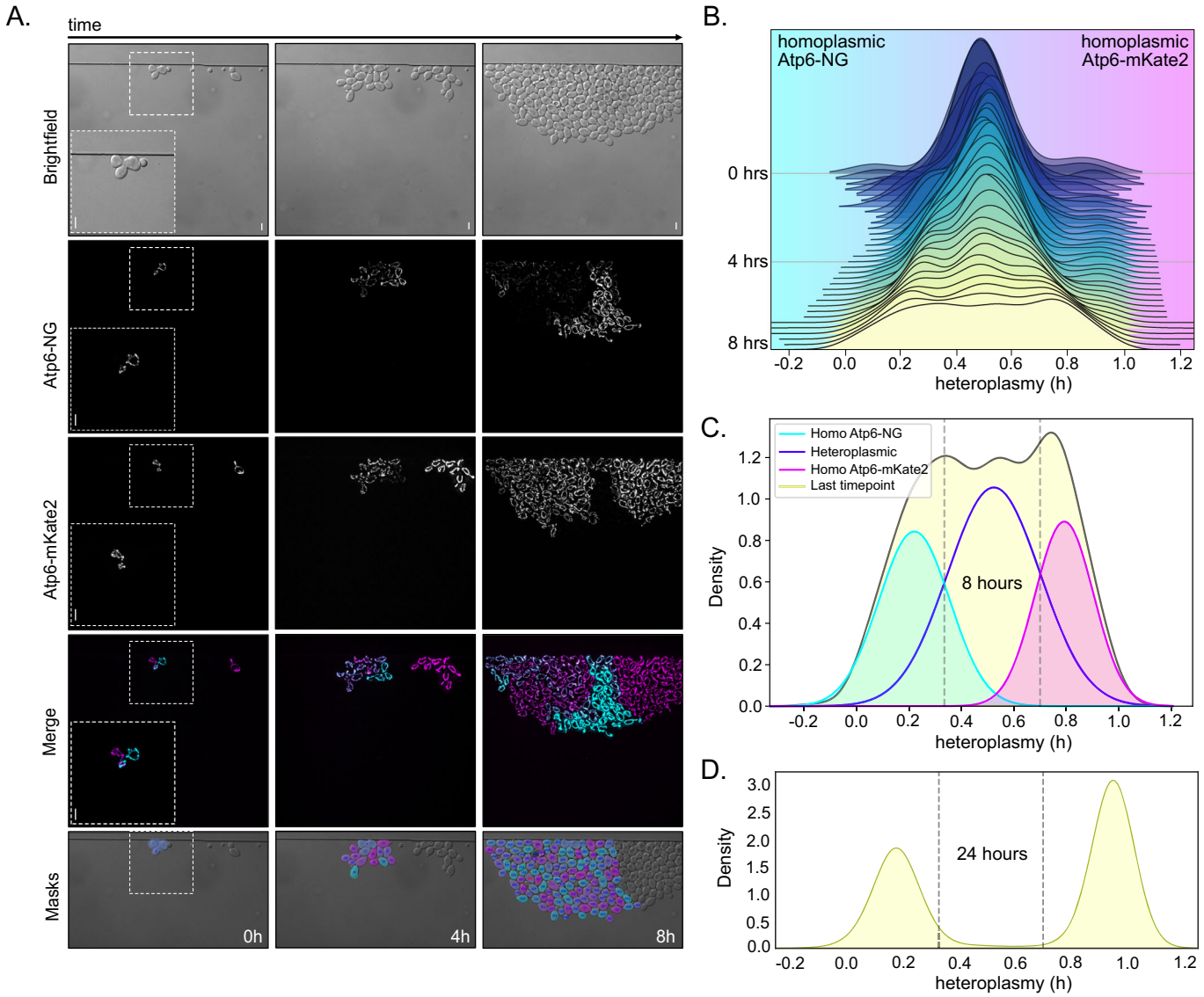

Figure 3. Rapid shift of mtDNA content in heteroplasmic cell populations.

(**A**) Representative images of a heteroplasmic population at indicated timepoints. Log-phase yeast cells harboring Atp6-NG (cyan) and Atp6-mKate2 (magenta) mtDNA were mated for 1.5 h prior to each microfluidic experiment. Individual heteroplasmic zygotes were chosen in a single field-of-view (FOV) and the growing cell populations were imaged for 8 h on a microfluidic chip. Fluorescence images are maximum-intensity projections of z-stacks, after deconvolution. Images representing the masks are derived from Cell-ACDC. Cells derived from a haploid cell present in the FOV were not segmented. Scale bars: 5 µm. (**B**) Joyplot of heteroplasmy levels of cells from a total of nine populations derived from heteroplasmic zygotes across the 8 h time-lapse recordings. (**C**) Single Gaussian curve fittings were applied on the three emerging peaks of the final cell distribution of the data at 8 h (density plot in light yellow, as in **B**). Three colored curves (cyan, purple, magenta) represent the cell distributions with more $mtDNA^{Atp6\text{-}NG}$ (cyan), more $mtDNA^{Atp6\text{-}mKate2}$ (magenta), or cells harboring both (purple). Homoplasmy thresholds were set based on the intersection points of Gaussian curves. An h-value of 0.33 was set as the homoplasmy threshold for cells mainly harboring $mtDNA^{Atp6\text{-}NG}$ and 0.71 as the threshold for $mtDNA^{Atp6\text{-}mKate2}$ homoplasmy, shown as gray dashed lines. (**D**) Density plot showing the heteroplasmy distribution of cells after 24 h. Atp6-NG and Atp6-mKate2 cells were mated for 2 h. Twenty individual zygotes were micro-dissected, upon growth on YPD plates for 24 h and heteroplasmic states of all cell populations were assessed by microscopy ($N = 20$ colonies, $n = 7538$ cells). Homoplasmy threshold values from the 8 h intersection points are shown in gray dashed lines. Source data are available online for this figure.

Atp6-NG and Atp6-mKate2 serve as valid proxies for the presence of the mtDNA by which they are encoded.

Rapid segregation of mtDNA variants

Next, we followed the segregation of $mtDNA^{Atp6\text{-}NG}$ and $mtDNA^{Atp6\text{-}mKate2}$ in populations derived from heteroplasmic zygotes, generated by mating parental cells harboring either mtDNA variant (Fig. 1A; Movie EV10). As expected, all newly formed zygotes displayed a fused mitochondrial network that exhibited signals in both fluorescent channels, indicative of carrying both mitochondrial genomes. We proceeded to generate time-lapse videos for a total duration of 8 h to track the mtDNA segregation across multiple generations. Remarkably, cell-to-cell

heterogeneity became rapidly evident in all populations, reflecting different heteroplasmy levels (Fig. 3A; Appendix Fig. S4A). Most interestingly, patches of cells emerged in all populations that had transitioned to exhibiting fluorescence only in a single channel during the time course, indicating that these cells had retained predominantly or exclusively one of both mtDNA variants.

To quantitatively assess the heteroplasmy levels within each cell and population, we applied the heteroplasmy formula $h = m1/(m1 + m2)$, (Aryaman et al, 2019; Johnston et al, 2015), where m1 and m2 are the fluorescent intensities of Atp6-NG and Atp6-mKate2 per cell that were normalized to cell volume as well as median fluorescence per timeframe. Furthermore, the background signal present in cell-free areas of images was subtracted from cellular fluorescence. As a result, an h-value of 0.5 is indicative of an equal ratio of both mtDNA variants within cells, equidistant to the homoplasmy extremes, which tend towards 1 or 0 when there is a shift towards $mtDNA^{Atp6\text{-}NG}$ or $mtDNA^{Atp6\text{-}mKate2}$, respectively. By plotting the quantities of cells with specific h-values over time, we observed a shift in heteroplasmic states (Fig. 3B). Initially, the heteroplasmy distribution was narrowly centered around the average value of 0.5, where most cells exhibited fluorescence for both Atp6 variants. As time progressed, the middle peak flattened and the overall heteroplasmy distribution broadened (Fig. 3B). Focusing on the final timepoint, two peaks at both ends of the spectrum became apparent, closer to h-values of either 1 or 0 (Fig. 3C; Appendix Fig. S4B), likely representing homoplasmic cells.

Of note, for all segregation experiments, zygotes were chosen that gave rise to medial buds, which inherit mitochondria from both parental cells and, therefore, end up being heteroplasmic (Strausberg and Perlman, 1978). The inheritance of a mixed content derived from both parental cells is apparent from the green and red fluorescence within the mitochondria of medial buds (Appendix Fig. S5A). Second-daughter cells from zygotes often bud off of lateral positions and predominantly or exclusively inherit mitochondrial content from the parental cell from which they originate. Importantly, the segregation pattern did not significantly change, when we excluded cells derived from second-generation daughter cells that had appeared on lateral zygote positions and, therefore, had started out with predominantly only one of both mtDNA variants (Appendix Fig. S5B).

To estimate the proportions of homo- and heteroplasmic cells, we fit three Gaussian curves to the observed trimodal heteroplasmy distribution at the final timepoint. These curves characterize cells primarily exhibiting homoplasmy for either $mtDNA^{Atp6\text{-}NG}$ (on the left) or $mtDNA^{Atp6\text{-}mKate2}$ (on the right), as well as heteroplasmic cells (in the middle). While definitively distinguishing between homo- and heteroplasmy is not feasible, we approximated their quantities by establishing thresholds at the intersections of individual Gaussian curves. Cells falling below an h-value of 0.35 or above 0.7 were classified as homoplasmic for $mtDNA^{Atp6\text{-}NG}$ or $mtDNA^{Atp6\text{-}mKate2}$, respectively (Fig. 3C). This approximation is further supported by the fact that residual non-mated haploid cells homoplasmic for either $mtDNA^{Atp6\text{-}NG}$ or $mtDNA^{Atp6\text{-}mKate2}$ exhibited h-values comparable to diploid cells classified as homoplasmic (Appendix Fig. S6). We posit that the homoplasmic peaks not being centered around 0 and 1 is primarily attributable to autofluorescence in the "absent" channel. To confirm that diploid homoplasmic cells indeed fall below or above these thresholds, we assessed heteroplasmic states of 20 independent populations derived from heteroplasmic zygotes after 24 h, where we expected virtually full segregation of mtDNA variants. Spatial limitations within the microfluidic system prevented its use for this approach. Therefore, we opted for a microdissection of heteroplasmic zygotes and observed mtDNA segregation in single cells after 24 h of growth on plates (Fig. EV2). Indeed, the 24 h cell distribution appeared bimodal, where the middle curve, representing heteroplasmic cells, was virtually absent (Fig. 3D). The two pronounced peaks fell below or above our homoplasmy thresholds, establishing them as good estimates to quantify homoplasmic cells. Based on these cutoffs, 97% of cells were characterized as homoplasmic, revealing, as expected, nearly complete segregation of two mtDNA variants within a growing yeast population after 24 h. Thus, our approach allows real-time imaging of mtDNA segregation dynamics at a single-cell level. Our analysis reveals rapid segregation, which can be observed already during the first 8 h and virtually completes within 24 h.

Mathematical modeling of mtDNA segregation dynamics

To better understand how the observed mtDNA segregation occurs, we developed a mathematical model that simulates the dynamics of segregation in a growing cell population arising from a single heteroplasmic cell. In vivo, mtDNA is distributed throughout a tubular mitochondrial network within cells and partitioning of mitochondria, including mtDNA, occurs via the transport of mitochondrial tubules into daughter cells during cell division (Osman et al, 2015). Hence, mtDNA copies present in the same segments of the tubular mitochondrial network are more likely to be segregated together into daughter or mother cells, respectively. Therefore, a simple random-pick model would not adequately capture the in vivo situation. To reflect this morphological aspect in the model, we used arrays, representing the tubular organization of mitochondria that contained two mtDNA variants either denoted as 0 or 1. Of note, we do not consider branching of the array. The length of this array represents the previously determined average of 32 mtDNA copies per diploid cell (Göke et al, 2020), neglecting the cell-to-cell variability in the copy numbers that may occur due to cell size differences. Importantly, we simulated zygotes with equal amounts of 0 and 1 s in an initial 'mixed' structure sequence of 01010101… (Fig. 4A). We substantiated the model's robustness through manipulation of the array, by mildly varying the mtDNA copy numbers between 26 and 38 (Appendix Fig. S7A), as well as by substituting the initial structure of the founder cell with a semi-mixed array ("0011100011…") or a non-mixed array ("0000011111…") (Appendix Fig. S7B,C).

To account for mitochondrial fission and fusion events, we introduced the *nspl* parameter, which represented the number of fragments an array could split into, followed by re-fusion in random order during growth. Upon completion of this shuffling process, the array was allowed to split into two parts, which partitioned to mother and daughter cells. The daughter cell received the shorter of both parts containing a specific amount of mtDNA copies, defined by the *ndau* parameter (Fig. 4A). Depending on the inherited mtDNA variants, each daughter cell consisted of either all 0 s, all 1 s, or a mixture of both. Upon division, mtDNA copies were allowed to replicate until the total number reached 32. To reflect relaxed mtDNA replication, we randomly chose mtDNA molecules for replication, allowing multiple rounds of replication

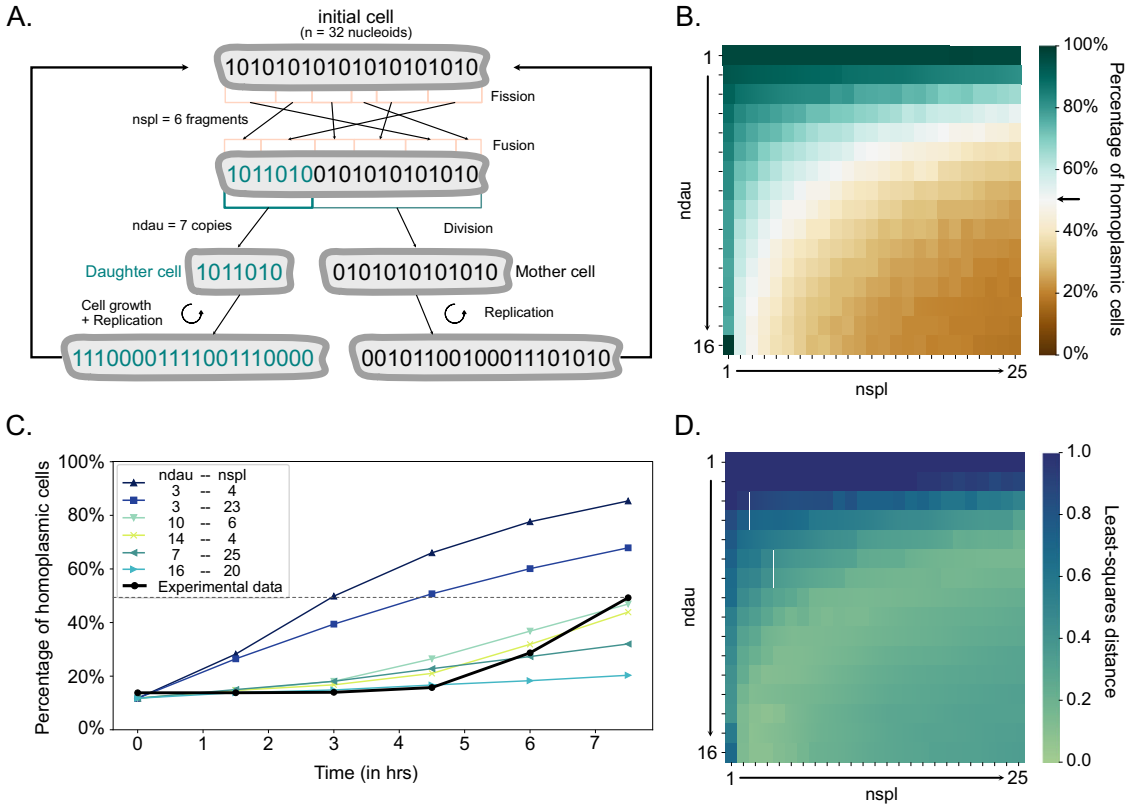

Figure 4. Mathematical modeling of mtDNA segregation dynamics.

(**A**) Mitochondria are simulated as arrays, where 0 and 1 s represent different mtDNA variants. Each single cell contains one such array with 32 mtDNA copies. The parameter *nspl* mimics the fission-fusion dynamics and the *ndau* parameter describes the number of mtDNA copies transferred to the daughter cell upon division. Each cell is allowed to give rise to a daughter cell once it reaches 32 mtDNA copies, upon random sequential replication of the inherited 0 and 1 s. In the shown example, where $nspl = 6$, the array splits into six fragments and then stochastically fuses back together. For simplicity, only 20 copies are shown. (**B**) Heatmap showing the percentage of homoplasmic cells at timepoint $t = 7.5$ h, for different *ndau* and *nspl* pairs. The arrow indicates the proportion (50%) of cells being virtually homoplasmic in the empirical data, based on the pre-established homoplasmy cutoffs. Each simulation with any given combination of the two parameters has been run ten times. (**C**) Curves display the proportion of homoplasmic cells in experimental (black line) or simulated data derived from different *ndau* and *nspl* combinations (colored lines) for timepoint $t = 0$, 1.5, 3, 4.5, 6, 7.5 h. The dashed line represents 50% homoplasmy. (**D**) Heatmap showing the least-squares distance of simulations with a given pair of *ndau* and *nspl* parameters from the experimental data, upon application of the homoplasmy thresholds. Each simulation with any given combination of the two parameters has been run ten times. Source data are available online for this figure.

for the same mtDNA molecule during the span of one cell cycle. Notably, newly replicated mtDNA copies were always placed next to the template mtDNA. We neglected the possibility of spontaneous cell death and mtDNA degradation.

First, we simulated the influence of *nspl* and *ndau* parameters on the segregation rate by modeling the amount of homoplasmic cells after 7.5 h (Fig. 4B). We observed that higher *nspl* or *ndau* parameters, corresponding to more shuffling or more mtDNA copies partitioned to daughter cells, predict a relatively low percentage of homoplasmic cells after 7.5 h. Conversely, lower *nspl* and/or *ndau* values lead to an acceleration of mtDNA segregation. Our simulations show that distinct *ndau-nspl* combinations can result in similar levels of homoplasmic cells after 7.5 h. We next asked, which of these combinations aligns with our experimental data. To this end, we applied the previously defined homoplasmy thresholds (Fig. 3C) to all timepoints within our 8-hr in vivo experiment and quantified amounts of homoplasmic cells (Fig. 4C, black curve). We compared the fractions of homoplasmic cells between the experimental and the simulated data at timepoints 1.5, 3, 4.5, 6, and 7.5 h by applying the least-squares criterion. We found the best-fitting parameter values to be $ndau = 14$ and $nspl = 4$ (Fig. 4C,D). However, we identified various combinations of *ndau* and *nspl* approximating the experimental results. In particular, there was an inverse relationship between the values for *nspl* and *ndau* that fit the data well, where higher *ndau* values required lower *nspl* ones, and vice versa. Specifically, the combinations of relatively higher *ndau* values (ranging from 10-16) and lower *nspl* values (within the range of 3–6) came closest to the empirical data (Fig. 4C, light green lines). In contrast, we observed a poor fit to the data, when *ndau* and *nspl* were simultaneously very low or very high (Fig. 4D). Thus, these results suggest that fusion and fission frequencies, representing shuffling events, as well as the number of mtDNA copies transferred to daughter cells are contributing to the segregation kinetics of mtDNA variants in a yeast population, under our neutral experimental setup.

Next, we used our model to examine how increased mtDNA copy numbers within cells may affect mtDNA variant segregation. To this end, we simulated segregation in cells with 56 (observed in

cells with increased mtDNA copy number lacking the gene *MRX6* (Göke et al, 2020)) or 90 mtDNA copies (as an extreme example) (Fig. EV4A,B) and compared segregation kinetics to the kinetics from the best-fitting simulations for cells with 32 mtDNA copy numbers, where *ndau* and *nspl* equaled 14 and 4, respectively (Fig. EV4C–E). We found that the segregation speed is very similar if the *nspl* value stays the same (nspl=4) and the same percentage of total copies of mtDNA are passed on to the daughter cell (e.g., ~44% would mean 14 copies in a cell with 32 copies, but ~25 or ~39 copies in a cell with 56 or 90 copies, respectively) (Fig. EV4C). However, it is also possible that increased mtDNA copy number affects the *ndau* and/or *nspl* parameters. Similar to our simulations for mtDNA copy number equal to 32 (Fig. 4D), our simulations suggest that also in scenarios with increased mtDNA copy number, a higher percentage of mtDNA copies transmitted to daughter cells and increased fusion-fission frequencies could result in slower segregation of mtDNA variants. On the contrary, a lower percentage of transmitted copies and decreased fission-fusion frequencies would result in faster segregation (Fig. EV4D,E).

Altogether, these results suggest that fusion and fission frequencies, representing shuffling events, as well as the number of mtDNA copies transferred to daughter cells are contributing to the segregation kinetics of mtDNA variants in a yeast population, under our neutral experimental setup.

Partitioning of a small subset of mtDNA copies to daughter cells promotes mtDNA homoplasmy

Our mathematical model suggests that multiple different combinations of *nspl* and *ndau* parameters could explain the observed segregation of mtDNA variants. With respect to the *ndau* parameter, the values range from seven to fifteen, representing about a fifth or half of available mtDNA copies passed on to the daughter cell, respectively. Therefore, we asked which of the possible model predictions reflects the in vivo situation. First, we examined our experimental heteroplasmy dataset to evaluate if equal or unequal amounts of mtDNA copies are partitioned to mother and daughter cells during cell division. If unequal amounts of mtDNA copies are transferred per division to the progeny, we would expect a lower correlation between heteroplasmy values between mothers (M) and daughter cells (D) compared to a correlation of h-values between mothers to themselves at a later timepoint (M_D). In a scenario where mtDNA copies are equally split between mother and daughter, the M-D and M-M_D h-value correlations are expected to be similar. Hence, we compared heteroplasmy levels of mother cells (M) at timepoint t_M to those of their daughters (D) at t_D or granddaughters (GD) at t_{GD}, as well as to those of their aging selves M_D and M_{GD} at t_D or t_{GD}, respectively (Fig. 5A). The two timepoints, t_D and t_{GD}, were chosen based on the same growth stage, where cells had small buds (1/5 bud-to-mother volume ratio). In line with an unequal partitioning of mtDNA copies, we observed a high correlation between M and M_D in contrast to a statistically significant lower correlation coefficient between M and D (Fig. 5B). Comparison of mothers to their granddaughters further supported this hypothesis, as the M-GD correlation further decreased compared to the M-D correlation. In contrast, aged mothers (M_{GD}) still displayed a stronger similarity to their original heteroplasmic state (M). These results underscore that cell division, most likely through the transmission of a limited number of mtDNA copies, is a major driver for the progressive divergence of heteroplasmic states in a proliferating yeast population.

Subsequently, we aimed to directly determine the number of mtDNA copies passed from mother to daughter per cell division. Therefore, we employed the mtLacO-LacI system, which allows the detection of single mtDNA copies by fluorescence live-cell microscopy (Osman et al, 2015). First, we quantified the number of fluorescent foci, representing mtDNA copies, migrating across the bud neck from a mother to its bud in 5-minute windows. Cells were in different cell cycle stages, however only mother-bud pairs whose mitochondrial network appeared interconnected or where mitochondrial fragments traveled from mother to daughter were considered. We observed that, on average, 1.18 mtDNA foci were transmitted to daughter cells within these 5 min (Fig. 5C,D; see Methods; Appendix Fig. S8A,B; Movie EV11). Next, we examined the duration for which the exchange of mitochondrial content occurred between mother-daughter pairs, by live-cell microscopy using the nuclear-encoded matrix-targeted mKate2 (see Methods). We did not observe mitochondrial content exchange, neither through continuous mitochondrial tubules spanning the mother-bud neck, nor through transport of mitochondrial fragments, after an average time period of $\Delta t = 47.5$ min (Fig. 5E; Appendix Fig. S8C; Movie EV12). This observation aligns well with a previous study that similarly observed that daughter cells gain mitochondrial volume at the expense of the mother during the first half of the cell cycle (Rafelski et al, 2012). Taken together, we estimate that, on average, 11.2 nucleoids migrate from mother to daughter in a single-cell division (Fig. 5F).

To further examine mtDNA transmission to daughter cells, we performed live-cell microscopy of diploid cells containing the mtLacO-LacI system over the duration of an entire cell cycle and assessed dynamic changes of mtDNA content in virgin mother and emerging daughter cells. In line with our observation that the exchange of mitochondrial content occurs between mother and daughter cells for about 45 min, we observed a reduction of mtDNA foci from about 35 to below 30 in the mother cells during this time period, whereas the number of foci increased to 15 in daughter cells. After 45 min, the number of foci remained constant in the mother cell, while the foci number further increased to about 30 in the daughter cell (Fig. EV4). These results suggest that mtDNA copy number is replenished in mother cells, while mtDNA copies are being passed on to daughters, and that after 45 min mtDNA replication continues in daughter cells. Of note, we did not observe that the starting foci number of 35 was reestablished in the mother cell or the daughter cell. We assume that this observation is due to continued imaging causing phototoxicity or bleaching.

Besides asymmetric apportioning of mtDNA copies to daughter cells, our mathematical model also predicts a critical role for mitochondrial fusion and fission cycles in determining the rate of mtDNA variant segregation by shuffling mtDNA copies in the mitochondrial network. To experimentally test this prediction, we performed mtDNA variant segregation experiments in cells lacking the gene *DNM1*, which is essential for mitochondrial fission. Specifically, we mated Δ*dnm1* cells containing $mtDNA^{Atp6\text{-}NG}$ or $mtDNA^{Atp6\text{-}mKate2}$, pre-grown in YPG medium to prevent mtDNA loss, and microscopically evaluated the percentage of heteroplasmic cells in colonies formed from individual zygotes after 18 h of growth on YPD plates. In line with our model, the

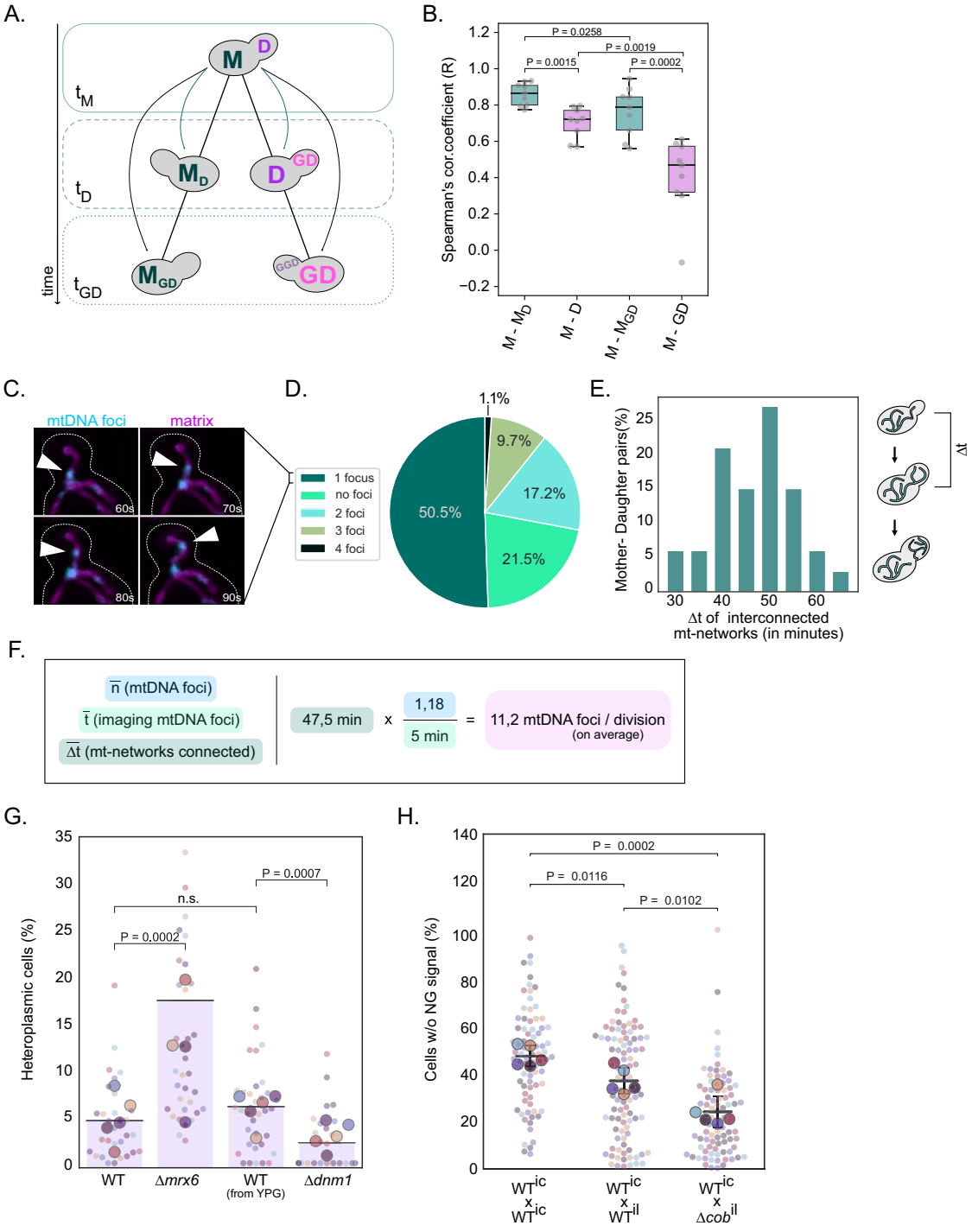

absence of mitochondrial fission resulted, on average, in a lower amount of heteroplasmic cells compared to mating between mtDNA$^{Atp6\text{-}NG}$ or mtDNA$^{Atp6\text{-}mKate2}$ WT cells, indicating faster segregation kinetics in the absence of mitochondrial fission (Fig. 5G). This conclusion is further supported by the observation that we detected exclusively homoplasmic cells in 57% of colonies derived from heteroplasmic Δ*dnm1* cells compared to 14% in WT cells (Appendix Fig. S9B).

We additionally experimentally tested the effect of increased mtDNA copy number on mtDNA segregation dynamics. To this end, we performed segregation experiments in Δ*mrx6* cells, that have previously been shown to have a twofold increase of mtDNA (Göke et al, 2020). We assessed the number of heteroplasmic cells in populations after growth for 18 h derived from Δ*mrx6* zygotes containing mtDNA$^{Atp6\text{-}NG}$ and mtDNA$^{Atp6\text{-}mKate2}$. Interestingly, mtDNA variant segregation was delayed in Δ*mrx6* cells and a higher percentage of cells remained heteroplasmic after 18 h of

Figure 5. Partitioning of a limited number of mtDNA molecules to the next generation facilitates rapid heteroplasmy changes.

(**A**) Schematic of cell relationship pairs. Correlations were calculated between mother cells and their progeny within a lineage (M-D-GD) or between themselves at later timepoints (M-M_D-M_{GD}). All cells were taken at the same growth stage, specifically 20% bud-to-mother volume ratio. (**B**) The box plot depicts Spearman's correlation coefficient for the aforementioned relationship pairs, among all cell populations ($N = 9$). Each cell population was derived from an individual zygote. The Spearman's correlation coefficient for each population is shown as a gray dot. The box extends from the lower to upper quartile values of the data, with a line at the median. Whiskers indicate the minimum and maximum values. $P < 0.05$: *, $P < 0.005$: **, $P < 0.0005$: ***, paired *t*-test. (**C**) Representative time-lapse of a spot being transferred to the bud. Yeast cells expressing 3xNG-LacI (cyan) and matrix-su9-mKate2 (magenta) labeling nucleoids and the matrix, respectively, were imaged for 5 min in 10 s intervals. The white arrowhead indicates a 3xNG-LacI focus crossing the bud neck. Amounts of foci crossing the bud neck during 5-min windows were counted. Fluorescent images are maximum-intensity projections of z-stacks, after deconvolution. Scale bar: 5 µm. (**D**) Percentile proportions of mtDNA foci crossing the mother-bud neck in 5 min ($N = 93$ mother-bud pairs). Budding cells were at different cell cycle stages. Each spot was counted as one mtDNA copy. (**E**) The bar plot shows the time duration during which mitochondrial networks remain connected between mothers and daughters. Mitochondrial network connectivity was examined in log-phase cells expressing matrix-targeted mKate2 ($n = 33$). Only cells with no visible bud at the beginning of the imaging were considered for analysis (see also Appendix Fig. S8C). (**F**) The calculation formula for the number of nucleoids passing per cell division, based on data derived from (**C**) and (**E**). (**G**) Heteroplasmy distribution in Δ*mrx6* and Δ*dnm1* deletion strains. Cells with increased copy number (Δ*mrx6*) or deficient for mitochondrial fission (Δ*dnm1*) were generated in strains containing $mtDNA^{Atp6\text{-}NG}$ or $mtDNA^{Atp6\text{-}mKate2}$. Cells containing $mtDNA^{Atp6\text{-}NG}$ or $mtDNA^{Atp6\text{-}mKate2}$ and the respective deletion were mated. After zygote formation and dissection, diploid colonies were grown for 18 h on a YPD plate. Each colony was imaged to assess the fraction of heteroplasmic cells (also see Appendix Fig. S9A for all data points). Of note, Δ*dnm1* cells were cultivated in YPG media before mating and dissection on YPD plates, to prevent mtDNA loss. For each genotype shown, the small dots represent the percentage of heteroplasmic cells in individual colonies ($n > 50$ cells/colony). Each bigger dot depicts the mean of each biological replicate ($N = 5$), and the line is the mean of all replicates for the corresponding mating. Statistical significance was determined by paired *t*-test. (**H**) 24 h heteroplasmy assessment in matings between cells containing mutated mtDNA (Δ*cob*) or intact mtDNA. Log-phase yeast cells harboring $mtDNA^{Atp6\text{-}NG}$ were mated with cells containing intact intron-containing mtDNA, intact intronless mtDNA, or intronless Δ*cob* mtDNA, all not expressing any fluorophore. After zygote formation and dissection, diploid colonies were grown for 24 h on a YPD plate. Each colony was imaged to assess the fraction of cells not expressing Atp6-NG. For each genotype shown, the small dots represent the percentage of heteroplasmic cells in individual colonies ($n > 100$ cells/colony). Each bigger dot depicts the mean of each biological replicate ($N = 5$), and the line is the mean of all replicates for the corresponding mating. Error bars indicate SD. Statistical significance was determined by paired *t*-test. Source data are available online for this figure.

growth (Fig. 5G), with none of the populations having entirely segregated (Appendix Fig. S9B). In conjunction with predictions from our model (Fig. EV3), the experimentally determined delayed segregation in Δ*mrx6* cells suggests that these cells have higher fission-fusion frequencies and/or transmit a higher percentage of mtDNA copies to daughter cells.

Thus, our experimental data suggest that unequal amounts of mtDNA copies are partitioned to daughter cells during the cell cycle, which appears to be a major driving force for mtDNA segregation. Additionally, we find that fission deficiency leads to faster mtDNA variant segregation, while increased mtDNA copy number results in slower homoplasmy establishment.

Finally, we asked if we could apply our experimental setup to observe purifying selection of intact over mutant mtDNA. Currently, no yeast strains are available that harbor a mutant mtDNA encoding a fluorescent protein. Therefore, we conducted experiments in which cells containing intact intron-containing $mtDNA^{Atp6\text{-}NG}$ were mated with cells containing "dark" intronless $mtDNA^{il\text{-}\Delta cob}$, lacking the open reading frame encoding Cytochrome b, which is essential for respiratory growth. Notably, deletion of *COB* was generated in mtDNA lacking introns (Gruschke et al, 2011). Therefore, we conducted control experiments where cells containing $mtDNA^{Atp6\text{-}NG}$ were mated with cells harboring intact intron-containing ($mtDNA^{ic}$) or intact intronless mtDNA ($mtDNA^{il}$), both lacking genes encoding fluorescent proteins. Upon growth for 24 h, we assessed the percentage of "dark" cells, lacking $mtDNA^{Atp6\text{-}NG}$, in populations arising from heteroplasmic zygotes (Fig. EV5). Our data show that in matings between cells harboring $mtDNA^{Atp6\text{-}NG}$ and cells harboring $mtDNA^{ic}$, no preference for either mtDNA variant was present as equal segregation into 'dark' and fluorescent cells was observed (Fig. 5H). Matings between cells harboring $mtDNA^{Atp6\text{-}NG}$ and cells harboring $mtDNA^{il}$ revealed a slight preference for the intron-containing mtDNA as less "dark" cells were detected. Most strikingly, the number of "dark" cells was significantly lower after the growth of zygotes containing $mtDNA^{Atp6\text{-}NG}$ and $mtDNA^{il\text{-}\Delta cob}$, indicating selection against the mutant mtDNA. This result confirms our previous finding that yeast cells favor generation of progeny with functional mtDNA copies (Jakubke et al, 2021), and that our experimental pipeline can be used to study the purifying selection of mtDNA.

Discussion

In this study, we unveil the dynamics of mtDNA heteroplasmy in a living cell population with unprecedented temporal resolution. Our findings demonstrate that proliferating heteroplasmic yeast populations exhibit rapid transitions towards homoplasmic states. Through the analysis of heteroplasmic variance in cell lineages, alongside mathematical modeling and direct mtDNA copy tracking, we demonstrate that asymmetric partitioning of mtDNA copy numbers and mitochondrial fission are important determinants for mtDNA segregation. Our finding, with smaller daughter cells receiving a lower copy number than their mothers, also aligns with our previous finding that mtDNA copy number correlates strongly with cell volume (Seel et al, 2023).

Understanding the principles and dynamics that underlie the segregation of mtDNA variants has been hampered by the inability to track their presence and quantities within living cells across multiple cell divisions. We overcome this hurdle and infer the presence of heteroplasmy levels within individual cells over time, by employing two mtDNA variants encoding Atp6 tagged with different fluorescent proteins. Our results demonstrate the efficacy of this approach in assessing mtDNA quantities, despite the fact that proteins indirectly represent mtDNA. First, we observed a rapid decrease in fluorescent signals upon translational inhibition with Chloramphenicol and a subsequent resurgence of signal upon drug removal. Second, deletion of the mitochondrial HMG-box protein Abf2, causing gradual loss of mtDNA (Schrott and Osman, 2023; Sia et al, 2009; Zelenaya-Troitskaya et al, 1998), results in

heterogeneity of fluorescent signals within populations, whereas fluorescent signals in wild-type populations show little cell-to-cell variance. Hence, our fluorescent readout detects changes in mtDNA abundance or its expression within the duration of our experiments. These findings strongly affirm the notion that rapid changes in fluorescent intensities within proliferating cell populations, derived from heteroplasmic zygotes, closely align with shifts in the level of heteroplasmy. Nevertheless, it is very probable that residual "fossil" Atp6 protein amounts persist within cells, even if the mtDNA genomes encoding these proteins are not present in cells anymore, which likely leads to an underestimation of the speed of mtDNA variant loss.

Examination of mtDNA segregation dynamics has so far largely been limited to in silico approaches (Aryaman et al, 2019; Glastad and Johnston, 2023; Johnston, 2019; Johnston et al, 2015; Kowald and Kirkwood, 2011; Tam et al, 2013). As our experimental setup allows assessment of this process in vivo, comparison of empirical data with mathematical modeling becomes possible. To this end, we performed simulations, which consider important aspects imposed on mtDNA segregation by mitochondrial morphology and dynamics as well as the relaxed replication of mtDNA. Our model identifies shuffling and unequal partitioning as important factors influencing the speed of mtDNA variant segregation. Decreased shuffling of mtDNA increases the speed of segregation, likely because mtDNA copies stay close to their template mtDNA after replication and to other molecules copied from the same template. Thus, it is more probable that larger numbers of mtDNA copies of the same type are passed on to the daughter cell, which also implies that the nucleoids staying in the mother cell are more homogeneous. Indeed, our experiments confirm the prediction that lack of mitochondrial fission accelerates mtDNA variant segregation. This finding is also in line with previous mathematical modeling (Tam et al, 2013) and the reported limited mobility of mtDNA (Jakubke et al, 2021; Nunnari et al, 1997), which likely prevents shuffling of different mtDNA variants within the mitochondrial network in the absence of mitochondrial fusion and fission.

Shuffling and unequal partitioning are both predicted to influence mtDNA segregation. Direct assessment of mtDNA partitioning to progeny cells reveals that under our experimental conditions, about a third of available mtDNA copies are partitioned to the daughter cell in wild-type cells. Our model suggests that for such an *ndau* value, a relatively low *nspl* parameter ($nspl = 5$) is required to match the observed speed of mtDNA variant segregation. We would like to emphasize that the absolute value of the *nspl* parameter predicted by our model should be regarded with care. Our model does not consider parameters such as the branching of mitochondrial tubules, the spatial organization of mitochondrial tubules in the cell, or a link between mtDNA replication and mitochondrial fission (Lewis et al, 2016; Murley et al, 2013). Such parameters likely affect shuffling of mtDNA variants (Glastad and Johnston, 2023), and thereby the outcome of mtDNA segregation. Nevertheless, we regard it as an interesting possibility that the number of mtDNA molecules partitioned to the daughter cell, as well as fusion-fission cycles, can be modulated by the cell, perhaps in response to stress conditions or altered mitochondrial physiology to either promote or reduce the speed of mtDNA segregation.

Interestingly, we find that mtDNA variant segregation is slowed down in Δ*mrx6* cells that exhibit an increased mtDNA copy number. In light of our simulations, this result suggests that Δ*mrx6* cells do either pass on a higher percentage of mtDNA copies to daughter cells or that the fusion-fission frequency is increased. Given the link between mtDNA replication and mitochondrial fission (Lewis et al, 2016; Murley et al, 2013), it is an interesting possibility that increased mtDNA copy number and, consequently, more replication events, may cause an elevated fission frequency. It will be interesting to determine the cause for decreased mtDNA segregation speed in cells with elevated mtDNA content in future experiments.

In addition to assessing the segregation dynamics of two neutral mtDNA variants that fully support mitochondrial function, we employed our experimental setup to investigate the competition between intact and mutant mtDNA. Our findings corroborate our previous observations that *S. cerevisiae* cells preferentially generate progeny with intact mtDNA (Jakubke et al, 2021). Therefore, we anticipate that our approach will be instrumental in examining mtDNA quality control and purifying selection in future studies.

Methods

Yeast strain construction

All yeast strains employed in this study were generated in the W303 background. Detailed genotypes are listed in Appendix Table S1. Construction of single deletion mutants followed the procedure described in (Janke et al, 2004). Primers and plasmid information are listed in Appendix Tables S2 and S3, respectively. For the deletion of *ABF2*, transformed cells were plated and kept on non-fermentable (YPG) carbon source, to avoid loss of mtDNA prior to the microfluidic experiment.

Yeast growth conditions

Prior to all experiments, cells were freshly streaked from −80 °C on YPD plates, left to grow at 30 °C overnight, and then inoculated in fermentable (YPD) liquid culture. The next day, cells were diluted to 0.1 OD_{600} and further incubated to reach the log phase. Of note, the Δ*abf2* cells, for either variant, were maintained on YPG, to prevent spontaneous mtDNA loss.

Growth assay and petite analysis

For the growth tests, log-phase cells were serially diluted and 3 µl of each dilution were spotted onto fermentable (YPD) and non-fermentable (YPG) plates. Plates were incubated at 30 and 37 °C, and were imaged after 24 and 48 h of growth. Appendix Fig. S1A shows the data after 48 h of growth. For the petite analyses to assess the loss of mtDNA in cells, 200 cells growing in log-phase were plated on YPG plates containing 0.1% glucose. Plates were imaged and colonies were counted after 3 days at 30 °C and classified into grande (big) or petite (small) colonies. Cells unable to properly respire show a petite phenotype.

Live cell microscopy

Time-lapse data was acquired using the microfluidics CellAsic ONIX system (Millipore) attached to a Nikon Eclipse Ti inverted microscope, equipped with a CFI Apochromat TIRF 100XC oil objective with a numerical aperture of 1.49 and a working distance of 0.12 mm (Nikon MRD01991). A TwinCam LS dual-camera splitter, coupled with two Photometrics Prime 95B 25-mm cameras, facilitated simultaneous imaging of red and green fluorophores. Every experiment was performed under the same settings for both fluorophores, with 40 ms exposure time, and 40% LED power. NeonGreen was excited at 506 nm wavelength, while mKate2 at 588 nm. Z-stacks were captured with increments of 0.3 µm over a total of 6 µm. Information on filters and dichroics can be made available upon request.

Both haploid and diploid cells were visualized for 8 up to 12 h, depending on the experiment, and images were acquired at 30 °C in 15 min intervals throughout the duration of the time-lapse using a temperature-controlled chamber around the microscope. Cells were continuously replenished with a fresh minimal medium at a flow rate of 15 kPa. For all microfluidic experiments, the CellAsic ONIX plates (Millipore) for haploid yeast cells were used. To obtain the diploid cells used for diploid live cell imaging, log-phase haploid cells harboring Atp6-NG were mated with haploid Atp6-mKate2 cells, in a 1:1 ratio on a YPD plate. After 2 h at 30 °C, once zygotes were formed, cells were resuspended in minimal medium, and single zygotes were picked in individual field of views to be monitored overnight using the CellAsic ONIX system.

Image processing and data acquisition

Cell segmentation and tracking was performed frame by frame based on the DIC channel using the Cell-ACDC software and the implemented YeastMate cell segmentation algorithm (Bunk et al, 2022; Padovani et al, 2022). Cell cycle annotations, mask correction, and lineage tracking errors, as well as cell volume calculation, were also performed through the Cell-ACDC software. All cell masks and traces were also manually verified. Fluorescent signals were quantified from the mean projection of the z-stack per timepoint from non-deconvolved video recordings. Fluorescent intensities per cell were first corrected by subtraction of background signal, measured in cell-free areas, and normalized to cell volume. Subsequently, for comparability between the different cell populations and to account for photobleaching, the cell signal intensity for the respective fluorophore was additionally normalized to the median intensity of all segmented cells of the given timepoint and technical replicate. Microscopy images in all figures were deconvolved with the Huygens software (Scientific Volume Imaging).

24-h heteroplasmy assessment

For assessing the proportion of homoplasmic Atp6-mKate2 and Atp6-NG cells after 24 h, the respective strains were grown to log phase and mated in a 1:1 ratio for 90 min on YPD plates. Once zygotes were formed, they were micro-dissected and placed in separate areas on a YPD plate, where they grew into single colonies overnight (Fig. EV2). The next morning, each distinct colony was picked and diluted into 200 µl and imaged on an Ibidi glass slide, previously coated with the immobilizing agent Concanavalin A (Jakubke et al, 2021). To get an estimate of heteroplasmy within the population, a minimum of 200 cells were imaged and evaluated from each individual colony. First, the h-value of all segmented cells was calculated, using the heteroplasmy equation (Johnston et al, 2015), and subsequently, after binning the data, cells were characterized as homoplasmic for Atp6-NG, Atp6-mKate2 or heteroplasmic if they fell within the middle range of heteroplasmy, defined by the intersection points of the single Gaussian curves (Fig. 3C).

For assessing the level of homoplasmy in cells competing between intact and mutant mtDNA, we mated WT strains harboring $mtDNA^{Atp6\text{-}NG}$ with cells containing intronless $mtDNA^{\Delta cob}$ (Gruschke et al, 2011). As a control, we also mated cells harboring $mtDNA^{Atp6\text{-}NG}$ with WT "dark" $mtDNA^{ic}$, or WT "dark" $mtDNA^{il}$. To assess the percentage of homoplasmic cells, we manually determined a threshold for 'signal' or 'no signal' by thresholding the fluorescent intensity of Atp6-NG based on the distribution of cells across each replicate as follows. Across all experiments, two distributions, exhibiting or virtually lacking fluorescent signals, were observed. The lowest value at the valley between the two peaks was set as the threshold for signal per replicate.

For assessing the heteroplasmy levels of cells with increased copy number (Δ*mrx6*) or fission-deficient ones (Δ*dnm1*), the zygote dissection pipeline was performed as described above, only that colonies were imaged after 18 h of growth on YPD plates. The rationale for earlier imaging was to capture differences in the percentage of remaining heteroplasmic cells more clearly compared to later imaging, where mtDNA variant segregation would have been virtually complete even in matings with a decreased rate of segregation.

mtDNA copy partitioning during cell division

To estimate the number of mtDNA copies crossing the mother-bud neck, we used a diploid strain developed in the lab, containing mtDNA with integrated LacO repeats and expressing the nuclear-encoded matrix-targeted 3xNG-LacI protein as well as a matrix-targeted mKate2 to monitor the mitochondrial network (3xNG-LacI-PGK1-su9-mKate2) (Osman et al, 2015). Log-phase cells, pre-grown in YPD, were visualized in 10-second intervals for 5 min in total, since longer exposure (with such frequent intervals) induces significant photobleaching.

By focusing exclusively on the neck region where the two cells are joined, we quantified the migration of mtDNA fluorescent foci from the maternal to the daughter side. Notably, we only analyzed cells where the mitochondrial networks between mother and bud were connected. Given that cells were at different stages of the cell cycle, we calculated the average amount of foci transmitted in 5 min, regardless of bud size. We cannot rule out that if two mtDNA foci are in close proximity, they might be counted as a single molecule. Of note, all aforementioned analysis was done using all z-slices and 3D modeling of each cell, and no maximum projection of z-stacks, to avoid loss or misinterpretation of the number of foci per cell pair.

To precisely determine the duration of content exchange between mothers and daughters, we employed the same strain but under different imaging conditions. Log-phase cells were

visualized for 120 min, in 5-min intervals, for successful monitoring of complete division cycles and mitochondrial network association between mothers and daughters. We defined the initiation of budding, when cells were in the very early S phase, as timepoint zero. We tracked the exchange process until the daughter's mitochondrial network had completely separated from that of the mother. At this point, just before the ultimate separation of networks, most daughter cells had developed into buds with an average cell volume equivalent to 55% of the mother's size, most likely corresponding to mid- to late G2 phase. In cases where mothers had large buds, we observed no network connectivity, indicating that these buds had already entered the late G2 phase in preparation for cytokinesis, which is consistent with existing literature (Koren et al, 2010). By analyzing 33 cells from timepoint zero to the last timepoint, we calculated an average mitochondrial content exchange period of 47.5 min, which was subsequently used to calculate an estimate of nucleoids transmitted per division.

mtDNA foci assessment during the cell cycle

In order to assess the number of mtDNA foci during a complete cell cycle, we used the same diploid strain (3xNG-LacI-PGK1-su9-mKate2) used for mtDNA foci assessment during mother-bud partitioning. Cells were harvested at log phase and imaged for 2 h at 7 min intervals. mKate2 and NeonGreen were simultaneously captured using the dual-camera system (50 ms exposure time, 30 and 100% light intensity, respectively). Of note, all aforementioned analyses were done using all z-slices and 3D modeling of each cell, and no maximum projection of z-stacks, to avoid loss or misinterpretation of the number of foci per cell pair. Foci were counted with custom-built Fiji Macros using the "3D Maxima finder" command. For the analysis, only virgin mothers, that is, cells that had just budded off from their mother, were considered. Timepoint zero was determined based on the point of bud emergence from the virgin mothers, per time-lapse video.

Mathematical model

In the model, we represent mitochondria as lists of 0 and 1 s, representing two different mtDNA genotypes. Mitochondria are modeled as one-dimensional objects without branches. When a mtDNA molecule is duplicated, the copy is placed right next to the original one. For the mtDNA copy number of diploid yeast cells, we apply actual measurements derived from (Göke et al, 2020), and set the average amount of mtDNA copies to 32 in each simulated cell. We additionally assume that one nucleoid contains one mtDNA copy and all mtDNA copies have identical replication rates. Importantly, the model neglects the possibility of a preferential replication of only a fixed subset of copies at any timepoint.

In order to accurately reflect the heteroplasmic state of founder cells, we define two different mtDNA variants in each zygote, mtDNA type 0 and mtDNA type 1. Hence, a cell can have two different states, homoplasmic for either 0 or 1, or a combination of both when heteroplasmic. In each simulation, founder cells were consistently characterized by virtually absolute heteroplasmy, featuring a distribution of mtDNA haplotypes according to the average of all nine biological replicates and a mitochondrion structure composed of alternating 0 and 1 sequences (that is 0101010101… in the case of 50% mtDNA haplotype 1). Given our experimental observations, where spontaneous mtDNA depletion is absent, we also postulate the absence of mtDNA depletion in each cell in silico. Furthermore, to simulate yeast lineages as close to the real data as possible, we allow each cell to divide only upon reaching the predefined mtDNA copy number. This way, when a daughter cell is created, it is allowed to first grow and replicate its content, before proceeding to division.

To account for the fission and fusion events in mitochondria, we establish the *nspl* parameter, defining the number of fragments every mitochondrial sequence splits into. This fragmentation leads to a reshuffling of the mtDNA copies within each mitochondrion, mimicking the fission-fusion dynamics. Upon this shuffling process, all fragments refuse and each cell is allowed to divide, by splitting into two parts. We also define a second variable *ndau* for the number of copies a mother cell gives to the daughter per division. We set the maximum *ndau* value to always be half of the total number of copies in the given founder cell. For example, in the simulations with increased copy number, where $n = 56$ or $n = 90$ copies/cell, each daughter cell could inherit a maximum of 28 or 45 copies, respectively. The *ndau* parameter, along with the *nspl*, are the only model parameters to be fitted to the data. Specifically, we first fit a sigmoid curve to the experimental heteroplasmy values at six timepoints ($t = 1.5$, 3, 4.5, 6, 7.5 h) and then identified the best-fitting pairs (*ndau*, *nspl*), using least-squares fitting.

Data analysis

Data analysis and statistics were performed in Python and the in silico mathematical modeling was constructed using R. A dependent two-sided *t*-test (scipy.stats.ttest_rel) was chosen for related lineage data (Fig. 5B). An independent two-sided *t*-test (scipy.stats.ttest_ind) was chosen for all data derived from independent samples (Fig. 5G,H). All scripts are provided in a GitHub repository under https://github.com/statgenlmu/yeast_mito_segregation.

Data availability

This study includes no data deposited in external repositories. Scripts and code for data analysis are deposited in the GitHub repository under https://github.com/statgenlmu/yeast_mito_segregation.

The source data of this paper are collected in the following database record: biostudies:S-SCDT-10_1038-S44318-024-00183-5.

Expanded view data, supplementary information, appendices are available for this paper at https://doi.org/10.1038/s44318-024-00183-5.

Peer review information

A peer review file is available at https://doi.org/10.1038/s44318-024-00183-5

References

Alber AB, Paquet ER, Biserni M, Naef F, Suter DM (2018) Single live cell monitoring of protein turnover reveals intercellular variability and cell-cycle dependence of degradation rates. Mol Cell 71:1079–1091.e9

Aryaman J, Bowles C, Jones NS, Johnston IG (2019) Mitochondrial network state scales mtDNA genetic dynamics. Genetics 212:1429–1443

Ashley MV, Laipis PJ, Hauswirth WW (1989) Rapid segregation of heteroplasmic bovine mitochondria. Nucleic Acids Res 17:7325–7331

Birky CW (1994) Relaxed and stringent genomes: why cytoplasmic genes don't obey Mendel's laws. J Heredity 85:355–365

Birky J (2001) The inheritance of genes in mitochondria and chloroplasts: laws, mechanisms, and models. Annu Rev Genet 35:125–148

Bunk D, Moriasy J, Thoma F, Jakubke C, Osman C, Hörl D (2022) YeastMate: neural network-assisted segmentation of mating and budding events in *S. cerevisiae*. Bioinformatics 38:2667–2669

Burgstaller JP, Kolbe T, Havlicek V, Hembach S, Poulton J, Piálek J, Steinborn R, Rülicke T, Brem G, Jones NS et al (2018) Large-scale genetic analysis reveals mammalian mtDNA heteroplasmy dynamics and variance increase through lifetimes and generations. Nat Commun 9:2488

Cao L, Shitara H, Sugimoto M, Hayashi JI, Abe K, Yonekawa H (2009) New evidence confirms that the mitochondrial bottleneck is generated without reduction of mitochondrial DNA content in early primordial germ cells of mice. PLoS Genet 5:e1000756

Chen XJ, Butow RA (2005) The organization and inheritance of the mitochondrial genome. Nat Rev Genet 6:815–25

Cree LM, Samuels DC, de Sousa Lopes SC, Rajasimha HK, Wonnapinij P, Mann JR, Dahl H-HM, Chinnery PF (2008) A reduction of mitochondrial DNA molecules during embryogenesis explains the rapid segregation of genotypes. Nat Genet 40:249–254

Dujon B, Slonimski PP, Weill L (1974) Mitochondrial genetics IX: a model for recombination and segregation of mitochondrial genomes in saccharomyces cerevisiae. Genetics 78:415–437

Floros VI, Pyle A, Dietmann S, Wei W, Tang WCW, Irie N, Payne B, Capalbo A, Noli L, Coxhead J et al (2018) Segregation of mitochondrial DNA heteroplasmy through a developmental genetic bottleneck in human embryos. Nat Cell Biol 20:144–151

Glastad RC, Johnston IG (2023) Mitochondrial network structure controls cell-to-cell mtDNA variability generated by cell divisions. PLoS Comput Biol 19:e1010953

Göke A, Schrott S, Mizrak A, Belyy V, Osman C, Walter P (2020) Mrx6 regulates mitochondrial DNA copy number in S. cerevisiae by engaging the evolutionarily conserved Lon protease Pim1. Mol Biol Cell 31:511–723

Gruschke S, Kehrein K, Römpler K, Gröne K, Israel L, Imhof A, Herrmann JM, Ott M (2011) Cbp3-Cbp6 interacts with the yeast mitochondrial ribosomal tunnel exit and promotes cytochrome b synthesis and assembly. J Cell Biol 193:1101–14

Hill JH, Chen Z, Xu H (2014) Selective propagation of functional mitochondrial DNA during oogenesis restricts the transmission of a deleterious mitochondrial variant. Nat Genet 46:389–92

Iborra FJ, Kimura H, Cook PR (2004) The functional organization of mitochondrial genomes in human cells. BMC Biol 14:1–14

Jajoo R, Jung Y, Huh D, Viana MP, Rafelski SM, Springer M, Paulsson J (2016) Accurate concentration control of mitochondria and nucleoids. Science 351:169–72

Jakubke C, Roussou R, Maiser A, Schug C, Thoma F, Bunk D, Hörl D, Leonhardt H, Walter P, Klecker T et al (2021) Cristae-dependent quality control of the mitochondrial genome. Sci Adv 7:eabi8886

Janke C, Magiera MM, Rathfelder N, Taxis C, Reber S, Maekawa H, Moreno-Borchart A, Doenges G, Schwob E, Schiebel E et al (2004) A versatile toolbox for PCR-based tagging of yeast genes: new fluorescent proteins, more markers and promoter substitution cassettes. Yeast 21:947–62

Johnston IG (2019) Varied mechanisms and models for the varying mitochondrial bottleneck. Front Cell Dev Biol 7:294

Johnston IG, Burgstaller JP, Havlicek V, Kolbe T, Rülicke T, Brem G, Poulton J, Jones NS (2015) Stochastic modelling, Bayesian inference, and new in vivo measurements elucidate the debated mtDNA bottleneck mechanism. Elife 4:e07464

Kauppila TES, Kauppila JHK, Larsson N-G (2017) Mammalian mitochondria and aging: an update. Cell Metab 25:57–71

Koren A, Soifer I, Barkai N (2010) MRC1-dependent scaling of the budding yeast DNA replication timing program. Genome Res 20:781–790

Kotrys AV, Durham TJ, Guo XA, Vantaku VR, Parangi S, Mootha VK (2024) Single-cell analysis reveals context-dependent, cell-level selection of mtDNA. Nature 629:458–466

Kowald A, Kirkwood TBL (2011) Evolution of the mitochondrial fusion-fission cycle and its role in aging. Proc Natl Acad Sci USA 108:10237–10242

Kukat C, Wurm CA, Spåhr H, Falkenberg M, Larsson N, Jakobs S (2011) Super-resolution microscopy reveals that mammalian mitochondrial nucleoids have a uniform size and frequently contain a single copy of mtDNA. Proc Natl Acad Sci USA 108:13534–13539

Lee HS, Ma H, Juanes RC, Tachibana M, Sparman M, Woodward J, Ramsey C, Xu J, Kang EJ, Amato P et al (2012) Rapid mitochondrial DNA segregation in primate preimplantation embryos precedes somatic and germline bottleneck. Cell Rep 1:506–515

Leonard PJ, Rathod PK, Golin J (1994) Loss of function mutation in the yeast multiple drug resistance gene PDR5 causes a reduction in chloramphenicol efflux. Antimicrob Agents Chemother 38:2492–2494

Lewis SC, Uchiyama LF, Nunnari J (2016) ER-mitochondria contacts couple mtDNA synthesis with mitochondrial division in human cells. Science 353:aaf5549

Lieber T, Jeedigunta SP, Palozzi JM, Lehmann R, Hurd TR (2019) Mitochondrial fragmentation drives selective removal of deleterious mtDNA in the germline. Nature 570:380–384

Ma H, Xu H, O'Farrell PH (2014) Transmission of mitochondrial mutations and action of purifying selection in Drosophila melanogaster. Nat Genet 46:393–397

Murley A, Lackner LL, Osman C, West M, Voeltz GK, Walter P, Nunnari J (2013) ER-associated mitochondrial division links the distribution of mitochondria and mitochondrial DNA in yeast. Elife 2:e00422

Nunnari J, Marshall WF, Straight A, Murray A, Sedat JW, Walter P (1997) Mitochondrial transmission during mating in Saccharomyces cerevisiae is determined by mitochondrial fusion and fission and the intramitochondrial segregation of mitochondrial DNA. Mol Biol Cell 8:1233–42

Okamoto K, Perlman PS, Butow RA (1998) The sorting of mitochondrial DNA and mitochondrial proteins in zygotes: preferential transmission of mitochondrial DNA to the medial bud. J Cell Biol 142:613–23

Olivo PD, Van De Walle MJ, Laipis PJ, Hauswirth WW (1983) Nucleotide sequence evidence for rapid genotypic shifts in the bovine mitochondrial DNA D-loop. Nature 306:400–402

Osman C, Noriega TR, Okreglak V, Fung JC, Walter P (2015) Integrity of the yeast mitochondrial genome, but not its distribution and inheritance, relies on mitochondrial fission and fusion. Proc Natl Acad Sci USA 112:E947–956

Otten ABC, Theunissen TEJ, Derhaag JG, Lambrichs EH, Boesten IBW, Winandy M, van Montfoort APA, Tarbashevich K, Raz E, Gerards M et al (2016) Differences in strength and timing of the mtDNA bottleneck between zebrafish germline and non-germline cells. Cell Rep 16:622–630

Padovani F, Mairhörmann B, Falter-Braun P, Lengefeld J, Schmoller KM (2022) Segmentation, tracking and cell cycle analysis of live-cell imaging data with cell-ACDC. BMC Biol 20:174

Park CB, Larsson N-G (2011) Mitochondrial DNA mutations in disease and aging. J Cell Biol 193:809–18

Rafelski SM, Viana MP, Zhang Y, Chan Y-HM, Thorn KS, Yam P, Fung JC, Li H, da F Costa L, Marshall WF (2012) Mitochondrial network size scaling in budding yeast. Science 338:822–4

Schrott S, Osman C (2023) Two mitochondrial HMG-box proteins, Cim1 and Abf2, antagonistically regulate mtDNA copy number in *Saccharomyces cerevisiae*. Nucleic Acids Res 51:11813–11835

Seel A, Padovani F, Mayer M, Finster A, Bureik D, Thoma F, Osman C, Klecker T, Schmoller KM (2023) Regulation with cell size ensures mitochondrial DNA homeostasis during cell growth. Nat Struct Mol Biol 30:1549–1560

Sia RA, Carrol S, Kalifa L, Hochmuth C, Sia EA (2009) Loss of the mitochondrial nucleoid protein, Abf2p, destabilizes repetitive DNA in the yeast mitochondrial genome. Genetics 181:331–334

Spelbrink JN (2010) Functional organization of mammalian mitochondrial DNA in nucleoids: history, recent developments, and future challenges. IUBMB Life 62:19–32

Stewart JB, Chinnery PF (2021) Extreme heterogeneity of human mitochondrial DNA from organelles to populations. Nat Rev Genet 22:106–118

Stewart JB, Larsson N-G (2014) Keeping mtDNA in shape between generations. PLoS Genet 10:e1004670

Strausberg RL, Perlman PS (1978) The effect of zygotic bud position on the transmission of mitochondrial genes in *Saccharomyces cerevisiae*. Mol Gen Genet 163:131–44

Tam ZY, Gruber J, Halliwell B, Gunawan R (2013) Mathematical modeling of the role of mitochondrial fusion and fission in mitochondrial DNA maintenance. PLoS ONE 8:e76230

Wai T, Teoli D, Shoubridge EA (2008) The mitochondrial DNA genetic bottleneck results from replication of a subpopulation of genomes. Nat Genet 40:1484–1488

Wei W, Tuna S, Keogh MJ, Smith KR, Aitman TJ, Beales PL, Bennett DL, Gale DP, Bitner-GlindziczÃ¢ MAK, Black GC et al (2019) Germline selection shapes human mitochondrial DNA diversity. Science 364:eaau6520

Zelenaya-Troitskaya O, Newman SM, Okamoto K, Perlman PS, Butow RA (1998) Functions of the high mobility group protein, Abf2p, in mitochondrial DNA segregation, recombination and copy number in Saccharomyces cerevisiae. Genetics 148:1763–1776

Acknowledgements

We thank Nadja Lebedeva and Johannes Hagen for their technical assistance. Appreciation is extended to all members of the Osman and Mokranjac groups for providing constructive feedback. Furthermore, we are grateful for the enriching discussions within the “Mito-Club”. This work was funded by a European Research Council Starting Grant (ERCStG-714739 IlluMitoDNA), a Human Frontier Science Program Research Grant (RGP021/2023) and a DFG Research Grant (HO 7333/1).

Author contributions

Rodaria Roussou: Conceptualization; Data curation; Formal analysis; Investigation; Methodology; Writing—original draft; Writing—review and editing. **Dirk Metzler**: Conceptualization; Software; Formal analysis; Writing—original draft; Writing—review and editing. **Francesco Padovani**: Software; Writing—review and editing. **Felix Thoma**: Formal analysis; Investigation; Methodology. **Rebecca Schwarz**: Formal analysis; Investigation. **Boris Shraiman**: Conceptualization. **Kurt M Schmoller**: Conceptualization; Software; Supervision; Funding acquisition; Writing—original draft; Writing—review and editing. **Christof Osman**: Conceptualization; Resources; Supervision; Funding acquisition; Methodology; Writing—original draft; Project administration; Writing—review and editing.

Source data underlying figure panels in this paper may have individual authorship assigned. Where available, figure panel/source data authorship is listed in the following database record: biostudies:S-SCDT-10_1038-S44318-024-00183-5.

Funding

Open Access funding enabled and organized by Projekt DEAL.

Disclosure and competing interests statement

The authors declare no competing interests.

Expanded View Figures

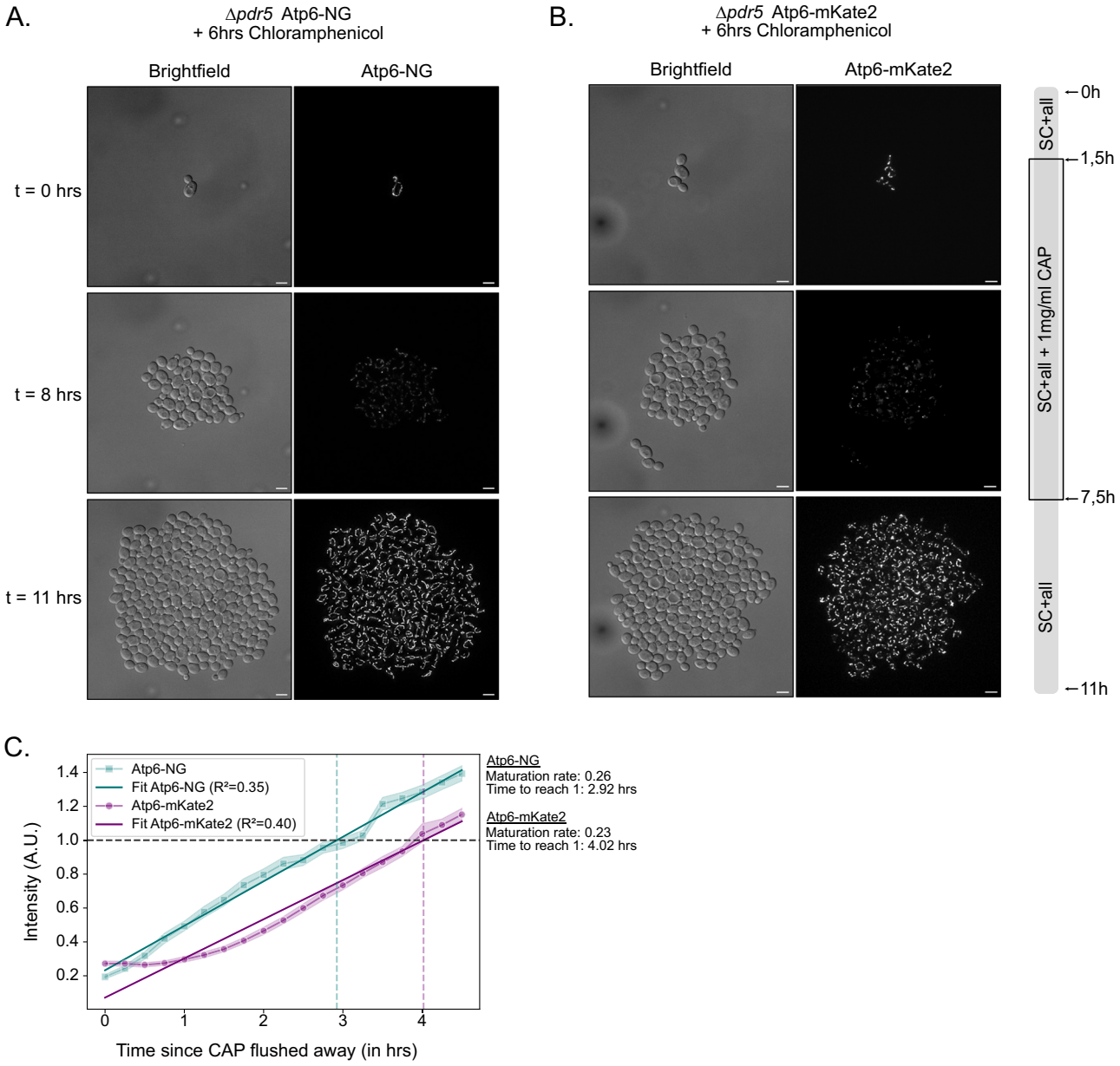

Figure EV1. mtDNA$^{Atp6\text{-}NG}$ and mtDNA$^{Atp6\text{-}mKate2}$ strains with temporary exposure to chloramphenicol.

(**A**, **B**) Yeast cells harboring mtDNA$^{Atp6\text{-}NG}$ (**A**) or mtDNA$^{Atp6\text{-}mKate2}$ (**B**) were imaged for 11 h ($N = 3$/strain). Chloramphenicol (1 mg/ml) was added after the first cell duplication, i.e., after 1.5 h of imaging, and was removed from the microfluidic chamber after 6 h of incubation. Fluorescence images are maximum-intensity projections of z-stacks, after deconvolution. Scale bars: 5 µm. (**C**) Line graph showing the fluorescent intensities of cells expressing Atp6-NG (cyan) or Atp6-mKate2 (magenta) upon washing off the Chloramphenicol (see Fig. 2F) after incubation with 1 mg/ml CAP for 6 h for sufficient mitochondrial translation inhibition. Curve fitting on the fluorescent intensity lines upon washing off the drug provides the maturation timings of the two Atp6 variants. Data represent the mean of all replicates per strain, and the shaded areas represent the 95% confidence interval. Fluorescent intensities were normalized to the cells at the first timepoint, for either of the fluorescent channels.

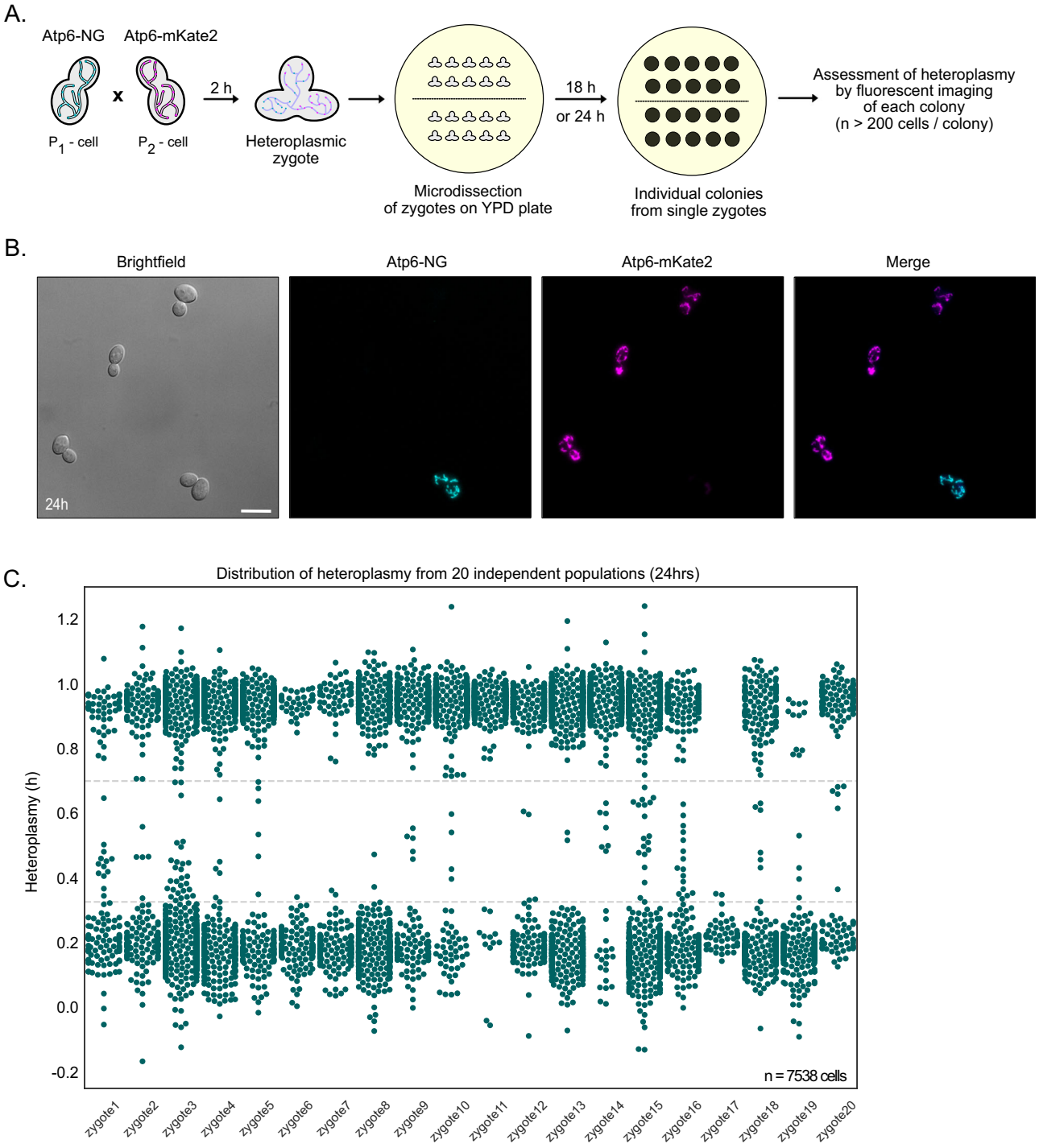

Figure EV2. 24-h heteroplasmy assessment from 20 independent populations.

(**A**) Schematic of the 24-h heteroplasmy assessment experiment. Cells harboring mtDNA$^{Atp6\text{-}NG}$ were mated with cells containing mtDNA$^{Atp6\text{-}mKate2}$ on a YPD plate. After a 2-h incubation, upon zygote formation, individual zygotes were micro-dissected and placed in different areas of a fresh YPD plate. Cells were kept for 24 h at 30 °C until colonies were formed. Cells from each colony, originating from a single zygote, were imaged to assess population homoplasmy levels, by calculating the proportion of cells exhibiting Atp6-NG and/or Atp6-mKate2 signal. (**B**) Representative image of a small field of view from one population, after 24 h. In total, 20 individual populations were screened, each originating from a diploid heteroplasmic zygote. Cells harboring mtDNA$^{Atp6\text{-}NG}$ are shown in cyan, while cells having kept the mtDNA$^{Atp6\text{-}mKate2}$ are depicted in magenta. Fluorescence images are maximum-intensity projections of z-stacks, after deconvolution. Scale bars: 5 µm. (**C**) Heteroplasmy distributions from all 20 independent diploid populations after 24 h of growth on the YPD plate ($N = 20$ zygotes/$n > 200$ cells/colony). Each dot represents a single cell. Heteroplasmy values below 0.33 or above 0.71, the homoplasmy thresholds, represent cells harboring mainly mtDNA$^{Atp6\text{-}NG}$ or mtDNA$^{Atp6\text{-}mKate2}$, respectively. As apparent from the graph, some cells for each population still exhibit a heteroplasmic state, which is evident from a h-value between 0.33 and 0.71.

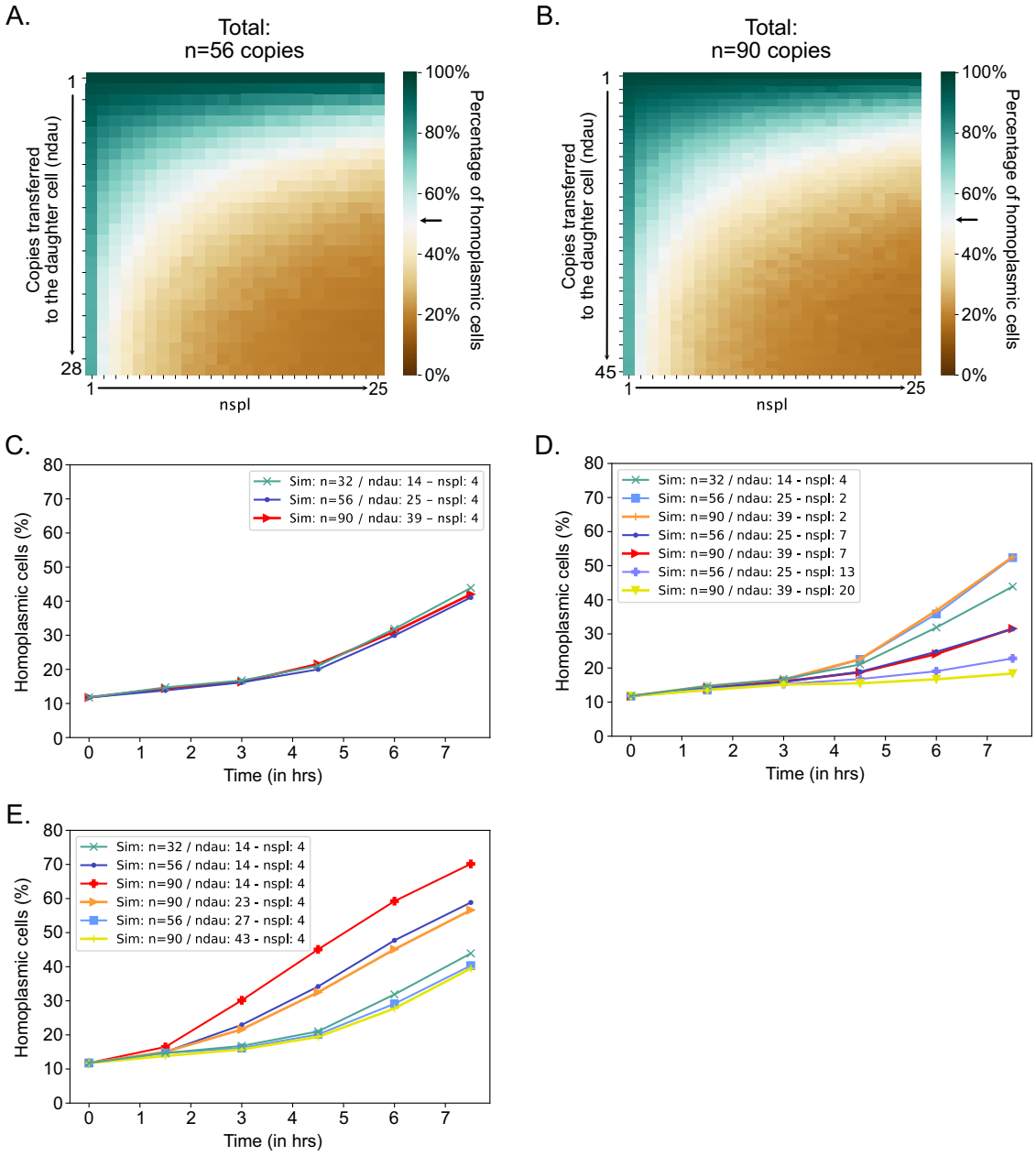

Figure EV3. Simulations of homoplasmy establishment in cell populations with increased mtDNA copy number.

(**A**) Heatmap showing the percentage of homoplasmic cells at timepoint $t = 7.5$ h, for different *ndau* and *nspl* pairs, for $n = 56$ mtDNA copies. The maximum value of *ndau* is defined by the half ($n = 28$) of the total mtDNA copies in the founder cell ($n = 56$). The arrow indicates the proportion (50%) of cells being virtually homoplasmic in the empirical data, based on the pre-established homoplasmy cutoffs. Each simulation with any given combination of the two parameters has been run ten times. (**B**) Heatmap showing the percentage of homoplasmic cells at timepoint $t = 7.5$ h, for different *ndau* and *nspl* pairs, for $n = 90$ mtDNA copies. The maximum value of *ndau* is defined by half ($n = 45$) of the total mtDNA copies in the founder cell ($n = 90$). The arrow indicates the proportion (50%) of cells being virtually homoplasmic in the empirical data, based on the pre-established homoplasmy cutoffs. Each simulation with any given combination of the two parameters has been run ten times. (**C**) Percentage of homoplasmic cells in simulated cell populations with $n = 32$ copies, relative to populations with $n = 56$ copies or $n = 90$ copies/cell. The number of copies transferred to the daughter cell (*ndau*) has been kept proportional to the total copy number in each of the simulations, that is 44\% of the total copies gets transferred to the daughter cell. The parameter *nspl* has been kept identical. (**D**) Percentage of homoplasmic cells in simulated cell populations with $n = 32$ copies, relative to populations with $n = 56$ copies or $n = 90$ copies/cell, with varying *nspl* values. The *ndau* parameter is proportional to the total copy number (44%), while the *nspl* parameter varies from low to high values per simulation. A comparison of these curves demonstrates the effect of lower or higher fission-fusion frequencies on the speed of segregation. The combination of $ndau = 14$ and $nspl = 4$ in cells with $n = 32$ copies is used as a point of reference, across all plots. (**E**) Percentage of homoplasmic cells in simulated cell populations with $n = 32$ copies, relative to populations with $n = 56$ copies or $n = 90$ copies/cell, with identical *nspl* values, and different levels of *ndau*. Comparison of these curves demonstrates the effect of lower or higher numbers of mtDNA copies being transferred to the daughter cells on the speed of segregation. The combination of $ndau = 14$ and $nspl = 4$ in cells with $n = 32$ copies is used as a point of reference, across all plots.

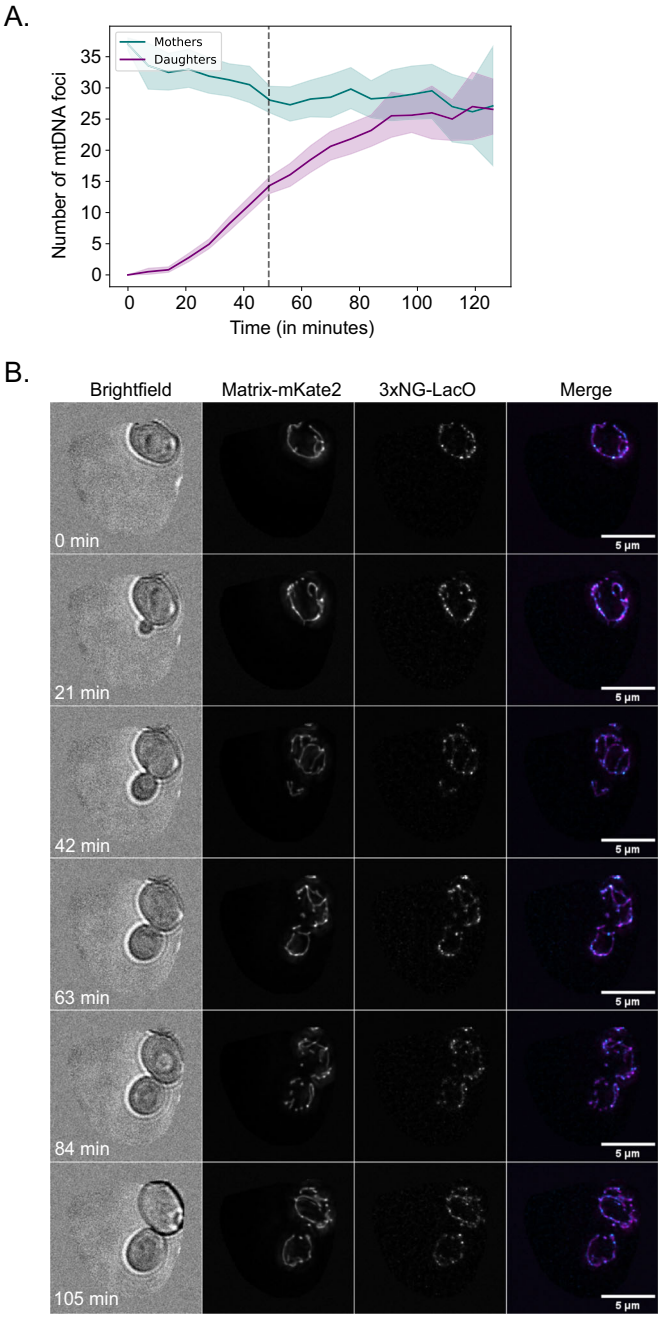

Figure EV4. Number of mtDNA foci in mother-daughter pairs during a complete cell cycle.

(**A**) Diploid cells expressing mitochondrially targeted 3xNG-LacI and mKate2 were harvested at the log phase and imaged for 2 h. The number of mtDNA foci were counted in virgin mothers (M) and their emerging daughters (D) ($n = 59$ M-D pairs). The dashed line represents the average period of time ($t = 47.5$ min) that mitochondrial content was exchanged between mothers and daughters, as shown in Fig. 5D. (**B**) Example time-lapse images of a virgin mother and its emerging bud. All cells express mitochondrially targeted 3xNG-LacI, used for visualizing the LacO-mtDNA foci, and mitochondrially targeted mKate2 to visualize the mitochondrial network. Mother-daughter pairs were cropped manually prior to segmentation and analysis.

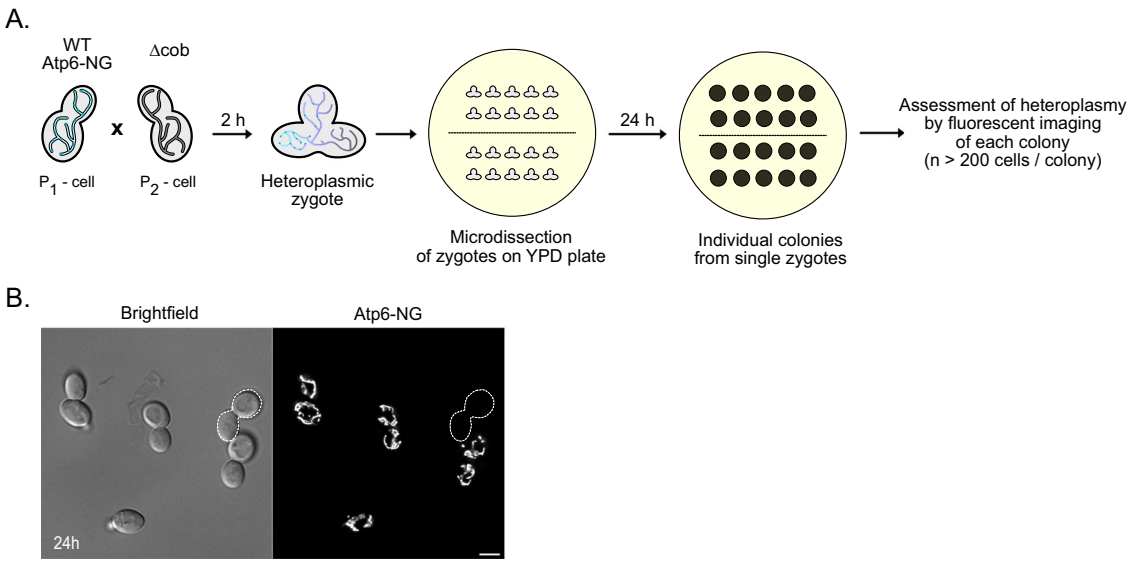

Figure EV5. 24-hr heteroplasmy assessment in colonies with competing mtDNA qualities.

(**A**) Schematic of the 24 h heteroplasmy assessment experiment of matings between cells harboring intact or mutant mtDNA. Cells harboring intron-containing mtDNA$^{Atp6\text{-}NG}$ were mated with cells containing intronless mtDNA$^{il\text{-}\Delta cob}$ on a YPD plate. After a 2 h incubation, upon zygote formation, individual zygotes were micro-dissected and placed in different areas of a fresh YPD plate. Cells were kept for 24 h at 30 °C until colonies had formed. Cells from each colony, originating from a single zygote, were imaged to assess the percentage of cells with fluorescent (mtDNA$^{Atp6\text{-}NG}$) or 'dark' (*mtDNA*$^{il\text{-}\Delta cob}$) mitochondria. (**B**) Representative image of a small field-of-view from one population, after 24 h. Diploid cells harboring mtDNA$^{Atp6\text{-}NG}$ are exhibiting fluorescence, while 'dark' cells (indicated by a white outline) do not contain mtDNA$^{Atp6\text{-}NG}$. Fluorescence images are maximum-intensity projections of z-stacks, after deconvolution. Scale bars: 5 μm.

Appendix

Real-time assessment of mitochondrial DNA heteroplasmy dynamics at the single-cell level

Rodaria Roussou et al.

*Corresponding author: osman@bio.lmu.de

Contents

Appendix Figure S1

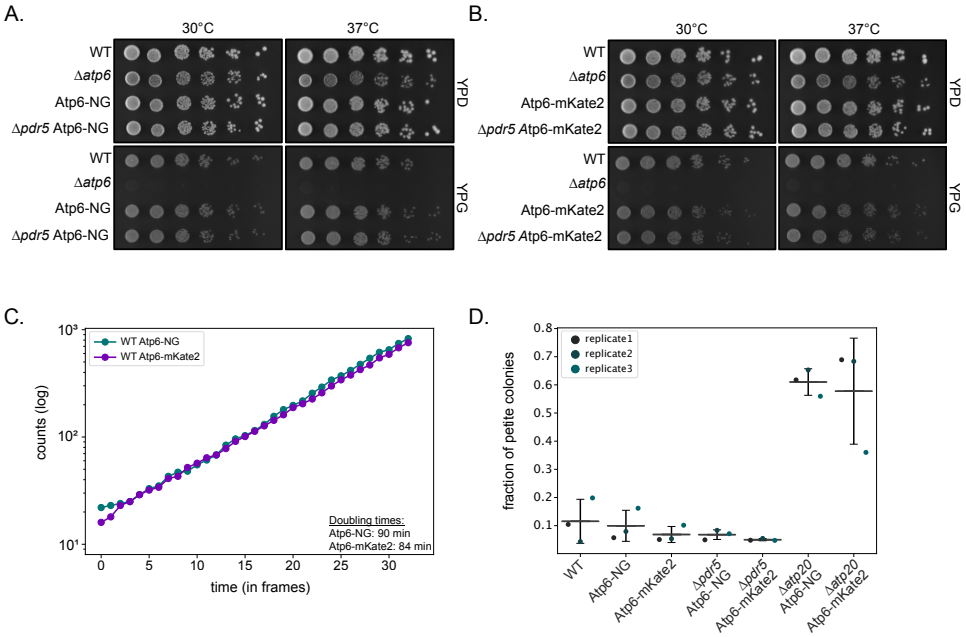

Growth and petite frequency of mtDNA$^{\text{Atp6-NG}}$ and mtDNA$^{\text{Atp6-mKate2}}$ strains. (A, B) Drop dilution growth analyses of strains harboring mtDNA$^{\text{Atp6-NG}}$ (A) or mtDNA$^{\text{Atp6-mKate2}}$ (B). Serial dilutions of the indicated strains were spotted on rich medium containing glucose or glycerol as carbon sources and incubated at 30°C or 37°C. **(C)** Growth curves of Atp6-NG and Atp6-mKate2 strains were assessed from timelapse microscopy data of 8-hr recordings (N=6/strain). Cell amounts were derived by segmentation of brightfield images in 15 min intervals. Cell amounts are depicted on the y axis in log scale. **(D)** Petite frequency of indicated strains (n=3). The Δ*atp20* strains, known to have elevated petite levels, were used as controls.

Appendix Figure S2

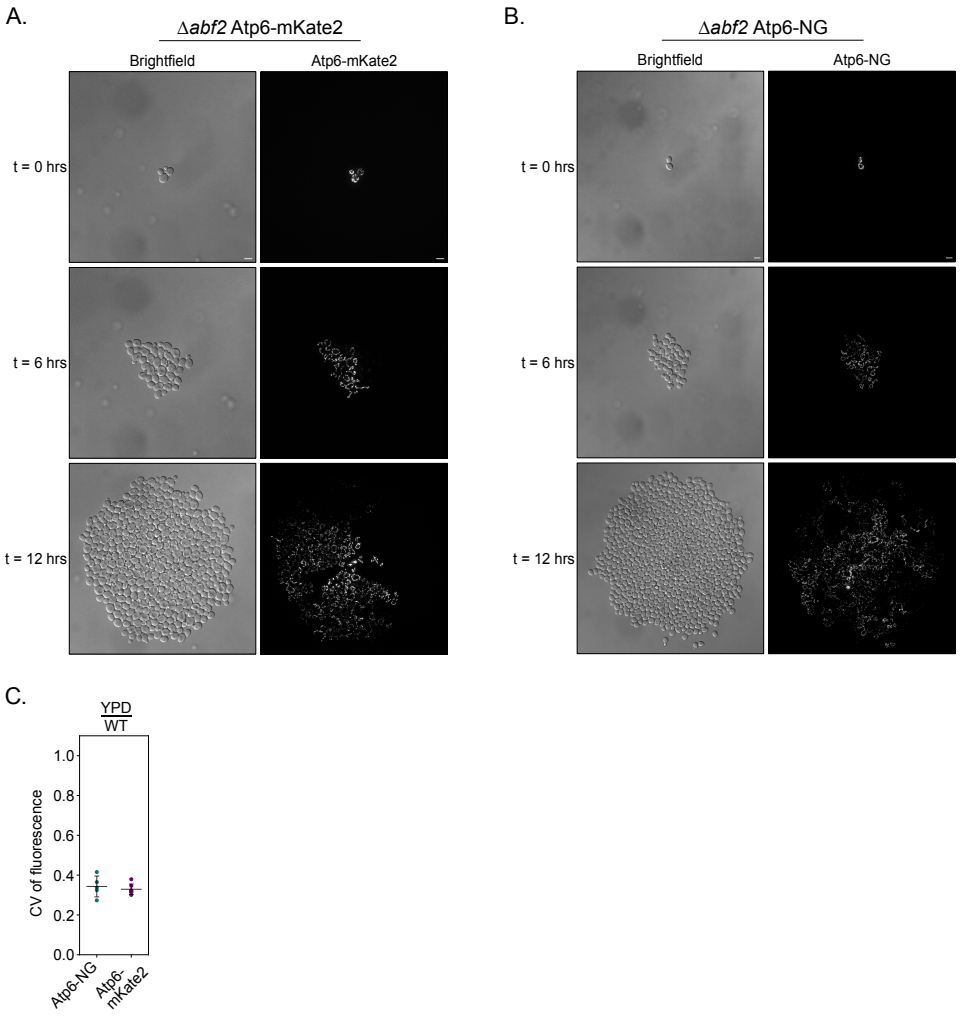

Expression of Atp6-NG and Atp6-mKate2 in Δ*abf2* cells over time. (A, B) Representative images from Δ*abf2* cells expressing (A) Atp6-NG or (B) Atp6-mKate2 (N=3/strain). Cells were imaged for 12 hrs, and three different timepoints are shown (t = 0, 6 and 12 hrs). Cells were first grown in YPG and maintained in minimal media during the microfluidic imaging, to assess mtDNA loss. Fluorescence images are maximum intensity projections

of z-stacks, after deconvolution. Scale bars: 5 μm. **(C)** Coefficient of variation (CV) of fluorescence calculated at the final timepoint of imaging for strains, harboring mtDNA$^{\text{Atp6-NG}}$ or mtDNA$^{\text{Atp6-mKate2}}$ (N=6/strain). Strains were pre-grown in glucose-containing media (YPD).

Appendix Figure S3

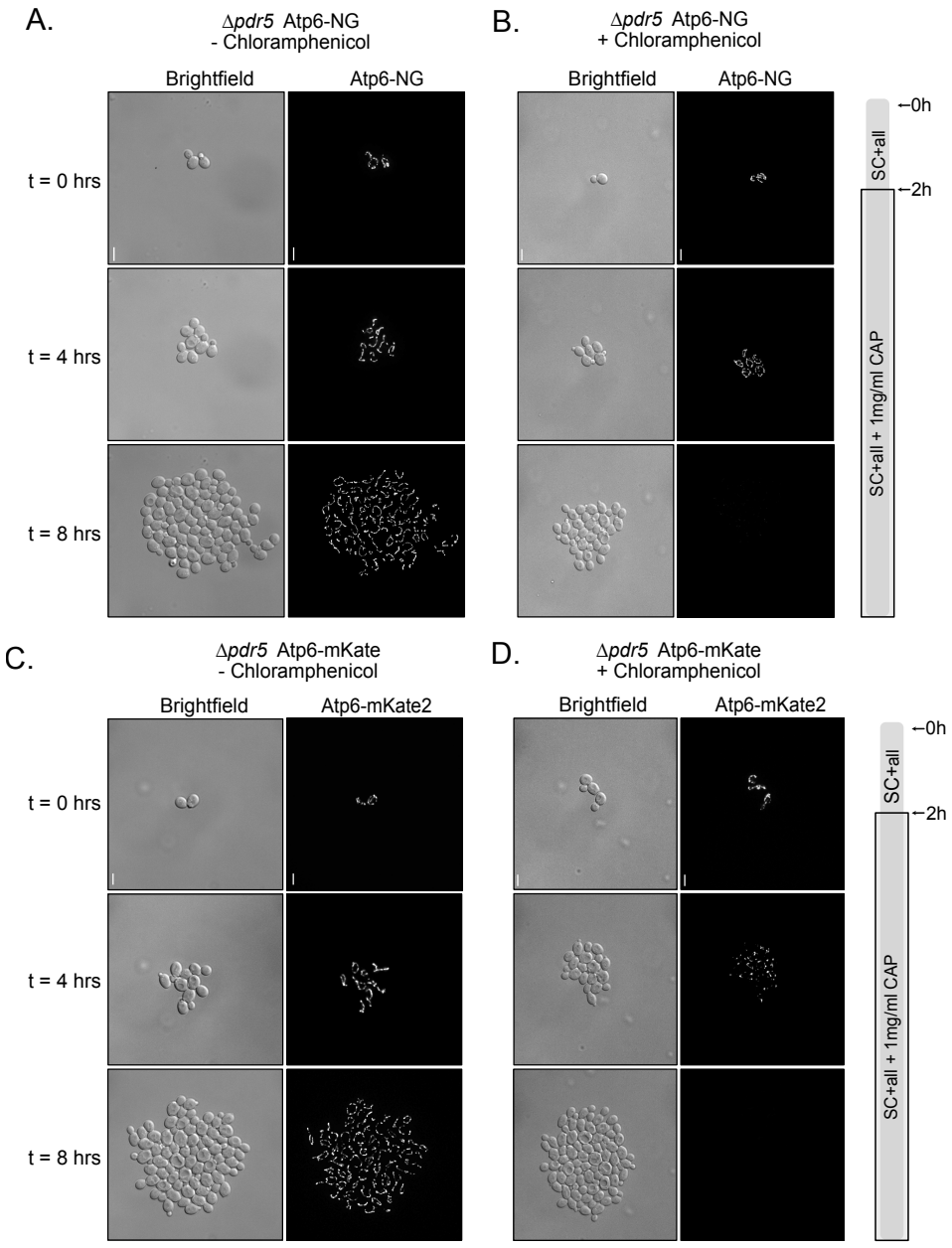

mtDNA$^{\text{Atp6-NG}}$ and mtDNA$^{\text{Atp6-mKate2}}$ strains with and without treatment with Chloramphenicol (CAP). (A, B, C, D) Representative images of Δ*pdr5* cells harboring mtDNA$^{\text{Atp6-NG}}$ (A, B) or mtDNA$^{\text{Atp6-mKate2}}$ (C, D). Cells were imaged for 8 hrs and fresh minimal media was provided throughout each experiment with (B, D) or without (A, C) addition of CAP (1 mg/ml) after the first 2 hrs of recording (N=3/strain). Fluorescence images are maximum intensity projections of z-stacks, after deconvolution. Scale bars: 5 μm.

Appendix Figure S4

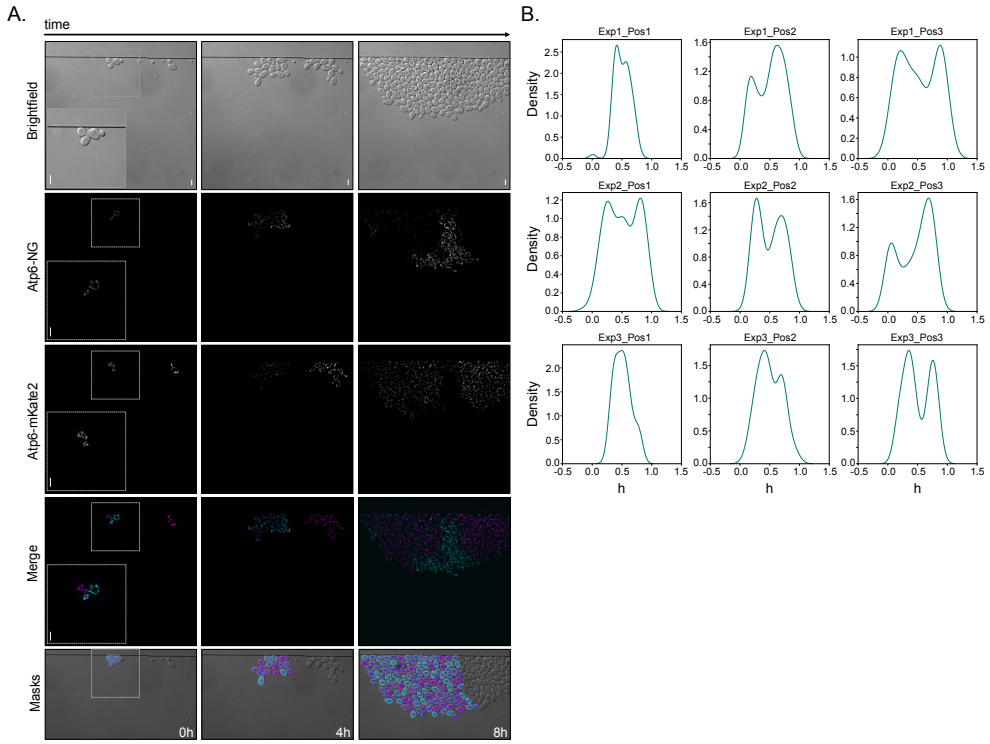

Heteroplasmy distribution amongst individual colonies. **(A)** The same representative images of Figure 3A, at timepoints 0h, 4h and 8 hrs, without histogram adjustment. Fluorescence images are maximum intensity projections of z-stacks, after deconvolution. Scale bars: 5 μm. **(B)** Heteroplasmy distribution from the last timepoint of each individual diploid population (N=9). An h-value of 0.5 represents a virtually absolute heteroplasmic state. Cells with h-values lower than 0.5 contain a higher proportion of mtDNA$^{\text{Atp6-NG}}$, while cells with h-values above 0.5 contain a higher proportion of mtDNA$^{\text{Atp6-mKate2}}$. Segregation can be observed across all independent populations, with cells distributed across two homoplasmic peaks. Notably, in three cases (Exp1Pos1, Exp3Pos1, Exp3Pos2) segregation is more subtle and the homoplasmic peaks less pronounced.

Appendix Figure S5

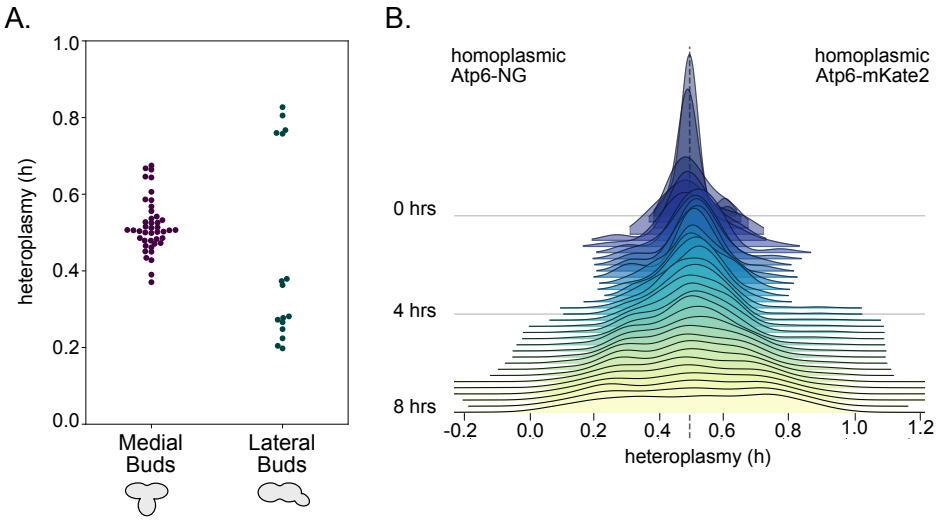

Heteroplasmy levels in medial and lateral buds. (A) Heteroplasmy values for medial and lateral buds from zygotes, assessed upon mating within the first 2hrs of growth in the microfluidic chamber. Each dot represents one single cell. Heteroplasmy (h) values below 0.33 or above 0.71, which are the homoplasmy thresholds, represent cells harboring mainly $\text{mtDNA}^{\text{Atp6-NG}}$ or $\text{mtDNA}^{\text{Atp6-mKate2}}$, respectively. **(B)** Joyplot of heteroplasmy levels of cells over time, from a total of nine populations, excluding all lateral buds and their progeny. All populations were derived from heteroplasmic zygotes across 8-hr timelapse recordings. The dashed line represents the virtually absolute heteroplasmy value of h=0.5.

Appendix Figure S6

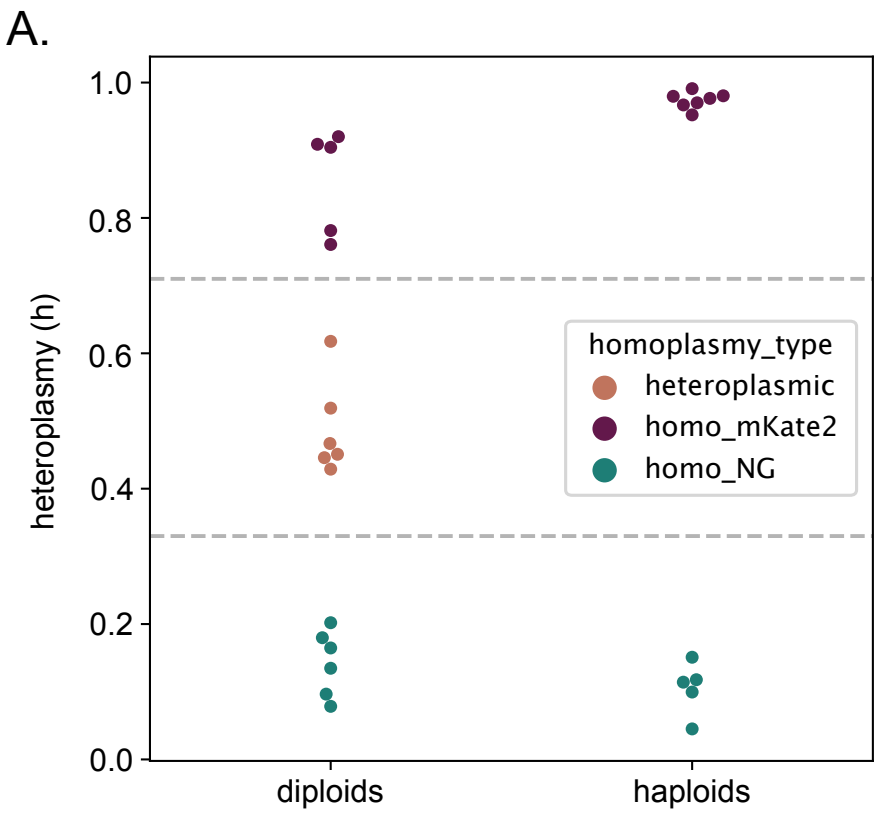

h-values of non-mated haploid cells present in timelapse videos of heteroplasmic diploid cells. (A) During recording of mtDNA heteroplasmy segregation in diploid populations over time, individual haploids cells that did not mate were also present in the same field of view. Diploid cells, classified as homoplasmic for either Atp6-NG or Atp6-mKate2, or still remaining heteroplasmic, were randomly selected from the final timepoint of the microfluidic videos, and their heteroplasmy values were compared to non-mated haploid homoplasmic cells. Application of the heteroplasmy equation places these haploid cells to the extremes of the heteroplasmy values, below 0.33 or above 0.71, comparable to diploid cells characterized as homoplasmic

based on the same homoplasmy thresholds. Each dot represents one single cell. Dashed lines indicate the homoplasmy thresholds, at h=0.33 and 0.71, respectively.

Appendix Figure S7

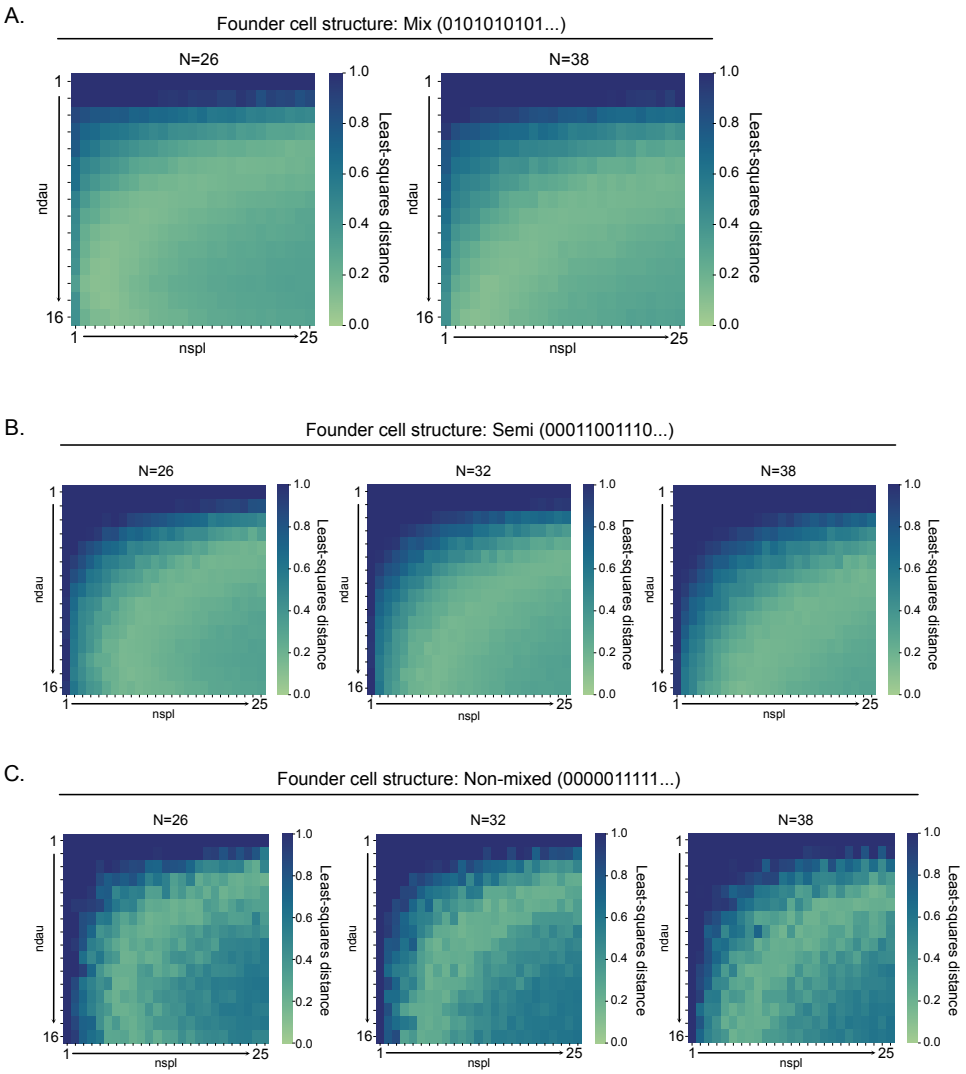

Robustness of the mtDNA segregation model. (A) Simulations for founder cell structure: mixed (0101010101..), and mildly varying the total number of mtDNA copies per cell. Heatmap shows the least-squares distance of simulations with a given pair of *ndau* and *nspl* parameters from the empirical data. Specifically, data represent two outcomes upon modeling

mtDNA segregation where the number of mtDNA molecules per cell prior to division is N=26 or N=38, respectively. *nspl* represents the number of sub-fragments the mother cell will break into , shuffle, and re-fuse prior to division, and *ndau* represents the number of mtDNA copies transferred to the daughter cell upon division. Higher values of the color gradient (blue) indicate larger distances, that is lower likelihood fitting to the data. Each simulation of any combination of parameters has been run 10 times, and the average least-squares distance was taken. **(B)**Simulations for founder cell structure: semi, and mildly varying the total number of mtDNA copies per cell. Heatmap shows the least-squares distance of simulations with a given pair of *ndau* and *nspl* parameters from the empirical data, with a different initial structure for the founder cell (semi: 1110001100011..). Specifically, data represent the outcomes of modeling mtDNA segregation with the number of mtDNA molecules per cell: N=26, N=32 or N=38, respectively. Robustness of the model was tested based on the similarity of the best hits upon varying the total number of copies per cell prior to division, as well as by altering structure of the founder cell. Each simulation of any combination of parameters has been run 10 times, and the average least-squares distance was taken. **(C)** Simulations for founder cell structure: non-mixed, and mildly varying the total number of mtDNA copies per cell. Heatmap shows the least-squares distance of simulations with a given pair of *ndau* and *nspl* parameters from the empirical data, with a different initial structure for the founder cell (non-mixed: 0000011111..). Specifically, data represent the outcomes of modeling mtDNA segregation with the number of mtDNA molecules per cell: N=26, N=32 or N=38, respectively. Robustness of the model was tested based on the similarity of the best hits upon varying the total number of copies per cell prior to division, as well as by altering the structure of the founder cell. Each simulation of any combination of parameters has been run 10 times, and the average least-squares distance was taken.

Appendix Figure S8

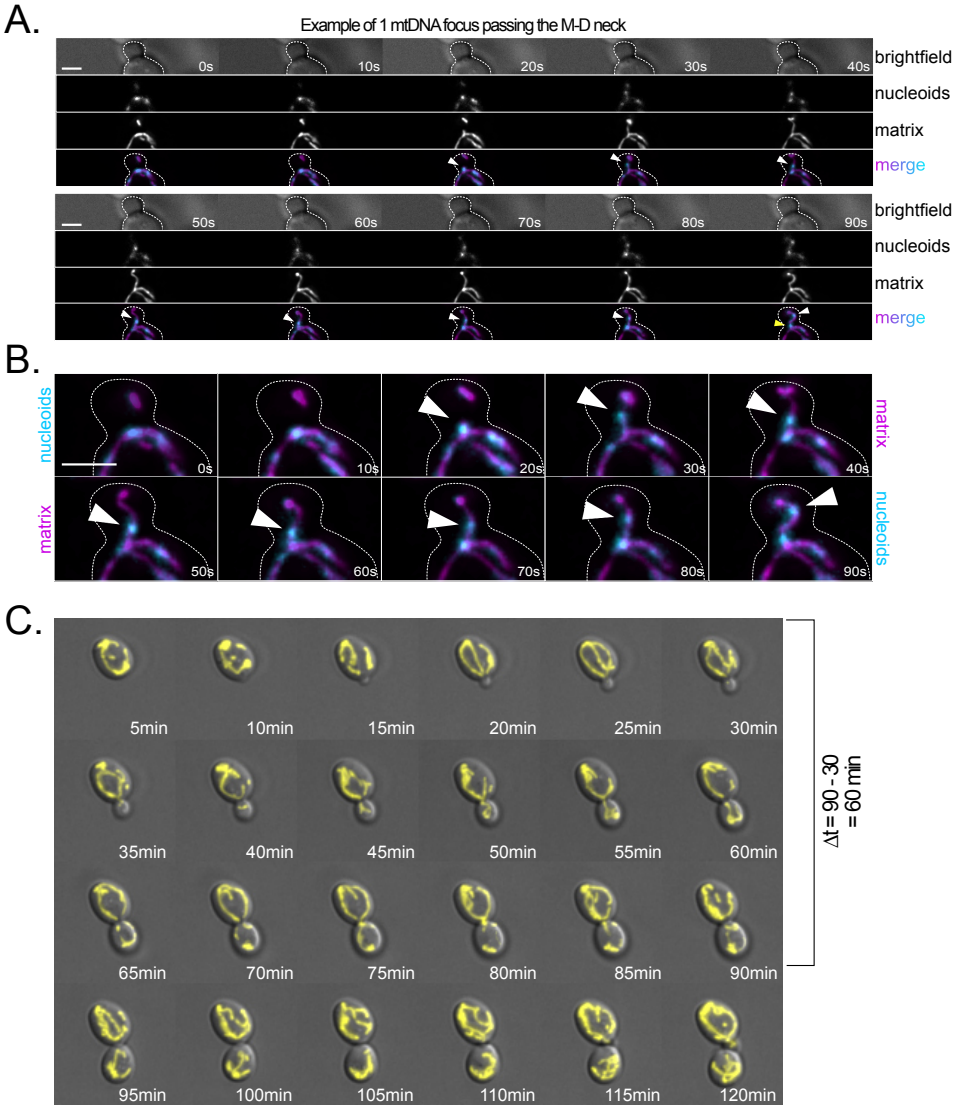

Inherited mtDNA foci and mitochondrial network connectivity of mother-bud pairs. (A) Representative images of one mother-bud pair in early S phase. Using the mtLacO-LacI system, each nucleoid is visible as a fluorescent foci, migrating across the bud-neck in the 5-minute window.

Nucleoids (cyan) are assumed to contain only one mtDNA copy. Mitochondrial network is shown in magenta. Log-phase cells from different cell cycle stages were examined (n=93 mother-bud pairs). Fluorescence images are maximum intensity projections of z-stacks, after deconvolution. Scale bars: 5 μm. **(B)** Enlarged images of the merge of S7A. Nucleoids represented in cyan, mitochondrial network in magenta. White arrows indicate one focus crossing the mother-bud neck. Scale bars: 5 μm. **(C)** Example timelapse images of a mother-bud pair with total mitochondrial network connectivity duration $\Delta t = 60$ minutes. Cells expressing the construct su9-matrix-mKate2 were used to visualize the mitochondrial network (yellow). Only cells in late G1 or early S phase were considered for the calculation, that is no visible bud by the start of imaging (n=33 cells).

Appendix Figure S9

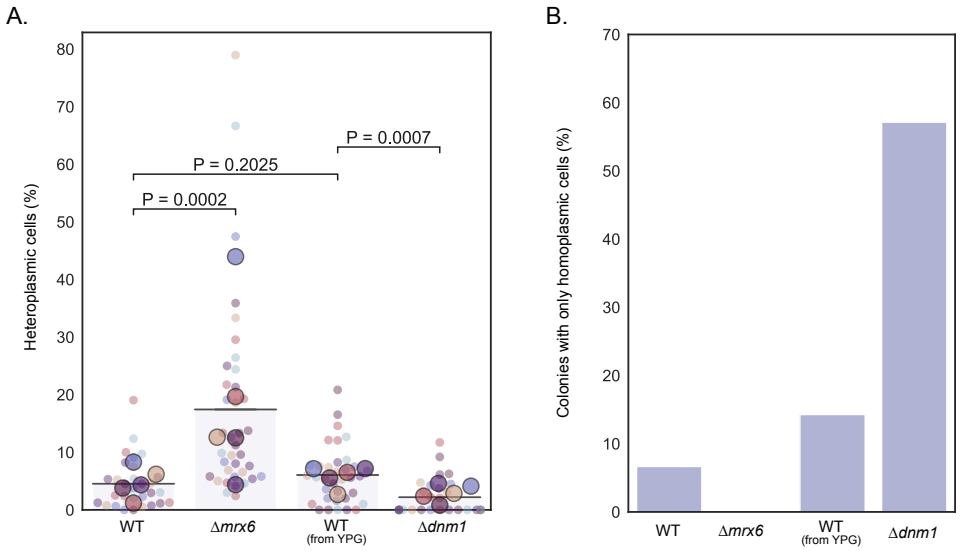

18-hr heteroplasmy assessment in Δ*mrx6* and Δ*dnm1* deletion strains. **(A)** Heteroplasmy levels in matings of Δ*mrx6* and Δ*dnm1* deletion strains. Cells with increased copy number (Δ*mrx6*) or fission-deficient (Δ*dnm1*) cells were generated in strains containing mtDNA$^{\text{Atp6-NG}}$ or mtDNA$^{\text{Atp6-mKate2}}$. After zygote formation and microdissection, diploid colonies were grown for 18 hrs on a YPD plate. Cells from each colony were imaged to assess the fraction of heteroplasmic cells (see also: Fig. S8). Of note, Δ*dnm1* cells were cultivated in YPG media, to prevent any mtDNA loss, before mating and dissection on YPD plates. For each genotype shown, the small dots represent the mean percentage of heteroplasmic cells in an individual colony (N>50 cells/colony). Each bigger dot depicts the mean of each biological replicate (N=5). The line represents the mean of all replicates for the corresponding mating. Statistical significance was determined by paired t-test. **(B)** Barplot of all populations derived from individual heteroplasmic zygotes, where no heteroplasmic cells were detected across all replicates, after 18 hrs. Mating of Δ*dnm1* cells resulted in a high percentage of populations, where only homoplasmic cells were detected. In contrast, for matings of

Δ*mrx6* cells, heteroplasmic cells were detected in all populations.

Appendix Table S1: Yeast Strains

Name	Genotype	Origin
yCO844	ade2-1 his3-11,15 trp1-1 leu2-3,112 ura3-1 CAN1 arg8::HIS3 MAT a (MR6)	Rak et al., 2006
yCO845	ade2-1 his3-11,15 trp1-1 leu2-3,112 ura3-1 CAN1 arg8::HIS3- Δ*atp6* MAT a (MR10)	Rak et al., 2006
yCO084	ade2-1 his3-11,15 trp1-1 leu2-3,112 ura3-1 CAN1 arg8::HIS3 ATP6-NeonGreen MAT alpha	Jakubke et al., 2021
yRR043	ade2-1 his3-11,15 trp1-1 leu2-3,112 ura3-1 CAN1 arg8::HIS3 ATP6-mKate2 MAT a	Jakubke et al., 2021
yFT019	leu2-3,112 can1-100 ura3-1 his3-11,15 Leu2-Pcup1-3xNG-LacI-PGK1-Su9-mKate2-Leu2 MAT a/alpha	this study
yRR195	ade2-1 his3-11,15 trp1-1 leu2-3,112 ura3-1 CAN1 arg8::HIS3 ATP6-NeonGreen Δ*pdr5*::Hyg MAT alpha	this study
yRR194	ade2-1 his3-11,15 trp1-1 leu2-3,112 ura3-1 CAN1 arg8::HIS3 ATP6-mKate2 Δ*pdr5*::Hyg MAT a	this study
yRR202	ade2-1 his3-11,15 trp1-1 leu2-3,112 ura3-1 CAN1 arg8::HIS3 ATP6-NeonGreen Δ*abf2*::Hyg MAT alpha	this study
yRR203	ade2-1 his3-11,15 trp1-1 leu2-3,112 ura3-1 CAN1 arg8::HIS3 ATP6-mKate2 Δ*abf2*::Hyg MAT a	this study
yRR187	ade2-1 his3-11,15 trp1-1 leu2-3,112 ura3-1 CAN1 arg8::HIS3 ATP6-NeonGreen Δ*dnm1*::Hyg MAT alpha	this study
yRR186	ade2-1 his3-11,15 trp1-1 leu2-3,112 ura3-1 CAN1 arg8::HIS3 ATP6-mKate2 Δ*dnm1*::Hyg MAT a	this study
yRR20	ade2-1 his3-11,15 trp1-1 leu2-3,112 ura3-1 CAN1 arg8::HIS3 ATP6-NeonGreen Δ*mrx6*::Nat MAT alpha	this study
yRR206	ade2-1 his3-11,15 trp1-1 leu2-3,112 ura3-1 CAN1 arg8::HIS3 ATP6-mKate2 Δ*mrx6*::Nat MAT a	this study
yCO354	ade2-1 his3-11,15 trp1-1 leu2-3,112 ura3-1 CAN1 arg8::HIS3 cob::ARG8M intronless mtDNA MAT alpha	Gruschke et al., 2011
yCO391	ade2-1 his3-11,15 trp1-1 leu2-3,112 ura3-1 CAN1 arg8::HIS3 intronless mtDNA MAT a	Gruschke et al., 2011

Appendix Table S2: Oligonucleotides

Name	Sequence	Purpose
CO2836	TTAAGTTTTCGTATCCGCTCGTTCGAAAGACTTT AGACAAAAATGCGTACGCTGCAGGTCGAC	PDR5 fwd (S1)
CO2837	CATCTTGGTAAGTTTCTTTTCTTAACCAAATTCA AAATTCTATTAATCGATGAATTCGAGCTCG	PDR5 rev (S2)
CO1158	GTAAACAGATTAACAAAGAAGCCAATCAATTACA ACAACAAATAACGTACGCTGCAGGTCGAC	ABF2 fwd (S1)
CO1159	ACGGAAAGAATAAAGGCATAAAAAACATTGTGAG AGTACCGCGGTATCGATGAATTCGAGCTCG	ABF2 rev (S2)
CO356	CATTAAGTAGCTACCAGCGAATCTAAATACGACG GATAAAGAATGCGTACGCTGCAGGTCGAC	DNM1 fwd (S1)
CO357	ACGCAATGTTGAAGTAAGATCAAAAATGAGATGA ATTATGCAATTAATCGATGAATTCGAGCTCG	DNM1 rev (S2)
CO870	TATGTCACATAATAGAGCAGTGGATAAGTACTCA ATGCAAAATCAATCGATGAATTCGAGCTCG	MRX6 fwd (S1)
CO914	AGATCATTGCAGAAGTAGTGAGATTTAGTCGTA CGTTACGTCATGCGTACGCTGCAGGTCGAC	MRX6 rev (S2)

Appendix Table S3: Plasmids

Name	Insert	Selection marker	Origin
pCO059	pFA6a-NatNT2	Nourseothricin	Janke et al., 2004
pCO021	pfa6a-kanMX6	G418	Janke et al., 2004
pCO074	pfa6a-hphNT1	Hygromycin	Janke et al., 2004
pCO494	pKT127-NeonGreen (Janke primers)	G418	Osman et al., 2015
pCO533	pKT127-mKate2 (Janke primers)	G418	Jakubke et al., 2021

Publication 2:
Cristae-dependent quality control of the mitochondrial genome

GENETICS

Cristae-dependent quality control of the mitochondrial genome

Christopher Jakubke[1,2†], Rodaria Roussou[1,2†], Andreas Maiser[1], Christina Schug[3], Felix Thoma[1,2], David Bunk[1], David Hörl[1], Heinrich Leonhardt[1], Peter Walter[4,5], Till Klecker[3], Christof Osman[1]*

Mitochondrial genomes (mtDNA) encode essential subunits of the mitochondrial respiratory chain. Mutations in mtDNA can cause a shortage in cellular energy supply, which can lead to numerous mitochondrial diseases. How cells secure mtDNA integrity over generations has remained unanswered. Here, we show that the single-celled yeast *Saccharomyces cerevisiae* can intracellularly distinguish between functional and defective mtDNA and promote generation of daughter cells with increasingly healthy mtDNA content. Purifying selection for functional mtDNA occurs in a continuous mitochondrial network and does not require mitochondrial fission but necessitates stable mitochondrial subdomains that depend on intact cristae morphology. Our findings support a model in which cristae-dependent proximity between mtDNA and the proteins it encodes creates a spatial "sphere of influence," which links a lack of functional fitness to clearance of defective mtDNA.

INTRODUCTION

Mitochondria contain their own genome, known as mitochondrial DNA (mtDNA), which in most organisms encodes core subunits of the respiratory chain and the adenosine triphosphate (ATP) synthase as well as transfer RNAs (tRNAs) and ribosomal RNAs (rRNAs) required for mitochondrial protein translation. Multiple copies of mtDNA are distributed throughout the mitochondrial network. Mutations in mtDNA can have detrimental consequences for mitochondrial function and can lead to a multitude of mitochondrial diseases, which have a prevalence of ~20 cases per 100,000 individuals (*1*). How cells maintain the integrity of mtDNA over generations, despite high mitochondrial mutation rates, has remained unclear. Studies in *Drosophila melanogaster* and mice have revealed that mutant copies of mtDNA are removed in the female germline in a process known as purifying selection (*2*–*4*). Mitochondrial fission has been proposed to contribute to this process in *D. melanogaster* (*5*, *6*). Generation of small mitochondrial fragments containing only one or a few mitochondrial genomes is believed to separate mtDNA copies from one another to prevent complementation of mutant mtDNA by gene products of intact mtDNA. Subsequently, mitochondrial fragments containing mutated mtDNA are proposed to be detected on the basis of a decreased membrane potential or ATP content and removed by mitophagy. In addition, it has been found that compromised protein import efficiency into damaged mitochondria leads to a decrease in mtDNA replication and hence disfavors propagation of mutated mtDNA copies (*3*, *7*). Despite this progress, many questions remain about the cellular mechanisms that facilitate selection against mutant mtDNA. By exploiting the possibility to genetically manipulate mtDNA in *Saccharomyces cerevisiae*, we establish budding yeast as a model system to study mtDNA quality control.

[1]Faculty of Biology, Ludwig-Maximilian-Universität München, 82152 Planegg-Martinsried, Germany. [2]Graduate School Life Science Munich, Planegg, Germany. [3]Zellbiologie, Universität Bayreuth, 95440 Bayreuth, Germany. [4]Howard Hughes Medical Institute and Department of Biochemistry and Biophysics, University of California, San Francisco, San Francisco, CA 94143, USA. [5]Department of Physiology, University of California, San Francisco, San Francisco, CA 94143, USA.
*Corresponding author. Email: osman@bio.lmu.de
†These authors contributed equally to this work.

RESULTS

A pedigree analysis reveals mtDNA quality control in *S. cerevisiae*

First, we asked whether the single-celled *S. cerevisiae* intracellularly distinguishes between intact and mutant mtDNA and supports generation of young progeny with a healthy mtDNA content. We devised an approach to genetically follow segregation of wild-type (WT) and mutant mtDNA copies from heteroplasmic single yeast cells. Two yeast strains of opposing mating types were used for this approach. The first strain is of mating type *a* and harbors WT mtDNA and a deletion of the nuclear-encoded *ARG8* gene that encodes the mitochondrially localized Arg8 protein and is required for synthesis of arginine. Therefore, this strain is able to grow on medium containing nonfermentable carbon sources but not on medium lacking arginine. The second strain is of mating type *alpha* and harbors a deletion of the nuclear-encoded *ARG8*, but contains mtDNA in which the *COB* gene is replaced by the *ARG8* gene (Δ*cob*::*ARG8*) (*8*). This latter strain can thus grow in the absence of arginine but not on nonfermentable carbon sources due to the deletion of the mtDNA-encoded *COB* gene. The open reading frames (ORFs) of *COB* and *ARG8* are 1158 and 1294 base pairs (bp) in size, respectively. Replacement of the *COB* gene, therefore, results in a minor increase of the overall size of the mtDNA of less than 0.2%, which is unlikely to confer a replicative disadvantage on the Δ*cob*::*ARG8* mtDNA due to larger size. Both strains contained comparable amounts of mtDNA as determined by quantitative real-time polymerase chain reaction (PCR; fig. S1A).

Both yeast strains were mated to obtain heteroplasmic diploid zygotes containing WT and Δ*cob*::*ARG8* mtDNA. Microdissection was used to transfer single zygotes to a cell-free area on an agar plate containing rich medium and glucose as a fermentable carbon source, which supports growth of cells containing WT, Δ*cob*::*ARG8*, or both mtDNA species. Once the first daughter cell had budded from the zygote, it was moved to a new location on the agar plate. Growth of this former daughter cell was again monitored, until the second-generation daughter cell had budded, which was again transferred to a new position. This procedure was repeated for up to five generations, and isolated cells were incubated to allow growth of colonies (Fig. 1, A and B). The mtDNA genotype in such colonies was inferred by

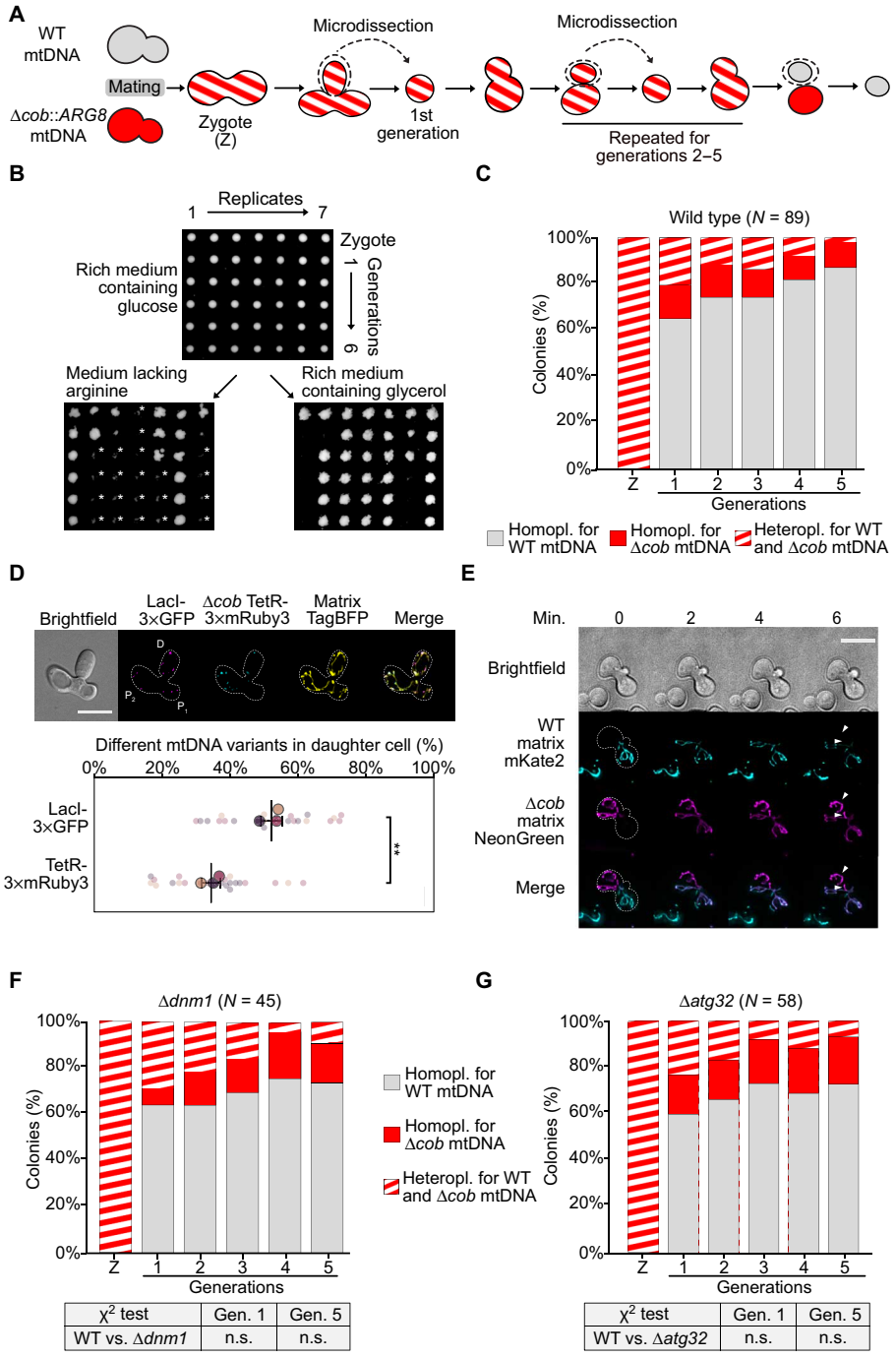

χ^2 test	Gen. 1	Gen. 5
WT vs. Δ*dnm1*	n.s.	n.s.

χ^2 test	Gen. 1	Gen. 5
WT vs. Δ*atg32*	n.s.	n.s.

Fig. 1. *S. cerevisiae* cells distinguish between WT and mutant mtDNA. (**A**) Schematic illustration of the pedigree analysis. Two Δ*arg8* yeast strains harboring WT or Δ*cob::ARG8* mtDNA were mated. Zygotes were isolated, and daughter cells from up to five consecutive generations were separated and placed on free spots on the agar plate by microdissection. (**B**) Growth pattern of the pedigree analysis after microdissection. Colonies were initially grown on rich medium containing glucose. The mtDNA genotype was inferred from the ability of colonies to grow on synthetic arginine lacking medium (Δ*cob::ARG8* mtDNA) or on medium containing the nonfermentable carbon source glycerol (WT mtDNA). Asterisks indicate cell material that was carried over by replica plating and failed to produce obvious colonies upon further incubation. For further illustrative explanation and confirmation of the pedigree analysis, refer to fig. S1 (B to D). (**C**) Pedigree analysis of WT cells. Striped bars indicate percentage of heteroplasmic cells containing WT and Δ*cob::ARG8* mtDNA. Gray or red bars indicate percentage of homoplasmic cells containing WT or Δ*cob::ARG8* mtDNA, respectively. (**D**) Inheritance of either intact or mutated mtDNA. Mating events between two cells either with WT-LacO (GFP, P_1) or Δ*cob::ARG8*-TetO (mRuby3, P_2) mtDNA. Both cells expressed a nuclear-encoded, matrix-targeted TagBFP. The percentage of either GFP or mRuby3 spots in the daughter cells relative to total number of the respective mtDNA variant have been plotted. Big circles represent the mean values from individual experiments. ***P*<0.01, *t* test. (**E**) Mitochondrial morphology during mating. Mating events between two cells containing either WT or Δ*cob::ARG8* mtDNA. Cells expressed either matrix-targeted mKate2 or mNeonGreen (NG). Mating events were monitored by live-cell microscopy. Time point before mixing of the matrix contents has been defined as T0. (**F** and **G**) Pedigree analysis of Δ*dnm1* or Δ*atg32* cells. Scale bars, 10 μm (D and E).

their ability to grow on medium containing a nonfermentable carbon source or medium lacking arginine, indicative of the presence of WT or Δ*cob*::*ARG8* mtDNA, respectively (Fig. 1B and fig. S1B). The presence or absence of mtDNA was further corroborated by PCR analysis of selected lineages (fig. S1C). Of note, this growth-based assay cannot distinguish whether mtDNA variants are entirely absent or present in insufficient amounts to support growth on the respective selective medium. Previous analyses in *S. cerevisiae* have revealed rapid segregation of mtDNA variants containing neutral genetic markers within less than 10 and often within one generation (*9*). We similarly observe rapid segregation; notably, however, we detected a strong bias for the WT mtDNA copy. More than 60% of the colonies derived from the first-generation daughter contained exclusively the WT mtDNA, while only about ~15% of the colonies contained exclusively the Δ*cob*::*ARG8* mtDNA and ~25% remained in a heteroplasmic state (Fig. 1C). A further segregation toward WT mtDNA was observed in following generations. More than 80% of colonies derived from daughters of the fifth generation contained only the WT mtDNA (Fig. 1C). Only 3% of the colonies of the fifth generation were heteroplasmic, indicating virtually complete segregation of both mtDNA types. Very similar results were obtained in pedigree analyses, where the mating types of the WT and the Δ*cob*::*ARG8* mtDNA containing strains had been switched, indicating that selection for WT mtDNA over Δ*cob*::*ARG8* mtDNA is independent of the mating type (fig. S2A). Furthermore, we did not observe selection against mtDNA variants with an *ARG8* gene inserted into a noncoding region of mtDNA, indicating that the *ARG8* gene does not impart a strong selective disadvantage on the mtDNA (fig. S2B).

We developed a microscopic approach to visualize selection of WT over Δ*cob* mtDNA during budding of daughter cells from zygotes. To this end, we used our previously generated strain that harbors tandem LacO repeats in a noncoding region of mtDNA upstream of *COX2* and expresses a nuclear-encoded LacI-3×GFP (green fluorescent protein) fusion protein harboring an N-terminal mitochondrial targeting sequence (*10*). In a separate strain, we replaced the mtDNA-encoded *COB* gene with tandem TetO repeats and introduced a gene encoding a mitochondrially targeted Tet-repressor fused to three repeats of the fluorescent protein mRuby3 into the nuclear genome. This strain contained very similar mtDNA levels compared to a reference strain, indicating that the TetO-TetR system does not lead to major defects in mtDNA maintenance (fig. S3A). In the strains used for this analysis, LacI-3×GFP and TetR-3×mRuby3 bind to the LacO and TetO repeats, respectively. To visualize mitochondria, both strains express the mitochondrially targeted blue fluorescent protein TagBFP. Both strains were mated, and zygotes were analyzed by fluorescence microscopy. We detected mutant mtDNA in the daughter cell. Quantitative image analysis, however, revealed that relative amounts of WT LacO-mtDNA were more abundant in the daughter cell than the Δ*cob* TetO-mtDNA (Fig. 1D and fig. S3B). While we cannot entirely rule out that the LacO-LacI or the TetO-TetR systems affect the mtDNA selection process or lead to biased results in this imaging approach, these data support the conclusion that *S. cerevisiae* cells can distinguish between WT and mutant mtDNA and promote generation of progeny with predominantly healthy mtDNA content.

Selection against mutant mtDNA occurs in a continuous mitochondrial network

Like in higher eukaryotes, mitochondria form a continuous tubular network in *S. cerevisiae* that is constantly rearranged by fusion and fission events. A simple explanation for rapid segregation of WT and mutant mtDNA could be that dysfunctional mitochondria do not fuse with healthy mitochondria to form a continuous network upon mating. In such a scenario, mutant and WT copies of mtDNA would not mix but be kept in separated mitochondrial compartments, which could facilitate efficient segregation. To examine this possibility, we used live-cell microscopy to monitor mitochondrial fusion during mating of two yeast strains expressing either mNeonGreen (NG) or mKate2 targeted to the mitochondrial matrix. We first examined mating events between two cells, both containing WT mtDNA. In line with previous observations, we observed fusion of mitochondria in newly formed zygotes (*11*–*13*). Fusion was characterized by quick and mostly complete equilibration of mKate2 and NG within 2 min throughout virtually all parts of the mitochondrial network in zygotes (fig. S4A). Similarly, we observed rapid fusion of mitochondrial networks in mating events between cells containing either WT or Δ*cob*::*ARG8* mtDNA (Fig. 1E, fig. S4B, and movie S1). Detection of both fluorescent proteins throughout the mitochondrial network was the result of fusion rather than ongoing translation, because unfused fragments could be distinguished during the mitochondrial fusion process in zygotes (arrowheads in Fig. 1E). Despite content mixing of mitochondria, our pedigree analysis reveals that yeast zygotes can still distinguish between mutant and WT mtDNA to produce daughter cells that predominantly contain WT mtDNA.

Mitochondrial fission or Atg32-mediated mitophagy is not required for selection against mutant mtDNA

We asked whether mitochondrial fission could facilitate selection against mutant mtDNA, as has been proposed for *D. melanogaster* (*5*, *6*). We did not observe increased mitochondrial fragmentation after mating between cells containing WT mtDNA or mating between cells containing either WT or Δ*cob*::*ARG8* mtDNA. Thus, excessive mitochondrial fragmentation does not occur during selection against mutant mtDNA in yeast zygotes (Fig. 1E; fig. S4, A and B; and movie S1).

To further assess the role of mitochondrial fission in selection against mutant mtDNA, we performed pedigree analyses of crosses between cells lacking the fission protein Dnm1 and harboring either WT or mutant Δ*cob*::*ARG8* mtDNA. Notably, the absence of mitochondrial fission did not compromise rapid selection for WT mtDNA in a colony produced by the first daughter cell of heteroplasmic yeast zygotes (Fig. 1F). Furthermore, live-cell microscopy of mating events between two Δ*dnm1* strains harboring either WT or mutant mtDNA and expressing matrix-targeted mKate2 or NG, respectively, revealed that mitochondria from both parental cells rapidly fused in zygotes (fig. S4C and movie S2). We also tested the importance of the mitophagy receptor Atg32 (*14*, *15*) for selection against mutant mtDNA. Δ*atg32* cells behaved similar to WT cells in pedigree analyses and exhibited complete mitochondrial fusion during the mating process (Fig. 1G, fig. S4D, and movie S3). Thus, neither mitochondrial fission nor Atg32-mediated mitophagy is essential for selection against mutant mtDNA during mating events of *S. cerevisiae* cells. Notably, selection for WT mtDNA in generations 2 to 5 appeared less prominent in pedigree analyses of Δ*dnm1* or Δ*atg32* cells compared to matings between WT cells. This observation could indicate that selection toward WT mtDNA in daughter cells of zygotes is independent of fission and mitophagy, whereas further selection in dividing diploids may be supported by these processes.

The mtDNA-encoded protein Atp6 exhibits severely limited diffusion rates

The fact that selection occurs in a continuous network that shares WT and mutant mtDNA presents a conundrum. How can cells distinguish between WT and mutant mtDNA if mitochondrial content equilibrates in a continuous network? We hypothesized that selection can only occur when subdomains are maintained within the mitochondrial network, whose functionality is determined by nearby copies of mtDNA. In such a scenario, it is important that mtDNA-encoded respiratory chain subunits do not exhibit rapid diffusion, because this would allow complementation of dysfunctional subdomains by gene products from WT mtDNA. To examine diffusion of an mtDNA-encoded protein, we modified mtDNA and fused an NG-tag to the C terminus of the mtDNA-encoded *ATP6* gene (fig. S5A). Yeast strains exclusively expressed the NG-tagged variant of Atp6 and did neither show growth defects on medium containing fermentable or nonfermentable carbon sources at 30° or 37°C nor exhibit increased formation of so-called petite cells that are respiratory deficient or display altered mtDNA or Atp6 protein levels (Fig. 2A and fig. S5, B to D). These observations indicate full functionality of the NG-tagged Atp6.

Fluorescence microscopy of diploid cells harboring the *ATP6-NG* mtDNA and expressing a nuclear-encoded matrix-targeted mScarlet revealed that, in contrast to the uniformly distributed mScarlet signal, Atp6-NG exhibited a patchy distribution in the mitochondrial network (fig. S5E). This distribution has also been observed previously

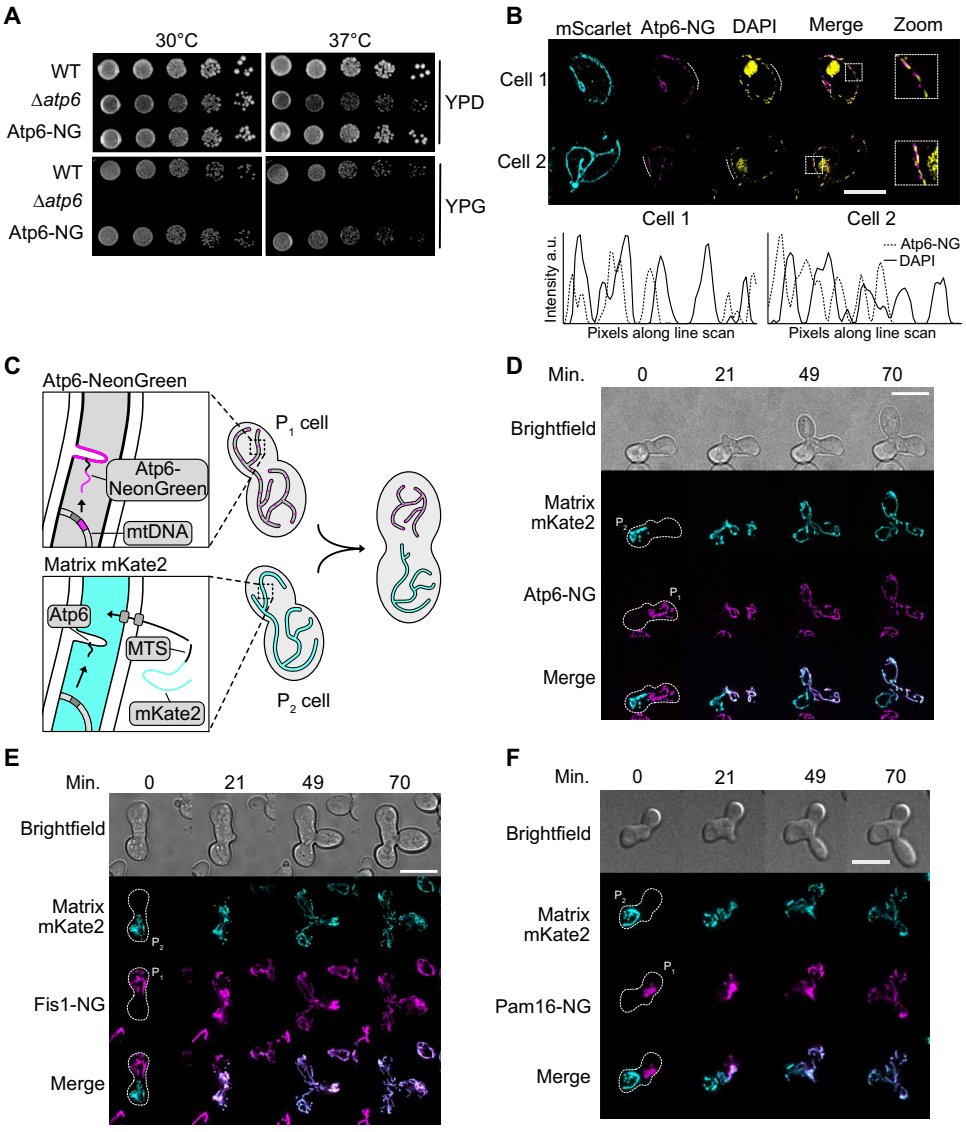

Fig. 2. mtDNA-encoded Atp6-NG exhibits limited diffusion. (**A**) Growth analyses of strains expressing NG-tagged Atp6. Serial dilutions of indicated strains were spotted on rich medium containing glucose or glycerol as carbon sources and incubated at 30° or 37°C. (**B**) Structured illumination microscopy of DAPI-stained cells expressing Atp6-NG and matrix-targeted mScarlet. Line graphs of pixel intensities along indicated lines are shown. a.u., arbitrary units. (**C**) Schematic illustration of the mating experiment of the Atp6-NG–tagged strain with a strain expressing the matrix labeling Su9-mKate2. (**D** to **F**) Diffusion of mitochondrial membrane proteins in fused mitochondria of zygotes. Cells expressing matrix-targeted mKate2 were mated with cells expressing mtDNA-encoded Atp6-NG (D), nuclear-encoded Fis1-NG (E), or Pam16-NG (F). Scale bars, 5 μm (B) and 10 μm (D to F).

using nuclear-encoded GFP-tagged variants of ATP synthase subunits, and it has been proposed that these patches report on mitochondrial cristae, in which the ATP synthase is enriched (*16*). We used structured illumination microscopy of 4′,6-diamidino-2-phenylindole (DAPI)–stained cells to query the relationship between Atp6-NG and mtDNA. Atp6-NG foci were spatially linked to mtDNA and were detected in the immediate surroundings of DAPI spots rather than directly colocalizing with them (Fig. 2B). This finding demonstrates that the ATP synthase localizes close to mtDNA but is largely excluded from areas occupied by mtDNA itself. This observation is in line with recent super-resolution data in HeLa cells that showed a lack of cristae in close proximity to mtDNA (*17*).

To further test whether Atp6-NG remains close to the copy of mtDNA by which it is encoded, we examined diffusion of Atp6-NG in living cells during a mating experiment. Cells harboring mtDNA encoding Atp6-NG were mated with cells expressing a nuclear-encoded matrix-targeted mKate2 and harboring nonmodified mtDNA. Equilibration of both fluorescent signals throughout the mitochondrial network of zygotes was studied over time by live-cell microscopy (Fig. 2C). In line with our previous observation, soluble mKate2 rapidly equilibrated throughout the mitochondrial network upon fusion of parental mitochondria. Notably, the Atp6-NG signal remained localized to mitochondria from the cell of its origin (Fig. 2D, fig. S6A, and movie S4). Only very small Atp6-NG amounts were present in the mitochondrial network of the mating partner ~80 min after mitochondrial fusion, when a daughter bud had already emerged at midpoint between both parental cells and had been invaded by mitochondria. To quantify equilibration of Atp6-NG in late zygotes harboring a large medial bud, we first segmented the mitochondrial network based on the mitochondrial mKate2 signal and assigned mitochondrial parts to either the parental Atp6-NG (P_1), the parental mKate2 (P_2), or the daughter cell. The Atp6-NG signal was then determined along the mitochondrial network parts that had been assigned to P_1, P_2, and daughter cell. The Atp6-NG signal was further normalized to the length of the subnetwork localized to the respective cells. This analysis revealed that on average only approximately 20% of the Atp6-NG was detected in the mitochondrial network of the other parental cell (Fig. 3B). In contrast, no difference in the mKate2 signal in both parental cells was apparent in this analysis, indicating complete mitochondrial fusion and full equilibration of this soluble matrix protein (fig. S7A). We cannot distinguish between preexisting and newly synthesized Atp6-NG in this assay but conclude that proteins from neither group efficiently populate the mitochondrial network of the parental cell that did not contain the Atp6-NG mtDNA.

To examine diffusion of another protein component of the oxidative phosphorylation (OXPHOS) complexes, we created a strain expressing an NG-tagged version of the nuclear-encoded protein Cox4, which is a subunit of complex IV. Cells expressing Cox4-NG cells were mated with cells expressing matrix-targeted mKate2. Of note, upon mating of these cells, continued cytosolic synthesis of Cox4-NG will lead to import of Cox4 into all parts of the mitochondrial network at later time points. Despite this complication and similar to our results obtained with Atp6-NG, Cox4-NG exhibited strongly reduced diffusion throughout the mitochondrial network of zygotes compared to the soluble matrix–targeted mKate2 and remained largely restricted to the cell of its origin during the duration of the microscopy experiment (fig. S6B).

Next, we asked whether limited diffusion of Atp6-NG or Cox4-NG was general to transmembrane (TM) proteins of mitochondrial membranes. We mated cells expressing matrix-targeted mKate2 with cells either expressing NG fused to the TM-domain of the outer membrane protein Fis1 or a functional Pam16-NG fusion protein (Fig. 2, E and F, and fig. S6, C and D). Pam16 is a subunit of the translocase of the inner mitochondrial membrane, which localizes predominantly to the inner boundary membrane (*18*). Time-lapse microscopy of such mating events revealed that diffusion of Fis1-TM-NG and Pam16-NG was slightly delayed compared to the soluble matrix protein mKate2, but both proteins equilibrated much faster than Atp6-NG throughout mitochondrial networks and no difference in signal intensity in both parental cells could be observed ~10 min after fusion of mitochondria in zygotes (fig. S6, E and F, and movies S5 and S6). In summary, mtDNA-encoded Atp6-NG and nuclear-encoded Cox4-NG, which are both subunits of respiratory chain complexes consisting of nuclear- and mtDNA-encoded subunits, are severely limited in equilibration throughout mitochondrial tubules compared to proteins of the inner boundary or the outer mitochondrial membranes.

Components important for cristae morphology affect diffusion rates of Atp6-NG

We hypothesized that components involved in maintenance of cristae morphology could be important for hindering diffusion of OXPHOS subunits and particularly mtDNA-encoded proteins within the mitochondrial network. Mic60 and Mic10 are components of the mitochondrial contact site (MICOS) complex, which stabilizes cristae junctions (*19*–*21*). Lack of Mic60 leads to cristae that are detached from the inner mitochondrial membrane but maintain their sheet-like morphology in the matrix. Atp20 and Atp21 are crucial for dimerization of the ATP synthase, which, in turn, stabilizes strongly bent cristae rims (*22*). Lack of the dimeric ATP synthase has been described to lead to an onion-like morphology of mitochondria, where uncontrolled proliferation of cristae membranes leads to a multilayered appearance (*23*). To examine the role of cristae in limiting equilibration of OXPHOS proteins, we quantified Atp6-NG mobility in our mating assay in Δ*atp20*, Δ*atp21*, Δ*atp20*Δ*atp21*, Δ*mic10*, or Δ*mic60* strains. Both parental cells contained the respective deletion in these crosses. In all mating events, the nuclear-encoded mKate2 equilibrated across the mitochondrial network (fig. S7A). We could observe a slightly less complete equilibration of mKate2 in zygotes lacking the dimeric ATP synthase, which is likely explained by septae that may create separate matrix compartments (*24*) and thereby may decrease efficiency of matrix content exchange. Δ*mic10* and Δ*mic60* cells exhibited increased diffusion of Atp6-NG between mitochondrial networks of parental cells compared to WT cells in our mating assay, which was characterized by a greater amount of Atp6-NG detected in the mating partner harboring the WT mtDNA (~35% compared to ~25% in WT cells; Fig. 3, A and B). Cells lacking Atp20, Atp21, or both proteins showed a strongly increased diffusion of Atp6-NG across the mitochondrial network in zygotes. In many cases, the source cell that contained *ATP6-NG*-mtDNA was hardly discernible from the mKate2 source cell in the zygotes. On average, ~45% of Atp6-NG was detected in the mating partner harboring the WT mtDNA in the absence of Atp20, Atp21, or both proteins (Fig. 3, A and B). In contrast to limited diffusion within the mitochondrial network formed by parental cells, Atp6-NG was readily detected in the budding daughter cells. In daughters from zygotes, the Atp6-NG signal was at ~70% compared to the *ATP6-NG* signal from the *ATP6-NG* parental cell in all mutants,

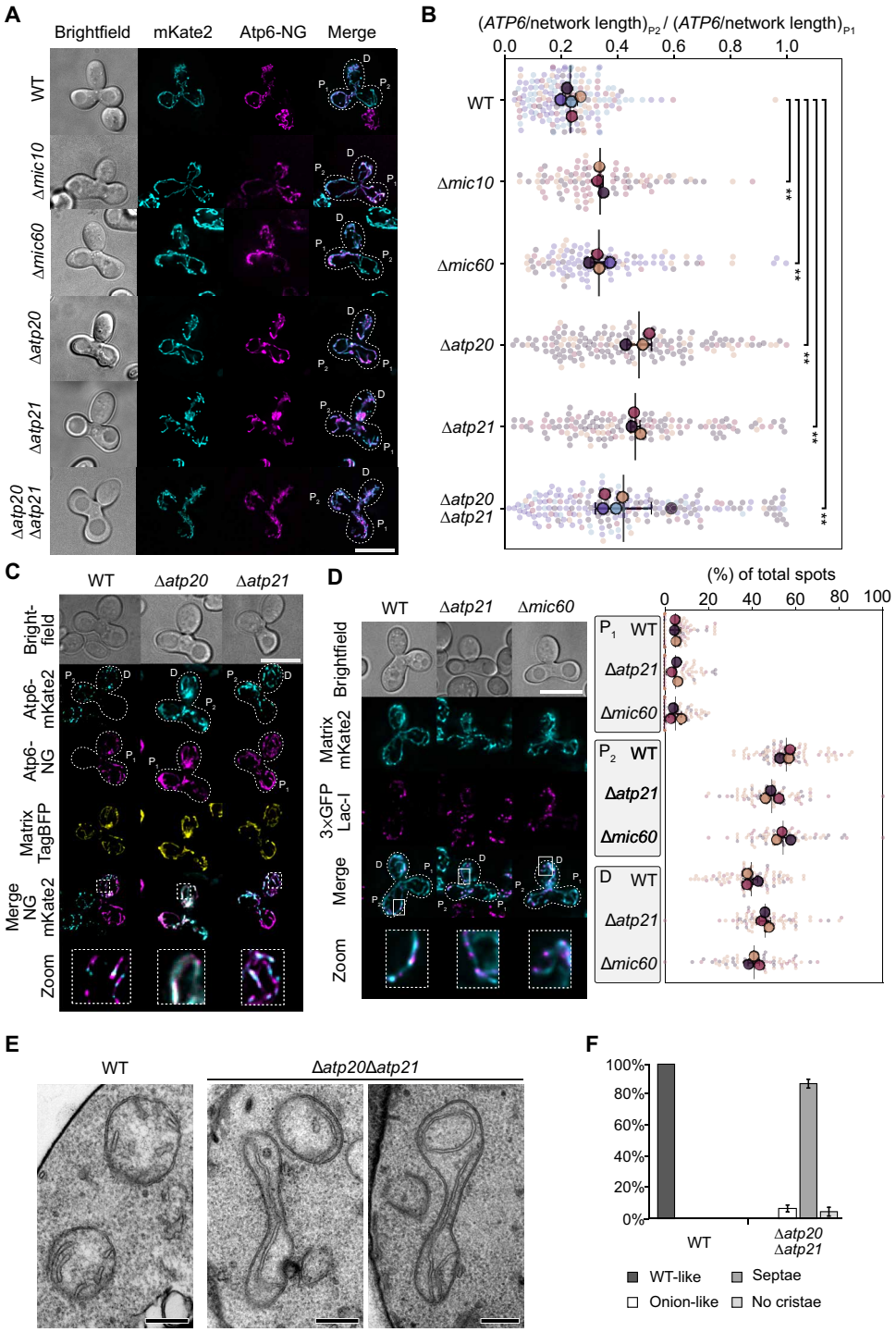

Fig. 3. Intact cristae morphology limits diffusion of mtDNA-encoded Atp6-NG. (**A**) Zygotes derived from mating events between WT or indicated mutant cells. In each mating event, one cell contained *ATP6*-NG mtDNA (P_1) and the other cell contained WT mtDNA and expressed matrix-targeted mKate2 (P_2). D, daughter cell. (**B**) The Atp6-NG signal was quantified in both parental cells of zygotes and normalized to the mitochondrial network length. The ratio of Atp6-NG signals in P_2 cells to P_1 cells of the same zygote is plotted; each point represents one zygote; $^{**}P < 0.01$, *t* test. (**C**) Mating events between WT, *Δatp20*, or *Δatp21* cells. Mating cells harbored either Atp6-NG mtDNA and nuclear-encoded Su9-TagBFP (P_1) or Atp6-mKate2 (P_2) mtDNA (D, daughter cell). (**D**) Mating events between WT, *Δatp21*, and *Δmic60* cells. Parental cell P_1 contained WT mtDNA and expressed matrix-targeted mKate2, whereas parental cell P_2 contained mtDNA with integrated LacO repeats (D, daughter cell). mtDNA-LacO spots in P_1, P_2, and D cells were counted and plotted as percentage of total number of spots in the zygote. Each data point in the plot represents one zygote. (**E**) Electron microscopic analysis of mitochondrial ultrastructure in WT and *Δatp20Δatp21* cells. (**F**) Quantification of electron microscopy data shown in (E). Scale bars, 10 μm (A, C, and D) and 250 nm (E).

with the exception of Δ*mic60* cells, where Atp6-NG levels only amounted to ~60% (fig. S7B). The reason why less Atp6-NG is found in the daughter cells of matings between Δ*mic60* cells is currently unclear. In summary, we observe increased diffusion of Atp6-NG in mutants lacking intact cristae morphology across existing mitochondrial networks of yeast zygotes. Because Δ*mic10* or Δ*mic60* mutants still have the dimeric form of the ATP synthase (*25*, *26*), our results strongly suggest that Atp6-NG mobility is increased due to compromised cristae morphology rather than conversion of the ATP synthase into the monomeric form in cells lacking Atp20 or Atp21.

We developed an additional assay to test the generation of mtDNA autonomous domains and the role of cristae therein. Cells expressing mtDNA-encoded Atp6-NG and nuclear-encoded matrix-targeted TagBFP were mated with cells expressing mtDNA-encoded Atp6-mKate2, and the patterns produced by the differently tagged Atp6 proteins were examined in zygotes. The Atp6-mKate2 strain grew normally on medium containing fermentable or nonfermentable carbon sources, and no increase in *petite* formation was observed, indicating that the mKate2-tagged variant of Atp6 was functional (fig. S7C). In line with our previous observations, the Atp6 proteins remained localized to their respective origin cells in zygotes in crosses between WT cells (Fig. 3C). Notably, we often observed an alternating, mostly nonoverlapping pattern of green and red signals along the TagBFP-stained mitochondrial network in the daughter cell produced by the zygote (Fig. 3C, zoom, and fig. S7D). Thus, Atp6-NG and Atp6-mKate2 occupy separate domains in the mitochondrial network and exhibit limited mixing. This result indicates that mtDNA copies encoding Atp6-NG or Atp6-mKate2 maintain semi-autonomous mitochondrial subdomains. The alternating pattern in the daughter cell further suggests a complex procedure in which mitochondrial domains from both parental cells are sorted into the daughter cell. In mating events between Δ*atp20* and Δ*atp21* cells expressing either Atp6-NG or Atp6-mKate2, both fluorescently tagged Atp6 variants showed a stronger colocalization in daughter cells and separate domains were hardly discernible (Fig. 3C and fig. S7D). These observations show that cristae are required for maintenance of inner membrane domains and prevent extensive mixing between gene products of different mtDNA copies.

mtDNA diffusion is limited in WT, Δ*atp21* and Δ*mic60* cells

Cristae could support mtDNA-mediated formation of mitochondrial subdomains via at least two mutually nonexclusive mechanisms: (i) Cristae could limit mobility of mtDNA within the mitochondrial matrix by forming physical barriers and thereby promote local synthesis of mtDNA-encoded proteins. (ii) Cristae could corral mtDNA-encoded proteins by preventing their diffusion through cristae junctions into the inner boundary membrane. To determine the importance of cristae in restricting mtDNA mobility, we used our recently developed mtDNA LacO-LacI-GFP system (*10*) to specifically mark mtDNA in one of the parental cells in a mating experiment (P_2 cell). The other parental strain used in the mating assay contained WT mtDNA lacking the LacO repeats and expressed the matrix-targeted mKate2 protein (P_1 cell). In mating events between two WT cells, two Δ*atp21*, or Δ*mic60* cells, LacO-marked mtDNA was evident in the daughter cells produced by zygotes, indicating efficient transport of mtDNA into daughter cells. Of note, we observed a slight increase of the percentage of LacO mtDNA spots in the daughter cell in matings between Δ*atp21* cells compared to matings between WT or Δ*mic60* cells (Fig. 3D). The underlying reason for this observation remains to be determined. LacO-marked mtDNA did not accumulate in the P_1 parental cell even at late zygotic stages in any of the matings (Fig. 3D). Thus, mobility of mtDNA remains limited in the mitochondrial network of parental cells in matings between Δ*atp21* or Δ*mic60* cells that contain strongly compromised cristae architecture. We conclude that WT-like cristae architecture plays a crucial role in limiting equilibration of the Atp6-NG protein, rather than diffusion of mtDNA.

To find a potential explanation for the rapid equilibration of Atp6-NG in the absence of dimer-specific ATP synthase subunits, we carefully examined WT, Δ*atp20*, Δ*atp21*, and Δ*atp20*Δ*atp21* cells by electron microscopy and also performed serial sectioning to obtain three-dimensional (3D) information about the mitochondrial ultrastructure. Mitochondria of WT cells showed cristae with the typical perpendicular orientation to the mitochondrial tubular axis. In mutant cells lacking dimeric ATP synthase, however, inner membrane structure was markedly altered and virtually no WT-like cristae were apparent. Instead, mitochondria exhibited onion- and balloon-like inner membrane profiles, as previously described. In accordance with previous work, we frequently observed strongly elongated cristae-like structures that traversed the whole mitochondrion (Fig. 3, E and F, and fig. S8) (*22*, *23*,*27*).

These observations provide a possible explanation for the inability of cells lacking dimeric ATP synthase to constrain diffusion of Atp6-NG. While respiratory chain complexes get trapped in cristae in WT cells, they are free to diffuse along the altered cristae membranes in Δ*atp20*, Δ*atp21*, and Δ*atp20*Δ*atp21* mutants.

Cristae morphology is required for mtDNA quality control

Having determined that mtDNA-encoded subunits exhibit a severely reduced mobility in the inner mitochondrial membrane that is dependent on normal cristae biogenesis, we asked whether mutants defective in cristae biogenesis would have problems to distinguish between WT and mutant mtDNA. We applied our pedigree analysis to follow inheritance of WT over Δ*cob::ARG8* mtDNA from heteroplasmic zygotes in the absences of *ATP20*, *ATP21*, *MIC10*, or *MIC60*. Deletion of these genes did not lead to greatly altered mtDNA levels in strains containing WT or Δ*cob::ARG8* mtDNA (fig. S9A). In particular, mtDNA levels of the mating partners of each pedigree mating pair did not differ significantly to one another. Notably, clearance of the mutant mtDNA was significantly delayed in the absence of any of these proteins. While 60% of lineages for the WT were already homoplasmic for WT mtDNA in the first generation, this value dropped to 40% in cristae mutants. Moreover, while only ~20% of cells of the first generation in WT cells still maintained a heteroplasmic state, ~40% of such cells were detected in the first generation of matings between cristae mutants. After five generations, a significantly smaller proportion of the lineages were homoplasmic for WT mtDNA in the cristae mutants (Fig. 4, A to F). Thus, the ability to choose WT over mutant mtDNA is severely compromised in mutants with defective cristae architecture. In line with these pedigree results and in accordance with previous work, Δ*atp20*, Δ*atp21*, Δ*atp20*Δ*atp21*, Δ*mic10*, or Δ*mic60* strains harboring exclusively WT mtDNA exhibit increased formation of *petites*, revealing a reduced ability to maintain a healthy mtDNA population in cells (fig. S9B) (*23*).

DISCUSSION

Our data reveal that the unicellular *S. cerevisiae* is able to promote generation of progeny with a healthy mtDNA population from

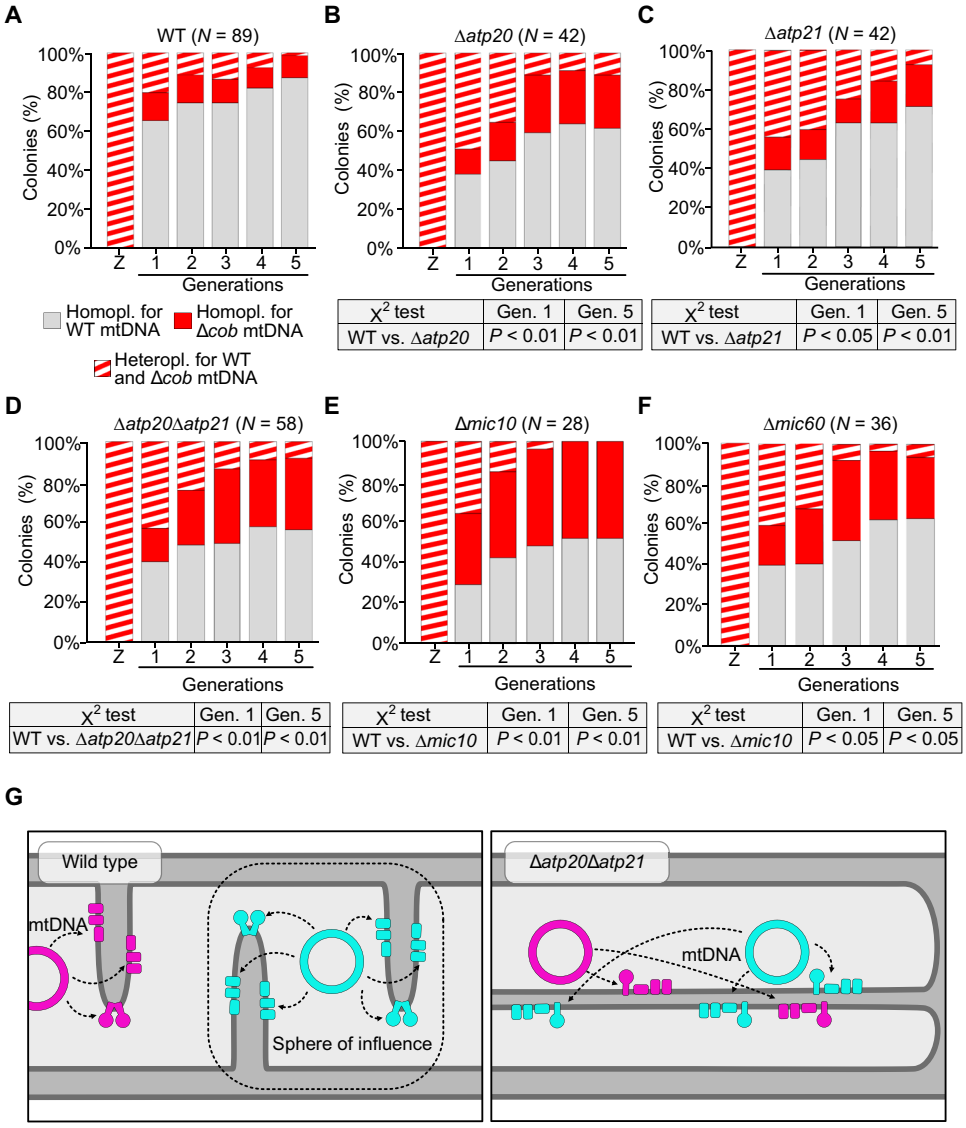

Fig. 4. mtDNA quality control depends on normal cristae morphology. (**A** to **F**) Pedigree analyses of strains lacking indicated genes. WT pedigree (A) is identical to Fig. 1C, shown to allow comparison to mutant analyses in (B) to (F). χ^2 test has been applied as statistical hypothesis tests to compare first- and fifth-generation data of mutant strains to the WT. (**G**) Model for quality control of mtDNA in a fused mitochondrial network. mtDNA copies in WT cells supply only the cristae in their immediate surrounding with mtDNA-encoded proteins. Respiratory chain complex containing mtDNA-encoded subunits has limited diffusion capability and is trapped within cristae, which leads to a sphere of influence of mtDNA. Limited diffusion of respiratory chain complexes is compromised in cells with compromised cristae structure.

heteroplasmic zygotes that contain WT and mutant mtDNA. So far, our demonstration of the purifying selection in yeast is limited to a model mutant mtDNA variant that entirely lacks the *COB* gene. It will be interesting to examine in future studies how yeast cells deal with deletions of other mtDNA-encoded genes or milder point mutations. Unexpectedly, we show that the purifying selection occurs in a continuous mitochondrial network and does not require mitochondrial fission. This finding raised the question how cells can detect mutant mtDNA copies among WT copies in a mitochondrial network, where soluble matrix proteins rapidly equilibrate and potentially even out physiological differences and thus conceal mutant copies.

A possible solution for this problem is provided by our finding that diffusion of OXPHOS components, namely, the mtDNA-encoded protein Atp6-NG and the nuclear-encoded Cox4-NG, is severely limited in WT cells compared to proteins localized to the inner boundary membrane, the outer membrane, or the matrix. Of particular interest in this respect is the observation that the mtDNA-encoded Atp6-NG forms subdomains that remain in the vicinity of the mtDNA by which it is encoded. These findings are in line with analyses in HeLa cells that have similarly demonstrated reduced mobility of OXPHOS proteins along the longitudinal axis of mitochondrial tubules (*28*, *29*). A previously proposed plausible explanation for the restricted mobility is that OXPHOS proteins, likely aided through their assembly into complexes and supercomplexes (*30*), get trapped within cristae membranes and are prevented from diffusion past cristae junctions into the inner boundary membrane (*18*, *31*). In strong support of this hypothesis, we find that the mtDNA-encoded Atp6-NG exhibits increased equilibration across the mitochondrial

network in mutants with defective cristae architecture, while movement of the mtDNA from which it originates remains restricted. Notably, our pedigree analysis revealed that mutants with defective cristae biogenesis are incapable of distinguishing effectively between WT and mutant mtDNA to support progeny with functional mtDNA.

Together, our findings are in line with a previously proposed model in which each mtDNA copy has a "sphere of influence" and remains spatially linked to its gene products (*32*, *33*). Our data support the hypothesis that such a sphere of influence is dependent on normal cristae architecture (Fig. 4G). According to this model, mutations in mtDNA would lead to mitochondrial subdomains with physiological defects that could flag such areas and facilitate purging of the linked mtDNA copy. In line with this idea, it has recently been shown that individual cristae within the same mitochondrial tubule can maintain independent membrane potentials (*34*). Defective cristae biogenesis would lead to defective subdomain formation and a weakened link between mtDNA and its gene products, which, in turn, would blur physiological differences caused by mtDNA mutations (Fig. 4G). As a consequence, detection and purging of mutated mtDNA would be hindered.

For such a system to work, not only the proteins but also their mRNAs need to remain close to the mtDNA copy from which they originate. In matings between two WT cells containing either regular or *ATP6-NG* mtDNA, we observe very low levels of Atp6-NG protein in parts of the mitochondrial network that does not contain the *ATP6-NG* mtDNA, even more than 80 min after mitochondria of both parental cells have fused (fig. S6A). This result indicates that little synthesis of Atp6-NG occurs in these parts of the network within the time frame of this analysis. It is, however, possible that biogenesis of OXPHOS complexes is generally low in the mitochondrial network of parental cells because of little OXPHOS turnover. In this case, we would see little synthesis of Atp6-NG even if its mRNA would be present. Not much is known from the literature about the mobility of mitochondrial mRNAs. It was recently proposed that mitochondrial transcription and translation may occur in a coupled manner in *S. cerevisiae* (*35*). Taking into account that insertion of mtDNA-encoded proteins into the mitochondrial inner membrane occurs cotranslationally (*36*, *37*) and, at least in part, at cristae membranes (*38*), all steps of mitochondrial gene expression from transcription to insertion of proteins into cristae membranes could be spatially linked. Nevertheless, characterization of mRNA mobility in mitochondria awaits further studies.

We demonstrate that yeast cells can distinguish between mutant and WT mtDNA and propose that cristae-dependent subdomains are an important prerequisite for efficient purging of mutant mtDNA. It remains an outstanding and exciting question how cells mechanistically detect and remove mutant mtDNA. Plausible physiological parameters that may serve as signals on dysfunctional mitochondria are a reduced membrane potential (*39*), decreased ATP levels (*5*), or altered redox states (*40*). What processes may remove mutant mtDNA from cells? Our microscopic analyses suggest that mutant mtDNA transfer to daughter cells of heteroplasmic zygotes may be reduced, but not entirely prevented (Fig. 1D). Preferential transport of fit mitochondria into daughter cells has been demonstrated in yeast previously (*40*). In combination with our pedigree analysis, where a large percentage of first-generation colonies appears homoplasmic (Fig. 1C), we suggest that further rounds of selection against mutant mtDNA likely occur in the daughter cells that eventually entirely purge mutant mtDNA. While we find that mitochondrial fission or Atg32-mediated mitophagy is not absolutely essential for selection against mutant mtDNA, especially during production of the first daughter cell of heteroplasmic zygotes, these processes may contribute to efficient clearance during further growth and cell divisions. Furthermore, WT mtDNA could also be preferentially replicated as suggested for *D. melanogaster* (*3*, *7*) or mutant mtDNA could be selectively degraded within mitochondria by nucleases. It was demonstrated in yeast that the mtDNA polymerase Mip1 degrades mtDNA through its exonuclease domain upon prolonged starvation (*41*). It remains to be determined whether such a mechanism could also be involved in clearance of mutant mtDNA. Together, selection against mutant mtDNA could entail a combination of mechanisms that may include selective transport of mitochondria containing healthy mtDNA to daughter cells, mitophagic removal of mitochondrial fragments containing mutant mtDNA, selective replication of healthy mtDNA, or selective degradation of mutant mtDNA by nucleases. The discovery of a purifying selection in *S. cerevisiae* combined with the tools we developed in this study will be of great value in elucidating molecular mechanisms responsible for clearance of mutant mtDNA.

MATERIALS AND METHODS

Yeast strains and plasmids

All yeast strains are derived from W303 background. Strain information can be found in table S1. Deletions of genes and C-terminal tagging of nuclear-encoded genes were performed in haploid strains using homologous recombination as described previously (*42*). For the experiment presented in fig. S3A, the mating type of strain yCO354 had to be switched from Mat *alpha* to Mat *a*. Mating type switching was performed by transient (90 min) galactose-induced expression of the HO endonuclease from the plasmid pJH132 (*43*). Subsequently, a Mat *a* strain that had lost the plasmid pJH132 was isolated. Primer and plasmid information can be found in tables S2 and S3, respectively.

Pedigree analysis

Approximately 1.85×10^7 cells from early post-log phase [optical density at 600 nm (OD_{600}) ~ 1.5] growing cultures of strains with opposing mating types were combined in a 1.5-ml reaction tube, vortexed, centrifuged at 3000 rpm for 3 min, and resuspended in 50 µl of rich medium containing glucose [yeast extract peptone dextrose (YPD)]. Subsequently, the cell suspension was spotted onto a YPD plate and incubated for 2 to 3 hours to allow mating of strains. A small amount of cells was scraped off the plate and was resuspended in 200 µl of YPD medium. From this mated cell suspension, 30 µl was spread as a line on a YPD plate. Individual zygotes were identified on the basis of their characteristic shape and transferred to free areas on the agar plate. Cell growth was monitored, and daughter cells were separated from zygotes or mother cells and transferred to free areas on the agar plate. This procedure was repeated for five generations (Fig. 1, A and B). After incubation for 2 days at 30°C, the grown colonies were replica-plated onto plates containing synthetic defined medium lacking arginine (SD-Arg) and plates containing rich medium and glycerol as a carbon source [yeast extract peptone glycerol (YPG)]. Those plates were again incubated for 24 to 48 hours, and growth was scored. Of note, colonies were scored as "growing" for SD-Arg or YPG even when only parts of the replicated colony displayed growth. Growth rates were not considered in this

experiment. The presence or absence of growth was verified by restreaking of cell material from selected colonies onto YPG or SD-Arg plates (fig. S1B). In addition, a mating-type test was performed to confirm that the initially picked cells were zygotes. Lineages were only considered when the starting zygotes were able to grow on YPG and SD-Arg plates, indicating a heteroplasmic state. Of note, we sporadically observed that mtDNA species were lost in one generation but reappeared at a later generation (e.g., replicate 2 in Fig. 1B). We attribute this observation to cases in which all copies of one particular mtDNA species are passed on to the daughter cell. In such a scenario, a mother cell lacking this mtDNA species is produced, whereas this species will be present in the daughter cell (fig. S1D).

Live-cell microscopy

For all live-cell microscopy experiments, yeast cells were imaged in ibidi 8-well µ-Slides (ibidi GmbH, Gräfelfing). For immobilization of yeast cells during microscopy, wells were coated with concanavalin A, a lectin that can bind the cell wall of yeast cells. In brief, wells were filled with 200 µl of concanavalin A (0.5 µg/ml) and incubated for 30 min. Concanavalin A was removed, and wells were dried for 30 min at room temperature. For single-frame images and videos of mating events, 1000 µl from two cultures with strains of opposing mating types was combined in a reaction tube, vortexed thoroughly, and centrifuged for 3 min at 5000 rpm. The pellet was resuspended in 50 µl of YPD medium and spotted onto a YPD plate to allow cells to mate. Plates were incubated for 3 hours for single-frame images and for 1.5 hours for videos. The premated cells were scraped off and resuspended in 400 µl of sterile-filtered 1× phosphate-buffered saline (PBS) buffer, and 200 µl was transferred into a concanavalin A–coated well of ibidi 8-well µ-Slide. The slides were centrifuged for 2 min at 2000 rpm to promote adherence of the cells to the bottom of the well. Wells were washed twice with 400 µl of filtered synthetic complete (SC) medium to remove floating cells and eventually resuspended in SC medium for imaging. Microscopy was performed at 30°C on a Nikon Ti2-Eclipse microscope equipped with a CFI Apochromat TIRF 100×/1.49 numerical aperture (NA) oil objective and a TwinCam LS dual-camera splitter attached to two Photometrics Prime 95B 25-mm cameras. The dual-camera setup enabled simultaneous imaging of red and green fluorophores. Specifications of filters and dichroics can be made available upon request. For time-lapse microscopy, cells were imaged every 2 or 7 min for indicated total periods of time. For quantification of the imaging presented in Fig. 1D, zygotes were only considered when patchy structures were apparent for GFP and mRuby3 signals. Cells harboring the TetO repeats often showed a diffuse red staining of mitochondria, which is likely explained by recombination of the TetO repeats.

Image processing and analysis

All images, except those obtained by structured illumination microscopy, were postprocessed by deconvolution with the Huygens software (Scientific Volume Imaging). Fluorescent channels acquired simultaneously on two different cameras were aligned using a custom-built Python script. Alignment parameters were obtained from simultaneous imaging in bright-field mode. For quantification of Atp6-NG levels presented in Fig. 3A, mitochondria were first segmented in 3D based on the matrix-mKate2 signal using the mitograph software (*44*). Binary masks for parental and daughter cells were manually created in Fiji by drawing outlines on the bright-field image. Masks were used in a next step to assign coordinates of the mitochondrial network to the respective cells. Then, Atp6-NG intensities were determined and summed up along the mitochondrial network of parental or daughter cells using custom-built Python scripts. To account for differences in the mitochondrial amount in different cells, the Atp6-NG signal was normalized to the mitochondrial network length present in the respective cell.

Quantification of colocalization of Atp6-NG and Atp6-mKate2, presented in fig. S7D, was performed as follows. The mitochondrial network was first segmented in 3D based on the matrix-TagBFP signal using the mitograph software. Manually created binary masks were used to assign parts of the mitochondrial network to parental or daughter cells. Fluorescent intensities of Atp6-NG and Atp6-mKate2 were then determined for pixels along the mitochondrial network. Next, Manders and Pearson correlation coefficients were determined between both signals. For determination of the Manders correlation coefficient, signals along the mitochondrial network were thresholded beforehand with Yen *et al.*'s method (*45*).

Genetic manipulation of mtDNA

Strains harboring mtDNA in which the *COB* gene was replaced with an arginine marker and a nonrecombinable TetO array were generated as follows. First, a synthesized TetO array, in which 21 TetO repeats are separated by spacers of varying length and sequence, was inserted after the stop codon of the *ARG8* gene in the plasmid pCOB-ST5 (*8*). This cloning step resulted in the plasmid pCO307, which thus contains an insert in which sequences homologous to the up- and downstream regions of the *COB* gene flank the ORF of *ARG8* followed by the TetO array. pCO307 was introduced into the *kar1-1* strain αDFS160 ρ^0 by biolistic transformation with the PDS-1000/He particle delivery system (Bio-Rad Laboratories), and transformants were selected by their ability to rescue the *cox2-62* mutation of the strain NB40-3C (*46*). pCO307 was then cytoducted into a Δ*arg8* W303 WT strain, which resulted in the deletion of the *COB* gene by *ARG8*-TetO through homologous recombination. Cells containing the Δ*cob*::*ARG8-TetO*-mtDNA were selected on the basis of their arginine prototrophy. Last, a construct (pCO407) consisting of the Cup1 promoter driving expression of an ORF in which the Su9 mitochondrial targeting sequence was fused to the TetR gene, which, in turn, was followed by three copies of the red fluorescent protein mRuby3, was chromosomally integrated into the HO locus (strain yCO460).

Strains harboring mtDNA in which the *ATP6* is tagged with either NG or mKate2 were generated as follows. First, synthesized gene fragments encoding NG and mKate2 compatible with the mitochondrial genetic code (Twist Bioscience, San Francisco) were fused to the C terminus of the coding region of *ATP6*, which was amplified from genomic DNA. *ATP6*-NG or *ATP6*-mKate2 was flanked with an 806-bp region homologous to the upstream region of *ATP6* and a 60-bp region homologous to the downstream region of *ATP6*. The entire fragments were then cloned into the Xho I site of the plasmid pPT24 (*47*), which resulted in either plasmid pCO444 or pCJ013 for ATP6-NG and ATP6-mKate2, respectively. pCO444 and pCJ013 were introduced into the *kar1-1* strain αDFS160 ρ^0 by biolistic transformation, and transformants were selected by their ability to rescue the cox2 mutation of NB40-3C (*46*). pCO444 and pCJ013 were then cytoducted into the strain MR10 (*48*). Colonies in which *ATP6*-NG (yCJ043) or *ATP6*-mKate2 (yCJ120) had successfully integrated into the *ATP6* locus were identified by their ability to grow on a nonfermentable carbon source. A strain containing *ATP6-NG*-mtDNA

and mating type *alpha* was obtained by mating yCJ043 with a ρ^0 W303 WT strain followed by sporulation and tetrad dissection (yCJ084).

Primer sequences used for cloning and plasmid maps can be made available upon request.

DAPI staining and structured illumination microscopy

Coverslips (no. 1.5) were coated with 50 µl of concanavalin A (0.5 µg/ml) and air-dried for 1 hour. Residual concanavalin A was removed, and coverslips were dried for 45 min before fixation. OD_{600} = 0.5 of log phase yeast cells were harvested at 5000 rpm for 3 min and washed using 1× PBS + 0.02% Tween 20. Cells were resuspended in 20 µl of 1× PBS + 0.02% Tween 20. Subsequently, all cells were placed on the concanavalin A–coated coverslips and incubated for 45 min to let cells settle on the coverslip. Then, cells were washed for 2 min with filtered SC medium. Cells were fixed using a 4% formaldehyde solution + DAPI (1 µg/ml) in filtered SC medium for 30 min. Cells were washed once more for 2 min using filtered SC medium. Twenty microliters of MOVIOL 4-88 (Roth) was added to the coverslips, and microscope slides were put onto the coverslips. Fixed immobilized cells were used for super-resolution imaging by structured illumination microscopy. The acquisition was performed on a 3D SIM DeltaVision OMX V3 microscope (General Electric) equipped with a 10× 1.4 NA oil immersion objective UPlanSApo (Olympus), 405-, 488-, and 593-nm diode lasers, and Cascade II electron-multiplying charge-coupled device (CCD) cameras (Photometrics). After acquisition with an appropriate refractive index oil, raw data were first reconstructed and corrected for color shifts using the provided software softWoRx 6.0 Beta 19 (unreleased). In a second step, a custom-made macro in Fiji (*49*) finalized the channel alignment and established composite TIFF (tag image file format) stacks, which were used for image analysis.

Electron microscopy

For electron microscopy, all strains were pregrown in YPG medium to select for functional mtDNA. Subsequently, cells were grown to log phase in YPD or rich medium containing galactose medium, as indicated. Sample preparation for electron microscopy was essentially performed as previously described (*50*) with two minor changes: The fixation with glutaraldehyde was performed for 1 hour, and all centrifugation steps were carried out at 1610*g* for 5 min. Ultrathin sectioning was performed using a Leica Ultracut UCT (Leica Microsystems, Wetzlar, Germany) ultramicrotome and an ultra 35° diamond knife (Diatome, Nidau, Switzerland). Ultrathin 50- to 70-nm sections were placed on Pioloform-coated copper slot grids (Plano, Wetzlar, Germany) and poststained for 15 min with uranyl acetate and 3 min with lead citrate, as previously described (*50*). Electron microscopy was performed using a JEOL JEM-1400 Plus transmission electron microscope (JEOL, Tokyo, Japan) operated at 80 kV. Images were taken with a JEOL Ruby CCD camera (3296 × 2472 pixels) and the TEM Center software Ver.1.7.12.1984 (JEOL, Tokyo, Japan).

Miscellaneous

Western blot analyses were performed with isolated mitochondria. Fifty micrograms of isolated mitochondria was preheated on 95°C for 5 min in 1× SDS loading buffer and separated on a 12% SDS gel. After transfer to polyvinylidene difluoride membranes, membranes were incubated with the following primary antibodies in 5% milk and tris-buffered saline: mouse anti-NG (1:1000; Chromotek GmbH), rabbit anti-aconitase1 (1:1000), and rabbit anti-Atp6 (1:1000). Quantitative real-time PCR experiments to determine mtDNA levels were performed as described previously (*51*). For the petite analysis, cells were grown overnight at 30°C, then freshly diluted to an OD_{600} = 0.2, and grown for another 3 hours. A total of 200 cells were plated onto YPG plates containing 0.1% glucose. Plates were incubated for 3 days at 30°C. Only cells proficient in respiratory growth are able to continue growth after all glucose has been consumed.

SUPPLEMENTARY MATERIALS

Supplementary material for this article is available at https://science.org/doi/10.1126/sciadv.abi8886

View/request a protocol for this paper from *Bio-protocol*.

REFERENCES AND NOTES

1. G. S. Gorman, P. F. Chinnery, S. DiMauro, M. Hirano, Y. Koga, R. McFarland, A. Suomalainen, D. R. Thorburn, M. Zeviani, D. M. Turnbull, Mitochondrial diseases. *Nat. Rev. Dis. Primers* **2**, 16080 (2016).
2. W. Fan, K. G. Waymire, N. Narula, P. Li, C. Rocher, P. E. Coskun, M. A. Vannan, J. Narula, G. R. Mac Gregor, D. C. Wallace, A mouse model of mitochondrial disease reveals germline selection against severe mtDNA mutations. *Science* **319**, 958–962 (2008).
3. J. H. Hill, Z. Chen, H. Xu, Selective propagation of functional mitochondrial DNA during oogenesis restricts the transmission of a deleterious mitochondrial variant. *Nat. Genet.* **46**, 389–392 (2014).
4. J. B. Stewart, C. Freyer, J. L. Elson, A. Wredenberg, Z. Cansu, A. Trifunovic, N.-G. Larsson, Strong purifying selection in transmission of mammalian mitochondrial DNA. *PLOS Biol.* **6**, e10 (2008).
5. T. Lieber, S. P. Jeedigunta, J. M. Palozzi, R. Lehmann, T. R. Hurd, Mitochondrial fragmentation drives selective removal of deleterious mtDNA in the germline. *Nature* **570**, 380–384 (2019).
6. Z. Chen, Z.-H. Wang, G. Zhang, C. K. E. Bleck, D. J. Chung, G. P. Madison, E. Lindberg, C. Combs, R. S. Balaban, H. Xu, Mitochondrial DNA segregation and replication restrict the transmission of detrimental mutation. *J. Cell Biol.* **219**, e201905160 (2020).
7. Y. Zhang, Z. H. Wang, Y. Liu, Y. Chen, N. Sun, M. Gucek, F. Zhang, H. Xu, PINK1 inhibits local protein synthesis to limit transmission of deleterious mitochondrial DNA mutations. *Mol. Cell* **73**, 1127–1137.e5 (2019).
8. S. Gruschke, K. Römpler, M. Hildenbeutel, K. Kehrein, I. Kühl, N. Bonnefoy, M. Ott, The Cbp3–Cbp6 complex coordinates cytochrome ***b*** synthesis with bc_1 complex assembly in yeast mitochondria. *J. Cell Biol.* **193**, 1101 (2011).
9. P. S. Philip, C. William Birky, R. L. Strausberg, Segregation of mitochondrial markers in yeast. *Methods Enzymol.* **56**, 139–154 (1979).
10. C. Osman, T. R. Noriega, V. Okreglak, J. C. Fung, P. Walter, Integrity of the yeast mitochondrial genome, but not its distribution and inheritance, relies on mitochondrial fission and fusion. *Proc. Natl. Acad. Sci. U.S.A.* **112**, E947–E956 (2015).
11. J. Nunnari, W. F. Marshall, A. Straight, A. Murray, J. W. Sedat, P. Walter, Mitochondrial transmission during mating in *Saccharomyces cerevisiae* is determined by mitochondrial fusion and fission and the intramitochondrial segregation of mitochondrial DNA. *Mol. Biol. Cell* **8**, 1233–1242 (1997).
12. K. Okamoto, P. S. Perlman, R. A. Butow, The sorting of mitochondrial DNA and mitochondrial proteins in zygotes: Preferential transmission of mitochondrial DNA to the medial bud. *J. Cell Biol.* **142**, 613–623 (1998).
13. R. Azpiroz, R. A. Butow, Patterns of mitochondrial sorting in yeast zygotes. *Mol. Biol. Cell* **4**, 21–36 (1993).
14. K. Okamoto, N. Kondo-Okamoto, Y. Ohsumi, Mitochondria-anchored receptor Atg32 mediates degradation of mitochondria via selective autophagy. *Dev. Cell* **17**, 87–97 (2009).
15. T. Kanki, K. Wang, Y. Cao, M. Baba, D. J. Klionsky, Atg32 is a mitochondrial protein that confers selectivity during mitophagy. *Dev. Cell* **17**, 98–109 (2009).
16. L. Jimenez, D. Laporte, S. Duvezin-Caubet, F. Courtout, I. Sagot, Mitochondrial ATP synthases cluster as discrete domains that reorganize with the cellular demand for oxidative phosphorylation. *J. Cell Sci.* **127**, –719, 726 (2014).
17. T. Stephan, A. Roesch, D. Riedel, S. Jakobs, Live-cell STED nanoscopy of mitochondrial cristae. *Sci. Rep.* **9**, 12419 (2019).
18. F. Vogel, C. Bornhövd, W. Neupert, A. S. Reichert, Dynamic subcompartmentalization of the mitochondrial inner membrane. *J. Cell Biol.* **175**, 237–247 (2006).
19. S. Hoppins, S. R. Collins, A. Cassidy-Stone, E. Hummel, R. M. Devay, L. L. Lackner, B. Westermann, M. Schuldiner, J. S. Weissman, J. Nunnari, A mitochondrial-focused genetic interaction map reveals a scaffold-like complex required for inner membrane organization in mitochondria. *J. Cell Biol.* **195**, 323–340 (2011).

20. K. von der Malsburg, J. M. Müller, M. Bohnert, S. Oeljeklaus, P. Kwiatkowska, T. Becker, A. Loniewska-Lwowska, S. Wiese, S. Rao, D. Milenkovic, D. P. Hutu, R. M. Zerbes, A. Schulze-Specking, H. E. Meyer, J.-C. Martinou, S. Rospert, P. Rehling, C. Meisinger, M. Veenhuis, B. Warscheid, I. J. van der Klei, N. Pfanner, A. Chacinska, M. van der Laan, Dual role of mitofilin in mitochondrial membrane organization and protein biogenesis. *Dev. Cell* **21**, 694–707 (2011).
21. M. Harner, C. Körner, D. Walther, D. Mokranjac, J. Kaesmacher, U. Welsch, J. Griffith, M. Mann, F. Reggiori, W. Neupert, The mitochondrial contact site complex, a determinant of mitochondrial architecture. *EMBO J.* **30**, 4356–4370 (2011).
22. K. M. Davies, C. Anselmi, I. Wittig, J. D. Faraldo-Gomez, W. Kuhlbrandt, Structure of the yeast F1Fo-ATP synthase dimer and its role in shaping the mitochondrial cristae. *Proc. Natl. Acad. Sci. U.S.A.* **109**, 13602–13607 (2012).
23. P. Paumard, J. Vaillier, B. Coulary, J. Schaeffer, V. Soubannier, D. M. Mueller, D. Brèthes, J. P. di Rago, J. Velours, The ATP synthase is involved in generating mitochondrial cristae morphology. *EMBO J.* **21**, 221–230 (2002).
24. M. E. Harner, A.-K. Unger, W. J. Geerts, M. Mari, T. Izawa, M. Stenger, S. Geimer, F. Reggiori, B. Westermann, W. Neupert, An evidence based hypothesis on the existence of two pathways of mitochondrial crista formation. *eLife* **5**, e18853 (2016).
25. R. Rabl, V. Soubannier, R. Scholz, F. Vogel, N. Mendl, A. Vasiljev-Neumeyer, C. Körner, R. Jagasia, T. Keil, W. Baumeister, M. Cyrklaff, W. Neupert, A. S. Reichert, Formation of cristae and crista junctions in mitochondria depends on antagonism between Fcj1 and Su e/g. *J. Cell Biol.* **185**, 1047–1063 (2009).
26. H. Rampelt, M. Bohnert, R. M. Zerbes, S. E. Horvath, B. Warscheid, N. Pfanner, M. van der Laan, Mic10, a core subunit of the mitochondrial contact site and cristae organizing system, interacts with the dimeric F 1 F o-ATP synthase. *J. Mol. Biol.* **429**, 1162–1170 (2017).
27. J. Velours, A. Dautant, B. Salin, I. Sagot, D. Brèthes, Mitochondrial F1F0-ATP synthase and organellar internal architecture. *Int. J. Biochem. Cell Biol.* **41**, 1783–1789 (2009).
28. V. Wilkens, W. Kohl, K. Busch, Restricted diffusion of OXPHOS complexes in dynamic mitochondria delays their exchange between cristae and engenders a transitory mosaic distribution. *J. Cell Sci.* **126**, 103–116 (2013).
29. T. Appelhans, C. P. Richter, V. Wilkens, S. T. Hess, J. Piehler, K. B. Busch, Nanoscale organization of mitochondrial microcompartments revealed by combining tracking and localization microscopy. *Nano Lett.* **12**, 610–616 (2012).
30. H. Schägger, K. Pfeiffer, Supercomplexes in the respiratory chains of yeast and mammalian mitochondria. *EMBO J.* **19**, 1777–1783 (2000).
31. R. W. Gilkerson, J. M. Selker, R. A. Capaldi, The cristal membrane of mitochondria is the principal site of oxidative phosphorylation. *FEBS Lett.* **546**, 355–358 (2003).
32. A. Kowald, T. B. L. Kirkwood, Evolution of the mitochondrial fusion-fission cycle and its role in aging. *Proc. Natl. Acad. Sci. U.S.A.* **108**, 10237–10242 (2011).
33. K. B. Busch, A. Kowald, J. N. Spelbrink, Quality matters: How does mitochondrial network dynamics and quality control impact on mtDNA integrity? *Philos. Trans. R. Soc. B* **369**, 20130442 (2014).
34. D. M. Wolf, M. Segawa, A. K. Kondadi, R. Anand, S. T. Bailey, A. S. Reichert, A. M. van der Bliek, D. B. Shackelford, M. Liesa, O. S. Shirihai, Individual cristae within the same mitochondrion display different membrane potentials and are functionally independent. *EMBO J.* **38**, e101056 (2019).
35. K. Kehrein, R. Schilling, B. V. Möller-Hergt, C. A. Wurm, S. Jakobs, T. Lamkemeyer, T. Langer, M. Ott, Organization of mitochondrial gene expression in two distinct ribosome-containing assemblies. *Cell Rep.* **10**, 843–853 (2015).
36. Y. Itoh, J. Andréll, A. Choi, U. Richter, P. Maiti, R. B. Best, A. Barrientos, B. J. Battersby, A. Amunts, Mechanism of membrane-tethered mitochondrial protein synthesis. *Science* **371**, 846–849 (2021).
37. G. Szyrach, M. Ott, N. Bonnefoy, W. Neupert, J. M. Herrmann, Ribosome binding to the Oxa1 complex facilitates co-translational protein insertion in mitochondria. *EMBO J.* **22**, 6448–6457 (2003).
38. S. Stoldt, D. Wenzel, K. Kehrein, D. Riedel, M. Ott, S. Jakobs, Spatial orchestration of mitochondrial translation and OXPHOS complex assembly. *Nat. Cell Biol.* **20**, 528–534 (2018).
39. S. M. Jin, M. Lazarou, C. Wang, L. A. Kane, D. P. Narendra, R. J. Youle, Mitochondrial membrane potential regulates PINK1 import and proteolytic destabilization by PARL. *J. Cell Biol.* **191**, 933–942 (2010).
40. J. R. McFaline-Figueroa, J. Vevea, T. C. Swayne, C. Zhou, C. Liu, G. Leung, I. R. Boldogh, L. A. Pon, Mitochondrial quality control during inheritance is associated with lifespan and mother-daughter age asymmetry in budding yeast. *Aging Cell* **10**, 885–895 (2011).
41. T. C. Medeiros, R. L. Thomas, R. Ghillebert, M. Graef, Autophagy balances mtDNA synthesis and degradation by DNA polymerase POLG during starvation. *J. Cell Biol.* **217**, 1601–1611 (2018).
42. C. Janke, M. M. Magiera, N. Rathfelder, C. Taxis, S. Reber, H. Maekawa, A. Moreno-Borchart, G. Doenges, E. Schwob, E. Schiebel, M. Knop, A versatile toolbox for PCR-based tagging of yeast genes: New fluorescent proteins, more markers and promoter substitution cassettes. *Yeast* **21**, 947–962 (2004).
43. J. A. Nickoloff, J. D. Singer, M. F. Hoekstra, F. Heffron, Double-strand breaks stimulate alternative mechanisms of recombination repair. *J. Mol. Biol.* **207**, 527–541 (1989).
44. S. M. Rafelski, M. P. Viana, Y. Zhang, Y.-H. M. Chan, K. S. Thorn, P. Yam, J. C. Fung, H. Li, L. da F Costa, W. F. Marshall, Mitochondrial network size scaling in budding yeast. *Science* **338**, 822–824 (2012).
45. J. C. Yen, F. J. Chang, S. Chang, A new criterion for automatic multilevel thresholding. *IEEE Trans. Image Process.* **4**, 370–378 (1995).
46. D. F. Steele, C. A. Butler, T. D. Fox, Expression of a recoded nuclear gene inserted into yeast mitochondrial DNA is limited by mRNA-specific translational activation. *Proc. Natl. Acad. Sci. U.S.A.* **93**, 5253–5257 (1996).
47. P. E. Thorsness, T. D. Fox, Nuclear mutations in *Saccharomyces cerevisiae* that affect the escape of DNA from mitochondria to the nucleus. *Genetics* **134**, 21–28 (1993).
48. M. Rak, E. Tetaud, F. Godard, I. Sagot, B. Salin, S. Duvezin-Caubet, P. P. Slonimski, J. Rytka, J.-P. di Rago, Yeast cells lacking the mitochondrial gene encoding the ATP synthase subunit 6 exhibit a selective loss of complex IV and unusual mitochondrial morphology. *J. Biol. Chem.* **282**, 10853–10864 (2007).
49. J. Schindelin, I. Arganda-Carreras, E. Frise, V. Kaynig, M. Longair, T. Pietzsch, S. Preibisch, C. Rueden, S. Saalfeld, B. Schmid, J.-Y. Tinevez, D. J. White, V. Hartenstein, K. Eliceiri, P. Tomancak, A. Cardona, Fiji: An open-source platform for biological-image analysis. *Nat. Methods* **9**, 676–682 (2012).
50. A. K. Unger, S. Geimer, M. Harner, W. Neupert, B. Westermann, Analysis of yeast mitochondria by electron microscopy, in *Methods in Molecular Biology* (Humana Press Inc., 2017), vol. 1567, pp. 293–314.
51. A. Göke, S. Schrott, A. Mizrak, V. Belyy, C. Osman, P. Walter, Mrx6 regulates mitochondrial DNA copy number in *Saccharomyces cerevisiae* by engaging the evolutionarily conserved Lon protease Pim1. *Mol. Biol. Cell* **31**, 511–545 (2019).

Acknowledgments: We thank T. Kautzleben and N. Lebedeva for technical assistance, L. Heiderscheid and M. Kroker for help with the experimental work, and S. Geimer for help with electron microscopy. OMX microscopy was performed at the Center for Advanced Light Microscopy (CALM). We thank M. Schuldiner and members of the Osman laboratory for critically reading the manuscript. We are grateful for stimulating discussions within the "Mito-Club" throughout the course of this project. We thank Martin Ott and Jean Velours for providing reagents. **Funding:** C.O., C.J., R.R., and F.T. are supported by a grant from the European Research Council (ERCStG-714739 IlluMitoDNA). T.K. is supported by the Elitenetzwerk Bayern through the "Biological Physics" program and by a grant from the Deutsche Forschungsgemeinschaft (DFG, project number 459304237). A.M., D.B., D.H., and H.L. are supported by the SPP 2202 Priority Program of the Deutsche Forschungsgemeinschaft (DFG, project number 422857584). **Author contributions:** C.O. and C.J. designed the project. C.O., C.J., R.R., A.M., F.T., C.S., and T.K. performed experiments and/or analyzed experimental data. D.B. and D.H. developed a software to automatically detect yeast zygotes in microscopic images. C.O., C.J., R.R., and T.K. wrote the manuscript, with contributions from all coauthors. H.L. supervised super-resolution microscopy experiments and development of zygote detection software. P.W. supervised early stages of the project. **Competing interests:** The authors declare that they have no competing interests. **Data and materials availability:** All data needed to evaluate the conclusions in the paper are present in the paper and/or the Supplementary Materials.

Submitted 7 April 2021
Accepted 8 July 2021
Published 1 September 2021
10.1126/sciadv.abi8886

Citation: C. Jakubke, R. Roussou, A. Maiser, C. Schug, F. Thoma, D. Bunk, D. Hörl, H. Leonhardt, P. Walter, T. Klecker, C. Osman, Cristae-dependent quality control of the mitochondrial genome. *Sci. Adv.* **7**, eabi8886 (2021).

Science Advances
AAAS

Supplementary Materials for

Cristae-dependent quality control of the mitochondrial genome

Christopher Jakubke, Rodaria Roussou, Andreas Maiser, Christina Schug, Felix Thoma, David Bunk, David Hörl, Heinrich Leonhardt, Peter Walter, Till Klecker, Christof Osman*

*Corresponding author. Email: osman@bio.lmu.de

Published 1 September 2021, *Sci. Adv.* **7**, eabi8886 (2021)
DOI: 10.1126/sciadv.abi8886

The PDF file includes:

Other Supplementary Material for this manuscript includes the following:

Supplementary materials

Figure S1

(A) Quantitative PCR analysis of mtDNA levels of WT or Δ*cob::ARG8* strains, which were used in the pedigree analysis (Fig. 1C). No difference in mtDNA levels between both strains are apparent. The average value is derived from three biological replicates. The value for each biological replicate was derived from three technical replicates; Error bars indicate SD. n. s. - non significant, t-test.

(B) Carry-over cell material does not support growth upon restreaking. Replica plating during the pedigree analysis results in carry-over of cell material. While such cell material is easily distinguished from growing cells by direct visual inspection of plates, it is difficult to discern on photos. For this experiment, cell material was restreaked on selective plate to demonstrate the difference between carry-over cell material and cell growth. Asterisks indicate carry-over cell material.

(C) PCR analysis corroborates results from the growth-based pedigree assay. Genomic DNA was extracted directly from YPD grown colonies without further incubation from three pedigree lineages and remaining cell material was replica plated onto YPG or SC-ARG (lacking arginine) plates. Presence of the *COB* gene (present in WT mtDNA, which supports growth on YPG) or the *ARG8* gene (present in Δ*cob::ARG8* mtDNA, which supports growth on SC-Arg) was tested by PCR using specific oligos for the respective genes. PCR results correlate perfectly with the growth based analysis.

(D) Schematic illustration of the pedigree analysis, explaining the skipping of generations on a respective medium. YPG - rich medium containing the non-fermentable carbon source glycerol, SC-Arg - synthetic defined medium lacking arginine.

Figure S2

(A) Pedigree analysis of WT cells. The experiment is virtually identical to the experiment presented in Fig. 1C with the difference that the starting strains for the pedigree analysis had switched mating types. Specifically, in this experiment the strain containing WT mtDNA had mating type *alpha*, whereas the strain containing Δ*cob::ARG8* had mating type *a*. Striped bars indicate percentage of heteroplasmic cells containing WT and Δ*cob::ARG8* mtDNA. Grey or red bars indicate percentage of homoplasmic cells containing WT or Δ*cob::ARG8* mtDNA, respectively.

(B) Pedigree analysis of cells containing *ARG8* inserted neutrally into mtDNA upstream of the *COX2* gene. We cannot distinguish between cells that are heteroplasmic for both mtDNA species and cells where *ARG8* had recombined into WT mtDNA. The shown result, however, indicates that *ARG8* does not confer a strong disadvantage on mtDNA, which could lead to its removal.

Figure S3

(A) Quantitative PCR analysis of mtDNA levels of WT or Δ*cob::ARG8-TetO*-TetR-3xmRuby3 strains, which were used for the microscopy experiments presented in Fig. 1D. A slight increase in the mtDNA levels of the Δ*cob::ARG8-TetO*-TetR-3xmRuby3 is apparent. The average value is derived from three biological replicates. The value for each biological replicate was derived from three technical replicates; Error bars indicate SD. n. s. - non significant, t-test.

(B) Additional microscopic images of the inheritance of either LacO-marked intact or TetO-marked Δ*cob::ARG8-TetO* mtDNA. Images complement data shown in Fig. 1D.

Scale bar: D 10 μm.

Figure S4

(A and B) Time-lapse microscopy of mating events between WT cells expressing either matrix-targeted NG or matrix-targeted mKate2. Mating events are shown, where either both cells contained WT mtDNA (A) or one cell contained WT mtDNA and the other contained Δ*cob::ARG8* mtDNA (B). Selected time-frames for (B) are shown in Fig. 1E.

(C and D) Similar to (A), except that cells with deletions of the nuclear-encoded Δ*dnm1* (C) or Δ*atg32* (D) were used.

Scale bars: A-D 10 μm.

Figure S5

(A) Schematic illustration of the NG-tagged *ATP6* within mtDNA.

(B) Quantitative PCR analysis of mtDNA levels of WT or strains expressing the Atp6-NG protein. The average value is derived from three biological replicates. The value for each biological replicate was derived from three technical replicates; Error bars indicate SD. n. s. - non significant, t-test.

(C) Petite frequency of the Atp6-NG strain in comparison to WT and the Δ*atp21* strains.

(D) Westernblot analysis of strains harbouring either WT or *ATP6-NG* mtDNA. Aconitase (Aco1) was used as a loading control.

(E) Widefield fluorescence microscopy images of diploid cells harbouring *ATP6*-NG mtDNA and expressing nuclear-encoded matrix-targeted mScarlet.
Scale bar: E 10 μm.

Figure S6

(A) Time-lapse microscopy of mating events between WT cells harbouring *ATP6*-NG mtDNA and WT cells harbouring WT mtDNA and expressing nuclear-encoded matrix-targeted Kate2.

(B) Time-lapse microscopy of mating events between cells expressing NG-tagged Cox4 and cells expressing nuclear-encoded matrix-targeted mKate2.

(C) Growth analysis of strains expressing NG fused to Pam16 or the transmembrane domain of Fis1 in comparison to WT. Strains were used in the time-lapse experiment presented in Fig. 2, E and F and Fig. S4D and E.

(D) Westernblot analysis of strains harbouring the NG-tagged version of Pam16. Aconitase was used as a loading control. Note that no signal for free NG is detectable indicating that NG is not cleaved off.

(E) Time-lapse microscopy of mating events between WT cells expressing NG fused to the transmembrane domain of Fis1 and WT cells expressing nuclear-encoded matrix-targeted mKate2.

(F) Time-lapse microscopy of mating events between cells expressing NG-tagged Pam16 and cells expressing nuclear-encoded matrix-targeted mKate2.

Scale bars: A and D-E 10 μm.

Figure S7

(A) Quantification of the equilibration of soluble Su9-mKate2 protein in mating experiments shown in Fig. 3A and B; ** P<0.01, t-test.

(B) Quantification of the Atp6-NG in the daughter cells of zygotes from mating experiments shown in Fig. 3A and B; * P<0.05, t-test.

(C) Spot test of strains expressing Atp6-NG or Atp6-mKate2 compared to the WT and a strain harbouring Δ*atp6* mtDNA.

(D) Quantification of the co-localization of Atp6-NG and Atp6-mKate2 in daughter cells derived from matings between WT, Δ*atp20* or Δ*atp20* cells, in which parental cells contained either *ATP6-NG* or *ATP6-mKate2* mtDNA. The Pearson (PCC) and Manders (MCC) correlation coefficients between Atp6-NG and Atp6-mKate2 signals along the mitochondrial network of daughter cells were determined for multiple cells in three independent experiments; * P<0.05, ** P<0.01, t-test.

Figure S8

(A) Electron micrographs of mitochondria from WT, Δ*atp20*, Δ*atp21*, and Δ*atp20* Δ*atp21* cells grown in rich medium containing glucose.

(B) Quantification of cristae shape from cells grown in rich medium containing glucose. For each strain, mitochondria from 50 cells were scored for mitochondrial ultrastructure and grouped into the indicated categories. Shown is the mean ± standard deviation from three independent experiments. Examples of mitochondria with altered cristae shape are depicted on the right.

(C) Electron micrographs of mitochondria from Δ*atp20* Δ*atp21* cells grown in rich medium containing galactose. Shown are two representative cells. For each cell, the same mitochondrion was imaged in consecutive 70 nm ultrathin sections.

Scale bars: A and C 500 nm; B 200 nm.

Figure S9

(A) Quantitative PCR analysis of mtDNA levels of WT, Δ*atp20*, Δ*atp21*, Δ*atp20*Δ*atp21*, Δ*mic10*, or Δ*mic60* strains containing WT or Δ*cob* mtDNA. Strains were used for the pedigree analysis presented in Figure 4A-F. The average value is derived from three biological replicates. The value for each biological replicate was derived from three technical replicates; Error bars indicate SD. n. s. - non significant, t-test.

(B) Petite frequency of the indicated deletion strains.

Movie S1

Mitochondrial morphology during mating events of WT cells. Mating events between two cells containing either WT or Δ*cob::ARG8* mtDNA. Cells expressed either matrix-targeted mKate2 (WT mtDNA, cyan) or NG (Δ*cob::ARG8* mtDNA, magenta). Mating events were monitored by live-cell microscopy. Brightfield, single fluorescent channels and a merge from both fluorescent channels are shown.

Movie S2

Mitochondrial morphology during mating events of Δ*dnm1* cells. Mating events between two Δ*dnm1* cells containing either WT or Δ*cob::ARG8* mtDNA. Cells expressed either matrix-targeted mKate2 (WT mtDNA, cyan) or NG (Δ*cob::ARG8* mtDNA, magenta). Mating events were monitored by live-cell microscopy. Brightfield, single fluorescent channels and a merge from both fluorescent channels are shown. Images were taken in 7 min intervals.

Movie S3

Mitochondrial morphology during mating events of Δ*atg32* cells. Mating events between two Δ*atg32* cells containing either WT or Δ*cob::ARG8* mtDNA. Cells expressed either matrix-targeted mKate2 (WT mtDNA, cyan) or NG (Δ*cob::ARG8* mtDNA, magenta). Mating events were monitored by live-cell microscopy. Brightfield, single fluorescent channels and a merge from both fluorescent channels are shown. Images were taken

in 7 min intervals.

Movie S4

Diffusion of mitochondrial-encoded Atp6-NG throughout the mitochondrial network of zygotes. Cells expressing matrix-targeted mKate2 (cyan) were mated with cells expressing mtDNA-encoded Atp6-NG (magenta) and were monitored by live cell imaging. Brightfield, single fluorescent channels and a merge from both fluorescent channels are shown. Images were taken in 7 min intervals.

Movie S5

Diffusion of Fis-NG throughout the mitochondrial network of zygotes. Cells expressing matrix-targeted mKate2 (cyan) were mated with cells expressing nuclear-encoded Fis1-NG (magenta) and were monitored by live cell imaging. Brightfield, single fluorescent channels and a merge from both fluorescent channels are shown. Images were taken in 7 min intervals.

Movie S6

Diffusion of Pam16-NG throughout the mitochondrial network of zygotes. Cells expressing matrix-targeted mKate2 (cyan) were mated with cells expressing nuclear-encoded Pam16-NG (magenta) and were monitored by live cell imaging. Brightfield, single

fluorescent channels and a merge from both fluorescent channels are shown. Images were taken in 7 min intervals.

Table S1

Yeast strains used in this study.

Table S2

Primers used in this study.

Table S3

Plasmids used in this study.

Supplemental Figure 1

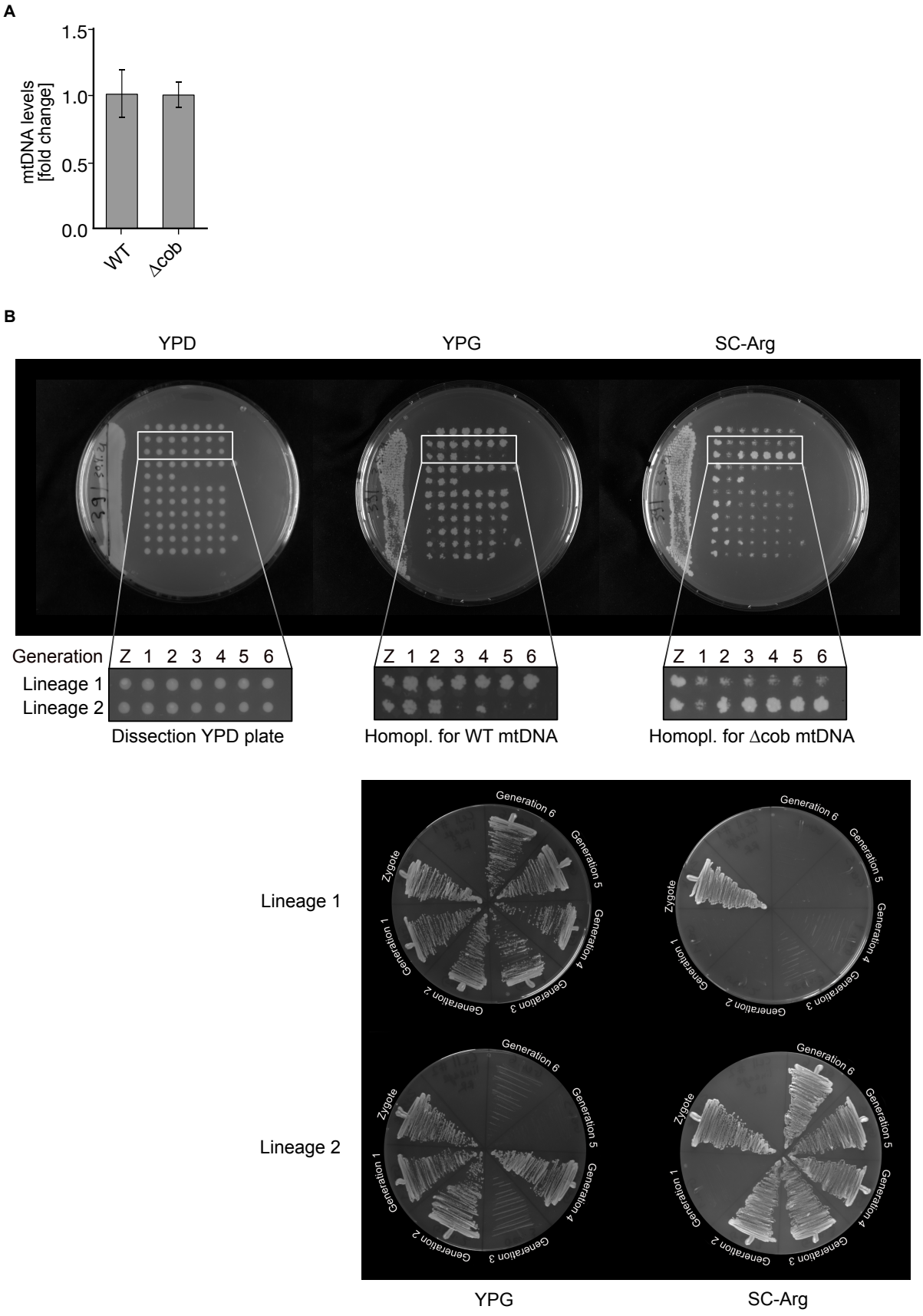

Supplemental Figure 1

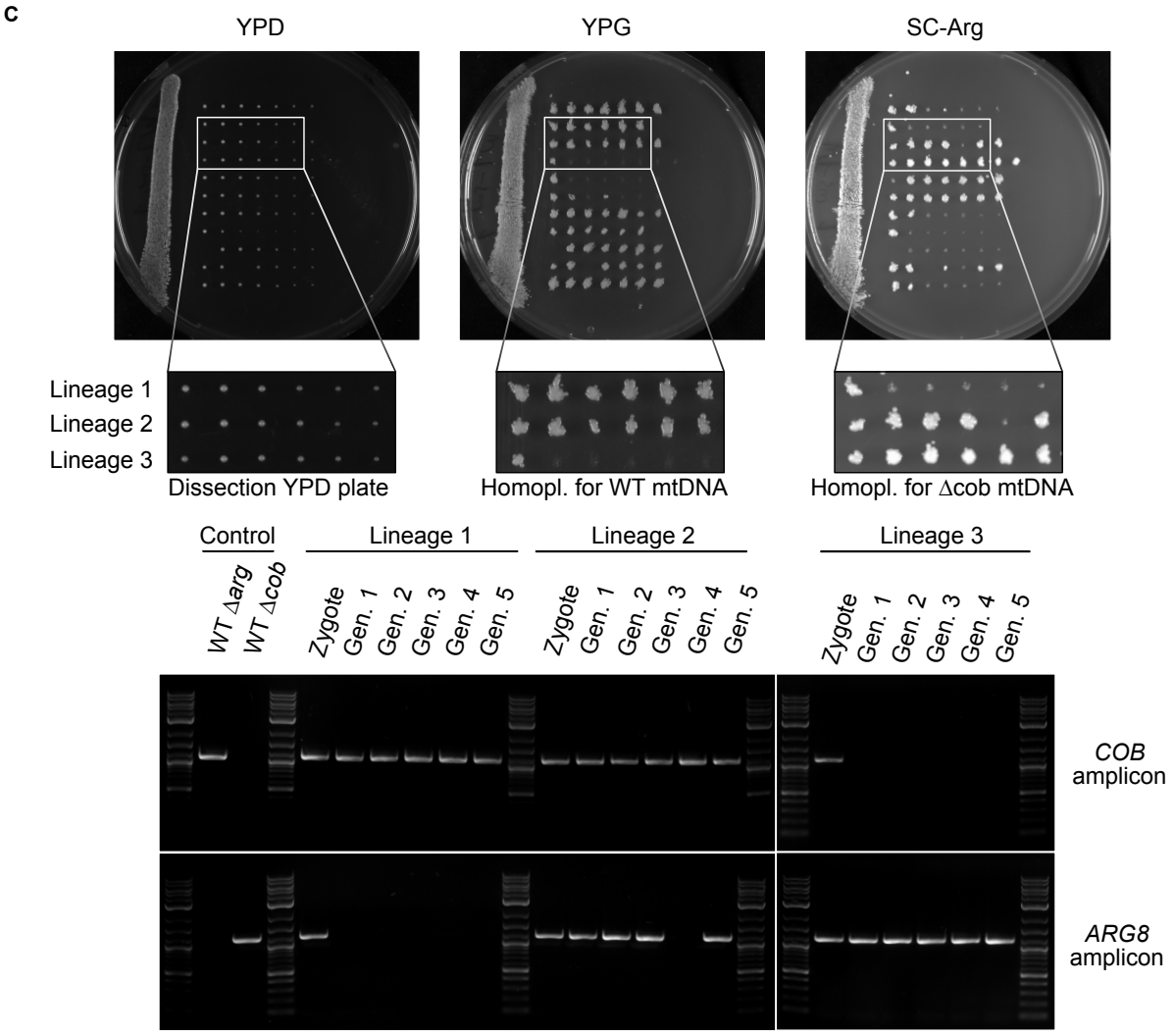

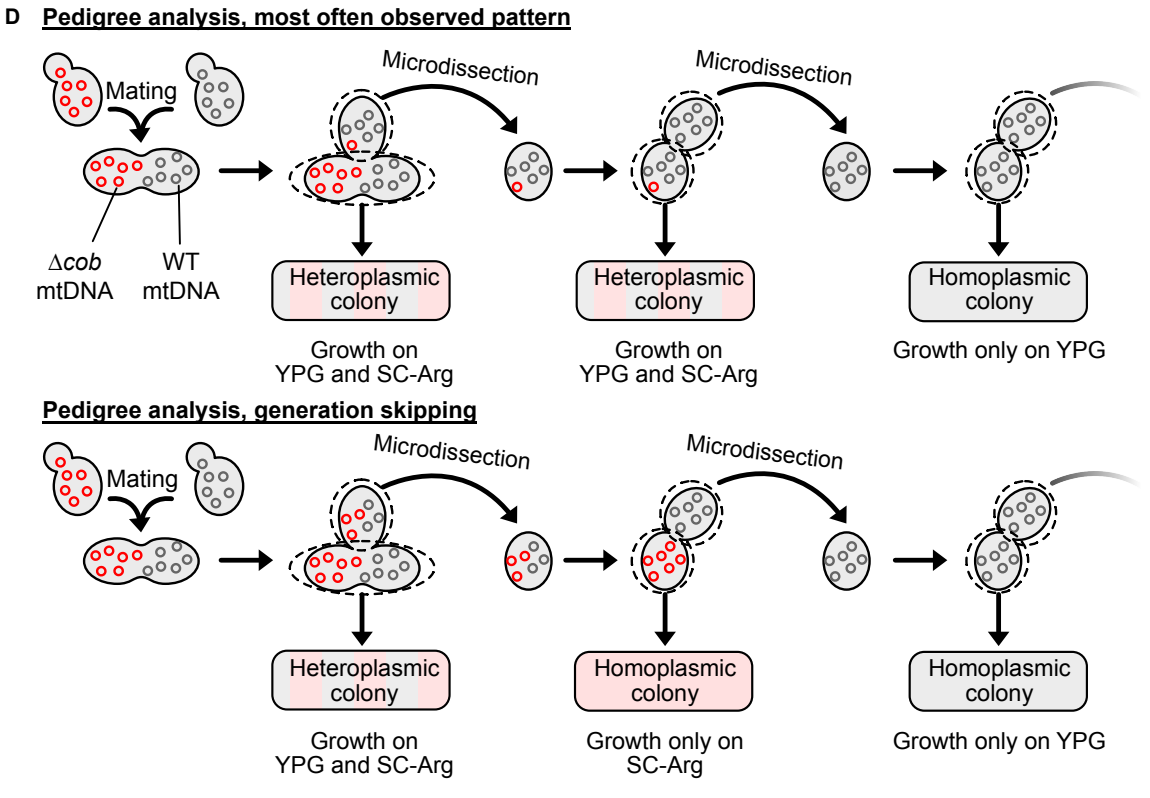

Supplemental Figure 2

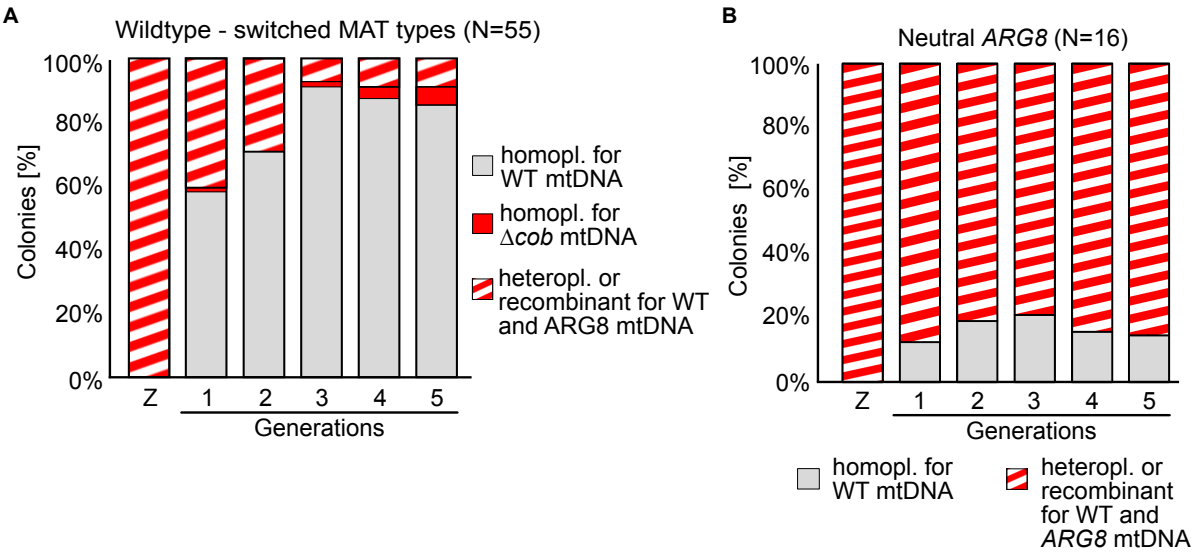

Supplemental Figure 3

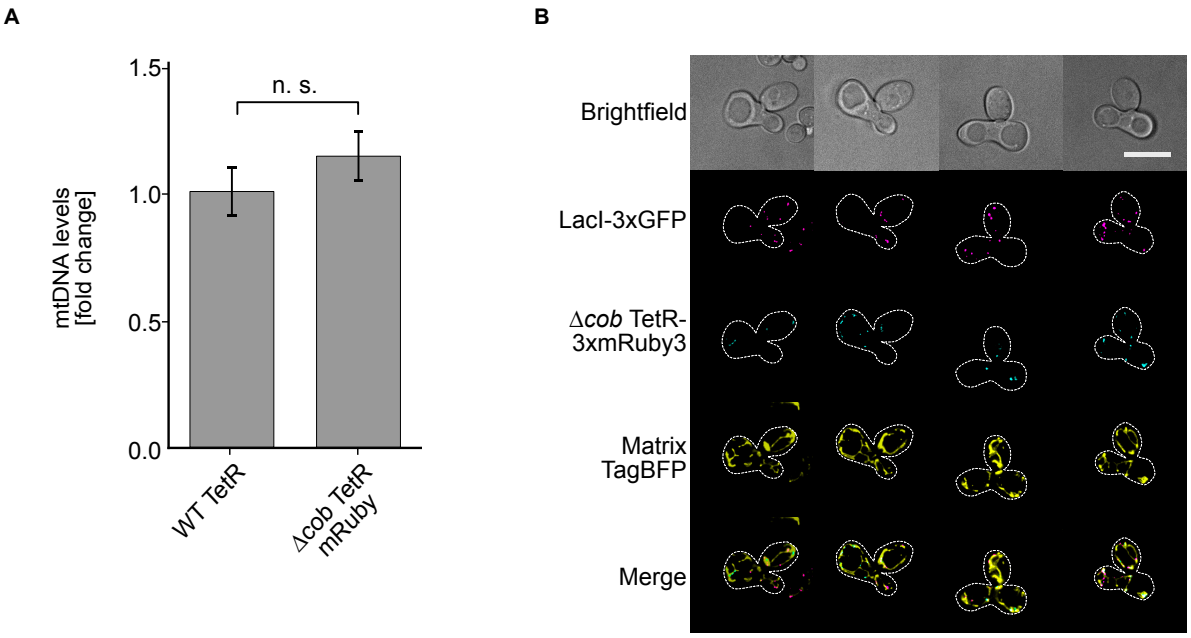

Supplemental Figure 4

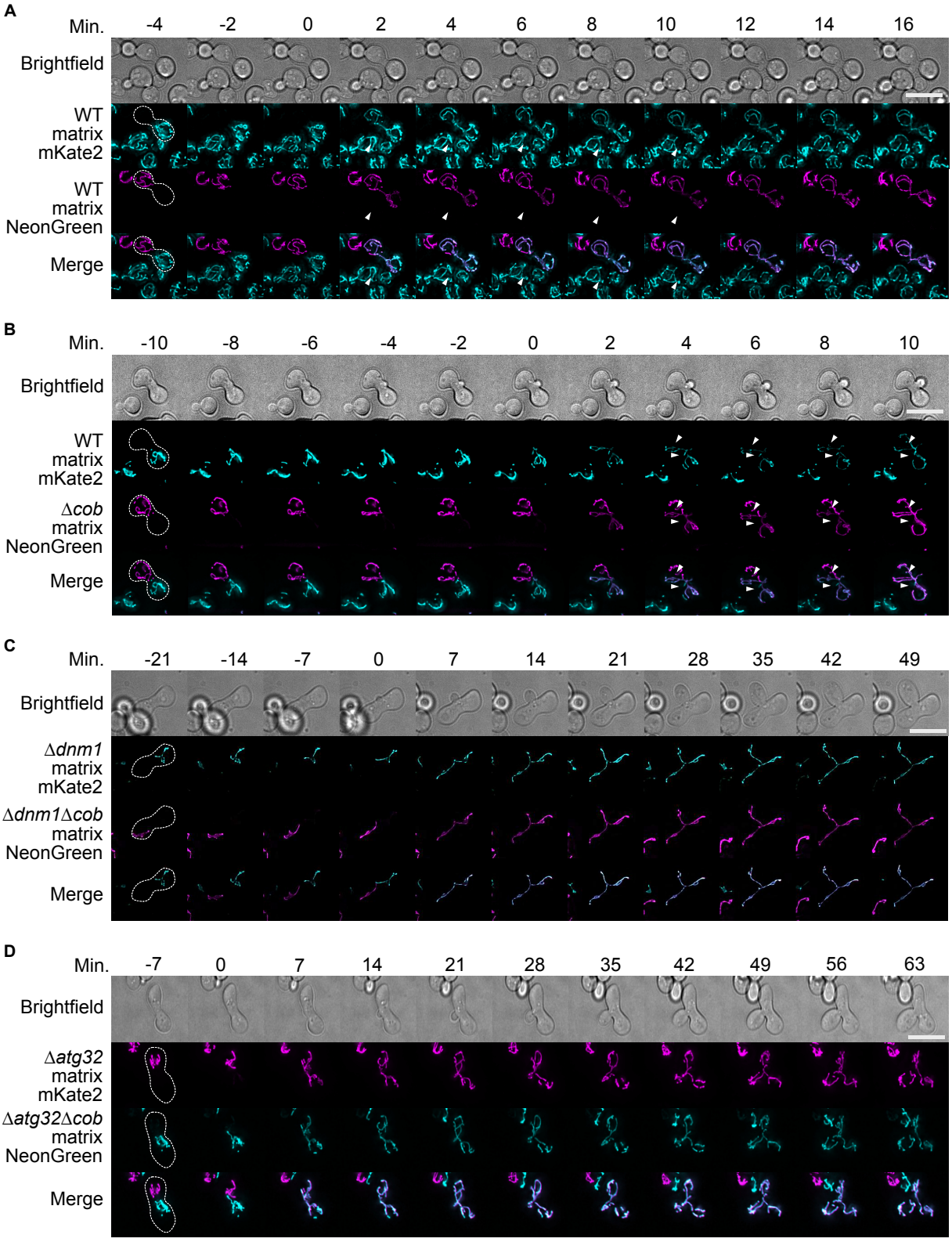

Supplemental Figure 5

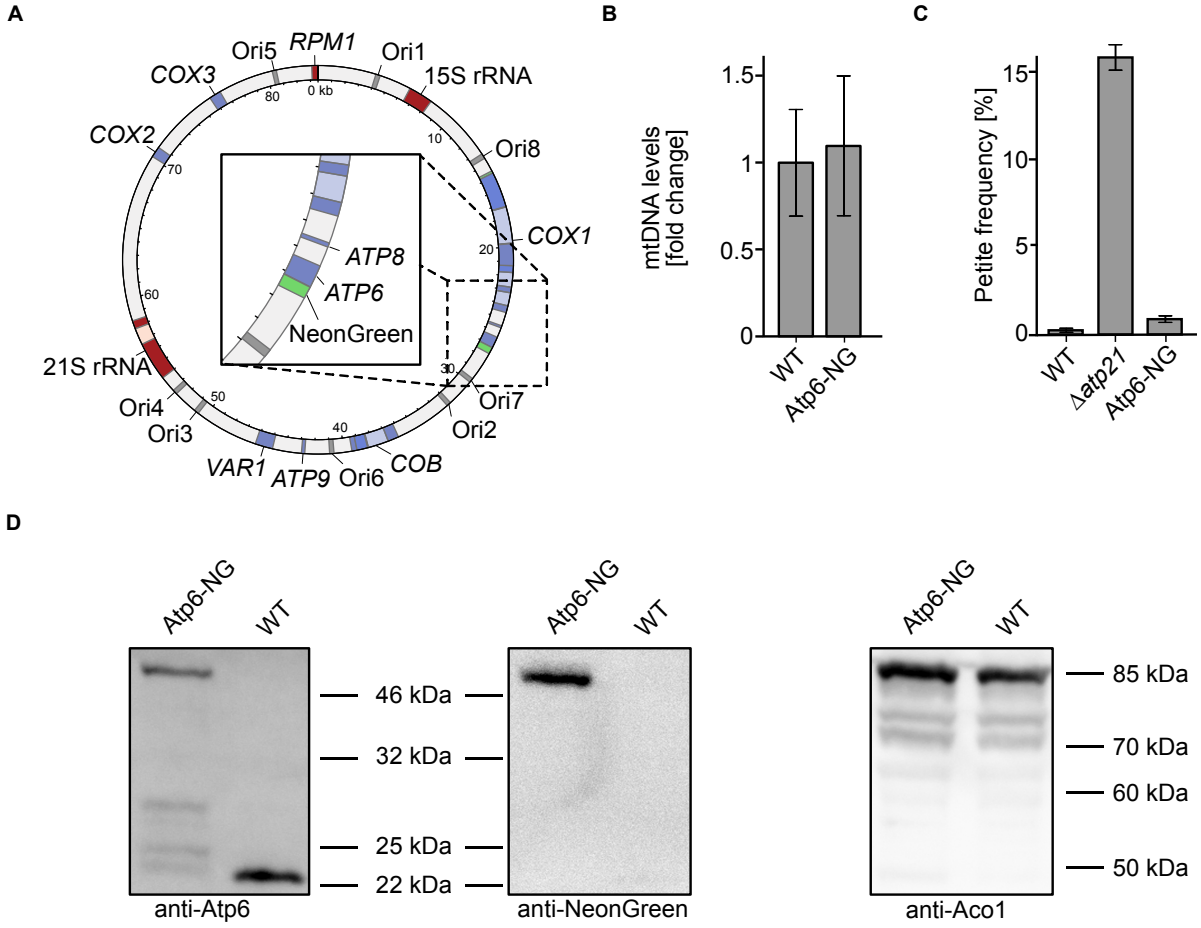

Supplemental Figure 6

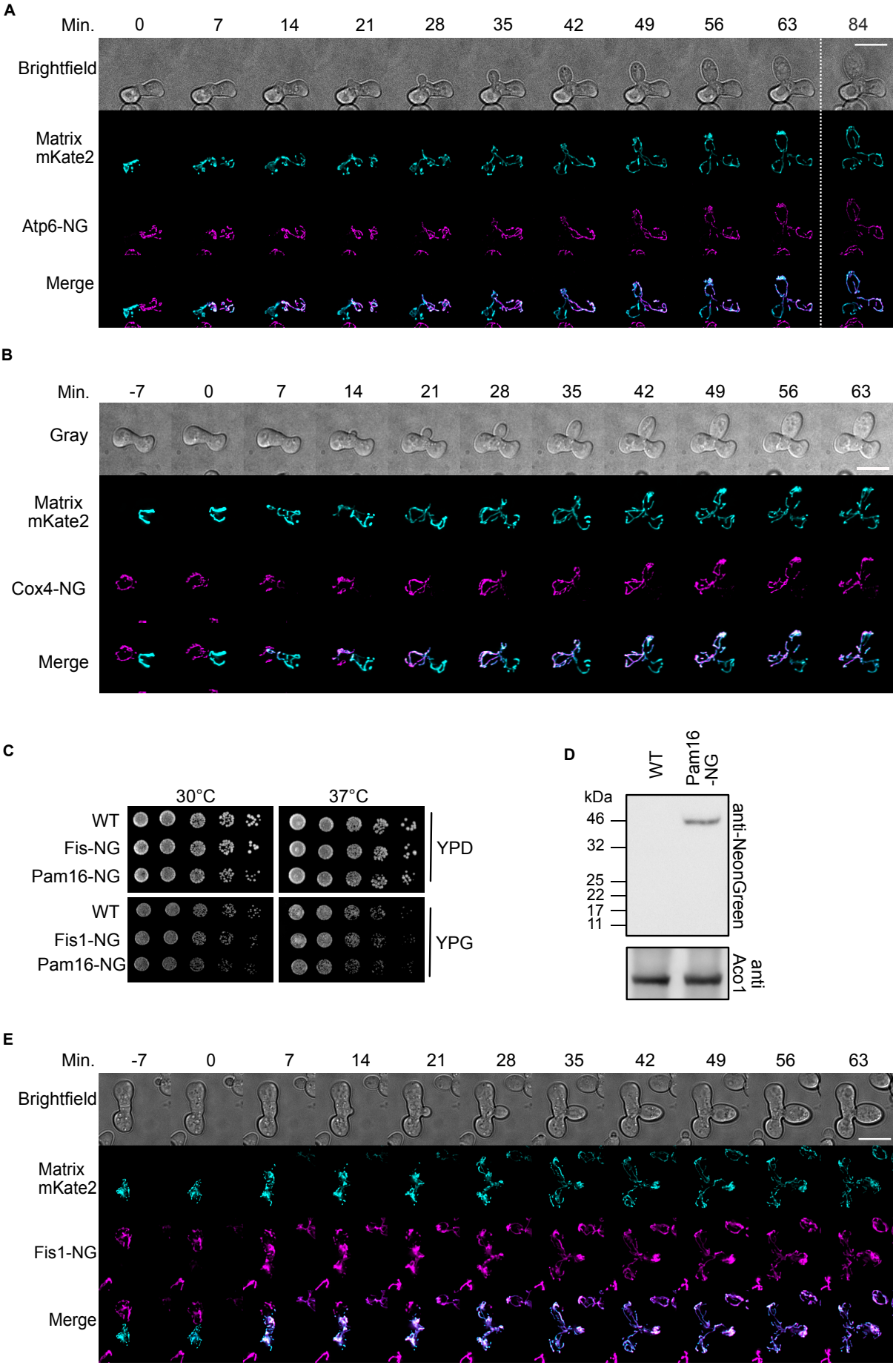

Supplemental Figure 6

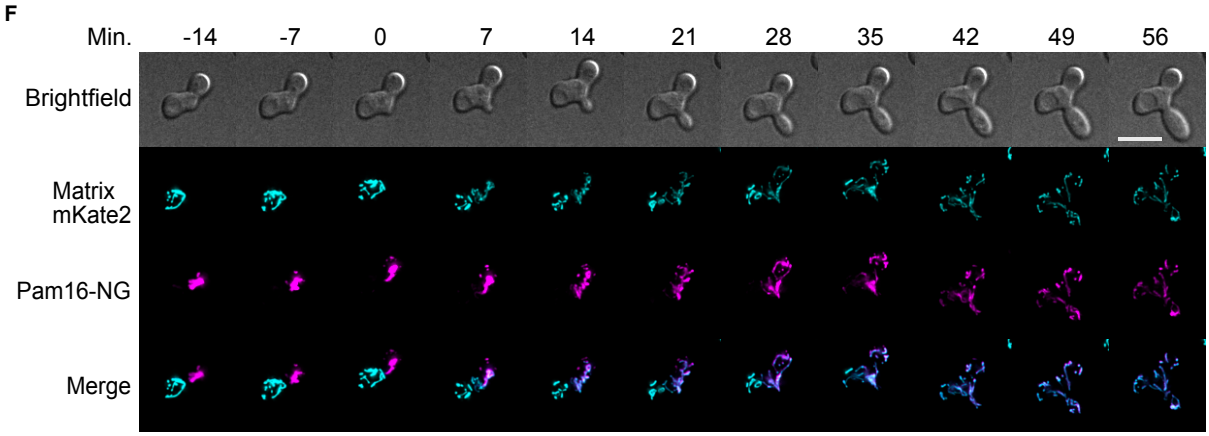

Supplemental Figure 7

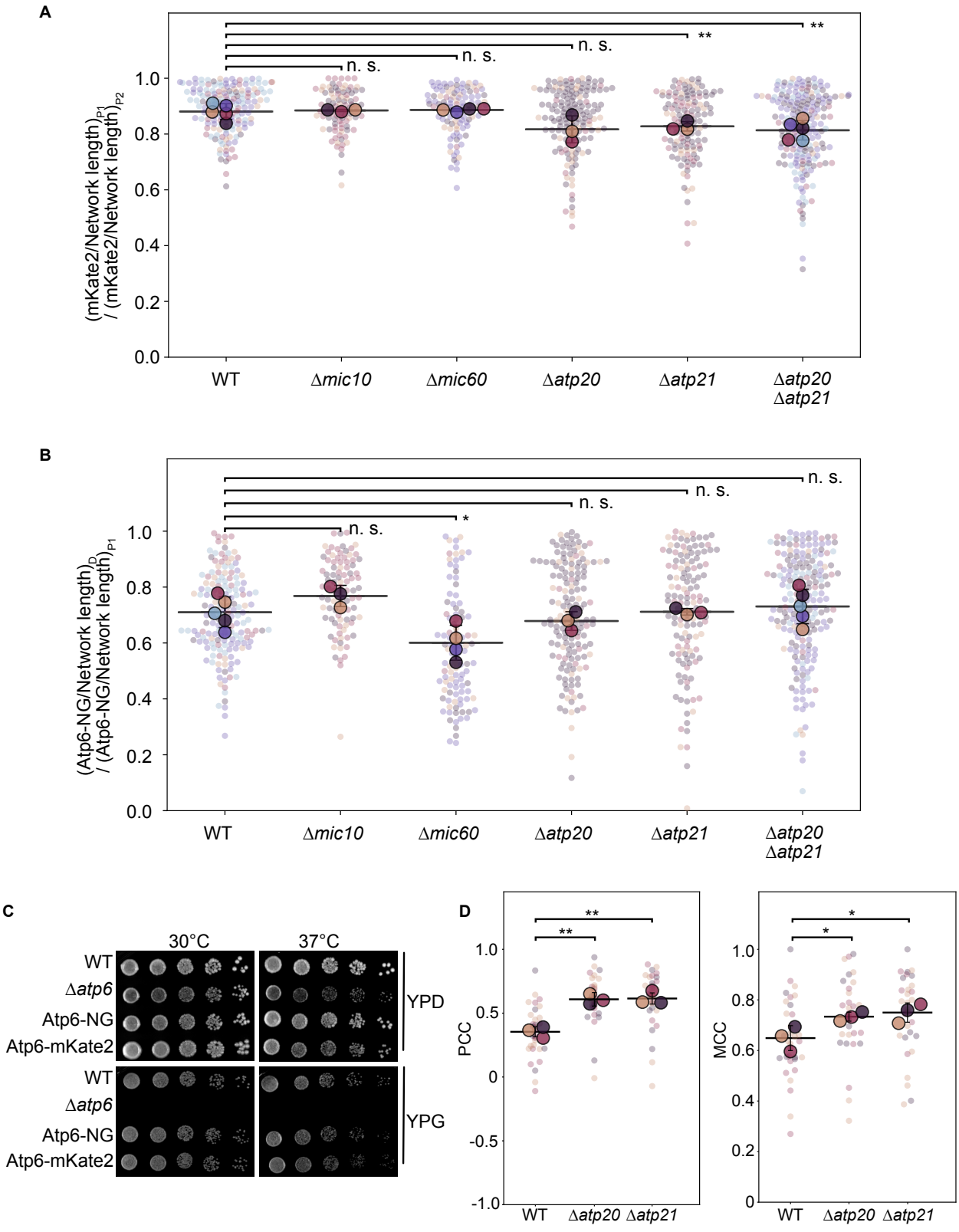

Supplemental Figure 8

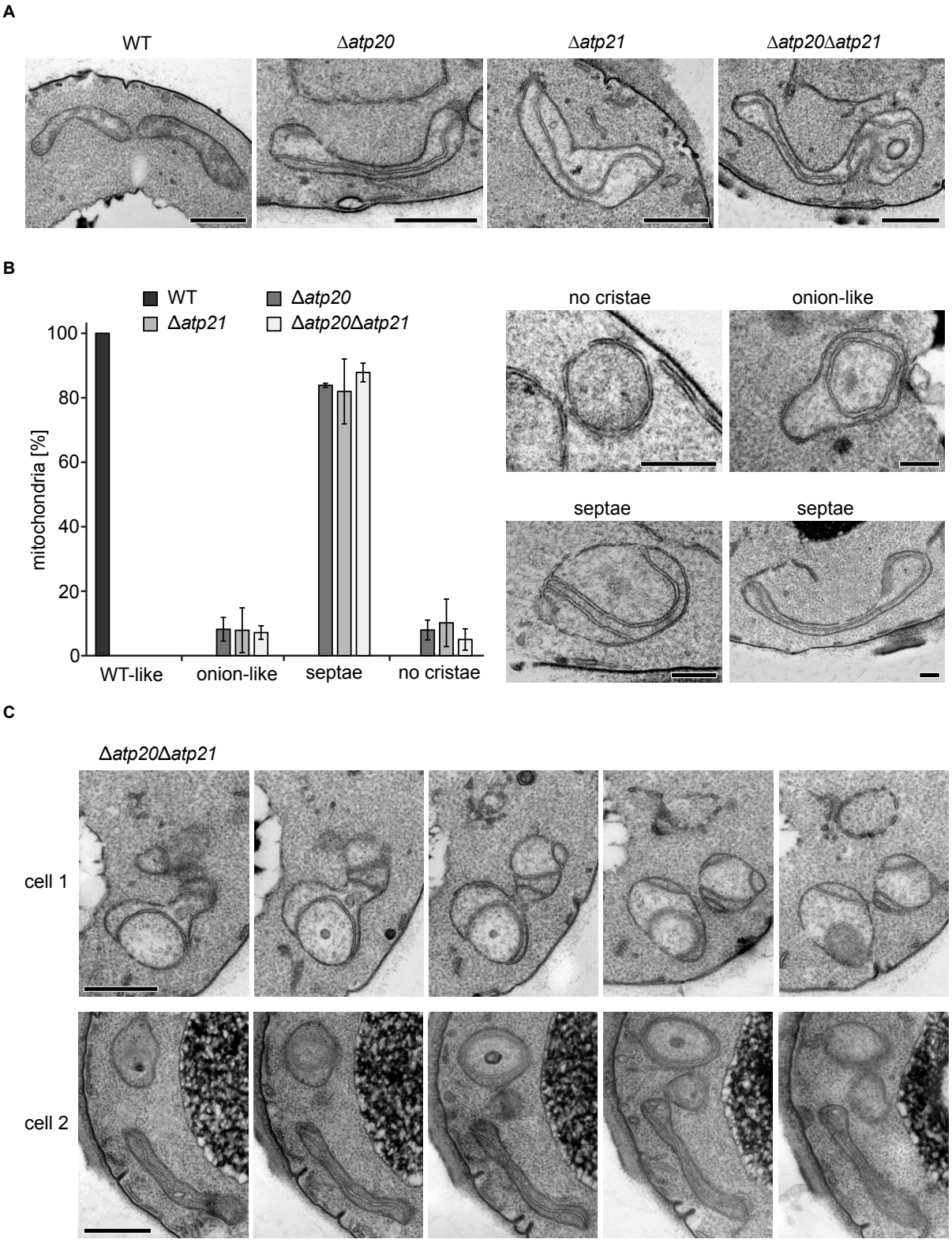

Supplemental Figure 9

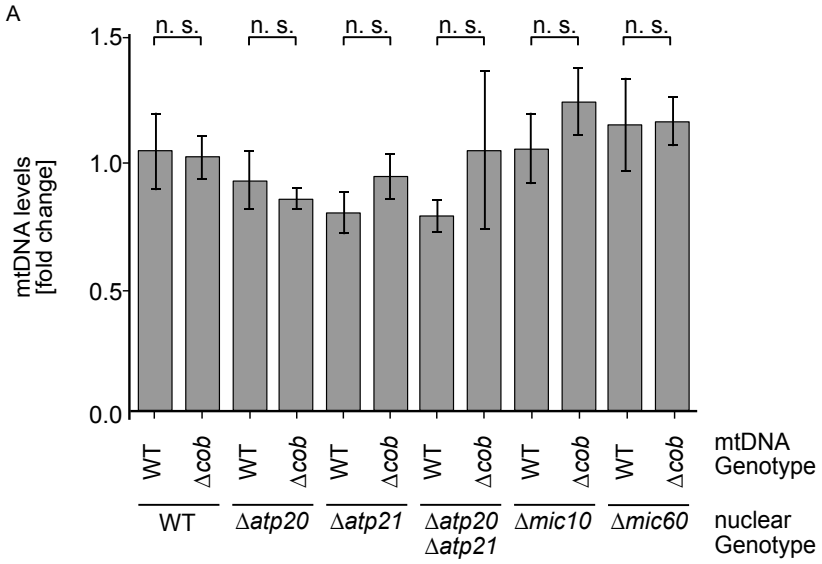

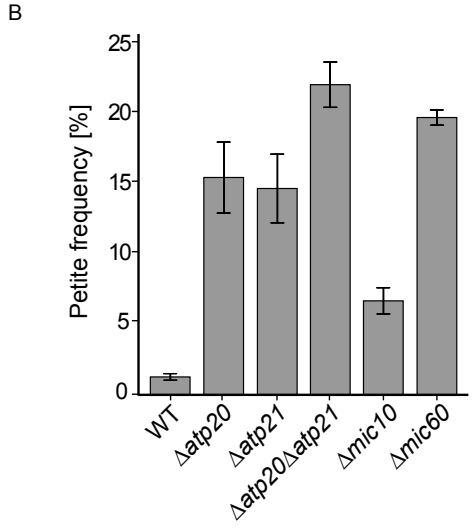

Table 1 - Yeast Strains used in this study

Name / Alias	Short description	Mating type	Genotype	Source
yCO380	WT	*Mat a*	*leu2-3,112 can1-100 ura3-1 his3-11,15 mt-LacO*	1
yCO381	WT	*Mat alpha*	*leu2-3,112 can1-100 ura3-1 his3-11,15 mt-LacO*	1
yCO391	*∆arg8*	*Mat a*	*ade2-1 his3-11,15 trp1-1 leu2-3,112 ura3-1 CAN1 arg8::HIS3 intronless mtDNA*	2
yCO354	*Δarg8::HIS3 Δcob::ARG8M*	*Mat alpha*	*ade2-1 his3-11,15 trp1-1 leu2-3,112 ura3-1 CAN1 arg8::HIS3 cob::ARG8M intronless mtDNA*	2
yCJ048	Neutral ARG8	*Mat alpha*	*leu2-3,112 can1-100 ura3-1 his3-11,15 ∆arg8::hphNT1 ARG8::mtDNA*	This study
yCO392	*∆arg8*	*Mat alpha*	*ade2-1 his3-11,15 trp1-1 leu2-3,112 ura3-1 CAN1 arg8::HIS3 intronless mtDNA*	This study
yCO969	*Δarg8::HIS3 Δcob::ARG8M*	*Mat a*	*ade2-1 his3-11,15 trp1-1 leu2-3,112 ura3-1 CAN1 arg8::HIS3 cob::ARG8M intronless mtDNA*	This study
yCO460	*Δcob::ARG8*-TetO-TetR-3xRuby	*Mat a*	*leu2-3,112 trp1-1 can1-100 ura3-1 his3-11,15 Δarg8::hphNT pvt100u-mtTagBFP HO-Su9-TetR-3xmRuby3--KanMX4-HO Δcob::ARG8-TetO*	This study
yCJ033	LacO-LacI-3xGFP	*Mat alpha*	*leu2-3,112 can1-100 ura3-1 his3-11,15 mt-LacO HO-Su9-TagBFP-Pcup-Su9-3xGFP-LacI::kanMX4*	This study
yCJ009	HO::Su9-mKate2	*Mat a*	*leu2-3,112 can1-100 ura3-1 his3-11,15 mt-LacO HO::Su9-mKate2::kanMX6*	This study

yCJ010	HO::Su9-NG	*Mat alpha*	*leu2-3,112 can1-100 ura3-1 his3-11,15 mt-LacO HO::Su9-NG::kanMX6*	This study
yCJ078	∆*arg8::HIS3* ∆cob::*ARG8M* HO::Su9-NG	*Mat alpha*	*ade2-1 his3-11,15 trp1-1 leu2-3,112 ura3-1 CAN1 arg8::HIS3 cob::ARG8M HO::Su9-NG-kanMX6 intronless mtDNA*	This study
yCJ081	∆*arg8::HIS3* HO::Su9-mKate2	*Mat a*	*ade2-1 his3-11,15 trp1-1 leu2-3,112 ura3-1 CAN1 arg8::HIS3 intronless mtDNA HO::Su9-mKate2::kanMX6*	This study
yCJ002	*Δdnm1 Δarg8::HIS3 Δcob::ARG8M*	*Mat alpha*	*ade2-1 his3-11,15 trp1-1 leu2-3,112 ura3-1 CAN1 arg8::HIS3 cob::ARG8M intronless mtDNA ∆dnm1::hphNT1*	This study
yCJ004	∆*dnm1 ∆arg8*	*Mat a*	*ade2-1 his3-11,15 trp1-1 leu2-3,112 ura3-1 CAN1 arg8::HIS3 intronless mtDNA ∆dnm1::hphNT1*	This study
yCJ085	*Δdnm1 Δarg8::HIS3 Δcob::ARG8M HO::Su9-NG*	*Mat alpha*	*ade2-1 his3-11,15 trp1-1 leu2-3,112 ura3-1 CAN1 arg8::HIS3 cob::ARG8M intronless mtDNA ∆dnm1::hphNT1 HO::Su9-NG-kanMX6*	This study
yCJ086	∆*dnm1 ∆arg8 HO::Su9-mKate2*	*Mat a*	*ade2-1 his3-11,15 trp1-1 leu2-3,112 ura3-1 CAN1 arg8::HIS3 intronless mtDNA ∆dnm1::hphNT1 HO::Su9-mKate2-kanMX6*	This study
yCJ074	*Δatg32 Δarg8::HIS3 Δcob::ARG8M*	*Mat alpha*	*ade2-1 his3-11,15 trp1-1 leu2-3,112 ura3-1 CAN1 arg8::HIS3 cob::ARG8M intronless mtDNA ∆atg32::hphNT1*	This study
yCJ075	∆*atg32 ∆arg8*	*Mat a*	*ade2-1 his3-11,15 trp1-1 leu2-3,112 ura3-1 CAN1 arg8::HIS3 intronless mtDNA ∆atg32::hphNT1*	This study
yCJ076	*Δatg32 Δarg8::HIS3 Δcob::ARG8M HO::Su9-NG*	*Mat alpha*	*ade2-1 his3-11,15 trp1-1 leu2-3,112 ura3-1 CAN1 arg8::HIS3 cob::ARG8M intronless mtDNA ∆atg32::hphNT1 HO::Su9-NG-kanMX6*	This study

yCJ077	Δ*atg32* Δ*arg8 HO::Su9-mKate2*	*Mat a*	*ade2-1 his3-11,15 trp1-1 leu2-3,112 ura3-1 CAN1 arg8::HIS3 intronless mtDNA Δatg32::hphNT1 HO::Su9-mKate2-kanMX6*	This study
yCO114	*rho^0*	*Mat alpha*	*leu2 ura3-52 ade2-101 arg8::URA3 kar1-1 rho^0*	3
yCO115	*rho$^+$ Δcox2*	*Mat a*	*lys2 leu2-3,112 ura3-52 his3HinDIII arg8::hisG rho$^+$ cox2-62*	3
yCJ025	MR6 WT	*Mat a*	*ade2-1 his3-11,15 trp1-1 leu2-3,112 ura3-1 CAN1 arg8::HIS3*	4
yCJ026	MR10 Δ*atp6*	*Mat a*	*ade2-1 his3-11,15 trp1-1 leu2-3,112 ura3-1 CAN1 arg8::HIS3 Δatp6*	4
yCJ043	*ATP6*-NG	*Mat a*	*ade2-1 his3-11,15 trp1-1 leu2-3,112 ura3-1 CAN1 arg8::HIS3 ATP6-NG*	This study
yCJ126	HO::Su9-mScarlet *ATP6*-NG	*Mat a/ alpha*	*ade2-1 his3-11,15 trp1-1 leu2-3,112 ura3-1 CAN1 arg8::HIS3 ATP6-NG HO::Su9-mScarlet-URA3*	This study
yCJ045	HO::Su9-mKate2	*Mat alpha*	*leu2-3,112 can1-100 ura3-1 his3-11,15 mt-LacO HO::Su9-mKate2-kanMX6*	This study
yCJ019	*COX*4-NeonGreen	*Mat alpha*	*leu2-3,112 can1-100 ura3-1 his3-11,15 mt-LacO Cox4-NeonGreen*	This study
yCJ072	Fis1-NG	*Mat a*	*ade2-1 his3-11,15 trp1-1 leu2-3,112 ura3-1 CAN1 arg8::HIS3 intronless mtDNA FIS1-NG::kanMX6*	This study
yCJ114	Pam16-NG	*Mata*	*leu2-3,112 can1-100 ura3-1 his3-11,15 mt-LacO PAM16-NG::kanMX*	This study
yCJ051	Δ*atp21 ATP6*-NG	*Mat a*	*ade2-1 his3-11,15 trp1-1 leu2-3,112 ura3-1 CAN1 arg8::HIS3 ATP6-NG Δatp21::hphNT1*	This study
yCJ052	Δ*atp21* HO::Su9-mKate2	*Mat alpha*	*leu2-3,112 can1-100 ura3-1 his3-11,15 mt-LacO Mito Δatp21::hphNT1 HO::Su9-mKate2-kanMX6*	This study

yCJ053	Δ*atp20 ATP6*-NG	*Mat a*	*ade2-1 his3-11,15 trp1-1 leu2-3,112 ura3-1 CAN1 arg8::HIS3 ATP6-NG Δatp20::hphNT1*	This study
yCJ054	Δ*atp20* HO::Su9-mKate2	*Mat alpha*	*leu2-3,112 can1-100 ura3-1 his3-11,15 mt-LacO Mito Δatp20::hphNT2 HO::Su9-mKate2-kanMX6*	This study
yCJ057	Δ*atp20*Δ*atp21 ATP6*-NG	*Mat a*	*ade2-1 his3-11,15 trp1-1 leu2-3,112 ura3-1 CAN1 arg8::HIS3 ATP6-NG Δatp21::hphNT1 Δatp20::hphNT2*	This study
yCJ058	Δ*atp20*Δ*atp21* HO::Su9-mKate2	*Mat alpha*	*leu2-3,112 can1-100 ura3-1 his3-11,15 mt-LacO Mito Δatp21::hphNT1 Δatp20::hphNT2 HO::Su9-mKate2-kanMX6*	This study
yCO754	Δ*mic10 ATP6*-NG	*Mat a*	*ade2-1 his3-11,15 trp1-1 leu2-3,112 ura3-1 CAN1 arg8::HIS3 ATP6-NG Δmic10::hphNT1*	This study
yCO755	Δ*mic10* HO::Su9-mKate2	*Mat alpha*	*leu2-3,112 can1-100 ura3-1 his3-11,15 mt-LacO Mito Δmic10::hphNT1 HO::Su9-mKate2-kanMX6*	This study
yCJ066	Δ*mic60 ATP6*-NG	*Mat a*	*ade2-1 his3-11,15 trp1-1 leu2-3,112 ura3-1 CAN1 arg8::HIS3 ATP6-NG Δmic60::hphNT1*	This study
yCJ067	Δ*mic60* HO::Su9-mKate2	*Mat alpha*	*leu2-3,112 can1-100 ura3-1 his3-11,15 mt-LacO Mito Δmic60::hphNT1 HO::Su9-mKate2-kanMX6*	This study
yCJ120	*ATP6*-mKate2	*Mat a*	*ade2-1 his3-11,15 trp1-1 leu2-3,112 ura3-1 CAN1 arg8::HIS3 ATP6-mKate2*	This study
yCJ084	*ATP6*-NG	*Mat alpha*	*leu2-3,112 can1-100 ura3-1 his3-11,15 ATP6-NG*	This study
yCJ123	ATP6-NG pvt100u-TagBFP	*Mat alpha*	*leu2-3,112 can1-100 ura3-1 his3-11,15 ATP6-NG pvt100u-TagBFP*	This study

yCJ124	ATP6-mKate2 pvt100u-TagBFP	*Mat a*	*ade2-1 his3-11,15 trp1-1 leu2-3,112 ura3-1 CAN1 arg8::HIS3 ATP6-mKate2 pvt100u-TagBFP*	This study
yCJ127	ATP6-NG Δ*atp20* pvt100u-TagBFP	*Mat alpha*	*leu2-3,112 can1-100 ura3-1 his3-11,15 ATP6-NG Δatp20::NatNT2 pvt100u-TagBFP*	This study
yCJ128	ATP6-mKate2 Δ*atp20* pvt100u-TagBFP	*Mat a*	*ade2-1 his3-11,15 trp1-1 leu2-3,112 ura3-1 CAN1 arg8::HIS3 ATP6-mKate2 Δatp20::NatNT2 pvt100u-TagBFP*	This study
yCJ130	ATP6-NG Δ*atp21* pvt100u-TagBFP	*Mat alpha*	*leu2-3,112 can1-100 ura3-1 his3-11,15 ATP6-NG Δatp21::hphNTI pvt100u-TagBFP*	This study
yCJ132	ATP6-mKate2 Δ*atp21* pvt100u-TagBFP	*Mat a*	*ade2-1 his3-11,15 trp1-1 leu2-3,112 ura3-1 CAN1 arg8::HIS3 ATP6-mKate2 Δatp21::hphNTI pvt100u-TagBFP*	This study
yCJ103	WT LacO-LacI	*Mat alpha*	*leu2-3,112 can1-100 ura3-1 his3-11,15 mt-LacO Su9-3xGFP-LacI::kanMX6*	This study
yCJ104	WT matrix-mKate2	*Mat a*	*leu2-3,112 trp1-1 can1-100 ura3-1 ade2-1 his3-11,15 HO-Su9-mKate2*	This study
yCJ105	LacO-LacI Δ*atp21*	*Mat alpha*	*leu2-3,112 can1-100 ura3-1 his3-11,15 mt-LacO Su9-3xGFP-LacI::kanMX6 Δatp21::NatNT2*	This study
yCJ106	matrix-mKate2 Δ*atp21*	*Mat a*	*leu2-3,112 trp1-1 can1-100 ura3-1 ade2-1 his3-11,15 HO-Su9-mKate2 Δatp21::NatNT2*	This study
yCJ134	LacO-LacI Δmic60	*Mat alpha*	*leu2-3,112 can1-100 ura3-1 his3-11,15 mt-LacO Su9-3xGFP-LacI::kanMX6 Δmic60::hphNT1*	This study
yCJ135	matrix-mKate2 Δmic60	*Mat a*	*leu2-3,112 trp1-1 can1-100 ura3-1 ade2-1 his3-11,15 HO-Su9-mKate2 Δmic60::hphNT1*	This study
yCJ020	*Δatp20 Δarg8::HIS3 Δcob::ARG8M*	*Mat alpha*	*ade2-1 his3-11,15 trp1-1 leu2-3,112 ura3-1 CAN1 arg8::HIS3 cob::ARG8M intronless mtDNA ∆atp20::hphNT1*	This study

yCJ022	*∆atp20 ∆arg8*	*Mat a*	*ade2-1 his3-11,15 trp1-1 leu2-3,112 ura3-1 CAN1 arg8::HIS3 intronless mtDNA ∆atp20::hphNT1*	This study
yCJ046	*Δatp20Δatp21 Δarg8::HIS3 Δcob::ARG8M*	*Mat alpha*	*ade2-1 his3-11,15 trp1-1 leu2-3,112 ura3-1 CAN1 arg8::HIS3 cob::ARG8M intronless mtDNA ∆atp21::hphNT1 ∆atp20:: kanMX6*	This study
yCJ047	*∆atp20∆atp21 ∆arg8*	*Mat a*	*ade2-1 his3-11,15 trp1-1 leu2-3,112 ura3-1 CAN1 arg8::HIS3 intronless mtDNA ∆atp21::hphNT1 ∆atp20::kanMX6*	This study
yCJ005	*Δatp21 Δarg8::HIS3 Δcob::ARG8M*	*Mat alpha*	*ade2-1 his3-11,15 trp1-1 leu2-3,112 ura3-1 CAN1 arg8::HIS3 cob::ARG8M intronless mtDNA ∆atp21::hphNT1*	This study
yCJ007	*∆atp21 ∆arg8*	*Mat a*	*ade2-1 his3-11,15 trp1-1 leu2-3,112 ura3-1 CAN1 arg8::HIS3 intronless mtDNA ∆atp21::hphNT1*	This study
yCO756	*Δmic10 Δarg8::HIS3 Δcob::ARG8M*	*Mat alpha*	*ade2-1 his3-11,15 trp1-1 leu2-3,112 ura3-1 CAN1 arg8::HIS3 cob::ARG8M intronless mtDNA ∆mic10::hphNT1*	This study
yCO757	*∆mic10 ∆arg8*	*Mat a*	*ade2-1 his3-11,15 trp1-1 leu2-3,112 ura3-1 CAN1 arg8::HIS3 intronless mtDNA ∆mic10::hphNT1*	This study
yCJ070	*Δmic60 Δarg8::HIS3 Δcob::ARG8M*	*Mat alpha*	*ade2-1 his3-11,15 trp1-1 leu2-3,112 ura3-1 CAN1 arg8::HIS3 cob::ARG8M intronless mtDNA ∆mic60::hphNT1*	This study
yCJ071	*∆mic60 ∆arg8*	*Mat a*	*ade2-1 his3-11,15 trp1-1 leu2-3,112 ura3-1 CAN1 arg8::HIS3 intronless mtDNA ∆mic60::hphNT1*	This study

[1] Osman et al. 2015
[2] Gruschke et al. 2011
[3]Steele et al. 1996
[4] Rak et al. 2007

Tabel 2 - Primers used in this study

Name / Alias	Sequence
CO356 Δ*dnm1* S1	CATTAAGTAGCTACCAGCGAATCTAAATACGACGGATAAAGAATG CGTACGCTGCAGGTCGAC
CO357 Δ*dnm1* S2	CGCAATGTTGAAGTAAGATCAAAAATGAGATGAATTATGCAATTA ATCGATGAATTCGAGCTCG
CO573 Δ*atg32* S1	TCACAAAAGCAAAAAAAATCTGCCAGGAACAGTAAA CATATGCGTACGCTGCAGGTCGAC
CO574 Δ*atg32* S2	GTGAGTAGGAACGTGTATGTTTGTGTATATTGGAA AAAGGTTAATCGATGAATTCGAGCTCG
CO888 Δ*mic10* S1	TGCTACGAGAGGGAATAAACACGGAAAAAGACAAAATATACCAT GCGTACGCTGCAGGTCGAC
CO889 Δ*mic10* S2	TATTTTTTTTTTTGAATATATATAAAGCATCGTCGCTTAAGACTAAT CGATGAATTCGAGCTCG
CO986 Δ*atp20* S1	ACCTGCCGATAAATCATATTTCAGAACGCTAATCAATTCATC ATGCGTACGCTGCAGGTCGAC
CO987 Δ*atp20* S2	ACGAATATACAAGGGTTTTGCGAATAGATAGAATTAAAAAGCT TAATCGATGAATTCGAGCTCG
CO1104 Δ*atp21* S1	CGGAACATAACGTATATAGGAACTAGCTGAGTGAGTTAAAG GATGCGTACGCTGCAGGTCGAC
CO1105 Δ*atp21* S2	TAATGTGCATTTTTAGTATCCTATTTATGTTGAAGCTTCTATTTA ATCGATGAATTCGAGCTCG
CO1114 qPCR *Cox1* fv	CTACAGATACAGCATTTCCAAGA
CO1115 qPCR *Cox1* rv	GTGCCTGAATAGATGATAATGGT
CO1116 qPCR *Act1* fv	CACCCTGTTCTTTTGACTGA
CO1117 qPCR *Act1* rv	CGTAGAAGGCTGGAACGTTG
CO1196 Δ*mic60* S1	GGCATAAGAACGCATTGAAAAGTCTAAAAAACTAATATTCGT ATGCGTACGCTGCAGGTCGAC

CO1197 Δ*mic60* S2	AGGTGTAATGACGTACATCTCTTTTCTCTTTGTATTATTCTTTC AATCGATGAATTCGAGCTCG
CO1268 tagging of *Fis1* fw	GTAATTATCTACTTTTTACAACAAATATAAAACAATGGTCTCAA AAGGGGAGG
CO1269 tagging of *Fis1* rv	CCAAGCTTCTTATATAATTCATCCATTCCCATGACA
CO1270 backbone for *Fis1*-NG fw	GGATGAATTATATAAGAAGCTTGGTCATGGTACTGA
CO1271 backbone for *Fis1*-NG rv	GCAAGCTAAACAGATCTTACCTTCTCTTGTTTCTTAAGAAGAAAC
CO1677 tagging of *Pam16* fw	CGAATTCAACAAATTCATCTGGTGCAGATAATAGTGCAAGC AGCAATCAGCGTACGCTGCAGGTCGAC
CO1678 tagging of *Pam16* rv	GCTGCATGCTTTCGATAACACTTGTGACGTAATGATGGAGGCTT CCTTGAATCGATGAATTCGAGCTCG
CO562 Amplification of *COB* for	AATCAAATGTGTATTTAAGTTTAGTG
CO562 Amplification of *COB* rev	TTATTTATTAACTCTACCGATATAGAAT
CO891 Amplification of *ARG8* for	TCAAGACCTGAAGATTTATGTATCACAAGAGG
CO601 Amplification of *ARG8* rev	TTAAGCATATACAGCTTCGATAGC
CO982 S3 tagging of Cox4	TACAAACTAAACCCTGTTGGTGTTCCAAATGATGACCACCATCA CGGTGACGGTGCTGGTTTA
CO982 S2 tagging of Cox4	AAAAAGTAAAAGAGAAACAGAAGGGCAACTTGAATGATAAGATT AATCGATGAATTCGAGCTCG

Table 3 - Plasmids used in this study

Name / Alias	Needed for	Source
pCO021	Janke deletion cassette G418 resistance	1
pCO059	Janke deletion cassette NAT resistance	1
pCO074	Janke deletion cassette hygromycin resistance	1
pCO151	pvt100u-TagBFP	This study
pCO282	pCOB-ST5	2
pCO441	HO-P_{PGK1}-Su9-mKate2-kanMX6-HO	This study
pCO442	HO-P_{PGK1}-Su9-NG-kanMX6-HO	This study
pCO307	pCOB/ST5 Arg8+Term+synth-TetO	This study
pCO408	HO-P_{CUP}-Su9-3xGFP-LacI—P_{PGK}-Su9-TagBFP-KanMX	This study
pCO407	HO-P_{CUP}-Su9-TetR-3xRuby3--P_{PGK1}-Su9-TagBFP-KanMX4-HO	This study
pCO444	Plasmid for biolistic transformation and generation of *ATP6*-mtNeonGreen	This study
pCO494	C-Terminal tagging of proteins with NeonGreen	This study
pCJ013	Plasmid for biolistic transformation and generation of *ATP6*-mtNeonGreen	This study

[1] Janke et al. 2004
[2] Gruschke et al. 2011

Discussion

9 Summary

The mechanisms of mitochondrial DNA quality control and purifying selection have been extensively studied in the past years, yet they continue to be incompletely understood. Whether and how cells are able to discern functional against mutated genomes in situations where both variants are fully mixed in a heteroplasmic soup within mitochondria of the same cell remains obscure. Heteroplasmy, the cellular state where different mtDNA haplotypes coexist, still lacks a thorough and complete understanding, as various processes have been proposed to contribute to this phenomenon.

What is well-known, however, is that mitochondrial genomes encode for vital components of the respiratory chain. Unlike nuclear DNA, mtDNA exists in multiple copies within cells. Heterogeneity among the mtDNA copies within a single cell, termed heteroplasmy, is not a rare phenomenon. Although not all heteroplasmic cells harbor mutated mtDNA copies, but just different haplotypes, the degree of heteroplasmy can frequently alter due to the inefficient mtDNA repair mechanisms occuring over time (Nissanka and Moraes, 2020). Mutations in mtDNA can lead to insufficiency in cellular energy production, resulting in various mitochondrial diseases. Consequently, gaining insights into the mitochondrial genome dynamics and the mechanisms governing the transition from heteroplasmy to homoplasmy is crucial. Moreover, given the impact of mutant mtDNA molecules on cellular health, understanding how mtDNA integrity is maintained across generations and how dysfunctional copies are eliminated during cell division events are paramount areas for investigation.

During the first chapter of my thesis, I addressed fundamental questions such as whether we can monitor heteroplasmy in yeast cells, and how rapidly this phenomenon dissipates. Heteroplasmy essentially creates a battlefield where coexisting mtDNA haplotypes compete for transmission to the next generation. The approach we followed was to first establish a pipeline that allowed for real-time single-cell tracking of mtDNA variant segregation in dividing yeast populations. We utilized mtDNA-based fluorescent markers, microfluidics, and automated cell tracking to follow neutral mtDNA variants in heteroplasmic populations. Briefly, this method revealed rapid segregation of mtDNA genomes and, in combination with direct mtDNA copy tracking, we identified asymmetric partitioning of mtDNA copies during division as a key factor for mtDNA haplotype segregation. Additionally, upon building a mathematical model based on empirical real-time segregation data we found that the kinetics of mtDNA heteroplasmy segregation are further impacted by mitochondrial fission and fusion frequencies. This finding was further supported by dissection- and microscopy-based analysis of fission-deficient cells, where the establishment of homoplasmy occurred faster than in wildtype ones. By investigating the influence of mtDNA copy number on the speed of segregation, we also found that in cells with increased number of mtDNA molecules the rate of mtDNA segregation slows significantly down.

During the second chapter of my work, we asked whether cells can distinguish between wildtype and mutant mtDNAs, and how the latter ones are successfully purged across generations. By applying the so-called pedigree analysis on mated cells carrying different intact and mutant mtDNA, we observed that *Saccharomyces cerevisiae* possesses the ability to internally differentiate between functional and defective mtDNA molecules. Additionally, we observed that daughter cells are produced with increasingly healthy mtDNA content, with the first generation daughter derived from heteroplasmic zygotes already exhibiting major preference towards the functional haplotypes. Interestingly, during the process of purifying selection, that occurs in a continuous mitochondrial network, we found that neither mitochondrial fission nor mitophagy are required using the pedigree pipeline. Nevertheless, our data indicates that these two processes could contribute to the clearance mechanism during subsequent cell divisions. Instead, a stable cristae morphology appeared as prerequisite for proper clearance. Based on our data, we propose that intact spatial organization retains mutated mtDNA copies and its encoded products in close proximity within sub-compartments, which can later be recognized and successfully eliminated.

In due course, using the microfluidic and pedigree pipelines, that allow assessment of segregation between intact and mutant mtDNA, it would be a fascinating direction to investigate the heteroplasmy dynamics under non-neutral scenarios, and we anticipate our approaches to be instrumental in deciphering the mechanisms underlying the purifying selection of mtDNA. With the combination of single-cell microscopy, microfluidics, live-cell tracking and microdissection, we are able to expand our understanding on mtDNA segregation and quality control, and actively contribute to the progress of mitochondrial research.

10 Chapter 1: Assessment of mtDNA heteroplasmy dynamics in *S. cerevisiae*

Monitoring the dynamics of mitochondrial genome segregation within single cells in a continuously evolving population presents inherent challenges. Until now, accurately inferring the quantity of mtDNA variants within living cells over time has not been experimentally possible. Therefore, dynamics of mtDNA molecules have been majorly studied using dry-lab computations (Glastad and Johnston, 2023; Johnston, 2019; Johnston et al., 2015; Tam et al., 2013). On the experimental level, it is rather difficult to gain information on single cells in a live-cell microscopy setup, as tagging and thus tracking of individual mtDNA copies has been proven very challenging. Additionally, there are multiple technical hurdles related to live cell imaging. For example, cells often grow out of the field of view or can be washed away while fresh media is flushed into microfluidic chambers during imaging (Bheda et al., 2020). Additionally, within a couple of rounds of divisions, cells become very dense and start to overlap, leading to potential errors in lineage tracking and inference of the inheritance pattern. Lastly, repeated fluorescence excitation in small intervals can induce phototoxicity, affecting cellular fitness. Our primary goal was to overcome all these obstacles, with minimum interference on the physiological processes driving the mtDNA heteroplasmy dynamics.

10.1 Dynamics of mtDNA segregation over time at the single-cell level

With this work, we established a cutting-edge pipeline based on microscopy and microfluidics, allowing real-time tracking of mtDNA heteroplasmy dynamics at the single-cell level. We utilized two neutral mtDNA-encoded Atp6 variants, tagged C-terminally either with NeonGreen or mKate2, as surrogate markers for distinct mtDNA haplotypes, which made tracing of individual cell trajectories and construction of multiple lineage trees possible. The specific pipeline was developed on growing yeast populations spanning up to 6 generations. Taking into account the aforementioned live-cell microfluidic limitations, the method could be also applied for genealogical trees with larger than 6-generation lineages.

Specifically, we overcame the hurdle of tagging mtDNA directly by creating two variants where the mtDNA-encoded Atp6 gene was tagged C-terminally with different fluorophores. By using two different tags, NeonGreen or mKate2, we established two rather identical strains expressing Atp6-NG or Atp6-mKate2, that were used as proxies for the respective mtDNA. Upon mating of both strains, our experiments revealed a rapid divergence from the heteroplasmic state within individual cells, with diploid populations achieving 50% absolute homoplasmy within 8 hours. In order to confirm the homoplasmy thresholds derived from the microfluidic distributions after 8 hours, we also developed an auxiliary method, which I refer to as 24-HASC (24h- **H**eteroplasmy **A**ssessment in **S**ingle **C**olonies). We used 24-HASC to rapidly estimate the heteroplasmy levels of multiple colonies after overnight growth upon microdissection. We found an almost perfect split between the homoplasmic proportions of the two Atp6 variants, among a total of 20 individual colonies analyzed. The 24-HASC approach is a simple straightforward experiment that can also be applied for examining heteroplasmic proportions in matings with competitive mtDNA haplotypes. Indeed, in cell populations from zygotes harboring wildtype and Δcob mtDNA, we observed a clear preference for wildtype mtDNA homoplasmy. As a side note, for the final assessment of mtDNA heteroplasmy distributions acquired from the microfluidic data, we did not exclude buds budding off of lateral zygote

positions ('lateral buds'), as we could not distinguish them when applying the 24-HASC. Lateral buds are often second daughter cells from zygotes and predominantly or even exclusively inherit mitochondrial content from the parental cell from which they originate. Notably, when we compared the heteroplasmy dynamics with and without lateral buds, no major differences were observed.

Using the aforementioned pipelines, the main objective of our work was to decipher the factors driving the rapid heteroplasmic shifts. Possible contributors to heteroplasmy alterations include relaxed replication, and unequal partitioning during cell divisions, as well as intracellular selection favoring a specific mtDNA haplotype in mother mitochondria even prior to inheritance. Modeling has shown that, even when mutated and wildtype mtDNA copies coexist and undergo non-selective replication, fluctuations and alterations in heteroplasmy levels can arise over time (Johnston, 2019; Chinnery and Samuels, 1999). Specifically, the non-selective replication can further delay the establishment of homoplasmy of a specific allele. Additionally, a physical bottleneck controlling the number of inherited mtDNA molecules and fission-fusion cycles, that reorganize the mitochondrial contents, are also factors that influence the segregation dynamics (Zhang, Burr, and Chinnery, 2018a; Twig et al., 2008; Radzvilavicius and Johnston, 2022). All the aforementioned processes collectively lead to heteroplasmy alterations and impact the homoplasmy fixation rate in all individual cells of a dividing yeast population.

To shed light on these phenomena, we built a simplified mathematical model that simulates mtDNA heteroplasmy segregation dynamics. Given the current limitations in what is known about mtDNA heteroplasmy regulation, we do not possess adequate data to develop an intricate model without relying on few unverified assumptions or unknown parameters, such as the frequency of fission events, the mtDNA replication frequency and speed, or whether new synthesis occurs while cell division and mtDNA exchange takes place. Consequently, the aim of the model was not to encapsulate the entire complexity of the mtDNA variant segregation, but rather to demonstrate that with a minimal set of assumptions and integrating known parameters involved in the process, similar dynamics like those observed experimentally could occur. We selected biologically reasonable values for all model parameters. Briefly, we defined two different mtDNA haplotypes by 0 or 1 in an array, representing the tubular organization of mitochondria. The length of this array was set to the previously determined average of 32 mtDNA copies per diploid cell (Göke et al., 2020). The founder cell of each simulated population had a randomized sequence of equal amounts of 0s and 1s. Additionally, all newly replicated mtDNA copies were always placed next to the template mtDNA. Of note, we excluded the possibility of cell death and mtDNA degradation. Additionally, we hypothesized that cells were allowed to divide only upon replication was complete, once the cell had reached the predefined mtDNA copy number (e.g. 32 copies), neglecting any cell-to-cell variabilities.

We limited our varying parameters to two, the fission-fusion frequency represented by *nspl*, and the number of inherited mtDNA molecules represented by *ndau*. We note that even though our model is reduced to two varying parameters, it is able to support the temporal heteroplasmy alterations observed *in vivo*, and recapitulates the homoplasmy fixation levels of the microfluidic data. We checked our model's robustness by alternative founder cell sequences, by changing the order between the two haplotypes from 'mix', to 'semi', or 'non-mixed', as well as by slightly varying the initial mtDNA copy number. We find that, in our model, the structure of the founder cell can influence the final speed of homoplasmy establishment, but not in a statistically significant manner. Similarly, small variations of the mtDNA

copy number of founder cells can lead to faster or slower segregation patterns, yet it does not result in a markedly distinct outcome. However, we find that a higher percentage of mtDNA copies transmitted to daughter cells and increased fusion-fission frequencies result in slower segregation of mtDNA variants. Interestingly, when *nspl* is about as high as the number of mtDNA molecules in a wildtype cell, the process of segregation corresponds to random independent sampling of nucleoids passed on to the daughter cell (Dujon, Slonimski, and Weill, 1974), and allele frequency alterations from mother to daughter cell resemble drift that majorly depends on uneven mitochondrial turnover (Campbell et al., 2023), as already known from population genetics.

Lastly, we anticipate that the transition from heteroplasmy to homoplasmy would occur even faster if the mtDNA haplotypes had distinct qualities, supporting the idea that segregation is less neutral in such scenarios. The current pipeline could be used to investigate the selection process in mutants that contain fluorescently-labeled proteins, by replacing mtDNA-encoded genes, that are expected to result in OXPHOS dysfunction, such as deletion of the Cytochrome b (COB) gene or the subunit 6 of the ATP synthase (ATP6). However, to date, this experiment remains pending, as generation of fluorescently labeled mutant mtDNA has proven to be rather challenging. On the upside, using the 24-HASC approach, our results indeed indicate that diploid cells favor the inheritance of functional mtDNA copies over the mutated ones, since more than 60% of the colonies appeared homoplasmic for the wildtype construct. Additionally, in strains lacking genes essential for proper segregation of mtDNA content between mother and daughter cells, or genes required for the correct positioning of mitochondria (Obara et al., 2022; Chen, Ping, and Lackner, 2018), the selection and mtDNA inheritance process are also expected to be compromised. For example, it has been observed that deletion of *MMR1* impairs bud tip anchorage of mitochondria, thus preventing binding of mitochondria to cER sheets, which has a detrimental effect on adequate mitochondrial inheritance. (Swayne et al., 2011). Another intriguing approach would be also to assess the process of mtDNA purification across multiple generations under different carbon sources or stress conditions, as the need for mitochondria and thus functional mtDNA genomes varies greatly under such circumstances.

10.2 Importance of cell division for establishing mtDNA homoplasmy

Why and how homoplasmy gets established in cells is still not fully understood. As mentioned in the introduction, there are multiple different mechanisms believed to contribute to this phenomenon. Briefly, the most prominent explanations for mtDNA segregation dynamics are the vegetative segregation (Birky, 2001; Birky, Fuerst, and Maruyama, 1989) and relaxed replication, together defined as random drift (Birky, Fuerst, and Maruyama, 1989), and the intercellular (Dujon, Slonimski, and Weill, 1974; Backer and Birky, 1985), and intracellular selection occurring in a non-random fashion for a specific genotype (Cree et al., 2008; Wai, Teoli, and Shoubridge, 2008; Zhang, Burr, and Chinnery, 2018b; Hill, Chen, and Xu, 2014; Klucnika and Ma, 2019). It is worth mentioning that establishing mtDNA homoplasmy may involve multiple of these processes simultaneously, rather than just one. Consequently, pinpointing the exact origin or cause of these transitions becomes even more challenging.

Importantly, mtDNA segregation mechanisms involve or even require cell division events. Therefore, in order to assess the direct influence of cell divisions on mtDNA segregation dynamics, we compared the changes between a mother and its

later self to the mother and its daughter at the same stage. The rationale behind this experiment was that in one scenario, equal numbers of mtDNA molecules could split between mother and daughter cells during cell division and a shift to homoplasmy could occur due to random selection of mtDNA molecules for replication and possibly also degradation. In this stochastic drift scenario, it would be expected that heteroplasmy values of mothers would correlate to similar extents with the heteroplasmy values of their later selves or their progeny. Alternatively, transmission of a limited number of mtDNA molecules from mothers to daughters would result in a bottleneck that samples mtDNA molecules from the mother's mtDNA pool. In this scenario, a lower correlation between heteroplasmy values should be observed when h-values of mother cells are compared to heteroplasmy values of their daughters rather than to h-values of themselves at a later timepoint.

What we observed was a reduced similarity between mothers and their offspring, with a higher correlation of mothers with their selves. This analysis highlighted that the decreased similarity between mothers and progeny is influenced by the division event, and also that unequal partitioning of mtDNA copies must take place in order to result in the statically significant difference observed across cell pairs. It is worth mentioning that the aging mother did differ from itself, suggesting a concurrent stochastic drift, potentially attributed to ongoing relaxed replication during aging. The observed difference in mother cells over time could also be due to the removal of mtDNA copies from the mother's pool since they are transmitted to the daughter cells. All in all, these results brought to the surface the major effect of cell divisions on the speed of mtDNA variant segregation. Our data also agree with recent computational studies, where cell divisions were shown to increase the variance of mtDNA heteroplasmy in mice and *in silico* (Johnston et al., 2015; Johnston and Jones, 2016). Another study of the mtDNA genetic bottleneck in human and mice primordial germ cells has also suggested that the process of mtDNA selection is facilitated by cell division (Floros et al., 2018), a finding further corroborating our conclusion. Importantly, cell division is an inevitable event in vegetatively growing cells. This means that either via a stochastic "spacing" or an "active-sorting" model (Aretz, Jakubke, and Osman, 2019), division will have a key role to the purifying selection process. For example, in the case of the "spacing" model, if equal partitioning of mitochondria occurs upon division, then faithful mtDNA partitioning to daughter cells will be achieved due to the uniform mtDNA distribution throughout the mitochondrial network. On the other hand, in the "active-sorting" scenario, directed movement of mtDNA to daughter cells would facilitate proper partitioning, by conjoining mtDNA copies with mitochondrial anchorage and motility before and during division. Put together, the process of cell division, most likely through transmission of a limited number of mtDNA copies, is a major driver for the progressive divergence of heteroplasmic states in a proliferating yeast population. Thus, we posit that while stochastic drift does occur over time within a cell trajectory, the alterations arising from division events have a more pronounced impact on shaping the cell's mtDNA composition.

10.3 mtDNA copy number transferred per cell division and fission-fusion frequencies influence mtDNA heteroplasmy dynamics

Apart from the unavoidable processes of drift and division taking place in proliferating cells, we next sought to identify whether there are active cellular mechanisms contributing to or even controlling the swift fixation to homoplasmy. Since mitochondrial genomes are not under Mendelian laws, as relaxed replication and partitioning influence their inheritance process (Birky, 1994), we integrated relaxed replication into our model, by allowing any mtDNA molecule to become a template for replication until division. This way, we were able to directly target the asymmetric vs symmetric partitioning question.

Upon fine-tuning of the computational simulations, we observed that a reduction of the inherited mtDNA molecules from mother to daughter cells significantly influenced the outcomes in heteroplasmy levels under a neutral scenario. Thus, we posit that reducing the number of mtDNA copies in a young cell could quickly expose different variants to present selective pressures. In line with this rationale, research in mice has demonstrated that a decrease in mtDNA molecules is responsible for the rapid heteroplasmy shifts during germline development (Cree et al., 2008). The genetic bottleneck has been widely investigated and suggested to account for the major heteroplasmy changes between generations (Zhang, Burr, and Chinnery, 2018b). Our results are also consistent with other bottleneck studies conducted across various model organisms (Cree et al., 2008; Tang et al., 2022; Zhang, Burr, and Chinnery, 2018a; Wai, Teoli, and Shoubridge, 2008; Marlow, 2017), emphasizing the importance of this process in broader evolutionary contexts.

Apart from a reduction in mtDNA copies transferred to the progeny, using our model, we also found fission-fusion frequencies to play a significant role in the rapid establishment of homoplasmy. Reduced shuffling of mtDNA seems to accelerate segregation, probably because mtDNA copies remain near their template mtDNA after replication and/or near other molecules copied from the same template. Consequently, it is more likely that larger numbers of the same mtDNA type are passed on to the daughter cell, thus rendering the remaining nucleoids in the mother cell more homogeneous (Figure 8). This result further aligns with previous mathematical modeling (Tam et al., 2013) and the restricted mobility of mtDNA (Nunnari et al., 1997), that could potentially hinder the mixing of different mtDNA variants within the mitochondrial network when fusion and fission are absent. Further evidence suggests that frequent mitochondrial fusion and fission play an important role in sustaining a healthy mitochondrial network, as they lead to content exchange across the mitochondrial tubules, which guarantees dilution of potentially harmful mtDNA mutations (Chan, 2012), and directly affects the speed of homoplasmy establishment. Furthermore, fission and fusion events occur continuously and rearrange mtDNAs within the matrix regardless of the nature or quality of the mtDNA molecule. Interestingly, fusion has been observed to occur near mtDNA so as to minimize the pressure for cristae remodeling (Ren et al., 2022). Concurrently, it has been recently suggested that mtDNA molecules are tethered to cristae and the IMM (Chapman, Ng, and Nicholls, 2020; Ren et al., 2022; Rajala et al., 2013; Prachař, 2016), which aids on the maintenance of cristae architecture. This is easily explained when we remember that cristae are arranged in such a manner that the nucleoids are placed in the in-between gaps of the IMM curvatures (Stephan et al., 2019). With this in mind, fusion and fission, which regulate the re-organization of mitochondrial tubules, can directly alter the positioning of mtDNA copies within the matrix. This

re-organisation further affects the cristae architecture, since it is often shaped according to the proximal mtDNA copies, which can in turn contribute to the heteroplasmy degree and the mtDNA inheritance patterns. Additionally, fission events have been linked to mtDNA replication (Lewis, Uchiyama, and Nunnari, 2016; Murley et al., 2013). Thus, it is probable that increased mtDNA replication and mtDNA copy number may lead to higher fission frequency, directly altering the heteroplasmic level of the cell. Put together, fragmentation and re-shuffling have a major influence on the cell's heteroplasmic state before and after segregation, and it will be interesting to decipher the speed of mtDNA segregation in cells with higher mtDNA contents and/or reduced fission.

One important experiment showcasing further the influence of effective shuffling on the speed of segregation was to track the heteroplasmy dynamics in strains lacking Dnm1. In such a scenario, since cells' mitochondria cannot undergo fission, we expect a faster establishment of mtDNA homoplasmy. This is expected as newly formed cells inherit mitochondrial tubules containing mtDNA copies from their mothers, which have not undergone any shuffling. Therefore, when fission is absent, no mixing can take place and patches of the same mtDNA haplotypes are generated and inherited, rendering the newly formed cells homoplasmic in fewer division rounds. Indeed, our *in vivo* experiments confirmed our hypothesis, with a rapid establishment of homoplasmy in Δ*dnm1* cells within 18 hours, in comparison to wildtype. Interestingly, we observed solely homoplasmic cells in 57% of colonies derived from heteroplasmic Δ*dnm1* cells in comparison to 14% in WT cells. Our proposition is that hindered shuffling of the mitochondrial contents potentially creates homogeneous patches within a cell, that upon division render a newly formed bud homoplasmic, or heteroplasmic with homogeneous sub-compartments. An alternative approach to check the role of fission in mtDNA segregation would be to create temperature-sensitive mutants of the inner membrane remodelling dynamin-related GTPase (Mgm1), as *MGM1* deletion leads to mtDNA loss. In such a scenario, the inner membrane fission would be halted, and thus monitoring of the influence of fission on the speed of segregation would be feasible. Temperature-sensitive Mgm1 mutants have been long established for studying the mitochondrial architecture, and notably the cristae structure is restored once the cells are returned to lower temperatures (Harner et al., 2016; Meeusen et al., 2006). Thus, these Mgm1 mutants would allow drastic, but reversible, shifts on mitochondrial dynamics, a fascinating tool to examine the effect of shuffling in mtDNA heteroplasmy in vegetatively growing cells over time.

We next investigated the effect of increased mtDNA copy number on mtDNA segregation dynamics. To achieve this, we conducted segregation experiments in Δ*mrx6* cells, which have been shown to have a higher total mtDNA copy number, specifically two-fold higher than the wildtype diploid cells (Göke et al., 2020). After mating Δ*mrx6* cells of opposing mating types containing $\text{mtDNA}^{\text{Atp6-NG}}$ and $\text{mtDNA}^{\text{Atp6-mKate2}}$, we quantified the number of heteroplasmic cells in populations after 18 hours of growth. Notably, mtDNA variant segregation was delayed in Δ*mrx6* cells, resulting in a higher percentage of heteroplasmic cells, and surprisingly with none of the populations achieving complete segregation, after 18 hours. The experimentally observed delayed segregation in Δ*mrx6* cells, combined with the predictions from our model, indicate that these cells exhibit either higher fission-fusion frequencies and/or transmit a higher percentage of mtDNA copies to the daughter cells. It would be a fascinating experiment to overexpress Dnm1, which causes mitochondrial fragmentation (Fukushima et al., 2001), in Δ*mrx6* cells and observe the

mtDNA inheritance dynamics in real-time. In such a scenario, mitochondrial fragments would be expected to contain an increased mtDNA copy number, leading to a very rapid homoplasmy fixation. If not, it could suggest that yeast cells regulate mtDNA replication as a tool for prolonged quality control. Furthermore, the LacO-LacI system that allows for direct visualization of the mtDNA foci could be used in the Δ*mrx6* strain, to assess whether more mtDNA copies get transferred from mother to daughter cells in the increased mtDNA copy number scenario. Of note, the LacO-LacI system carry specific photo-bleaching limitations, thus an improved construct is necessary for this approach to work.

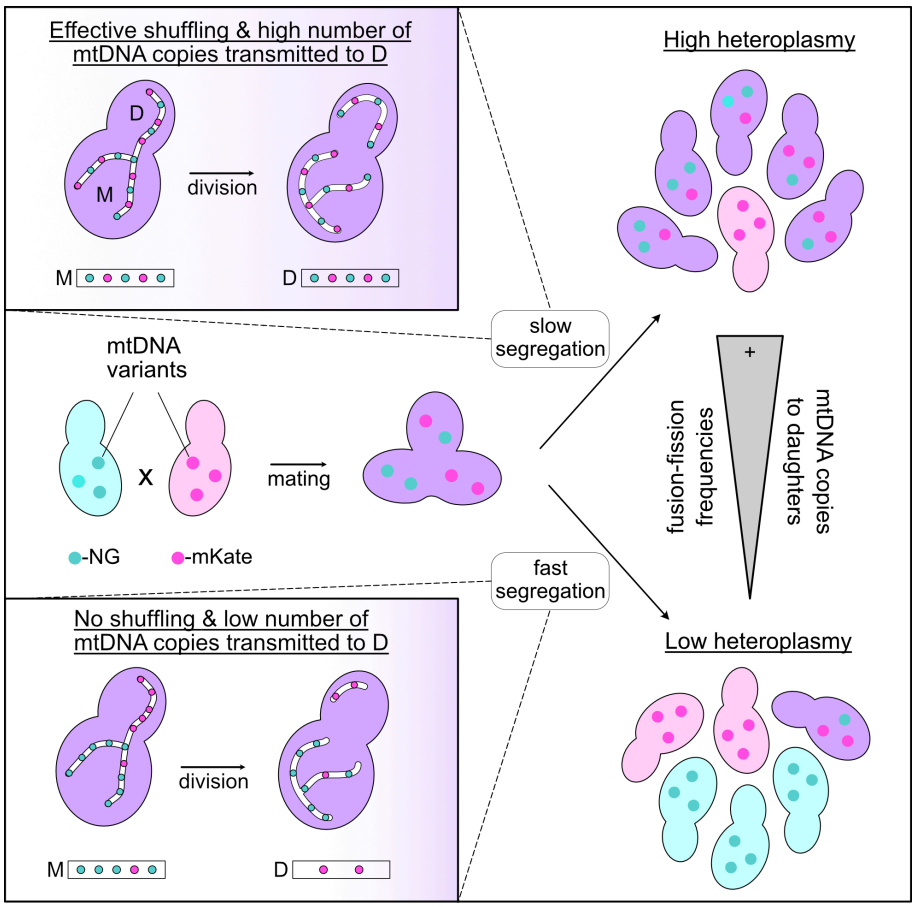

FIGURE 8: Model for mtDNA heteroplasmy dynamics, adapted from Roussou et al., 2024. Cells containing different mtDNA variants are termed heteroplasmic. Real-time imaging of heteroplasmy in dividing *S. cerevisiae* populations shows that the number of mtDNA copies passed to daughter cells and the degree of mitochondrial fission influence the speed of mtDNA variant segregation. Specifically, when a high number of mtDNA copies gets transferred to the daughters cell per cell division, while effective shuffling has taken place, segregation of mtDNA variants and the establishment of homoplasmy is slow. In contrast, when no shuffling occurs and only very few mtDNA copies are transferred to the progeny, cells become homoplasmic in fewer generations.

Regarding our model, one important limitation worth mentioning is that we cannot entirely rule out that stochastic *de novo* mtDNA mutations may still account for some of the observed heteroplasmy dynamics, as the *nspl* parameter fragments mitochondria in random lengths and reshuffling occurs stochastically. Thus, neighboring mtDNA copies may remain in proximity to each other and get inherited together, especially if the *nspl* parameter is low. Importantly, our data do not align with Kimura's "fixation by randomness" theory, which relies on specific assumptions,

such as a finite and constant population size, no *de novo* mutation, non-overlapping generations, and no migration (Wonnapinij, Chinnery, and Samuels, 2008; Li, 1996). Therefore, since our model is built on the biological characteristics of dividing yeast populations, we attribute the observed heteroplasmy rates on both the *nspl* and *ndau* parameters, for the simulated conditions.

Acknowledging cell divisions as a fundamental player in establishing mtDNA homoplasmy brings us closer to a better understanding of the mtDNA segregation dynamics. However, it is wise to keep in mind that in this study, the microfluidic data are derived from heteroplasmic cells with neutral mtDNA variants. Based on this specific setup, we identify fusion-fission frequencies along with a reduced number of mtDNA copies passing per segregation event from mother to daughter (specifically 1/3) as the key players of mtDNA heteroplasmy dynamics (Figure 8). Nonetheless, in a non-neutral setting, whether the cells' mtDNA composition during segregation is the reason for or the result of selection remains to be addressed. Therefore, before answering this cause-or-effect question, we ought to examine in real-time how yeast cells actively select for the healthy mitochondrial genomes in a scenario where haplotypes of different qualities coexist, as we observed in the 24-HASC microdissection experiment.

11 Chapter 2: mtDNA quality control is cristae-dependent

Monitoring mtDNA segregation dynamics in real time at the single-cell level is a milestone in the field and can pave the way for more detailed studies. Building on our pipeline and previous findings, it is also intriguing to investigate whether, upon absolute fusion of mitochondrial contents from cells harboring distinct qualities of mtDNA, the cells possess the capability to discern and transmit the functional mtDNA copies to their offspring. In the second part of my work, we addressed this question, and also explored factors expected to be involved in the purifying selection process. Firstly, we reproduced previous studies which demonstrated that mixing of soluble proteins, such as matrix ones, occurs during mating (Nunnari et al., 1997; Okamoto, Perlman, and Butow, 1998). We did so by using fluorescent proteins tagged with a mitochondrial targeting sequence (su9-mKate2 or su9-NeonGreen) in mating of two wildtype strains. Then, we investigated how cells discerned the WT mtDNA copies over the defective Δ*cob* ones, when containing both, and whether the cristae morphology influenced the selection process.

11.1 Yeast cells distinguish between WT and mutant mtDNA

By mating two parental cell lines, one harboring wildtype and the other defective mtDNA, we created zygotes with heteroplasmic mtDNA. This resulted in fully intermixed mtDNA molecules, coexisting and competing within the mitochondrial network. Using the pedigree analysis, our results indicate that indeed the unicellular organism *S. cerevisiae* can produce offspring with healthy mtDNA populations originating from heteroplasmic zygotes, and preferably generate progeny with intact mtDNA. Employing our microfluidic-based pipeline fully corroborated the aforementioned finding, since the degree of homoplasmy in populations carrying WT and mutant mtDNA reached a 50% homoplasmy after 24 hours. Notably, during the pedigree analyses, we observed sporadic cases where mtDNA species were lost in one generation but reappeared in the next one. This observation can be attributed to occasions where all copies of one particular mtDNA haplotype are passed on to the daughter cell, resulting in the mother cell lacking this mtDNA type, and the daughter containing it. More important, however, is to mention that the acquired data are limited to the specific deletion of the COB gene defining the mutant mtDNA strain. Therefore, it would be worth exploring different scenarios where yeast cells lack other mtDNA-encoded genes, or contain mtDNA with less severe mutations, as the effect of the mutation could greatly affect the efficiency of mtDNA selection. It would be also worth investigating how cells containing mutated mtDNA variants segregate in real-time, as so far we have acquired data using our two microdissection approaches, pedigree and 24-HASC. Our hypothesis is that the mtDNA segregation speed will exceed that of neutral variants, and that a 50% homoplasmy will be established in less than 5 generations.

Next, upon observing the clear pattern of selection in wildtype cells with competing mtDNA molecules, we assessed the potential mechanistic causes. Therefore, we deleted Dnm1 as well as Atg32, to check whether fission and mitophagy, respectively, influenced the clearance pattern of mutant mtDNA. Interestingly, neither fission nor mitophagy appeared to dramatically impact the mtDNA quality control, within this experimental setup. This raised questions on how cells can discern mutant mtDNA copies amidst wildtype copies in a mitochondrial network, where soluble matrix proteins quickly intermix, potentially obscuring physiological differences and thus protecting the mutant mtDNA copies.

Notably, prior investigations in yeast have demonstrated the preferential transport of healthy mitochondria into daughter cells (McFaline-Figueroa et al., 2011). Our pedigree analysis reveals a high proportion of first-generation colonies already exhibiting homoplasmy for the healthy mtDNA haplotype. However, our data also suggest that subsequent rounds of selection against mutant mtDNA, occurring in daughter cells, lead to the complete elimination of those mtDNA molecules. Although we find that mitochondrial fission or Atg32-mediated mitophagy may not be necessary for purging mutant mtDNA, during the generation of the very first daughter cells, these two processes may still contribute to the clearance process during further growth and subsequent cell divisions. In support to our data, where healthy mtDNA copies are preferentially inherited to daughter cells, it was recently shown that yeast mother cells retain dysfunctional mitochondria, via a mechanism where fusion is inhibited and the motor protein Myo2 is lost (Chelius et al., 2023). Yeast mitochondria are transported into the bud by the motor protein Myo2 attached to actin cables, with the help of Mmr1 (Obara et al., 2022; Chernyakov, Santiago-Tirado, and Bretscher, 2013; Itoh et al., 2002; Itoh, Toh-e, and Matsui, 2004). Chelius et al. proposed an inheritance mechanism where healthy mitochondria are successfully transferred to the progeny, leading to qualitative rejuvenation of the daughter cells, in a Mmr1-dependent manner. This qualitative inheritance could be further linked to the mtDNA quality, as dysfunctional mitochondrial tubules are often the outcome of the type of mtDNA copies they contain. Specifically, Chelius et al. suggest that Mmr1, functioning as the adapter of Myo2, detects mitochondrial dysfunction and/or ROS stress, leading to the dissociation of Myo2 from the mitochondrial surface and as a result, the defective mitochondria become immobilized and stay in the mother cells during cell division (Chelius et al., 2023).

Moreover, as mentioned in the introduction, heteroplasmy can be influenced by a relaxed replication mechanism. In this context, it is plausible that wildtype mtDNA is preferentially replicated, as previously suggested in *D. melanogaster* (Hill, Chen, and Xu, 2014; Zhang et al., 2019). This way, the proportion of functional mtDNA copies surpasses that of mutant in the total mtDNA pool, thereby increasing the likelihood that daughter cells will inherit WT mtDNA. Another explanation of the rapid removal of dysfunctional mtDNA copies could be that mutant mtDNA undergoes selective degradation by nucleases within the related mitochondrial subcompartments. Studies in yeast have demonstrated that the mitochondrial DNA polymerase, Mip1, degrades mtDNA through its exonuclease domain under prolonged starvation conditions (Medeiros et al., 2018), which could be linked to a more effective selection against mutated mtDNA under these conditions. However, further investigations are needed to ascertain whether such a mechanism contributes to the clearance of mutated mtDNA. All in all, the clearance of mutant mitochondrial genomes potentially involves a combination of mechanisms, including selective inheritance of wildtype mtDNA molecules to the progeny, mitophagic removal of fragments containing dysfunctional mtDNA, selective replication of healthy mtDNA, and/or even selective degradation of mutant mtDNA by nucleases.

11.2 mtDNA-encoded proteins remain in the vicinity of their mtDNA template

As multiple factors are involved in the selection process, we next aimed to comprehend how cells can differentiate between WT and mutant mtDNA while the

mitochondrial networks fully fuse. We hypothesized that selection can only operate when distinct subdomains persist within the mitochondrial network, each influenced by the nearby mtDNA copies. In such a case, mtDNA-encoded respiratory chain subunits should not diffuse rapidly, otherwise dysfunctional subdomains could be complemented by gene products from WT mtDNA. To assess the diffusion of an mtDNA-encoded protein, we used the previously established Atp6-NG strain, where we engineered the mitochondrial genome by tagging the C-terminus of the mtDNA-encoded *ATP6* gene with the NeonGreen tag.

Upon fluorescence microscopy of cells expressing *ATP6-NG* and the nuclear-encoded mScarlet in the matrix, we observed a patchy distribution of Atp6, contrasting the uniformly distributed mScarlet signal. Importantly, this distribution pattern agreed with previously observed data on GFP-tagged variants of ATP synthase subunits (Jimenez et al., 2014), which have been claimed to likely reflect mitochondrial cristae enrichment where the ATP synthase resides. We also found that Atp6-NG foci were spatially associated with mtDNA, located around the DAPI (mtDNA) spots rather than directly overlapping with them, indicating that Atp6-NG remains close to the mtDNA copy from which it originates. Based on this observation, we concluded that the ATP synthase localizes in close proximity to mtDNA and is majorly excluded from areas occupied by mtDNA. This can be interpreted as that there is a lack of cristae proximal to mtDNA, which also fully aligns with recent microscopy data in HeLa cells (Stephan et al., 2019), where lamellar cristae were shown to be arranged in groups, and the in-between gaps be occupied by mitochondrial nucleoids.

We also investigated whether Atp6-NG remained localized to the mitochondria from its original cell, upon mitochondrial fusion. Indeed this was the case, in contrast to the soluble mKate2 signal that equilibrated rapidly throughout the mitochondrial network. We obtained similar results with a nuclear-encoded subunit of Complex IV (Cox4-NG), indicating restricted diffusion of these proteins compared to soluble matrix proteins. Importantly, we cannot differentiate between pre-existing and newly synthesized Atp6-NG. However, even after the mitochondria of both parental cells had fully fused, we observed very low levels of Atp6-NG, in the cell without the respective mtDNA, indicating rather limited synthesis and/or restricted diffusion of Atp6-NG within the timeframe of our analysis. One approach to investigate this finding would be to use an adapted MS2-MCP system. By tagging endogenous transcripts with MS2 hairpins, live-cell tracking of the dynamics of mRNAs becomes possible (Tocchini and Mango, 2024). Essentially, upon expression of the MS2 Coat Protein (MCP), such a method would allow the visualization of the mRNA and whether it remains in the vicinity of the respective mtDNA copy. Additionally this method could be used for investigating the mRNA dynamics between mother and daughter cells in real time. Another experiment to differentiate between newly synthesized and "old" pre-existing Atp6-NG would be to use photoactivatable photoconvertible fluorescent tags, that allow quantitative tracking of a distinct protein in real time. Despite the limited knowledge on the dynamics of mitochondrial mRNAs, but taking into account that in yeast mitochondrial transcription and translation occur in a coupled manner (Kehrein et al., 2015), we posit that proteins encoding respiratory chain subunits remain largely restricted to the cell of its origin. All in all, we could show that in WT cells subunits of respiratory chain complexes remained local and in close proximity to the mtDNA they derive from, and the respective mtDNA-encoded proteins did not diffuse to the other parental cell during mating.

11.3 Selection occurs in a continuous mitochondrial network under intact cristae morphology

So far, this work has presented the complexity of the mtDNA inheritance in various levels. The last chapter of this work was focused on the role of cristae in the clearance of mutated mtDNA molecules. To examine the influence of cristae on purifying selection of mtDNA across generations, cristae-related genes were deleted and using the pedigree analysis, their effect on mtDNA quality control was assessed. Specifically, deletions of *ATP20*, *ATP21*, as well as the double deletion Atp20-Atp21, were observed to delay mtDNA quality control. Furthermore, deletion of *MIC10* and *MIC60*, as major determinants of the cristae junctions, led to a detrimental inability of the cell to distinguish between functional and mutant mtDNA.

Using the previously introduced strain, in which cells harbor WT mtDNA tagged with NeonGreen, we observed that in mutants with impaired cristae architecture the Atp6-NG signal exhibits increased movement throughout the mitochondrial network, while the mobility of the mtDNA from which it originates remains limited. This observation can be easily explained when considering cristae as diffusion boundaries. In line with this idea, studies have proposed that OXPHOS proteins get trapped within cristae membranes and are hindered from diffusing past the cristae junctions into the IMM (Schägger and Pfeiffer, 2000; Gilkerson, Selker, and Capaldi, 2003; Vogel et al., 2006). Studies conducted in HeLa cells also indicate that OXPHOS proteins along the longitudinal axis of the mitochondrial tubules exhibit diminished mobility (Wilkens, Kohl, and Busch, 2013; Appelhans et al., 2012).

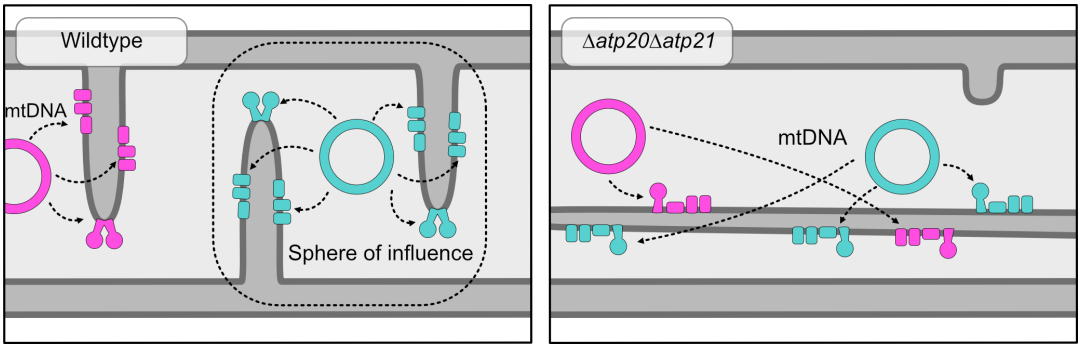

FIGURE 9: Model for mtDNA quality control in a fused mitochondrial network, adapted from Jakubke et al., 2021. In wildtype cells, mtDNA copies (in cyan) supply mtDNA-encoded proteins only to the cristae in their immediate vicinity. Respiratory chain complexes containing mtDNA-encoded subunits do not diffuse and remain local and confined within the cristae, creating a sphere of influence of mtDNA. However, in cells with compromised cristae structure, the limited diffusion of respiratory chain complexes is disrupted. In this case, proteins from the mutated mtDNA (in magenta) can be shadowed by proximal functional WT mtDNA-encoded products.

Based on our data, we posit that in healthy mitochondria, an intact cristae structure facilitates correct segregation of different mtDNA molecules and the proteins they encode. Due to the invaginations of the IMM, distinct sub-compartments are generated hosting mtDNA molecules, with their own sphere of influence. Subsequently, the cell can utilize this organization, for example in the case of reduced membrane potential (Jin et al., 2010), to efficiently identify and remove defective mtDNA copies from the mitochondrial network. Hence, the loss of cristae disrupts the organization of mtDNA-encoded proteins, allowing the respiratory chain complexes to freely diffuse along the altered cristae membranes, abolishing the concept

of a sphere of influence. As a result, the cell's ability to recognize and eliminate dysfunctional mtDNA is compromised, leading to the observed inefficient selection. Areas of defective mitochondria, containing mutated mtDNA, can be identified based on decreased respiratory chain efficiency. Within this rationale, a reduced proton gradient (Jin et al., 2010), lower ATP levels (Lieber et al., 2019), or altered redox states (McFaline-Figueroa et al., 2011) could serve as markers for cells to pinpoint defective mtDNA within the mitochondrial network, and could be used further for mutant mtDNA elimination. This experimental approach is further supported by a recent study, where individual cristae within the same mitochondrial tubule have been shown to maintain independent membrane potentials (Wolf et al., 2019). Our findings are also consistent with a previously proposed model positing that each mtDNA copy maintains a 'sphere of influence,' and remains spatially associated with its gene products (Kowald and Kirkwood, 2011; Busch, Kowald, and Spelbrink, 2014). Put together, we claim that the process of mtDNA purifying selection highly depends on normal cristae architecture and the sub-compartmentalisation of mitochondria (Figure 9).

All in all, with these results we underline that intact cristae architecture is a major determinant for the distribution of respiratory chain proteins across the mitochondrial matrix. We conclude that upon elimination of the cristae structure, selection is significantly impaired and thereby clearance against mutant mtDNAs is delayed.

12 Clinical significance

Mutations in mtDNA have been long associated and thus targeted for prevention of neurodegenerative, muscular and cardiovascular diseases. Deficient mtDNA maintenance contributes even to normal aging and diabetes (Al-Ghamdi et al., 2022; Amorim et al., 2022). Hence, heteroplasmy, which inevitably occurs over time, has also been shown to contribute to (if not cause) a plethora of myo-, neuropathies and cancer (Pérez-Amado et al., 2021; Habbane et al., 2021; Edwards et al., 2021). Additionally, although we currently lack direct experimental evidence, recent studies have indicated that proper mitochondrial function and the amount of mtDNA copies within a cell are also important determinants of oocyte quality and female fertility (Fragouli et al., 2015; Diez-Juan et al., 2015). Consequently, our understanding on how heteroplasmy comes to persist (or not), and how mtDNA mutations are selected against across generations and lineages become imperative topics to address.

Specifically, mutations in the mitochondrial genome have been associated with structural and functional alterations of crucial subunits of the OXPHOS complexes. Most of the times, they lead to dysfunction of the OXPHOS system, which eventually modifies concentrations of important metabolites, such as pyruvate and acetyl-CoA. The imbalance of these molecules has been linked to specific myopathies (Dengler et al., 1996), and production of ROS has been observed elevated in tumor cells as a result of increased metabolic rate, gene mutation and hypoxia, a cell state associated with malignant cell proliferation (Pérez-Amado et al., 2021; Perillo et al., 2020; Kondoh et al., 2013; Tafani et al., 2016). Therefore, heteroplasmy has been proposed as a potential biomarker of tracking the development and progression in cancer (Pérez-Amado et al., 2021). Furthermore, a strategy for effective elimination of dysfunctional mtDNA copies could involve active manipulation of the mtDNA using the CRISPR-Cas9 system (Schmiderer et al., 2022). Mitochondria-targeted Cas9 base-editing could be of great use for repairing mutated copies, keeping heteroplasmy below the biochemical threshold for pathologies (Stewart and Chinnery, 2015). However, the CRISPR-Cas9 system has yet to be applied for mitochondrial editing, as the guide RNA cannot enter inside mitochondria. In general, despite its advantages in mammalian cells, genome editing should be approached with caution as unintended mutations, called "off-targeting", as well as polymorphisms may occur when applying it (Rasul et al., 2022). Manipulating the degree of heteroplasmy within cells and/or tissues, could prove an extraordinary therapeutic strategy for tackling mitochondrial disorders, or at least delaying their onset, but there are still some safety concerns that need to be overcome.

Deleterious mutations have been also shown to cause early-onset diseases as they rapidly segregate toward homoplasmy by vegetative segregation (Wallace et al., 1995). That being so, cell divisions become fundamental in preventing such mutations to perpetuate across generations. Normally, in the germline harmful mutations are promptly eliminated by purifying selection, however selection errors do occur, as some mutated copies still pass on to the next generation. Consequently, examining the spatio-temporal dynamics of segregation, for example by following fluorescently-labeled mtDNA in real-time in different cell tissues *in vivo*, using whole-mount tissue live imaging, could yield valuable insights for advancing therapy development in the field. Certain mutations in mtDNA have been further associated with severe impacts on mitochondrial function during germline development in mammalian cells (Chiaratti and Chinnery, 2022). As those mtDNA mutations interfere with OXPHOS, they alter the OXPHOS-derived ATP, altering the ATP requirements of a particular cell, and thus negatively influence the mtDNA replication

and copy number of female germline stem cells during oogenesis (St. John, 2019). Given the significance of the genetic bottleneck to a cell's development, it is crucial to investigate mtDNA integrity in conjunction with inheritance, across all different stages of cell specification.

Lastly, since cristae morphology plays a fundamental role in the quality control process, it would be worth exploring the potential of tailored gene therapies that support new cristae biogenesis, thereby restoring probable purifying selection defects. Of course, it comes without saying that since our data are derived from yeast cells, it would be necessary to first confirm these findings in higher eukaryotes. Along these lines, investigating the phosphorylation status of subunits e and g of ATP synthase, that are responsible for the IMM curvatures, could yield valuable insights, given their implication in cristae architecture and structural integrity of mitochondria (Reinders et al., 2007). Specifically, the unphosphorylated form of subunit g (Atp20) has been reported to be required for the dimerization of the ATP synthase, which leads to the characteristic mitochondrial cristae morphology. Absence of Atp20 phosphorylation results in the formation of ATP synthase dimers as well as monomers. Hence, fine-tuning the phosphorylation state of such subunits could shift the cristae architecture as necessary, in order to increase IMM invaginations, that would eventually improve the process of mtDNA selection.

To conclude, despite substantial advancements in mitochondrial genome biology, a plethora of questions remain unanswered and a variety of diseases remain inadequately understood. Nonetheless, foundational research, such as investigating the dynamics of mtDNA segregation in a single-cell eukaryote, holds promise for paving the way towards understanding the mechanisms that underlie mtDNA variant segregation and purifying selection.

Bibliography

Al-Ghamdi, Bandar Ali et al. (Dec. 2022). "Role of mitochondrial DNA in diabetes Mellitus Type I and Type II". In: *Saudi Journal of Biological Sciences* 29.12, p. 103434. ISSN: 1319-562X. DOI: 10.1016/j.sjbs.2022.103434. URL: http://dx.doi.org/10.1016/j.sjbs.2022.103434.

Alberts Bruce, Bray Dennis Lewis Julian Raff Martin Roberts Keith and James D Watson (1994). "Molecular Biology of the Cell. 3rd edition." In: *New York: Garland Science*. URL: https://www.ncbi.nlm.nih.gov/books/NBK20684/.

Alexander, Christiane et al. (Oct. 2000). "OPA1, encoding a dynamin-related GTPase, is mutated in autosomal dominant optic atrophy linked to chromosome 3q28". In: *Nature Genetics* 26.2, 211–215. ISSN: 1546-1718. DOI: 10.1038/79944. URL: http://dx.doi.org/10.1038/79944.

Alkhaja, Alwaleed K. et al. (Jan. 2012). "MINOS1 is a conserved component of mitofilin complexes and required for mitochondrial function and cristae organization". In: *Molecular Biology of the Cell* 23.2. Ed. by Thomas D. Fox, 247–257. ISSN: 1939-4586. DOI: 10.1091/mbc.e11-09-0774. URL: http://dx.doi.org/10.1091/mbc.E11-09-0774.

Allen, John F. (Jan. 1992). "Protein phosphorylation in regulation of photosynthesis". In: *Biochimica et Biophysica Acta (BBA) - Bioenergetics* 1098.3, 275–335. ISSN: 0005-2728. DOI: 10.1016/s0005-2728(09)91014-3. URL: http://dx.doi.org/10.1016/s0005-2728(09)91014-3.

Allen, John F (May 2015). "Why chloroplasts and mitochondria retain their own genomes and genetic systems: Colocation for redox regulation of gene expression". In: *Proceedings of the National Academy of Sciences* 112.33, 10231–10238. ISSN: 1091-6490. DOI: 10.1073/pnas.1500012112. URL: http://dx.doi.org/10.1073/pnas.1500012112.

Amorim, João A. et al. (Feb. 2022). "Mitochondrial and metabolic dysfunction in ageing and age-related diseases". In: *Nature Reviews Endocrinology* 18.4, 243–258. ISSN: 1759-5037. DOI: 10.1038/s41574-021-00626-7. URL: http://dx.doi.org/10.1038/s41574-021-00626-7.

Andersson, G. E. et al. (Jan. 2003). "On the origin of mitochondria: a genomics perspective". In: *Philosophical Transactions of the Royal Society of London. Series B: Biological Sciences* 358.1429. Ed. by J. F. Allen and J. A. Raven, 165–179. ISSN: 1471-2970. DOI: 10.1098/rstb.2002.1193. URL: http://dx.doi.org/10.1098/rstb.2002.1193.

Andrews, Richard M. et al. (Oct. 1999). "Reanalysis and revision of the Cambridge reference sequence for human mitochondrial DNA". In: *Nature Genetics* 23.2, 147–147. ISSN: 1546-1718. DOI: 10.1038/13779. URL: http://dx.doi.org/10.1038/13779.

Appelhans, Timo et al. (Feb. 2012). "Nanoscale organization of mitochondrial microcompartments revealed by combining tracking and localization microscopy". In: *Nano Letters* 12.2, pp. 610–616. ISSN: 15306984. DOI: 10.1021/nl203343a. URL: https://pubmed.ncbi.nlm.nih.gov/22201267/.

Archer, Stephen L. (Dec. 2013). "Mitochondrial Dynamics — Mitochondrial Fission and Fusion in Human Diseases". In: *New England Journal of Medicine* 369.23. Ed. by Dan L. Longo, 2236–2251. ISSN: 1533-4406. DOI: 10.1056/nejmra1215233. URL: http://dx.doi.org/10.1056/NEJMra1215233.

Aretz, Ina, Christopher Jakubke, and Christof Osman (Dec. 2019). "Power to the daughters – mitochondrial and mtDNA transmission during cell division". In: *Biological Chemistry* 401.5, 533–546. ISSN: 1431-6730. DOI: 10.1515/hsz-2019-0337. URL: http://dx.doi.org/10.1515/hsz-2019-0337.

Arnold, I. (Dec. 1998). "Yeast mitochondrial F1F0-ATP synthase exists as a dimer: identification of three dimer-specific subunits". In: *The EMBO Journal* 17.24, 7170–7178. ISSN: 1460-2075. DOI: 10.1093/emboj/17.24.7170. URL: http://dx.doi.org/10.1093/emboj/17.24.7170.

Arselin, Geneviève et al. (Sept. 2004). "The Modulation in Subunits e and g Amounts of Yeast ATP Synthase Modifies Mitochondrial Cristae Morphology". In: *Journal of Biological Chemistry* 279.39, 40392–40399. ISSN: 0021-9258. DOI: 10.1074/jbc.m404316200. URL: http://dx.doi.org/10.1074/jbc.M404316200.

Ashley, M. V., P. J. Laipis, and W. W. Hauswirth (Sept. 1989). "Rapid segregation of heteroplasmic bovine mitodiondria". In: *Nucleic Acids Research* 17 (18), pp. 7325–7331. ISSN: 03051048. DOI: 10.1093/nar/17.18.7325.

Backer, James S. and C. William Birky (Jan. 1985). "The origin of mutant cells: mechanisms by whichSaccharomyces cerevisiae produces cells homoplasmic for new mitochondrial mutations". In: *Current Genetics* 9.8, 627–640. ISSN: 1432-0983. DOI: 10.1007/bf00449815. URL: http://dx.doi.org/10.1007/BF00449815.

Bacman, Sandra R et al. (Aug. 2013). "Specific elimination of mutant mitochondrial genomes in patient-derived cells by mitoTALENs". In: *Nature Medicine* 19.9, 1111–1113. ISSN: 1546-170X. DOI: 10.1038/nm.3261. URL: http://dx.doi.org/10.1038/nm.3261.

Berden, J.A and A.F Hartog (May 2000). "Analysis of the nucleotide binding sites of mitochondrial ATP synthase provides evidence for a two-site catalytic mechanism". In: *Biochimica et Biophysica Acta (BBA) - Bioenergetics* 1458.2–3, 234–251. ISSN: 0005-2728. DOI: 10.1016/s0005-2728(00)00076-1. URL: http://dx.doi.org/10.1016/s0005-2728(00)00076-1.

Berk, Arnold J. and David A. Clayton (July 1974). "Mechanism of mitochondrial DNA replication in mouse L-cells: Asynchronous replication of strands, segregation of circular daughter molecules, aspects of topology and turnover of an initiation sequence". In: *Journal of Molecular Biology* 86.4, 801–824. ISSN: 0022-2836. DOI: 10.1016/0022-2836(74)90355-6. URL: http://dx.doi.org/10.1016/0022-2836(74)90355-6.

Bheda, Poonam et al. (Dec. 2020). "Microfluidics for single-cell lineage tracking over time to characterize transmission of phenotypes in Saccharomyces cerevisiae". In: *STAR Protocols* 1.3, p. 100228. ISSN: 2666-1667. DOI: 10.1016/j.xpro.2020.100228. URL: http://dx.doi.org/10.1016/j.xpro.2020.100228.

Birky, C. W. (Sept. 1994). "Relaxed and Stringent Genomes: Why Cytoplasmic Genes Don't Obey Mendel's Laws". In: *Journal of Heredity* 85 (5), pp. 355–365. ISSN: 1465-7333. DOI: 10.1093/oxfordjournals.jhered.a111480. URL: https://academic.oup.com/jhered/article/887369/Relaxed.

Birky, C W, P Fuerst, and T Maruyama (Mar. 1989). "Organelle gene diversity under migration, mutation, and drift: equilibrium expectations, approach to equilibrium, effects of heteroplasmic cells, and comparison to nuclear genes." In: *Genetics* 121.3, 613–627. ISSN: 1943-2631. DOI: 10.1093/genetics/121.3.613. URL: http://dx.doi.org/10.1093/genetics/121.3.613.

Birky, C. William et al. (Jan. 1978). "Vegetative segregation of mitochondria in yeast: Estimating parameters using a random model". In: *Molecular and General Genetics MGG* 158.3, 251–261. ISSN: 1432-1874. DOI: 10.1007/bf00267196. URL: http://dx.doi.org/10.1007/BF00267196.

Birky, Jr (2001). "The inheritance of genes in mitochondria and chloroplasts: laws, mechanisms, and models". In: *Annual review of genetics* 35, pp. 125–148. ISSN: 0066-4197. DOI: 10.1146/ANNUREV.GENET.35.102401.090231. URL: https://pubmed.ncbi.nlm.nih.gov/11700280/.

Björkholm, Patrik et al. (Dec. 2016). "Why mitochondria need a genome revisited". In: *FEBS Letters* 591.1, 65–75. ISSN: 1873-3468. DOI: 10.1002/1873-3468.12510. URL: http://dx.doi.org/10.1002/1873-3468.12510.

Bleazard, William et al. (Aug. 1999). "The dynamin-related GTPase Dnm1 regulates mitochondrial fission in yeast". In: *Nature Cell Biology* 1.5, 298–304. ISSN: 1476-4679. DOI: 10.1038/13014. URL: http://dx.doi.org/10.1038/13014.

Boekema, Egbert J. and Hans-Peter Braun (Jan. 2007). "Supramolecular Structure of the Mitochondrial Oxidative Phosphorylation System". In: *Journal of Biological Chemistry* 282.1, 1–4. ISSN: 0021-9258. DOI: 10.1074/jbc.r600031200. URL: http://dx.doi.org/10.1074/jbc.R600031200.

Bohnert, Maria et al. (Oct. 2012). "Role of mitochondrial inner membrane organizing system in protein biogenesis of the mitochondrial outer membrane". In: *Molecular Biology of the Cell* 23.20. Ed. by Benjamin S. Glick, 3948–3956. ISSN: 1939-4586. DOI: 10.1091/mbc.e12-04-0295. URL: http://dx.doi.org/10.1091/mbc.E12-04-0295.

Boussau, Bastien et al. (June 2004). "Computational inference of scenarios for -proteobacterial genome evolution". In: *Proceedings of the National Academy of Sciences* 101.26, 9722–9727. ISSN: 1091-6490. DOI: 10.1073/pnas.0400975101. URL: http://dx.doi.org/10.1073/pnas.0400975101.

Brand, M.D. et al. (June 2013). "The role of mitochondrial function and cellular bioenergetics in ageing and disease: Mitochondrial function in ageing and disease". In: *British Journal of Dermatology* 169, 1–8. ISSN: 0007-0963. DOI: 10.1111/bjd.12208. URL: http://dx.doi.org/10.1111/bjd.12208.

Brewer, Laurence R. et al. (Oct. 2003). "Packaging of Single DNA Molecules by the Yeast Mitochondrial Protein Abf2p". In: *Biophysical Journal* 85.4, 2519–2524. ISSN: 0006-3495. DOI: 10.1016/s0006-3495(03)74674-8. URL: http://dx.doi.org/10.1016/S0006-3495(03)74674-8.

Burgstaller, Joerg P. et al. (Dec. 2018). "Large-scale genetic analysis reveals mammalian mtDNA heteroplasmy dynamics and variance increase through lifetimes and generations". In: *Nature Communications* 9 (1), p. 2488. ISSN: 2041-1723. DOI: 10.1038/s41467-018-04797-2.

Busch, Karin B, Axel Kowald, and Johannes N Spelbrink (July 2014). "Quality matters: how does mitochondrial network dynamics and quality control impact on mtDNA integrity?" In: *Philosophical transactions of the Royal Society of London. Series B, Biological sciences* 369.1646, p. 20130442. ISSN: 1471-2970. DOI: 10.1098/rstb.2013.0442. URL: http://www.ncbi.nlm.nih.gov/pubmed/24864312http://www.pubmedcentral.nih.gov/articlerender.fcgi?artid=PMC4032518.

Bustillo-Zabalbeitia, Itsasne et al. (July 2014). "Specific Interaction with Cardiolipin Triggers Functional Activation of Dynamin-Related Protein 1". In: *PLoS ONE* 9.7. Ed. by Stefan Strack, e102738. ISSN: 1932-6203. DOI: 10.1371/journal.pone.0102738. URL: http://dx.doi.org/10.1371/journal.pone.0102738.

Calvo, Sarah E. and Vamsi K. Mootha (Sept. 2010). "The Mitochondrial Proteome and Human Disease". In: *Annual Review of Genomics and Human Genetics* 11.1, 25–44. ISSN: 1545-293X. DOI: 10.1146/annurev-genom-082509-141720. URL: http://dx.doi.org/10.1146/annurev-genom-082509-141720.

Campbell, Peter et al. (June 2023). "Mitochondrial mutation, drift and selection during human development and ageing". In: *Research Square*. DOI: 10.21203/rs.3.rs-3083262/v1. URL: http://dx.doi.org/10.21203/rs.3.rs-3083262/v1.

Cao, Liqin et al. (Dec. 2009). "New Evidence Confirms That the Mitochondrial Bottleneck Is Generated without Reduction of Mitochondrial DNA Content in Early Primordial Germ Cells of Mice". In: *PLOS Genetics* 5.12, pp. 1–8. DOI: 10.1371/journal.pgen.1000756. URL: https://doi.org/10.1371/journal.pgen.1000756.

Carling, Phillippa J., Lynsey M. Cree, and Patrick F. Chinnery (Sept. 2011). "The implications of mitochondrial DNA copy number regulation during embryogenesis". In: *Mitochondrion* 11.5, 686–692. ISSN: 1567-7249. DOI: 10.1016/j.mito.2011.05.004. URL: http://dx.doi.org/10.1016/j.mito.2011.05.004.

Cerveny, Kara L., J. Michael McCaffery, and Robert E. Jensen (Feb. 2001). "Division of Mitochondria Requires a NovelDNM1-interacting Protein, Net2p". In: *Molecular Biology of the Cell* 12.2. Ed. by Douglas Koshland, 309–321. ISSN: 1939-4586. DOI: 10.1091/mbc.12.2.309. URL: http://dx.doi.org/10.1091/mbc.12.2.309.

Chakraborty, Arka et al. (Nov. 2016). "DNA structure directs positioning of the mitochondrial genome packaging protein Abf2p". In: *Nucleic Acids Research* 45.2, 951–967. ISSN: 1362-4962. DOI: 10.1093/nar/gkw1147. URL: http://dx.doi.org/10.1093/nar/gkw1147.

Chan, David C. (Dec. 2012). "Fusion and Fission: Interlinked Processes Critical for Mitochondrial Health". In: *Annual Review of Genetics* 46.1, 265–287. ISSN: 1545-2948. DOI: 10.1146/annurev-genet-110410-132529. URL: http://dx.doi.org/10.1146/annurev-genet-110410-132529.

Chapman, James, Yi Shiau Ng, and Thomas J. Nicholls (Aug. 2020). "The Maintenance of Mitochondrial DNA Integrity and Dynamics by Mitochondrial Membranes". In: *Life* 10.9, p. 164. ISSN: 2075-1729. DOI: 10.3390/life10090164. URL: http://dx.doi.org/10.3390/life10090164.

Chelius, Xenia et al. (Sept. 2023). "Selective retention of dysfunctional mitochondria during asymmetric cell division in yeast". In: *PLOS Biology* 21.9. Ed. by Jonathon Pines, e3002310. ISSN: 1545-7885. DOI: 10.1371/journal.pbio.3002310. URL: http://dx.doi.org/10.1371/journal.pbio.3002310.

Chen, WeiTing, Holly A. Ping, and Laura L. Lackner (Sept. 2018). "Direct membrane binding and self-interaction contribute to Mmr1 function in mitochondrial inheritance". In: *Molecular Biology of the Cell* 29.19. Ed. by Thomas D. Fox, 2346–2357. ISSN: 1939-4586. DOI: 10.1091/mbc.e18-02-0122. URL: http://dx.doi.org/10.1091/mbc.E18-02-0122.

Chen, Xi et al. (1995). "Rearranged mitochondrial genomes are present in human oocytes." In: *American journal of human genetics* 57 2, pp. 239–47. URL: https://api.semanticscholar.org/CorpusID:40342322.

Chen, Xin Jie and Ronald A Butow (Nov. 2005a). "The organization and inheritance of the mitochondrial genome." In: *Nature reviews. Genetics* 6 (11), pp. 815–25. ISSN: 1471-0056. DOI: 10.1038/nrg1708. URL: http://dx.doi.org/10.1038/nrg1708.

Chen, Xin Jie and Ronald A. Butow (Sept. 2005b). "The organization and inheritance of the mitochondrial genome". In: *Nature Reviews Genetics* 6.11, 815–825. ISSN: 1471-0064. DOI: 10.1038/nrg1708. URL: http://dx.doi.org/10.1038/nrg1708.

Chen, Zhiyong, Marine Berquez, and Alessandro Luciani (June 2020). "Mitochondria, mitophagy, and metabolic disease: towards assembling the puzzle". In: *Cell Stress* 4.6, 147–150. ISSN: 2523-0204. DOI: 10.15698/cst2020.06.222. URL: http://dx.doi.org/10.15698/cst2020.06.222.

Chernyakov, Irina, Felipe Santiago-Tirado, and Anthony Bretscher (Sept. 2013). "Active Segregation of Yeast Mitochondria by Myo2 Is Essential and Mediated by Mmr1 and Ypt11". In: *Current Biology* 23.18, 1818–1824. ISSN: 0960-9822. DOI: 10.1016/j.cub.2013.07.053. URL: http://dx.doi.org/10.1016/j.cub.2013.07.053.

Chiaratti, Marcos R. and Patrick F. Chinnery (Nov. 2022). "Modulating mitochondrial DNA mutations: factors shaping heteroplasmy in the germ line and somatic cells". In: *Pharmacological Research* 185, p. 106466. ISSN: 1043-6618. DOI: 10.1016/j.phrs.2022.106466. URL: http://dx.doi.org/10.1016/j.phrs.2022.106466.

Chinnery, P. F. and G. Hudson (May 2013). "Mitochondrial genetics". In: *British Medical Bulletin* 106.1, 135–159. ISSN: 1471-8391. DOI: 10.1093/bmb/ldt017. URL: http://dx.doi.org/10.1093/bmb/ldt017.

Chinnery, Patrick F. and David C. Samuels (Apr. 1999). "Relaxed Replication of mtDNA: A Model with Implications for the Expression of Disease". In: *The American Journal of Human Genetics* 64.4, 1158–1165. ISSN: 0002-9297. DOI: 10.1086/302311. URL: http://dx.doi.org/10.1086/302311.

Cho, Jae Hyoung et al. (Oct. 1998). "A Novel DNA-Binding Protein Bound to the Mitochondrial Inner Membrane Restores the Null Mutation of Mitochondrial Histone Abf2p in Saccharomyces cerevisiae". In: *Molecular and Cellular Biology* 18.10, 5712–5723. ISSN: 1098-5549. DOI: 10.1128/mcb.18.10.5712. URL: http://dx.doi.org/10.1128/MCB.18.10.5712.

Choi, Woo Suk and Miguel Garcia-Diaz (Dec. 2021). "A minimal motif for sequence recognition by mitochondrial transcription factor A (TFAM)". In: *Nucleic Acids Research* 50.1, 322–332. ISSN: 1362-4962. DOI: 10.1093/nar/gkab1230. URL: http://dx.doi.org/10.1093/nar/gkab1230.

Colina-Tenorio, L. et al. (Feb. 2020). "Shaping the mitochondrial inner membrane in health and disease". In: *Journal of Internal Medicine* 287.6, 645–664. ISSN: 1365-2796. DOI: 10.1111/joim.13031. URL: http://dx.doi.org/10.1111/joim.13031.

Colpman, Pierce, Asish Dasgupta, and Stephen L. Archer (July 2023). "The Role of Mitochondrial Dynamics and Mitotic Fission in Regulating the Cell Cycle in Cancer and Pulmonary Arterial Hypertension: Implications for Dynamin-Related Protein 1 and Mitofusin2 in Hyperproliferative Diseases". In: *Cells* 12.14, p. 1897. ISSN: 2073-4409. DOI: 10.3390/cells12141897. URL: http://dx.doi.org/10.3390/cells12141897.

Cree, Lynsey M. et al. (Feb. 2008). "A reduction of mitochondrial DNA molecules during embryogenesis explains the rapid segregation of genotypes". In: *Nature Genetics* 40 (2), pp. 249–254. ISSN: 10614036. DOI: 10.1038/ng.2007.63.

Cuppari, Anna et al. (May 2019). "DNA specificities modulate the binding of human transcription factor A to mitochondrial DNA control region". In: *Nucleic Acids Research* 47.12, 6519–6537. ISSN: 1362-4962. DOI: 10.1093/nar/gkz406. URL: http://dx.doi.org/10.1093/nar/gkz406.

Dai, Enyong et al. (Feb. 2024). "A guideline on the molecular ecosystem regulating ferroptosis". In: *Nature Cell Biology*. ISSN: 1476-4679. DOI: 10.1038/s41556-024-01360-8. URL: http://dx.doi.org/10.1038/s41556-024-01360-8.

Daley, Daniel O and James Whelan (2005). "Why genes persist in organelle genomes". In: *Genome Biology* 6.5, p. 110. ISSN: 1465-6906. DOI: 10.1186/gb-2005-6-5-110. URL: http://dx.doi.org/10.1186/gb-2005-6-5-110.

Darshi, Manjula et al. (Jan. 2011). "ChChd3, an Inner Mitochondrial Membrane Protein, Is Essential for Maintaining Crista Integrity and Mitochondrial Function". In: *Journal of Biological Chemistry* 286.4, 2918–2932. ISSN: 0021-9258. DOI: 10.1074/jbc.m110.171975. URL: http://dx.doi.org/10.1074/jbc.M110.171975.

Davies, K. M. et al. (Aug. 2012). "Structure of the yeast F1Fo-ATP synthase dimer and its role in shaping the mitochondrial cristae". In: *Proceedings of the National Academy of Sciences* 109.34, pp. 13602–13607. ISSN: 0027-8424. DOI: 10.1073/pnas.1204593109. URL: http://www.ncbi.nlm.nih.gov/pubmed/22864911http://www.pubmedcentral.nih.gov/articlerender.fcgi?artid=PMC3427116http://www.pnas.org/cgi/doi/10.1073/pnas.1204593109.

Delettre, Cécile et al. (Oct. 2000). "Nuclear gene OPA1, encoding a mitochondrial dynamin-related protein, is mutated in dominant optic atrophy". In: *Nature Genetics* 26.2, 207–210. ISSN: 1546-1718. DOI: 10.1038/79936. URL: http://dx.doi.org/10.1038/79936.

Dengler, Reinhard et al. (Apr. 1996). "Muscle fatigue, lactate, and pyruvate in mitochondrial myopathy with progressive external ophthalmoplegia". In: *Muscle amp; Nerve* 19.4, 456–462. ISSN: 1097-4598. DOI: 10.1002/(sici)1097-4598(199604)19:4<456::aid-mus5>3.0.co;2-b. URL: http://dx.doi.org/10.1002/(SICI)1097-4598(199604)19:4<456::AID-MUS5>3.0.CO;2-B.

Diaz, F. (Nov. 2002). "Human mitochondrial DNA with large deletions repopulates organelles faster than full-length genomes under relaxed copy number control". In: *Nucleic Acids Research* 30.21, 4626–4633. ISSN: 1362-4962. DOI: 10.1093/nar/gkf602. URL: http://dx.doi.org/10.1093/nar/gkf602.

Diez-Juan, Antonio et al. (Sept. 2015). "Mitochondrial DNA content as a viability score in human euploid embryos: less is better". In: *Fertility and Sterility* 104.3, 534–541.e1. ISSN: 0015-0282. DOI: 10.1016/j.fertnstert.2015.05.022. URL: http://dx.doi.org/10.1016/j.fertnstert.2015.05.022.

Diffley, J.F. and B Stillman (Feb. 1992). "DNA binding properties of an HMG1-related protein from yeast mitochondria." In: *Journal of Biological Chemistry* 267.5, 3368–3374. ISSN: 0021-9258. DOI: 10.1016/s0021-9258(19)50740-2. URL: http://dx.doi.org/10.1016/s0021-9258(19)50740-2.

DiMauro, Salvatore and Eric A. Schon (June 2003). "Mitochondrial Respiratory-Chain Diseases". In: *New England Journal of Medicine* 348.26, 2656–2668. ISSN: 1533-4406. DOI: 10.1056/nejmra022567. URL: http://dx.doi.org/10.1056/NEJMra022567.

Dixon, Scott J. et al. (May 2012). "Ferroptosis: An Iron-Dependent Form of Nonapoptotic Cell Death". In: *Cell* 149.5, 1060–1072. ISSN: 0092-8674. DOI: 10.1016/j.

cell.2012.03.042. URL: http://dx.doi.org/10.1016/j.cell.2012.03.042.

Dudkina, Natalya V. et al. (Aug. 2011). "Interaction of complexes I, III, and IV within the bovine respirasome by single particle cryoelectron tomography". In: *Proceedings of the National Academy of Sciences* 108.37, 15196–15200. ISSN: 1091-6490. DOI: 10.1073/pnas.1107819108. URL: http://dx.doi.org/10.1073/pnas.1107819108.

Dujon, B, P P Slonimski, and L Weill (Sept. 1974). "Mitochondrial genetics IX: A model for recombination and segregation of mitochondrial genomes in *Saccharomyces cerevisiae*". In: *Genetics* 78.1, pp. 415–437. ISSN: 1943-2631. DOI: 10.1093/genetics/78.1.415. eprint: https://academic.oup.com/genetics/article-pdf/78/1/415/34394392/genetics0415.pdf. URL: https://doi.org/10.1093/genetics/78.1.415.

D'Erchia, Anna Maria et al. (Jan. 2015). "Tissue-specific mtDNA abundance from exome data and its correlation with mitochondrial transcription, mass and respiratory activity". In: *Mitochondrion* 20, 13–21. ISSN: 1567-7249. DOI: 10.1016/j.mito.2014.10.005. URL: http://dx.doi.org/10.1016/j.mito.2014.10.005.

Edwards, David M. et al. (Apr. 2021). "Avoiding organelle mutational meltdown across eukaryotes with or without a germline bottleneck". In: *PLOS Biology* 19.4. Ed. by Thomas B.L. Kirkwood, e3001153. ISSN: 1545-7885. DOI: 10.1371/journal.pbio.3001153. URL: http://dx.doi.org/10.1371/journal.pbio.3001153.

Ekstrand, M. I. (Mar. 2004). "Mitochondrial transcription factor A regulates mtDNA copy number in mammals". In: *Human Molecular Genetics* 13.9, 935–944. ISSN: 1460-2083. DOI: 10.1093/hmg/ddh109. URL: http://dx.doi.org/10.1093/hmg/ddh109.

Embley, T. Martin and William Martin (Mar. 2006). "Eukaryotic evolution, changes and challenges". In: *Nature* 440.7084, 623–630. ISSN: 1476-4687. DOI: 10.1038/nature04546. URL: http://dx.doi.org/10.1038/nature04546.

Fan, Weiwei et al. (Feb. 2008). "A Mouse Model of Mitochondrial Disease Reveals Germline Selection Against Severe mtDNA Mutations". In: *Science* 319.5865, 958–962. ISSN: 1095-9203. DOI: 10.1126/science.1147786. URL: http://dx.doi.org/10.1126/science.1147786.

Fekkes, Peter, Kelly A. Shepard, and Michael P. Yaffe (Oct. 2000). "Gag3p, an Outer Membrane Protein Required for Fission of Mitochondrial Tubules". In: *The Journal of Cell Biology* 151.2, 333–340. ISSN: 1540-8140. DOI: 10.1083/jcb.151.2.333. URL: http://dx.doi.org/10.1083/jcb.151.2.333.

Filograna, R. et al. (Apr. 2019). "Modulation of mtDNA copy number ameliorates the pathological consequences of a heteroplasmic mtDNA mutation in the mouse". In: *Science Advances* 5.4. ISSN: 2375-2548. DOI: 10.1126/sciadv.aav9824. URL: http://dx.doi.org/10.1126/sciadv.aav9824.

Floros, VI et al. (Feb. 2018). "Segregation of mitochondrial DNA heteroplasmy through a developmental genetic bottleneck in human embryos". In: *Nature Cell Biology* 20 (2), pp. 144–151. ISSN: 14764679. DOI: 10.1038/s41556-017-0017-8.

Foury, Françoise et al. (Dec. 1998). "The complete sequence of the mitochondrial genome of Saccharomyces cerevisiae". In: *FEBS Letters* 440.3, 325–331. ISSN: 1873-3468. DOI: 10.1016/s0014-5793(98)01467-7. URL: http://dx.doi.org/10.1016/s0014-5793(98)01467-7.

Fragouli, Elpida et al. (June 2015). "Altered Levels of Mitochondrial DNA Are Associated with Female Age, Aneuploidy, and Provide an Independent Measure of Embryonic Implantation Potential". In: *PLOS Genetics* 11.6. Ed. by Stuart K. Kim, e1005241. ISSN: 1553-7404. DOI: 10.1371/journal.pgen.1005241. URL: http://dx.doi.org/10.1371/journal.pgen.1005241.

Frasch, Wayne D., Zain A. Bukhari, and Seiga Yanagisawa (Aug. 2022). "F1FO ATP synthase molecular motor mechanisms". In: *Frontiers in Microbiology* 13. ISSN: 1664-302X. DOI: 10.3389/fmicb.2022.965620. URL: http://dx.doi.org/10.3389/fmicb.2022.965620.

Friedman, Jonathan R et al. (Apr. 2015). "MICOS coordinates with respiratory complexes and lipids to establish mitochondrial inner membrane architecture". In: *eLife* 4. ISSN: 2050-084X. DOI: 10.7554/elife.07739. URL: http://dx.doi.org/10.7554/eLife.07739.

Fukushima, Noelle H. et al. (Sept. 2001). "The GTPase Effector Domain Sequence of the Dnm1p GTPase Regulates Self-Assembly and Controls a Rate-limiting Step in Mitochondrial Fission". In: *Molecular Biology of the Cell* 12.9. Ed. by Lawrence S. Goldstein, 2756–2766. ISSN: 1939-4586. DOI: 10.1091/mbc.12.9.2756. URL: http://dx.doi.org/10.1091/mbc.12.9.2756.

Gilkerson, Robert W., Jeanne M.L. Selker, and Roderick A. Capaldi (July 2003). "The cristal membrane of mitochondria is the principal site of oxidative phosphorylation". In: *FEBS Letters* 546.2-3, pp. 355–358. ISSN: 00145793. DOI: 10.1016/S0014-5793(03)00633-1. URL: https://pubmed.ncbi.nlm.nih.gov/12832068/.

Glastad, Robert C. and Iain G. Johnston (Mar. 2023). "Mitochondrial network structure controls cell-to-cell mtDNA variability generated by cell divisions". In: *PLoS Computational Biology* 19 (3 March), e1010953. ISSN: 15537358. DOI: 10.1371/journal.pcbi.1010953.

Göke, Aylin et al. (Sept. 2020). "Mrx6 regulates mitochondrial DNA copy number in *S. cerevisiae* by engaging the evolutionarily conserved Lon protease Pim1". In: *Molecular Biology of the Cell* 31 (7), pp. 511–723. ISSN: 1059-1524. DOI: 10.1091/mbc.e19-08-0470.

Haag-Liautard, Cathy et al. (Aug. 2008). "Direct Estimation of the Mitochondrial DNA Mutation Rate in Drosophila melanogaster". In: *PLoS Biology* 6.8. Ed. by Laurence D Hurst, e204. ISSN: 1545-7885. DOI: 10.1371/journal.pbio.0060204. URL: http://dx.doi.org/10.1371/journal.pbio.0060204.

Habbane, Mouna et al. (Oct. 2021). "Human Mitochondrial DNA: Particularities and Diseases". In: *Biomedicines* 9.10, p. 1364. ISSN: 2227-9059. DOI: 10.3390/biomedicines9101364. URL: http://dx.doi.org/10.3390/biomedicines9101364.

Hagstrom, E. et al. (Oct. 2013). "No recombination of mtDNA after heteroplasmy for 50 generations in the mouse maternal germline". In: *Nucleic Acids Research* 42.2, 1111–1116. ISSN: 1362-4962. DOI: 10.1093/nar/gkt969. URL: http://dx.doi.org/10.1093/nar/gkt969.

Harner, Max et al. (Nov. 2011). "The mitochondrial contact site complex, a determinant of mitochondrial architecture". In: *The EMBO Journal* 30.21, pp. 4356–4370. ISSN: 02614189. DOI: 10.1038/emboj.2011.379. URL: http://www.ncbi.nlm.nih.gov/pubmed/22009199http://www.pubmedcentral.nih.gov/articlerender.fcgi?artid=PMC3230385http://emboj.embopress.org/cgi/doi/10.1038/emboj.2011.379.

Harner, Max E. et al. (Nov. 2016). "An evidence based hypothesis on the existence of two pathways of mitochondrial crista formation". In: *eLife* 5.NOVEMBER2016.

ISSN: 2050084X. DOI: 10.7554/eLife.18853. URL: https://pubmed.ncbi.nlm.nih.gov/27849155/.

Harner, Max Emanuel et al. (Apr. 2014). "Aim24 and MICOS modulate respiratory function, tafazzin-related cardiolipin modification and mitochondrial architecture". In: *eLife* 3. ISSN: 2050-084X. DOI: 10.7554/elife.01684. URL: http://dx.doi.org/10.7554/eLife.01684.

Hauswirth, W. W. and P. J. Laipis (1982). "Mitochondrial DNA polymorphism in a maternal lineage of Holstein cows". In: *Proceedings of the National Academy of Sciences of the United States of America* 79 (15), pp. 4686–4690. ISSN: 0027-8424. DOI: 10.1073/PNAS.79.15.4686. URL: https://pubmed.ncbi.nlm.nih.gov/6289312/.

Hermann, Greg J. et al. (Oct. 1998). "Mitochondrial Fusion in Yeast Requires the Transmembrane GTPase Fzo1p". In: *The Journal of Cell Biology* 143.2, 359–373. ISSN: 1540-8140. DOI: 10.1083/jcb.143.2.359. URL: http://dx.doi.org/10.1083/jcb.143.2.359.

Higuchi-Sanabria, Ryo et al. (2016). "Live-cell imaging of mitochondria and the actin cytoskeleton in budding yeast". In: *Methods in Molecular Biology* 1365. ISSN: 10643745. DOI: 10.1007/978-1-4939-3124-8_2.

Hill, Jahda H, Zhe Chen, and Hong Xu (Mar. 2014). "Selective propagation of functional mitochondrial DNA during oogenesis restricts the transmission of a deleterious mitochondrial variant". In: *Nature Genetics* 46.4, 389–392. ISSN: 1546-1718. DOI: 10.1038/ng.2920. URL: http://dx.doi.org/10.1038/ng.2920.

Hoppins, S. et al. (Oct. 2011). "A mitochondrial-focused genetic interaction map reveals a scaffold-like complex required for inner membrane organization in mitochondria". In: *The Journal of Cell Biology*, jcb.201107053–. ISSN: 0021-9525. DOI: 10.1083/jcb.201107053. URL: http://jcb.rupress.org/cgi/content/abstract/jcb.201107053v1.

Iborra, Francisco J., Hiroshima Kimura, and Peter R. Cook (May 2004). "The functional organization of mitochondrial genomes in human cells". In: *BMC Biology* 2, p. 9. ISSN: 17417007. DOI: 10.1186/1741-7007-2-9. URL: https://pubmed.ncbi.nlm.nih.gov/15157274/.

Ikeda, Masataka et al. (Mar. 2015). "Overexpression of TFAM or Twinkle Increases mtDNA Copy Number and Facilitates Cardioprotection Associated with Limited Mitochondrial Oxidative Stress". In: *PLOS ONE* 10.3. Ed. by Junichi Sadoshima, e0119687. ISSN: 1932-6203. DOI: 10.1371/journal.pone.0119687. URL: http://dx.doi.org/10.1371/journal.pone.0119687.

Iovine, Joseph C., Steven M. Claypool, and Nathan N. Alder (Nov. 2021). "Mitochondrial compartmentalization: emerging themes in structure and function". In: *Trends in Biochemical Sciences* 46.11, 902–917. ISSN: 0968-0004. DOI: 10.1016/j.tibs.2021.06.003. URL: http://dx.doi.org/10.1016/j.tibs.2021.06.003.

Itoh, Takashi, Akio Toh-e, and Yasushi Matsui (June 2004). "Mmr1p is a mitochondrial factor for Myo2p-dependent inheritance of mitochondria in the budding yeast". In: *The EMBO Journal* 23.13, 2520–2530. ISSN: 1460-2075. DOI: 10.1038/sj.emboj.7600271. URL: http://dx.doi.org/10.1038/sj.emboj.7600271.

Itoh, Takashi et al. (Nov. 2002). "Complex Formation with Ypt11p, a rab-Type Small GTPase, Is Essential To Facilitate the Function of Myo2p, a Class V Myosin, in Mitochondrial Distribution in Saccharomyces cerevisiae". In: *Molecular and Cellular Biology* 22.22, 7744–7757. ISSN: 1098-5549. DOI: 10.1128/mcb.22.22.7744-

7757.2002. URL: http://dx.doi.org/10.1128/MCB.22.22.7744-7757.2002.

Iwata, Momi et al. (Sept. 2012). "The structure of the yeast NADH dehydrogenase (Ndi1) reveals overlapping binding sites for water- and lipid-soluble substrates". In: *Proceedings of the National Academy of Sciences* 109.38, 15247–15252. ISSN: 1091-6490. DOI: 10.1073/pnas.1210059109. URL: http://dx.doi.org/10.1073/pnas.1210059109.

Jajoo, Rishi et al. (Jan. 2016). "Accurate concentration control of mitochondria and nucleoids". In: *Science* 351 (6269), pp. 169–172. ISSN: 10959203. DOI: 10.1126/science.aaa8714.

Jakubke, Christopher et al. (Sept. 2021). "Cristae-dependent quality control of the mitochondrial genome". In: *Science advances* 7 (36), eabi8886. ISSN: 2375-2548. DOI: 10.1126/SCIADV.ABI8886. URL: https://pubmed.ncbi.nlm.nih.gov/34516914/.

Jenuth, Jack P. et al. (Oct. 1996). "Random genetic drift in the female germline explains the rapid segregation of mammalian mitochondrial DNA". In: *Nature Genetics* 14.2, 146–151. ISSN: 1546-1718. DOI: 10.1038/ng1096-146. URL: http://dx.doi.org/10.1038/ng1096-146.

Jimenez, Laure et al. (Dec. 2014). "Mitochondrial ATP synthases cluster as discrete domains that reorganize with the cellular demand for oxidative phosphorylation." In: *Journal of cell science* 127.4, pp. 719–726. ISSN: 1477-9137. DOI: 10.1242/jcs.137141. URL: http://www.ncbi.nlm.nih.gov/pubmed/24338369.

Jin, Seok Min et al. (Nov. 2010). "Mitochondrial membrane potential regulates PINK1 import and proteolytic destabilization by PARL". In: *Journal of Cell Biology* 191.5, pp. 933–942. ISSN: 00219525. DOI: 10.1083/jcb.201008084. URL: /pmc/articles/PMC2995166/pmc/articles/PMC2995166/?report=abstracthttps://www.ncbi.nlm.nih.gov/pmc/articles/PMC2995166/.

John, Philip and F. R. Whatley (Apr. 1975). "Paracoccus denitrificans and the evolutionary origin of the mitochondrion". In: *Nature* 254.5500, 495–498. ISSN: 1476-4687. DOI: 10.1038/254495a0. URL: http://dx.doi.org/10.1038/254495a0.

Johnston, Iain G. (Nov. 2019). "Varied Mechanisms and Models for the Varying Mitochondrial Bottleneck". In: *Frontiers in Cell and Developmental Biology* 7, p. 294. ISSN: 2296634X. DOI: 10.3389/fcell.2019.00294.

Johnston, Iain G. and Nick S. Jones (Nov. 2016). "Evolution of Cell-to-Cell Variability in Stochastic, Controlled, Heteroplasmic mtDNA Populations". In: *The American Journal of Human Genetics* 99.5, 1150–1162. ISSN: 0002-9297. DOI: 10.1016/j.ajhg.2016.09.016. URL: http://dx.doi.org/10.1016/j.ajhg.2016.09.016.

Johnston, Iain G. et al. (June 2015). "Stochastic modelling, Bayesian inference, and new in vivo measurements elucidate the debated mtDNA bottleneck mechanism". In: *eLife* 4 (JUNE2015), e07464. ISSN: 2050-084X. DOI: 10.7554/ELIFE.07464. URL: https://pubmed.ncbi.nlm.nih.gov/26035426/.

Kanki, Tomotake et al. (Nov. 2004). "Architectural Role of Mitochondrial Transcription Factor A in Maintenance of Human Mitochondrial DNA". In: *Molecular and Cellular Biology* 24.22, 9823–9834. ISSN: 1098-5549. DOI: 10.1128/mcb.24.22.9823-9834.2004. URL: http://dx.doi.org/10.1128/MCB.24.22.9823-9834.2004.

Kauppila, Timo E.S., Johanna H.K. Kauppila, and Nils-Göran Larsson (Jan. 2017). "Mammalian Mitochondria and Aging: An Update". In: *Cell Metabolism* 25 (1),

pp. 57–71. ISSN: 15504131. DOI: 10.1016/j.cmet.2016.09.017. URL: http://www.ncbi.nlm.nih.gov/pubmed/28094012http://linkinghub.elsevier.com/retrieve/pii/S1550413116305022.

Kehrein, Kirsten et al. (Feb. 2015). "Organization of Mitochondrial Gene Expression in Two Distinct Ribosome-Containing Assemblies." English. In: *Cell reports* 10.6, pp. 843–853. ISSN: 2211-1247. DOI: 10.1016/j.celrep.2015.01.012. URL: http://www.cell.com/article/S221112471500025X/fulltext.

Khan, Altmash, Gifty Kuriachan, and Radhakrishnan Mahalakshmi (Sept. 2021). "Cellular Interactome of Mitochondrial Voltage-Dependent Anion Channels: Oligomerization and Channel (Mis)Regulation". In: *ACS Chemical Neuroscience* 12.19, 3497–3515. ISSN: 1948-7193. DOI: 10.1021/acschemneuro.1c00429. URL: http://dx.doi.org/10.1021/acschemneuro.1c00429.

Kitami, Toshimori et al. (Mar. 2012). "A Chemical Screen Probing the Relationship between Mitochondrial Content and Cell Size". In: *PLoS ONE* 7.3. Ed. by Yidong Bai, e33755. ISSN: 1932-6203. DOI: 10.1371/journal.pone.0033755. URL: http://dx.doi.org/10.1371/journal.pone.0033755.

Kleele, Tatjana et al. (May 2021). "Distinct fission signatures predict mitochondrial degradation or biogenesis". In: *Nature* 593.7859, 435–439. ISSN: 1476-4687. DOI: 10.1038/s41586-021-03510-6. URL: http://dx.doi.org/10.1038/s41586-021-03510-6.

Klucnika, Anna and Hansong Ma (Mar. 2019). "A battle for transmission: the cooperative and selfish animal mitochondrial genomes". In: *Open Biology* 9.3. ISSN: 2046-2441. DOI: 10.1098/rsob.180267. URL: http://dx.doi.org/10.1098/rsob.180267.

Koehler, C M et al. (Sept. 1991). "Replacement of bovine mitochondrial DNA by a sequence variant within one generation." In: *Genetics* 129.1, 247–255. ISSN: 1943-2631. DOI: 10.1093/genetics/129.1.247. URL: http://dx.doi.org/10.1093/genetics/129.1.247.

Kondoh, Miyako et al. (Nov. 2013). "Hypoxia-Induced Reactive Oxygen Species Cause Chromosomal Abnormalities in Endothelial Cells in the Tumor Microenvironment". In: *PLoS ONE* 8.11. Ed. by Ryuichi Morishita, e80349. ISSN: 1932-6203. DOI: 10.1371/journal.pone.0080349. URL: http://dx.doi.org/10.1371/journal.pone.0080349.

Kowald, Axel and Tom B L Kirkwood (June 2011). "Evolution of the mitochondrial fusion-fission cycle and its role in aging." In: *Proceedings of the National Academy of Sciences of the United States of America* 108 (25), pp. 10237–42. ISSN: 1091-6490. DOI: 10.1073/pnas.1101604108. URL: http://www.pubmedcentral.nih.gov/articlerender.fcgi?artid=3121810&tool=pmcentrez&rendertype=abstract.

Kukat, Christian et al. (Aug. 2011). "Super-resolution microscopy reveals that mammalian mitochondrial nucleoids have a uniform size and frequently contain a single copy of mtDNA". In: *Proceedings of the National Academy of Sciences of the United States of America* 108 (33), pp. 13534–13539. ISSN: 00278424. DOI: 10.1073/pnas.1109263108.

Kuroiwa, Tsuneyoshi et al. (July 1982). "Epifluorescent microscopic evidence for maternal inheritance of chloroplast DNA". In: *Nature* 298.5873, 481–483. ISSN: 1476-4687. DOI: 10.1038/298481a0. URL: http://dx.doi.org/10.1038/298481a0.

Kühlbrandt, Werner (June 2019). "Structure and Mechanisms of F-Type ATP Synthases". In: *Annual Review of Biochemistry* 88.1, 515–549. ISSN: 1545-4509. DOI:

10.1146/annurev-biochem-013118-110903. URL: http://dx.doi.org/10.1146/annurev-biochem-013118-110903.

Lasserre, Jean-Paul et al. (June 2015). "Yeast as a system for modeling mitochondrial disease mechanisms and discovering therapies". In: *Disease Models amp; Mechanisms* 8.6, 509–526. ISSN: 1754-8403. DOI: 10.1242/dmm.020438. URL: http://dx.doi.org/10.1242/dmm.020438.

Lee, Hyo Sang et al. (May 2012). "Rapid Mitochondrial DNA Segregation in Primate Preimplantation Embryos Precedes Somatic and Germline Bottleneck". In: *Cell Reports* 1 (5), pp. 506–515. ISSN: 22111247. DOI: 10.1016/j.celrep.2012.03.011.

Leite, Ana Cláudia, Vítor Costa, and Clara Pereira (Aug. 2023). "Mitochondria and the cell cycle in budding yeast". In: *International Journal of Biochemistry and Cell Biology* 161. ISSN: 18785875. DOI: 10.1016/j.biocel.2023.106444.

Lemasters, John J (May 2007). "Modulation of mitochondrial membrane permeability in pathogenesis, autophagy and control of metabolism". In: *Journal of Gastroenterology and Hepatology* 22.s1. ISSN: 1440-1746. DOI: 10.1111/j.1440-1746.2006.04643.x. URL: http://dx.doi.org/10.1111/j.1440-1746.2006.04643.x.

Lenaz, G. and M.L. Genova (2013). "Quinones". In: *Encyclopedia of Biological Chemistry*. Elsevier, 722–729. ISBN: 9780123786319. DOI: 10.1016/b978-0-12-378630-2.00204-8. URL: http://dx.doi.org/10.1016/B978-0-12-378630-2.00204-8.

Lewis, Samantha C., Lauren F. Uchiyama, and Jodi Nunnari (July 2016). "ER-mitochondria contacts couple mtDNA synthesis with Mitochondrial division in human cells". In: *Science* 353 (6296), aaf5549. ISSN: 10959203. DOI: 10.1126/science.aaf5549.

Li, Wen-Hsiung (1996). "Kimura's Contributions to Molecular Evolution". In: *theoretical population biology* 49, p. 146153.

Lieber, Toby et al. (June 2019). "Mitochondrial fragmentation drives selective removal of deleterious mtDNA in the germline". In: *Nature* 570 (7761), pp. 380–384. ISSN: 14764687. DOI: 10.1038/s41586-019-1213-4. URL: /pmc/articles/PMC6614061/?report=abstracthttps://www.ncbi.nlm.nih.gov/pmc/articles/PMC6614061/.

Ling, Feng, Akiko Hori, and Takehiko Shibata (Feb. 2007). "DNA Recombination-Initiation Plays a Role in the Extremely Biased Inheritance of Yeast [rho] Mitochondrial DNA That Contains the Replication Origin ori5". In: *Molecular and Cellular Biology* 27.3, 1133–1145. ISSN: 1098-5549. DOI: 10.1128/mcb.00770-06. URL: http://dx.doi.org/10.1128/MCB.00770-06.

Lopez, J and S W G Tait (Mar. 2015). "Mitochondrial apoptosis: killing cancer using the enemy within". In: *British Journal of Cancer* 112.6, 957–962. ISSN: 1532-1827. DOI: 10.1038/bjc.2015.85. URL: http://dx.doi.org/10.1038/bjc.2015.85.

Luttik, Marijke A.H. et al. (Sept. 1998). "The Saccharomyces cerevisiae NDE1 and NDE2 Genes Encode Separate Mitochondrial NADH Dehydrogenases Catalyzing the Oxidation of Cytosolic NADH". In: *Journal of Biological Chemistry* 273.38, 24529–24534. ISSN: 0021-9258. DOI: 10.1074/jbc.273.38.24529. URL: http://dx.doi.org/10.1074/jbc.273.38.24529.

Ma, Hansong, Hong Xu, and Patrick H O'Farrell (Mar. 2014). "Transmission of mitochondrial mutations and action of purifying selection in Drosophila melanogaster". In: *Nature Genetics* 46.4, 393–397. ISSN: 1546-1718. DOI: 10.1038/ng.2919. URL: http://dx.doi.org/10.1038/ng.2919.

MacAlpine, David M., Philip S. Perlman, and Ronald A. Butow (June 1998). "The high mobility group protein Abf2p influences the level of yeast mitochondrial DNA recombination intermediates in vivo". In: *Proceedings of the National Academy of Sciences* 95.12, 6739–6743. ISSN: 1091-6490. DOI: 10.1073/pnas.95.12.6739. URL: http://dx.doi.org/10.1073/pnas.95.12.6739.

Maleszka, R., P.J. Skelly, and G.D. Clark-Walker (Dec. 1991). "Rolling circle replication of DNA in yeast mitochondria." In: *The EMBO Journal* 10.12, 3923–3929. ISSN: 0261-4189. DOI: 10.1002/j.1460-2075.1991.tb04962.x. URL: http://dx.doi.org/10.1002/j.1460-2075.1991.tb04962.x.

Malina, Carl, Christer Larsson, and Jens Nielsen (Apr. 2018). "Yeast mitochondria: an overview of mitochondrial biology and the potential of mitochondrial systems biology". In: *FEMS Yeast Research* 18.5. ISSN: 1567-1364. DOI: 10.1093/femsyr/foy040. URL: http://dx.doi.org/10.1093/femsyr/foy040.

Malsburg, Karina von der et al. (Oct. 2011). "Dual role of mitofilin in mitochondrial membrane organization and protein biogenesis." In: *Developmental cell* 21.4, pp. 694–707. ISSN: 1878-1551. DOI: 10.1016/j.devcel.2011.08.026. URL: http://www.ncbi.nlm.nih.gov/pubmed/21944719.

Margulis, Lynn (1970). "Origin of Eukaryotic Cells". In.

Marlow, Florence L. (May 2017). "Mitochondrial matters: Mitochondrial bottlenecks, self-assembling structures, and entrapment in the female germline". In: *Stem Cell Research* 21, 178–186. ISSN: 1873-5061. DOI: 10.1016/j.scr.2017.03.004. URL: http://dx.doi.org/10.1016/j.scr.2017.03.004.

Martin, William and Miklós Müller (Mar. 1998). "The hydrogen hypothesis for the first eukaryote". In: *Nature* 392.6671, 37–41. ISSN: 1476-4687. DOI: 10.1038/32096. URL: http://dx.doi.org/10.1038/32096.

McCutcheon, John P. and Nancy A. Moran (Nov. 2011). "Extreme genome reduction in symbiotic bacteria". In: *Nature Reviews Microbiology* 10.1, 13–26. ISSN: 1740-1534. DOI: 10.1038/nrmicro2670. URL: http://dx.doi.org/10.1038/nrmicro2670.

McFaline-Figueroa, José Ricardo et al. (Oct. 2011). "Mitochondrial quality control during inheritance is associated with lifespan and mother-daughter age asymmetry in budding yeast." In: *Aging cell* 10.5, pp. 885–95. ISSN: 1474-9726. DOI: 10.1111/j.1474-9726.2011.00731.x. URL: http://www.pubmedcentral.nih.gov/articlerender.fcgi?artid=3173513&tool=pmcentrez&rendertype=abstract.

Medeiros, Tânia Catarina et al. (May 2018). "Autophagy balances mtDNA synthesis and degradation by DNA polymerase POLG during starvation". In: *Journal of Cell Biology* 217.5, pp. 1601–1611. ISSN: 15408140. DOI: 10.1083/jcb.201801168. URL: https://pubmed.ncbi.nlm.nih.gov/29519802/.

Meeusen, Shelly et al. (Oct. 2006). "Mitochondrial Inner-Membrane Fusion and Crista Maintenance Requires the Dynamin-Related GTPase Mgm1". In: *Cell* 127.2, 383–395. ISSN: 0092-8674. DOI: 10.1016/j.cell.2006.09.021. URL: http://dx.doi.org/10.1016/j.cell.2006.09.021.

Michikawa, Yuichi et al. (Oct. 1999). "Aging-Dependent Large Accumulation of Point Mutations in the Human mtDNA Control Region for Replication". In: *Science* 286.5440, 774–779. ISSN: 1095-9203. DOI: 10.1126/science.286.5440.774. URL: http://dx.doi.org/10.1126/science.286.5440.774.

Miettinen, Teemu P. and Mikael Björklund (Nov. 2016). "Cellular Allometry of Mitochondrial Functionality Establishes the Optimal Cell Size". In: *Developmental Cell* 39.3, 370–382. ISSN: 1534-5807. DOI: 10.1016/j.devcel.2016.09.004. URL: http://dx.doi.org/10.1016/j.devcel.2016.09.004.

Miyakawa, Isamu (2017). "Organization and dynamics of yeast mitochondrial nucleoids". In: *Proceedings of the Japan Academy, Series B* 93.5, 339–359. ISSN: 1349-2896. DOI: 10.2183/pjab.93.021. URL: http://dx.doi.org/10.2183/pjab.93.021.

Montoya, J et al. (Dec. 1982). "Identification of initiation sites for heavy-strand and light-strand transcription in human mitochondrial DNA." In: *Proceedings of the National Academy of Sciences* 79.23, 7195–7199. ISSN: 1091-6490. DOI: 10.1073/pnas.79.23.7195. URL: http://dx.doi.org/10.1073/pnas.79.23.7195.

Moretton, Amandine et al. (Apr. 2017). "Selective mitochondrial DNA degradation following double-strand breaks". In: *PLOS ONE* 12.4. Ed. by Maria Sola, e0176795. ISSN: 1932-6203. DOI: 10.1371/journal.pone.0176795. URL: http://dx.doi.org/10.1371/journal.pone.0176795.

Mozdy, A.D., J.M. McCaffery, and J.M. Shaw (Oct. 2000). "Dnm1p Gtpase-Mediated Mitochondrial Fission Is a Multi-Step Process Requiring the Novel Integral Membrane Component Fis1p". In: *The Journal of Cell Biology* 151.2, 367–380. ISSN: 1540-8140. DOI: 10.1083/jcb.151.2.367. URL: http://dx.doi.org/10.1083/jcb.151.2.367.

Muller, H.J. (May 1964). "The relation of recombination to mutational advance". In: *Mutation Research/Fundamental and Molecular Mechanisms of Mutagenesis* 1.1, 2–9. ISSN: 0027-5107. DOI: 10.1016/0027-5107(64)90047-8. URL: http://dx.doi.org/10.1016/0027-5107(64)90047-8.

Murley, Andrew et al. (May 2013). "ER-associated mitochondrial division links the distribution of mitochondria and mitochondrial DNA in yeast". In: *eLife* 2, e00422. ISSN: 2050-084X. DOI: 10.7554/eLife.00422. URL: http://www.ncbi.nlm.nih.gov/pubmed/23682313http://www.pubmedcentral.nih.gov/articlerender.fcgi?artid=PMC3654481http://elifesciences.org/lookup/doi/10.7554/eLife.00422.

Murphy, Bonnie J. et al. (June 2019). "Rotary substates of mitochondrial ATP synthase reveal the basis of flexible F1-Fo coupling". In: *Science* 364.6446. ISSN: 1095-9203. DOI: 10.1126/science.aaw9128. URL: http://dx.doi.org/10.1126/science.aaw9128.

Nagashima, Shun et al. (Mar. 2020). "Golgi-derived PI (4) P-containing vesicles drive late steps of mitochondrial division". In: *Science* 367.6484, 1366–1371. ISSN: 1095-9203. DOI: 10.1126/science.aax6089. URL: http://dx.doi.org/10.1126/science.aax6089.

Navarro-Espíndola, Raful, Fernando Suaste-Olmos, and Leonardo Peraza-Reyes (Nov. 2020). "Dynamic Regulation of Peroxisomes and Mitochondria during Fungal Development". In: *Journal of Fungi* 6.4, p. 302. ISSN: 2309-608X. DOI: 10.3390/jof6040302. URL: http://dx.doi.org/10.3390/jof6040302.

Neupert, Walter (June 1997). "PROTEIN IMPORT INTO MITOCHONDRIA". In: *Annual Review of Biochemistry* 66.1, 863–917. ISSN: 1545-4509. DOI: 10.1146/annurev.biochem.66.1.863. URL: http://dx.doi.org/10.1146/annurev.biochem.66.1.863.

Newman, S. (Jan. 1996). "Analysis of mitochondrial DNA nucleoids in wild-type and a mutant strain of Saccharomyces cerevisiae that lacks the mitochondrial HMG box protein Abf2p". In: *Nucleic Acids Research* 24.2, 386–393. ISSN: 1362-4962. DOI: 10.1093/nar/24.2.386. URL: http://dx.doi.org/10.1093/nar/24.2.386.

Nicolson, Garth L. (2014). "Mitochondrial dysfunction and chronic disease: treatment with natural supplements." In: *Alternative therapies in health and medicine* 20

Suppl 1, pp. 18–25. URL: https://api.semanticscholar.org/CorpusID:25717326.

Nissanka, Nadee and Carlos T Moraes (Feb. 2020). "Mitochondrial heteroplasmy in disease and targeted nuclease-based therapeutic approaches". In: *EMBO reports* 21.3. ISSN: 1469-3178. DOI: 10.15252/embr.201949612. URL: http://dx.doi.org/10.15252/embr.201949612.

Nolfi-Donegan, Deirdre, Andrea Braganza, and Sruti Shiva (Oct. 2020). "Mitochondrial electron transport chain: Oxidative phosphorylation, oxidant production, and methods of measurement". In: *Redox Biology* 37, p. 101674. ISSN: 2213-2317. DOI: 10.1016/j.redox.2020.101674. URL: http://dx.doi.org/10.1016/j.redox.2020.101674.

Nunnari, J et al. (July 1997). "Mitochondrial transmission during mating in Saccharomyces cerevisiae is determined by mitochondrial fusion and fission and the intramitochondrial segregation of mitochondrial DNA." In: *Molecular Biology of the Cell* 8.7, 1233–1242. ISSN: 1939-4586. DOI: 10.1091/mbc.8.7.1233. URL: http://dx.doi.org/10.1091/mbc.8.7.1233.

Obara, Keisuke et al. (Apr. 2022). "Proteolysis of adaptor protein Mmr1 during budding is necessary for mitochondrial homeostasis in Saccharomyces cerevisiae". In: *Nature Communications* 13.1. ISSN: 2041-1723. DOI: 10.1038/s41467-022-29704-8. URL: http://dx.doi.org/10.1038/s41467-022-29704-8.

Okamoto, K, P S Perlman, and R A Butow (Aug. 1998). "The sorting of mitochondrial DNA and mitochondrial proteins in zygotes: preferential transmission of mitochondrial DNA to the medial bud." In: *The Journal of cell biology* 142 (3), pp. 613–23. ISSN: 0021-9525. URL: http://www.pubmedcentral.nih.gov/articlerender.fcgi?artid=2148178&tool=pmcentrez&rendertype=abstract.

Olivo, Paul D. et al. (1983). "Nucleotide sequence evidence for rapid genotypic shifts in the bovine mitochondrial DNA D-loop". In: *Nature* 306 (5941), pp. 400–402. ISSN: 1476-4687. DOI: 10.1038/306400a0. URL: https://www.nature.com/articles/306400a0.

Osman, Christof et al. (Mar. 2015). "Integrity of the yeast mitochondrial genome, but not its distribution and inheritance, relies on mitochondrial fission and fusion". In: *Proceedings of the National Academy of Sciences of the United States of America* 112 (9), E947–E956. ISSN: 10916490. DOI: 10.1073/pnas.1501737112.

Otsuga, Denichiro et al. (Oct. 1998). "The Dynamin-related GTPase, Dnm1p, Controls Mitochondrial Morphology in Yeast". In: *The Journal of Cell Biology* 143.2, 333–349. ISSN: 1540-8140. DOI: 10.1083/jcb.143.2.333. URL: http://dx.doi.org/10.1083/jcb.143.2.333.

Otten, Auke B.C. et al. (July 2016). "Differences in Strength and Timing of the mtDNA Bottleneck between Zebrafish Germline and Non-germline Cells". In: *Cell Reports* 16 (3), pp. 622–630. ISSN: 22111247. DOI: 10.1016/j.celrep.2016.06.023.

Palozzi, Jonathan M., Swathi P. Jeedigunta, and Thomas R. Hurd (Dec. 2018). "Mitochondrial DNA Purifying Selection in Mammals and Invertebrates". In: *Journal of Molecular Biology* 430.24, 4834–4848. ISSN: 0022-2836. DOI: 10.1016/j.jmb.2018.10.019. URL: http://dx.doi.org/10.1016/j.jmb.2018.10.019.

Paumard, Patrick et al. (Feb. 2002). "The ATP synthase is involved in generating mitochondrial cristae morphology". In: *EMBO Journal* 21.3, pp. 221–230. ISSN: 02614189. DOI: 10.1093/emboj/21.3.221. URL: https://pubmed.ncbi.nlm.nih.gov/11823415/.

Perillo, Bruno et al. (Feb. 2020). "ROS in cancer therapy: the bright side of the moon". In: *Experimental amp; Molecular Medicine* 52.2, 192–203. ISSN: 2092-6413. DOI: 10.1038/s12276-020-0384-2. URL: http://dx.doi.org/10.1038/s12276-020-0384-2.

Pfanner, Nikolaus et al. (Mar. 2014). "Uniform nomenclature for the mitochondrial contact site and cristae organizing system". In: *Journal of Cell Biology* 204.7, 1083–1086. ISSN: 0021-9525. DOI: 10.1083/jcb.201401006. URL: http://dx.doi.org/10.1083/jcb.201401006.

Pinto, Milena and Carlos T. Moraes (Aug. 2015). "Mechanisms linking mtDNA damage and aging". In: *Free Radical Biology and Medicine* 85, 250–258. ISSN: 0891-5849. DOI: 10.1016/j.freeradbiomed.2015.05.005. URL: http://dx.doi.org/10.1016/j.freeradbiomed.2015.05.005.

Piškur, Jure (May 1994). "Inheritance of the Yeast Mitochondrial Genome". In: *Plasmid* 31.3, 229–241. ISSN: 0147-619X. DOI: 10.1006/plas.1994.1025. URL: http://dx.doi.org/10.1006/plas.1994.1025.

Poole, Angela C. et al. (Apr. 2010). "The Mitochondrial Fusion-Promoting Factor Mitofusin Is a Substrate of the PINK1/Parkin Pathway". In: *PLoS ONE* 5.4. Ed. by Mark R. Cookson, e10054. ISSN: 1932-6203. DOI: 10.1371/journal.pone.0010054. URL: http://dx.doi.org/10.1371/journal.pone.0010054.

Posakony, JW, JM England, and G Attardi (Aug. 1977). "Mitochondrial growth and division during the cell cycle in HeLa cells". In: *The Journal of Cell Biology* 74.2, 468–491. ISSN: 0021-9525. DOI: 10.1083/jcb.74.2.468. URL: http://dx.doi.org/10.1083/jcb.74.2.468.

Prachař, Jarmil (2016). "Ultrastructure of mitochondrial nucleoid and its surroundings". In: *General physiology and biophysics* 35.03, 273–286. ISSN: 1338-4325. DOI: 10.4149/gpb_2016008. URL: http://dx.doi.org/10.4149/gpb_2016008.

Pérez-Amado, Carlos Jhovani et al. (July 2021). "Mitochondrial Heteroplasmy Shifting as a Potential Biomarker of Cancer Progression". In: *International Journal of Molecular Sciences* 22.14, p. 7369. ISSN: 1422-0067. DOI: 10.3390/ijms22147369. URL: http://dx.doi.org/10.3390/ijms22147369.

Raap, Anton K. et al. (Dec. 2012). "Non-Random mtDNA Segregation Patterns Indicate a Metastable Heteroplasmic Segregation Unit in m.3243Agt;G Cybrid Cells". In: *PLoS ONE* 7.12. Ed. by Yidong Bai, e52080. ISSN: 1932-6203. DOI: 10.1371/journal.pone.0052080. URL: http://dx.doi.org/10.1371/journal.pone.0052080.

Rabl, Regina et al. (June 2009). "Formation of cristae and crista junctions in mitochondria depends on antagonism between Fcj1 and Su e/g." In: *The Journal of cell biology* 185.6, pp. 1047–63. ISSN: 1540-8140. DOI: 10.1083/jcb.200811099. URL: http://jcb.rupress.org/content/185/6/1047.full.

Radzvilavicius, Arunas L. and Iain G. Johnston (Oct. 2022). "Organelle bottlenecks facilitate evolvability by traversing heteroplasmic fitness valleys". In: *Frontiers in Genetics* 13. ISSN: 1664-8021. DOI: 10.3389/fgene.2022.974472. URL: http://dx.doi.org/10.3389/fgene.2022.974472.

Rafelski, Susanne M. et al. (2012). "Mitochondrial Network Size Scaling in Budding Yeast". In: *Science* 338.6108. URL: http://science.sciencemag.org/content/338/6108/822.long.

Rajala, N. et al. (Oct. 2013). "Replication factors transiently associate with mtDNA at the mitochondrial inner membrane to facilitate replication". In: *Nucleic Acids Research* 42.2, 952–967. ISSN: 1362-4962. DOI: 10.1093/nar/gkt988. URL: http://dx.doi.org/10.1093/nar/gkt988.

Rapaport, Doron et al. (Aug. 1998). "Fzo1p Is a Mitochondrial Outer Membrane Protein Essential for the Biogenesis of Functional Mitochondria in Saccharomyces cerevisiae". In: *Journal of Biological Chemistry* 273.32, 20150–20155. ISSN: 0021-9258. DOI: 10.1074/jbc.273.32.20150. URL: http://dx.doi.org/10.1074/jbc.273.32.20150.

Rasul, Mohammed Fatih et al. (Mar. 2022). "Strategies to overcome the main challenges of the use of CRISPR/Cas9 as a replacement for cancer therapy". In: *Molecular Cancer* 21.1. ISSN: 1476-4598. DOI: 10.1186/s12943-021-01487-4. URL: http://dx.doi.org/10.1186/s12943-021-01487-4.

Reinders, Jörg et al. (Nov. 2007). "Profiling Phosphoproteins of Yeast Mitochondria Reveals a Role of Phosphorylation in Assembly of the ATP Synthase". In: *Molecular amp; Cellular Proteomics* 6.11, 1896–1906. ISSN: 1535-9476. DOI: 10.1074/mcp.m700098-mcp200. URL: http://dx.doi.org/10.1074/mcp.M700098-MCP200.

Ren, Wei et al. (Dec. 2022). "Visualization of mitochondrial cristae and mtDNA evolvement and interactions with super-resolution microscopy". In: DOI: 10.1101/2022.12.26.521907. URL: http://dx.doi.org/10.1101/2022.12.26.521907.

Rickwood, D., J.A.A. Chambers, and M. Barat (May 1981). "Isolation and preliminary characterisation of DNA-protein complexes from the mitochondria of Saccharomyces cerevisiae". In: *Experimental Cell Research* 133.1, 1–13. ISSN: 0014-4827. DOI: 10.1016/0014-4827(81)90350-5. URL: http://dx.doi.org/10.1016/0014-4827(81)90350-5.

Roger, Andrew J., Sergio A. Muñoz-Gómez, and Ryoma Kamikawa (Nov. 2017). "The Origin and Diversification of Mitochondria". In: *Current Biology* 27.21, R1177–R1192. ISSN: 0960-9822. DOI: 10.1016/j.cub.2017.09.015. URL: http://dx.doi.org/10.1016/j.cub.2017.09.015.

Roussou, Rodaria et al. (Aug. 2024). "Real-time assessment of mitochondrial DNA heteroplasmy dynamics at the single-cell level". In: *The EMBO Journal* 0.0, pp. 1–20. DOI: https://doi.org/10.1038/s44318-024-00183-5. URL: https://www.embopress.org/doi/abs/10.1038/s44318-024-00183-5.

Saraste, Matti (Mar. 1999). "Oxidative Phosphorylation at the fin de siècle". In: *Science* 283.5407, 1488–1493. ISSN: 1095-9203. DOI: 10.1126/science.283.5407.1488. URL: http://dx.doi.org/10.1126/science.283.5407.1488.

Sastri, Mira et al. (Oct. 2017). "Sub-mitochondrial localization of the genetic-tagged mitochondrial intermembrane space-bridging components Mic19, Mic60 and Sam50". In: *Journal of Cell Science* 130.19, 3248–3260. ISSN: 0021-9533. DOI: 10.1242/jcs.201400. URL: http://dx.doi.org/10.1242/jcs.201400.

Sauer, Heinrich, Maria Wartenberg, and Juergen Hescheler (2001). "Reactive Oxygen Species as Intracellular Messengers During Cell Growth and Differentiation". In: *Cellular Physiology and Biochemistry* 11.4, 173–186. ISSN: 1421-9778. DOI: 10.1159/000047804. URL: http://dx.doi.org/10.1159/000047804.

Sazanov, Leonid A. (May 2015). "A giant molecular proton pump: structure and mechanism of respiratory complex I". In: *Nature Reviews Molecular Cell Biology* 16.6, 375–388. ISSN: 1471-0080. DOI: 10.1038/nrm3997. URL: http://dx.doi.org/10.1038/nrm3997.

Schägger, Hermann and Kathy Pfeiffer (Apr. 2000). "Supercomplexes in the respiratory chains of yeast and mammalian mitochondria". In: *EMBO Journal* 19.8, pp. 1777–1783. ISSN: 02614189. DOI: 10.1093/emboj/19.8.1777. URL: https://pubmed.ncbi.nlm.nih.gov/10775262/.

Schmiderer, Ludwig et al. (Nov. 2022). "Site-specific CRISPR-based mitochondrial DNA manipulation is limited by gRNA import". In: *Scientific Reports* 12.1. ISSN: 2045-2322. DOI: 10.1038/s41598-022-21794-0. URL: http://dx.doi.org/10.1038/s41598-022-21794-0.

Schrott, Simon and Christof Osman (Nov. 2023). "Two mitochondrial HMG-box proteins, Cim1 and Abf2, antagonistically regulate mtDNA copy number in Saccharomyces cerevisiae". In: *Nucleic acids research* 51 (21), pp. 11813–11835. ISSN: 1362-4962. DOI: 10.1093/NAR/GKAD849. URL: https://pubmed.ncbi.nlm.nih.gov/37850632/.

Sedman, Tiina et al. (Mar. 2000). "A DNA Helicase Required for Maintenance of the Functional Mitochondrial Genome in Saccharomyces cerevisiae". In: *Molecular and Cellular Biology* 20.5, 1816–1824. ISSN: 1098-5549. DOI: 10.1128/mcb.20.5.1816-1824.2000. URL: http://dx.doi.org/10.1128/mcb.20.5.1816-1824.2000.

Seel, Anika et al. (Oct. 2023). "Regulation with cell size ensures mitochondrial DNA homeostasis during cell growth". In: *Nature Structural and Molecular Biology* 30 (10), pp. 1549–1560. ISSN: 15459985. DOI: 10.1038/s41594-023-01091-8.

Segui-Real, B. et al. (May 1993). "Functional independence of the protein translocation machineries in mitochondrial outer and inner membranes: passage of preproteins through the intermembrane space." In: *The EMBO Journal* 12.5, 2211–2218. ISSN: 0261-4189. DOI: 10.1002/j.1460-2075.1993.tb05869.x. URL: http://dx.doi.org/10.1002/j.1460-2075.1993.tb05869.x.

Sesaki, Hiromi and Robert E. Jensen (Nov. 1999). "Division versus Fusion: Dnm1p and Fzo1p Antagonistically Regulate Mitochondrial Shape". In: *The Journal of Cell Biology* 147.4, 699–706. ISSN: 1540-8140. DOI: 10.1083/jcb.147.4.699. URL: http://dx.doi.org/10.1083/jcb.147.4.699.

Shadel, Gerald S. (Nov. 1999). "Yeast as a Model for Human mtDNA Replication". In: *The American Journal of Human Genetics* 65.5, 1230–1237. ISSN: 0002-9297. DOI: 10.1086/302630. URL: http://dx.doi.org/10.1086/302630.

Shadel, Gerald S (June 2005). "Mitochondrial DNA, aconitase 'wraps' it up". In: *Trends in Biochemical Sciences* 30.6, 294–296. ISSN: 0968-0004. DOI: 10.1016/j.tibs.2005.04.007. URL: http://dx.doi.org/10.1016/j.tibs.2005.04.007.

Shapiro, Lucille et al. (May 1968). "Physical studies on the structure of yeast mitochondrial DNA". In: *Journal of Molecular Biology* 33.3, 907–922. ISSN: 0022-2836. DOI: 10.1016/0022-2836(68)90327-6. URL: http://dx.doi.org/10.1016/0022-2836(68)90327-6.

Shaw, Janet M and Jodi Nunnari (Apr. 2002). "Mitochondrial dynamics and division in budding yeast". In: *Trends in Cell Biology* 12.4, 178–184. ISSN: 0962-8924. DOI: 10.1016/s0962-8924(01)02246-2. URL: http://dx.doi.org/10.1016/s0962-8924(01)02246-2.

Shepard, Kelly A. and Michael P. Yaffe (Feb. 1999). "The Yeast Dynamin-like Protein, Mgm1p, Functions on the Mitochondrial Outer Membrane to Mediate Mitochondrial Inheritance". In: *The Journal of Cell Biology* 144.4, 711–720. ISSN: 1540-8140. DOI: 10.1083/jcb.144.4.711. URL: http://dx.doi.org/10.1083/jcb.144.4.711.

Siekevitz, Philip (July 1957). "Powerhouse of the Cell". In: *Scientific American* 197.1, 131–144. ISSN: 0036-8733. DOI: 10.1038/scientificamerican0757-131. URL: http://dx.doi.org/10.1038/scientificamerican0757-131.

Spelbrink, Johannes N. (2010). "Functional organization of mammalian mitochondrial DNA in nucleoids: history, recent developments, and future challenges".

In: *IUBMB life* 62 (1), pp. 19–32. ISSN: 1521-6551. DOI: 10.1002/IUB.282. URL: https://pubmed.ncbi.nlm.nih.gov/20014006/.

Spinelli, Jessica B. and Marcia C. Haigis (June 2018). "The multifaceted contributions of mitochondria to cellular metabolism". In: *Nature Cell Biology* 20.7, 745–754. ISSN: 1476-4679. DOI: 10.1038/s41556-018-0124-1. URL: http://dx.doi.org/10.1038/s41556-018-0124-1.

St. John, Justin C. (Aug. 2019). "Mitochondria and Female Germline Stem Cells—A Mitochondrial DNA Perspective". In: *Cells* 8.8, p. 852. ISSN: 2073-4409. DOI: 10.3390/cells8080852. URL: http://dx.doi.org/10.3390/cells8080852.

Stephan, Till et al. (Dec. 2019). "Live-cell STED nanoscopy of mitochondrial cristae". In: *Scientific Reports* 9.1. ISSN: 20452322. DOI: 10.1038/s41598-019-48838-2. URL: https://pubmed.ncbi.nlm.nih.gov/31455826/.

Stewart, James B. and Patrick F. Chinnery (Aug. 2015). "The dynamics of mitochondrial DNA heteroplasmy: implications for human health and disease". In: *Nature Reviews Genetics* 16.9, 530–542. ISSN: 1471-0064. DOI: 10.1038/nrg3966. URL: http://dx.doi.org/10.1038/nrg3966.

Stewart, James B and Patrick F. Chinnery (Feb. 2021). "Extreme heterogeneity of human mitochondrial DNA from organelles to populations". In: *Nature reviews. Genetics* 22 (2), pp. 106–118. ISSN: 1471-0064. DOI: 10.1038/S41576-020-00284-X. URL: https://pubmed.ncbi.nlm.nih.gov/32989265/.

Stewart, James B and Nils-Göran Larsson (Oct. 2014). "Keeping mtDNA in Shape between Generations." In: *PLoS genetics* 10 (10), e1004670. ISSN: 1553-7404. DOI: 10.1371/journal.pgen.1004670. URL: http://www.pubmedcentral.nih.gov/articlerender.fcgi?artid=4191934&tool=pmcentrez&rendertype=abstract.

Stewart, James Bruce et al. (Jan. 2008). "Strong Purifying Selection in Transmission of Mammalian Mitochondrial DNA". In: *PLoS Biology* 6.1. Ed. by Laurence D Hurst, e10. ISSN: 1545-7885. DOI: 10.1371/journal.pbio.0060010. URL: http://dx.doi.org/10.1371/journal.pbio.0060010.

Stumpf, J. D. et al. (Feb. 2010). "mip1 containing mutations associated with mitochondrial disease causes mutagenesis and depletion of mtDNA in Saccharomyces cerevisiae". In: *Human Molecular Genetics* 19.11, 2123–2133. ISSN: 1460-2083. DOI: 10.1093/hmg/ddq089. URL: http://dx.doi.org/10.1093/hmg/ddq089.

Swayne, Theresa C. et al. (Dec. 2011). "Role for cER and Mmr1p in Anchorage of Mitochondria at Sites of Polarized Surface Growth in Budding Yeast". In: *Current Biology* 21.23, 1994–1999. ISSN: 0960-9822. DOI: 10.1016/j.cub.2011.10.019. URL: http://dx.doi.org/10.1016/j.cub.2011.10.019.

Tafani, Marco et al. (2016). "The Interplay of Reactive Oxygen Species, Hypoxia, Inflammation, and Sirtuins in Cancer Initiation and Progression". In: *Oxidative Medicine and Cellular Longevity* 2016, 1–18. ISSN: 1942-0994. DOI: 10.1155/2016/3907147. URL: http://dx.doi.org/10.1155/2016/3907147.

Tam, Zhi Yang et al. (Oct. 2013). "Mathematical Modeling of the Role of Mitochondrial Fusion and Fission in Mitochondrial DNA Maintenance". In: *PLoS ONE* 8 (10), e76230. ISSN: 19326203. DOI: 10.1371/journal.pone.0076230.

Tang, Junhui et al. (May 2019). "Sam50–Mic19–Mic60 axis determines mitochondrial cristae architecture by mediating mitochondrial outer and inner membrane contact". In: *Cell Death amp; Differentiation* 27.1, 146–160. ISSN: 1476-5403. DOI: 10.1038/s41418-019-0345-2. URL: http://dx.doi.org/10.1038/s41418-019-0345-2.

Tang, Zhongjie et al. (Apr. 2022). "A Genetic Bottleneck of Mitochondrial DNA During Human Lymphocyte Development". In: *Molecular Biology and Evolution* 39.5. Ed. by Bing Su. ISSN: 1537-1719. DOI: 10.1093/molbev/msac090. URL: http://dx.doi.org/10.1093/molbev/msac090.

Temperley, Richard J. et al. (June 2010). "Human mitochondrial mRNAs—like members of all families, similar but different". In: *Biochimica et Biophysica Acta (BBA) - Bioenergetics* 1797.6–7, 1081–1085. ISSN: 0005-2728. DOI: 10.1016/j.bbabio.2010.02.036. URL: http://dx.doi.org/10.1016/j.bbabio.2010.02.036.

Tieu, Quinton and Jodi Nunnari (Oct. 2000). "Mdv1p Is a Wd Repeat Protein That Interacts with the Dynamin-Related Gtpase, Dnm1p, to Trigger Mitochondrial Division". In: *The Journal of Cell Biology* 151.2, 353–366. ISSN: 1540-8140. DOI: 10.1083/jcb.151.2.353. URL: http://dx.doi.org/10.1083/jcb.151.2.353.

Tocchini, Cristina and Susan E. Mango (Mar. 2024). "An adapted MS2-MCP system to visualize endogenous cytoplasmic mRNA with live imaging in Caenorhabditis elegans". In: *PLOS Biology* 22.3. Ed. by René F. Ketting, e3002526. ISSN: 1545-7885. DOI: 10.1371/journal.pbio.3002526. URL: http://dx.doi.org/10.1371/journal.pbio.3002526.

Tomar, Namrata et al. (Feb. 2022). "Substrate-dependent differential regulation of mitochondrial bioenergetics in the heart and kidney cortex and outer medulla". In: *Biochimica et Biophysica Acta (BBA) - Bioenergetics* 1863.2, p. 148518. ISSN: 0005-2728. DOI: 10.1016/j.bbabio.2021.148518. URL: http://dx.doi.org/10.1016/j.bbabio.2021.148518.

Twig, Gilad et al. (Jan. 2008). "Fission and selective fusion govern mitochondrial segregation and elimination by autophagy". In: *The EMBO Journal* 27.2, 433–446. ISSN: 1460-2075. DOI: 10.1038/sj.emboj.7601963. URL: http://dx.doi.org/10.1038/sj.emboj.7601963.

Tzagoloff, Alexander and Alan M. Myers (June 1986). "GENETICS OF MITOCHONDRIAL BIOGENESIS". In: *Annual Review of Biochemistry* 55.1, 249–285. ISSN: 1545-4509. DOI: 10.1146/annurev.bi.55.070186.001341. URL: http://dx.doi.org/10.1146/annurev.bi.55.070186.001341.

Uetz, Peter et al. (Feb. 2000). "A comprehensive analysis of protein–protein interactions in Saccharomyces cerevisiae". In: *Nature* 403.6770, 623–627. ISSN: 1476-4687. DOI: 10.1038/35001009. URL: http://dx.doi.org/10.1038/35001009.

Ugarte-Uribe, Begoña et al. (Oct. 2014). "Dynamin-related Protein 1 (Drp1) Promotes Structural Intermediates of Membrane Division". In: *Journal of Biological Chemistry* 289.44, 30645–30656. ISSN: 0021-9258. DOI: 10.1074/jbc.m114.575779. URL: http://dx.doi.org/10.1074/jbc.M114.575779.

Velours, Jean and Geneviéve Arselin (2000). "The Saccharomyces cerevisiae ATP synthase". In: *Journal of Bioenergetics and Biomembranes* 32.4, 383–390. ISSN: 0145-479X. DOI: 10.1023/a:1005580020547. URL: http://dx.doi.org/10.1023/a:1005580020547.

Vogel, Frank et al. (Oct. 2006). "Dynamic subcompartmentalization of the mitochondrial inner membrane". In: *The Journal of Cell Biology* 175.2, pp. 237–247. ISSN: 0021-9525. DOI: 10.1083/jcb.200605138. URL: http://www.ncbi.nlm.nih.gov/pubmed/17043137http://www.pubmedcentral.nih.gov/articlerender.fcgi?artid=PMC2064565http://www.jcb.org/lookup/doi/10.1083/jcb.200605138.

Vosseberg, Julian et al. (Oct. 2020). "Timing the origin of eukaryotic cellular complexity with ancient duplications". In: *Nature Ecology amp; Evolution* 5.1, 92–100.

ISSN: 2397-334X. DOI: 10.1038/s41559-020-01320-z. URL: http://dx.doi.org/10.1038/s41559-020-01320-z.

Vries, Simon de and Carla A.M. Marres (Jan. 1987). "The mitochondrial respiratory chain of yeast. Structure and biosynthesis and the role in cellular metabolism". In: *Biochimica et Biophysica Acta (BBA) - Reviews on Bioenergetics* 895.3, 205–239. ISSN: 0304-4173. DOI: 10.1016/s0304-4173(87)80003-4. URL: http://dx.doi.org/10.1016/s0304-4173(87)80003-4.

Wai, Timothy, Daniella Teoli, and Eric A Shoubridge (Nov. 2008). "The mitochondrial DNA genetic bottleneck results from replication of a subpopulation of genomes". In: *Nature Genetics* 40.12, 1484–1488. ISSN: 1546-1718. DOI: 10.1038/ng.258. URL: http://dx.doi.org/10.1038/ng.258.

Wallace, Douglas C. et al. (May 1995). "Mitochondrial DNA mutations in human degenerative diseases and aging". In: *Biochimica et Biophysica Acta (BBA) - Molecular Basis of Disease* 1271.1, 141–151. ISSN: 0925-4439. DOI: 10.1016/0925-4439(95)00021-u. URL: http://dx.doi.org/10.1016/0925-4439(95)00021-u.

Wang, Zhang and Martin Wu (Jan. 2015). "An integrated phylogenomic approach toward pinpointing the origin of mitochondria". In: *Scientific Reports* 5.1. ISSN: 2045-2322. DOI: 10.1038/srep07949. URL: http://dx.doi.org/10.1038/srep07949.

Watt, Ian N. et al. (Sept. 2010). "Bioenergetic cost of making an adenosine triphosphate molecule in animal mitochondria". In: *Proceedings of the National Academy of Sciences* 107.39, 16823–16827. ISSN: 1091-6490. DOI: 10.1073/pnas.1011099107. URL: http://dx.doi.org/10.1073/pnas.1011099107.

Weber, Tobias A. et al. (May 2013). "APOOL Is a Cardiolipin-Binding Constituent of the Mitofilin/MINOS Protein Complex Determining Cristae Morphology in Mammalian Mitochondria". In: *PLoS ONE* 8.5. Ed. by Paul A. Cobine, e63683. ISSN: 1932-6203. DOI: 10.1371/journal.pone.0063683. URL: http://dx.doi.org/10.1371/journal.pone.0063683.

Wei, Wei et al. (May 2019). "Germline selection shapes human mitochondrial DNA diversity". In: *Science* 364 (6442), eaau6520. ISSN: 10959203. DOI: 10.1126/science.aau6520.

Westermann, Benedikt (July 2014). "Mitochondrial inheritance in yeast". In: *Biochimica et Biophysica Acta (BBA) - Bioenergetics* 1837.7, 1039–1046. ISSN: 0005-2728. DOI: 10.1016/j.bbabio.2013.10.005. URL: http://dx.doi.org/10.1016/j.bbabio.2013.10.005.

Wiesner, Rudolf J., J.Caspar Rüegg, and Ingo Morano (Mar. 1992). "Counting target molecules by exponential polymerase chain reaction: Copy number of mitochondrial DNA in rat tissues". In: *Biochemical and Biophysical Research Communications* 183.2, 553–559. ISSN: 0006-291X. DOI: 10.1016/0006-291x(92)90517-o. URL: http://dx.doi.org/10.1016/0006-291x(92)90517-o.

Wilkens, Verena, Wladislaw Kohl, and Karin Busch (Jan. 2013). "Restricted diffusion of OXPHOS complexes in dynamic mitochondria delays their exchange between cristae and engenders a transitory mosaic distribution". In: *Journal of Cell Science* 126.1, pp. 103–116. ISSN: 0021-9533. DOI: 10.1242/jcs.108852. URL: http://www.ncbi.nlm.nih.gov/pubmed/23038773http://jcs.biologists.org/lookup/doi/10.1242/jcs.108852.

Wittig, Ilka and Hermann Schägger (June 2009). "Supramolecular organization of ATP synthase and respiratory chain in mitochondrial membranes". In: *Biochimica et Biophysica Acta (BBA) - Bioenergetics* 1787.6, 672–680. ISSN: 0005-2728. DOI: 10.

1016/j.bbabio.2008.12.016. URL: http://dx.doi.org/10.1016/j.bbabio.2008.12.016.

Wolf, Dane M et al. (Nov. 2019). "Individual cristae within the same mitochondrion display different membrane potentials and are functionally independent". In: *The EMBO Journal* 38.22. ISSN: 0261-4189. DOI: 10.15252/embj.2018101056. URL: https://pubmed.ncbi.nlm.nih.gov/31609012/.

Wong, Edith D. et al. (Oct. 2000). "The Dynamin-Related Gtpase, Mgm1p, Is an Intermembrane Space Protein Required for Maintenance of Fusion Competent Mitochondria". In: *The Journal of Cell Biology* 151.2, 341–352. ISSN: 1540-8140. DOI: 10.1083/jcb.151.2.341. URL: http://dx.doi.org/10.1083/jcb.151.2.341.

Wonnapinij, Passorn, Patrick F. Chinnery, and David C. Samuels (Nov. 2008). "The Distribution of Mitochondrial DNA Heteroplasmy Due to Random Genetic Drift". In: *American Journal of Human Genetics* 83 (5), pp. 582–593. ISSN: 00029297. DOI: 10.1016/j.ajhg.2008.10.007.

Wu, Zhihao, Winson S. Ho, and Rongze Lu (Sept. 2021). "Targeting Mitochondrial Oxidative Phosphorylation in Glioblastoma Therapy". In: *NeuroMolecular Medicine* 24.1, 18–22. ISSN: 1559-1174. DOI: 10.1007/s12017-021-08678-8. URL: http://dx.doi.org/10.1007/s12017-021-08678-8.

Zamaroczy, Miklos de and Giorgio Bernardi (Jan. 1986). "The GC clusters of the mitochondrial genome of yeast and their evolutionary origin". In: *Gene* 41.1, 1–22. ISSN: 0378-1119. DOI: 10.1016/0378-1119(86)90262-3. URL: http://dx.doi.org/10.1016/0378-1119(86)90262-3.

Zelenaya-Troitskaya, Olga et al. (Apr. 1998). "Functions of the High Mobility Group Protein, Abf2p, in Mitochondrial DNA Segregation, Recombination and Copy Number in Saccharomyces cerevisiae". In: *Genetics* 148.4, 1763–1776. ISSN: 1943-2631. DOI: 10.1093/genetics/148.4.1763. URL: http://dx.doi.org/10.1093/genetics/148.4.1763.

Zerbes, Ralf M. et al. (Sept. 2012). "Role of MINOS in Mitochondrial Membrane Architecture: Cristae Morphology and Outer Membrane Interactions Differentially Depend on Mitofilin Domains". In: *Journal of Molecular Biology* 422.2, 183–191. ISSN: 0022-2836. DOI: 10.1016/j.jmb.2012.05.004. URL: http://dx.doi.org/10.1016/j.jmb.2012.05.004.

Zhang, Haixin, Stephen P. Burr, and Patrick F. Chinnery (June 2018a). "The mitochondrial DNA genetic bottleneck: inheritance and beyond". In: *Essays in Biochemistry* 62.3. Ed. by Caterina Garone and Michal Minczuk, 225–234. ISSN: 1744-1358. DOI: 10.1042/ebc20170096. URL: http://dx.doi.org/10.1042/EBC20170096.

Zhang, Haixin, Stephen P. Burr, and Patrick F. Chinnery (June 2018b). "The mitochondrial DNA genetic bottleneck: inheritance and beyond". In: *Essays in Biochemistry* 62.3. Ed. by Caterina Garone and Michal Minczuk, 225–234. ISSN: 1744-1358. DOI: 10.1042/ebc20170096. URL: http://dx.doi.org/10.1042/EBC20170096.

Zhang, Yi et al. (2019). "PINK1 Inhibits Local Protein Synthesis to Limit Transmission of Deleterious Mitochondrial DNA Mutations". In: *Molecular Cell* 73.6, pp. 1127–1137. ISSN: 10972765. DOI: 10.1016/j.molcel.2019.01.013. URL: https://linkinghub.elsevier.com/retrieve/pii/S1097276519300139.

Ziviani, Elena, Ran N. Tao, and Alexander J. Whitworth (Mar. 2010). "Drosophila Parkin requires PINK1 for mitochondrial translocation and ubiquitinates Mitofusin". In: *Proceedings of the National Academy of Sciences* 107.11, 5018–5023. ISSN:

1091-6490. DOI: 10.1073/pnas.0913485107. URL: http://dx.doi.org/10.1073/pnas.0913485107.

Zorkau, Matthew et al. (Feb. 2021). "High-resolution imaging reveals compartmentalization of mitochondrial protein synthesis in cultured human cells". In: *Proceedings of the National Academy of Sciences* 118.6, e2008778118. ISSN: 0027-8424. DOI: 10.1073/pnas.2008778118. URL: https://pubmed.ncbi.nlm.nih.gov/33526660/.

Acknowledgements

First and foremost, my big thanks go to my supervisor Prof. Dr. Christof Osman, who gave me the opportunity and freedom to work on multiple exciting projects. Christof, thank you for the guidance, the optimism on challenging moments, and the fruitful discussions throughout these years. I am thankful for all the knowledge, but most importantly the lessons on perseverance in both scientific and life matters.

Many thanks go out to my thesis advisory committee: PD. Dr. Philipp Korber, Prof. Dr. Dirk Metzler and Prof. Dr. Christof Osman. The yearly meetings we had were detrimental for my research progress and for setting ambitious but always achievable goals.

A big thanks to the LSM Graduate School and to Nadine Hamze for the great workshops, initiatives and the ever-present support.

Sincere thanks also go to all colleagues and members of the Osman-Mokranjac Monday meetings and Mito-club meetings. Your feedback were instrumental in the continuous improvement and completion of my work. I am incredibly grateful for the opportunity I had to collaborate and exchange ideas with such motivated individuals. It has always been rewarding.

My thanks further extend to my colleagues and friends Nupur, Felix, Johannes for their invaluable insights, collaboration, and scientific and non-scientific support. Working with you was always a great pleasure, and not working with you was an even bigger one. I have been extremely lucky having you as partners on this journey.

I would also like to express my heartfelt gratitude to all my friends in Munich and those around the world. Those that I met before this journey, those that became an essential part during it, and those that showed up for me at the end of it. Thank you for the uncountable moments of laughter, connection and unwavering presence. Thank you Edu, Janet, Beth, Shalini, Gonz and many more!

An immense thanks goes to Chara and Roza, who, even from afar, have always been there for me all these years. A special thanks also goes to Cristina and Sarah. Your encouragement during the challenges and your celebration of my successes mean the world to me. I am incredibly grateful for our camaraderie.

Last but not least, I want to thank my friend Jan Bolmer, who stood by my side during this effort, witnessed my weakest moments, and actively helped me to advance.

I also thank my dog Bira, who has been my best emotional support buddy, and taught me that life is all about cuddles, tag-of-wars and maintaining a kind heart, no matter what. Thank you for your tremendous personality lady B.

Wholeheartedly, finally, I want to thank my family and mostly my parents and my sister, because without their support this work would not have been possible. You are always by my side, offering me the strength and motivation to keep moving forward. Thank you from the bottom of my heart for your unlimited love, encouragement and for believing in me all these years.